Impact of platelet-mediated inflammation on Alzheimer's disease progression and the interaction between collagen receptor glycoprotein VI and amyloid-β 40

Inaugural-Dissertation

zur Erlangung des Doktorgrades
der Mathematisch-Naturwissenschaftlichen Fakultät
der Heinrich-Heine-Universität Düsseldorf

vorgelegt von

Laura Mara Toska
aus Düsseldorf

Düsseldorf, Juni 2023

aus dem Institut für Experimentelle Vaskuläre Medizin
der Heinrich-Heine-Universität Düsseldorf

Gedruckt mit der Genehmigung der
Mathematisch-Naturwissenschaftlichen Fakultät der
Heinrich-Heine-Universität Düsseldorf

Berichterstatter:

1. Prof. Dr. Patricia Hidalgo

2. Prof. Dr. Margitta Elvers

Tag der mündlichen Prüfung: 15.06.2023

Table of content

Abstract

With the aging population, neurodegenerative diseases such as Alzheimer's disease (AD) are becoming a major health problem worldwide. AD is a multifactorial neurodegenerative disorder associated with the development of cognitive impairment due to neuronal cell loss. Neuropathologically, AD is characterized by extracellular amyloid-β (Aβ) plaques, intracellular neurofibrillary tangles and neuroinflammation in the brain. In addition, Aβ can also accumulate in cerebral blood vessels, which is referred to as cerebral amyloid angiopathy (CAA). CAA is associated with the degeneration of the vessel wall, resulting in decreased cerebral blood flow and progressive cognitive impairment. Platelets are key players in the regulation of hemostasis and are involved in acute and chronic inflammatory processes through their interaction with inflammatory and endothelial cells. In recent years, there has been increasing evidence for platelets to be involved in the progression of AD. In this context, short-term treatment of the transgenic APP23 mouse model of AD with the platelet antagonist clopidogrel resulted in a reduction of CAA burden.

The aim of the present study was to further investigate the role of platelets and, in particular, the role of the major platelet collagen receptor GPVI, in the progression of AD. In the present study, GPVI was identified as a direct binding partner of Aβ40 at the platelet surface. Binding of Aβ40 to GPVI triggered GPVI surface externalization, ATP release and platelet aggregation. In addition, GPVI is critically involved in platelet-mediated formation of amyloid-β aggregates *in vitro*. Thus, blocking or deletion of GPVI led to a significant reduction of Aβ aggregation *in vitro.* Moreover, platelet stimulation with Aβ40 has been shown to trigger, in part via GPVI receptor, the release of fibrinogen that co-localized with amyloid-β aggregates *in vitro*. Furthermore, the present study investigated the influence of Aβ40 on platelet-triggered inflammation and neutrophil recruitment. Stimulation of murine platelets with Aβ40 induced the formation of platelet-neutrophil aggregates. Subsequent *in vitro* analysis of human and murine neutrophils revealed increased platelet-mediated neutrophil adhesion after Aβ40 and ADP stimulation. However, the formation of neutrophil extracellular traps was not observed under these conditions. In contrast to platelets, murine neutrophils were not substantially involved in the formation of amyloid-β aggregates *in vitro*. Stimulation of platelets with Aβ40 triggered GPVI-dependent ROS production and, to some extent, GPVI-dependent TGF-β1 release. Moreover, this work describes for the first time an age-dependent migration of platelets into the brain parenchyma in *WTmT/mG;PF4Cre+* and *APP23mT/mG;PF4Cre+* mice, with an earlier onset in the hippocampus of *APP23mT/mG;PF4Cre+* mice. In the brain of aged *APP23-mT/mG;PF4Cre+,* platelets were localized around amyloid plaques and in close contact to microglia.

Taken together, this work identified the GPVI receptor as binding partner for Aβ40 at the platelet surface that contributes to the formation of amyloid-β aggregates by platelets *in vitro*. Moreover, the results of this work suggest that Aβ40 impact the platelet-mediated inflammation. In addition, platelets were detected around amyloid plaques in the brain parenchyma of aged *APP23mT/mG;PF4Cre+* mice. This work provides further knowledge about the role of platelets in AD and suggests that anti-thrombotic therapy might be beneficial of patients with AD.

Zusammenfassung

Mit der alternden Bevölkerung werden neurodegenerative Erkrankungen wie die Alzheimer-Krankheit (AK) weltweit zu einem großen Gesundheitsproblem. Die AK ist eine multifaktorielle neurodegenerative Erkrankung, die mit der Entwicklung kognitiver Beeinträchtigungen aufgrund des Verlusts neuronaler Zellen einhergeht. Neuropathologisch ist die AK durch extrazelluläre Amyloid-β (Aβ) -Plaques und intrazelluläre neurofibrilläre Ablagerungen im Gehirn, sowie Neuroinflammation gekennzeichnet. Darüber hinaus kann sich Aβ auch in den Blutgefäßen des Gehirns ablagern, was als zerebrale Amyloidangiopathie (ZAA) bezeichnet wird. Die ZAA kann mit einer Degeneration der Blutgefäßwände einhergehen. Dies führt zu einem verminderten zerebralen Blutfluss und einer fortschreitenden kognitiven Beeinträchtigung. Thrombozyten spielen eine Schlüsselrolle bei der Regulierung der Blutstillung und sind durch ihre Interaktion mit Entzündungszellen und dem Endothel auch an akuten und chronischen Inflammationsprozessen beteiligt. In den letzten Jahren mehren sich die Hinweise auf eine Beteiligung der Thrombozyten an der Progression der AK. In diesem Zusammenhang führte eine kurzfristige Behandlung des transgenen APP23Mausmodells der AK mit dem Thrombozytenantagonisten Clopidogrel zu einer Reduktion der ZAA im Gehirn dieser Tiere.

Ziel der vorliegenden Studie war es, die Rolle der Thrombozyten und insbesondere die Rolle des wichtigsten Kollagenrezeptors der Thrombozyten, GPVI, beim Fortschreiten der AK weiter zu untersuchen. In der vorliegenden Studie wurde GPVI als direkter Bindungspartner von Aβ40 an der Thrombozytenoberfläche identifiziert. Die Bindung von Aβ40 an GPVI löste die Externalisierung von GPVI an die Oberfläche, die Freisetzung von ATP und die Aggregation der Thrombozyten aus. Darüber hinaus ist GPVI entscheidend an der durch Thrombozyten-vermittelten Bildung von Amyloid-β-Aggregaten *in vitro* beteiligt. So führte die Blockierung oder Deletion von GPVI zu einer deutlichen Reduktion der Aβ-Aggregation *in vitro*. Weitergehend hat sich gezeigt, dass die Stimulation von Thrombozyten mit Aβ40, zum Teil über den GPVI-Rezeptor, die Freisetzung von Fibrinogen auslöst, welches *in vitro* mit Amyloid-β-Aggregaten kolokalisiert. Darüber hinaus wurde in der vorliegenden Studie der Einfluss von Aβ40 auf die durch Thrombozyten ausgelöste Inflammation und die Rekrutierung von Neutrophilen untersucht. Die Stimulation von murinen Thrombozyten mit Aβ40 induzierte die Bildung von Thrombozyten-Neutrophilen-Aggregaten. Die anschließende *in vitro* Analyse humanerund muriner Neutrophilen zeigte eine erhöhte Thrombozyten-vermittelte Adhäsion von Neutrophilen nach Aβ40- und ADP-Stimulation. Jedoch wurde keine Bildung von Neutrophil Extracellular Traps (NETs) unter diesen Bedingungen festgestellt. Im Gegensatz zu Thrombozyten waren Neutrophile nicht wesentlich an der Bildung von Amyloid-β-Aggregaten *in vitro* beteiligt. Die Stimulation von Thrombozyten mit Aβ40 löste eine GPVI-abhängige ROS-Produktion und eine GPVI-abhängige TGF-β1-Freisetzung aus. Darüber hinaus wird in dieser Arbeit erstmals eine altersabhängige Migration von Thrombozyten in das Hirnparenchym von WT*mT/mG;PF4Cre+* und APP23*mT/mG;PF4Cre+* Mäusen beschrieben, die im Hippocampus von APP23*mT/mG;PF4Cre+* Mäusen früher einsetzt. Im Gehirn von gealterten APP23-*mT/mG;PF4Cre+* Mäusen wurden Thrombozyten um die Amyloid-Plaques und in engem Kontakt mit den Mikroglia nachgewiesen.

Zusammenfassend konnte in dieser Arbeit der Kollagenrezeptor GPVI als neuer Bindungspartner von Aβ40 identifiziert werden, der zur Thrombozyten- vermittelten Bildung von Amyloid-β-Aggregaten *in vitro* beiträgt. Erste Untersuchungen dieser Arbeit legen nahe, dass Thrombozyten in Gegenwart von Aβ40 sowie zur Inflammation beitragen könnten. Darüber hinaus wurden Thrombozyten in amyloidreichen Regionen des Gehirnparenchyms von *APP23mT/mG;PF4Cre+* Mäusen nachgewiesen. Diese Arbeit trägt daher zum Verständnis über die Rolle von Thrombozyten in der AK bei und legt nahe, dass eine antithrombotische Therapie für Patienten mit AK von Nutzen sein könnte.

List of Tables

List of Figures

List of Abbreviation

ACID	APP intracellular domain
AD	Alzheimer´s disease
ADP	Adenosine 5′-diphosphate
ApoE	Apolipoprotein E gene
APP	Amyloid precursor protein
ATP	Adenosine triphosphate
Aβ	Amyloid-β
AβOs	Aβ42 oligomers
BACE1; BACE2	APP-cleaving enzyme 1 and 2
BBB	Blood–brain barrier
BLI	Bio-layer interferometry
CAA	Cerebral amyloid angiopathy
CAP37	Cationic antimicrobial protein of 37 kDa
CD40L	CD40 ligand
CD42	Platelet Glycoprotein Ib
CG	Cathepsin G
CNS	Central nervous system
CRP	Collagen releated peptide
CTF-α	C-terminal fragment
Cvx	Convulxin
DAG	1,2-diacylglycerol
DAPI	4′,6-Diamidine-2′-phenylindole dihydrochloride
ELISA	Enzyme-linked immunosorbent assays
EOAD	Early onset Alzheimer’s disease
FAD	Familial AD
FBS	Fetal Bovine Serum
FcRγ	Fc receptor γ-chain
FDA	Food and Drug Administration
FELASA	Federation of European Laboratory Animal Science Association
GP	Glycoprotein
GPCRs	G protein–coupled receptors
GPIb-V-IX	Glycoprotein-Ib-V-IX
GWAS	large-scale Genome-wide association studies
h	Hour
HIV	Human immunodeficiency
HRP	Streptavidin-coupled horseradish-peroxidase
IF	Immunofluorescence
Ig	Immunoglobulin
IgG	Immunoglobulin G
IP3	Inositol 1,4,5-trisphosphate
ITAM	Immunoreceptor tyrosine–based activation motif
LAT	Linker of activated T cells

LOAD	Late onset Alzheimer's disease
LY6G	Lymphocyte antigen 6 complex, locus
Mac-1	Integrin-αMβ2
MCA	Middle cerebral artery
MCAO	Middle cerebral artery occlusion
mG	EGFP cassette
min	Minute
MMPs	Matrix metalloproteinases
MPO	Myeloperoxidase
MRI	Magnetic resonance imaging
mT	tdTomato
Mwm	Morris water maze
NE	Neutrophil elastase
NETs	Neutrophil extracellular traps
NFT	Neurofibrillary tangles
NIA	National institute of Aging
OCS	Open canalicular system
PAR	Protease-activated receptors
PBS	Phosphate-buffered saline
PECAM	Platelet endothelial cell adhesion molecule
PET	Positron emission tomography
PLCγ2	Phospholipase C γ2
PMA	Phorbol myristate acetate
PNA	Platelet-neutrophil aggregates
PSEN1	Presenilin 1
PSEN2	Presenilin 2
PSGL-1	Glycoprotein Ligand-1
ROS	Reactive oxygen species
SPF	Specific pathogen-free
SPR	Surface plasmon resonance
Syk	Splenic tyrosine kinase
TGF-β1	Tumour growth factor β 1
TNF-α	Tumor necrosis factor-α
TP	Thromboxane A2 receptor
TRAP	Thrombin receptor-activating peptide
TxA2	Thromboxane A2
vWF	Willebrand factor
WHO	World Health organization
WT	Wildtype

1 Introduction

1.1 Alzheimer’s disease

1.1.1 Epidemiology and public health impact of Alzheimer´s disease

World Health organization (WHO) estimates around 55 million people living with dementia and nearly 10 million new cases every year worldwide [1]. In Germany approximately 1.6 million people are affected from dementia with an increasing tendency up to 2.4-2.8 million in 2050 [2]. Alzheimer's disease (AD) is a progressive neurodegenerative disease and the leading cause of age-related dementia, accounting for 70-80% of all dementia cases [3].

The U.S. National Institute of Aging [NIA] ranked AD on place 6 of the leading causes of death in the United States. Among citizens age 65 or above it is ranked on place 5 [4]. While deaths from stroke, human immunodeficiency virus (HIV) and heart disease decreased between 2000 and 2018, it is expected that the incidence of people with AD will increase in the next decades [4]. The economic burden of Alzheimer's disease treatment is estimated to be approximately $305 billion in the United States by 2020 and will continue to increase as the population ages [5]. To date, no effective treatment exists that could cure Alzheimer's disease or effectively stop its progression. Numerous Phase 3 clinical trials have failed, making AD one of the biggest world health burdens in the next decades and emphasizing the importance of new therapeutic strategies [6].

1.1.2 Genetic predisposition

AD is a multifactorial disease with genetic and environmental causes [7]. Most of the AD cases could be classified in three subtypes: The smallest subgroup is the autosomal dominant familial AD (FAD) with an average age onset of 46.2 years. FAD only causes less than 1% of all AD cases [8] and requires the patient to have a positive family history for AD and usually implies multiple affected persons in more than one generation [9]. To date, three genes have been associated with FAD: amyloid precursor protein (APP; 1.1.3), Presenilin 1 (PSEN1) and Presenilin 2 (PSEN2) [10]. The other type with an early onset is early onset Alzheimer’s disease (EOAD), which defines affected individuals under the age of 65. This group accounts for about 5% - 6% of the pathologically diagnosed AD cases.

EOAD also includes a large genetic predisposition for example familial mutations or summed polygenic risk [11, 12]. Patients with trisomy 21 for example often develop clinical AD symptoms after the age of 50. Here the triplication of the APP gene on chromosome 21 has been linked to increased brain amyloid levels [13-15].

The most common form of AD is late onset AD (LOAD), defined by those affected at age 65 or above. LOAD is considered as sporadic and to be multifactorial, however the large-scale genome-wide association studies (GWAS) identified more than 30 genes involved in LOAD pathogenesis. These genes not only affect APP and tau but also influence lipid (cholesterol) metabolism, endocytosis and synaptic function as well as immune response and inflammation [15-17]. To date, the most considered genetic risk factor for LOAD is the apolipoprotein E (*ApoE*) gene, which plays a key role in lipid metabolism. The *ApoE* gene is encoded by three genetic different allele variants (ε2, ε3, and ε4) resulting in three ApoE E2/E3/E4 protein isoforms, leading to isoform-specific differences in total serum cholesterol levels [18, 19]. One ε4 allele increases the risk of developing AD up to three times greater than persons with two copies of the ε3 allele [19]. Moreover genetic variation of the *ApoE* gene has also been linked to differential risk factors of cardiovascular diseases like atherosclerosis or hypertension [20]. In addition to genetic risk factors and increasing age studies demonstrated that the risk of developing AD or vascular dementia increases by conditions like heart disease, diabetes, stroke, high blood pressure and high cholesterol [21]. Also lifestyle factors like diet, social activity, education, smoking or alcohol and exercising might influence the risk of developing LOAD [22].

1.1.3 Neuropathology of Alzheimer's disease

In 1906 Alois Alzheimer described a neurodegenerative disorder, giving it the name Alzheimer's disease. He first reported the two neuropathological features, extracellular amyloid-β (Aβ) plaques and intracellular neurofibrillary tangles (NFT) [23]. For a long time, the definitive diagnosis of AD was just possible post mortem by histological staining of these two neuropathological features. But since Magnetic resonance imaging (MRI) and Positron emission tomography (PET) scans become more common, biomarkers of AD are able to detect molecular changes *in vivo* to analyze AD pathologies [24]. Here, patients are categorized based on biomarker evidence of pathology using the so-called ATN classification system: The presence of amyloid-β (A), hyperphosphorylation of Tau (T) and neurodegeneration (N) [25].

Amyloid-β plaques mostly contain Aβ40 and Aβ42 peptides, produced by an abnormal processing of the APP (section 1.1.4) and an imbalance of the production and clearance pathway in the brain.

Many types of nonvascular amyloid deposits have been described, but diffuse plaques and dense core plaques are mostly seen in AD brains [26, 27]. Diffuse plaques contain fine fibrillary Aβ protein, mostly Aβ42 and to a lesser degree Aβ40. They are free of swollen neurites and do not show accumulation of activated microglia and reactive astrocytes in their surroundings [28]. Core plaques contain Aβ42 and additionally more Aβ40. Core plaques have compact dense amyloid structures, implicating more fibrillogenic forms of Aβ [26]. Most of these dense core plaques are associated with activated microglial cells as well as hyperphosphorylated-tau-positive and dystrophic neurites [27, 29].

NFT are aggregates of abnormally phosphorylated tau proteins in neurons. Under physiological condition tau is located mainly in axons of neurons, associated to the microtubule for cytoskeleton stabilization or acting as a cross bridge which enables microtubules to interconnect with other cytoskeletal components such as actin and neuro-filaments [30]. Under pathophysiological conditions an increased tau phosphorylation results in a decreased tau binding to microtubules leading to dissociation. This process produces detached tau proteins which in turn undergo self-aggregation, forming oligomers and tau aggregates, leading to neuronal cell death [31, 32].

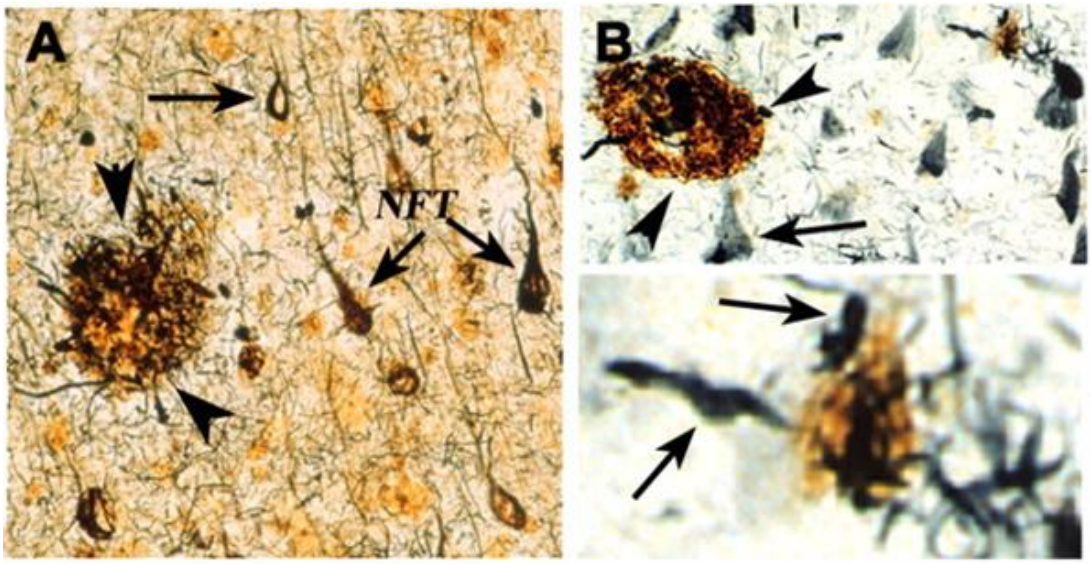

Figure 1: Neuropathological features of Alzheimer's disease.
(A) Extracellular senile plaques, mainly consisting of aggregated Aβ peptides (arrowheads), and intracellular neurofibrillary tangles (NFTs) of hyperphosphorylated tau protein aggregates (arrows) in brain tissue of Alzheimer's disease patients stained by Bielschowski silver staining. (B) Specific antibody staining of paired helical filaments (PHF) of hyperphosphorylated tau protein (arrows), and Aβ-aggregates (arrowheads). Shown are PHF-containing neurites associated with Aβ deposits. Aβ=amyloid-β peptide; NFTs = neurofibrillary tangles; PHF = paired helical filaments (Adopted from Nixon et al., 2007 [33];ISSN: 0021-9533).

1.1.4 Amyloid precursor protein processing in Alzheimer's disease

APP is a ubiquitous expressed transmembrane protein, consisting of a long extracellular N-Terminus and a short intracellular C-Terminus. The transmembrane domain is more hydrophobic. In humans, APP is encoded by a single gene located on chromosome 21, containing 18 exons [34, 35]. Three major isoforms produced by alternative splicing of APP are possible: APP695, APP751 und APP770. While APP695 is predominantly expressed in neurons in the central nervous system (CNS), APP751 and APP770 have been shown to be the predominant isoforms expressed by platelets and many other tissues [36, 37]. To date, various pathogenic APP mutations have been identified (Italian mutation: A713T) which are associated with an early-onset of AD and one APP mutation which is associated with a protective function (Icelandic: A673T) [38]. The physiological function has not been fully elucidated; however, it is suggested that APP may modulate synapse formation and function [39, 40] or act as a cell surface receptor [41].

Once APP is translocated from the endoplasmic reticulum to the cell surface it can be cleaved by two different processing pathways, the amylogenic und non amylogenic, producing biologically active fragments.

During the physiologically predominant non-amylogenic pathway APP is cleaved by the α-secretases within the amyloid-β region. In neurons, the major α-secretase is the metalloprotease ADAM10 (disintegrin and metalloproteinase domain-containing protein 10) [42]. The cleavage produces two peptides: The extracellular soluble APPα (sAPPα) and the C-terminal fragment (CTF-α). sAPPα has been shown to induce the upregulation of neuroprotective signaling pathways. For example, it supports neuronal resistance to acute hypoxia [43] or enhances neuronal resistance to brain injury [44]. CTF-α consists of a transmembrane and intracellular domain. It is cleaved by γ-secretase producing the extracellular P3 fragment and the APP intracellular domain (ACID) [45]. The role of these two peptides are not completely clear but it is supposed that ACID might play a role in regulating synaptic plasticity [40].

As previously reported (section 1.1.3), Aβ is the major component of senile plaques and is formed by proteolysis of APP during the amylogenic pathway. APP is cleaved by a β-secretase, namely APP-cleaving enzyme 1 and 2 (BACE1; BACE2), between Met596 and Asp597, producing a soluble APP N-terminal fragment (sAPPβ) and a C-terminal fragment (CTF-β) [45]. The remaining C-terminal fragment (CTF-β) is cleaved by the γ-secretase. The γ-secretase cleaving side is between the amino acid residues 37 to 43 of the Aβ domain, resulting in the generation of different Aβ proteins [46].

Here, Aβ40 and Aβ42 are the dominant products while other minor cleavage products include Aβ38, Aβ39, and Aβ43 [47].

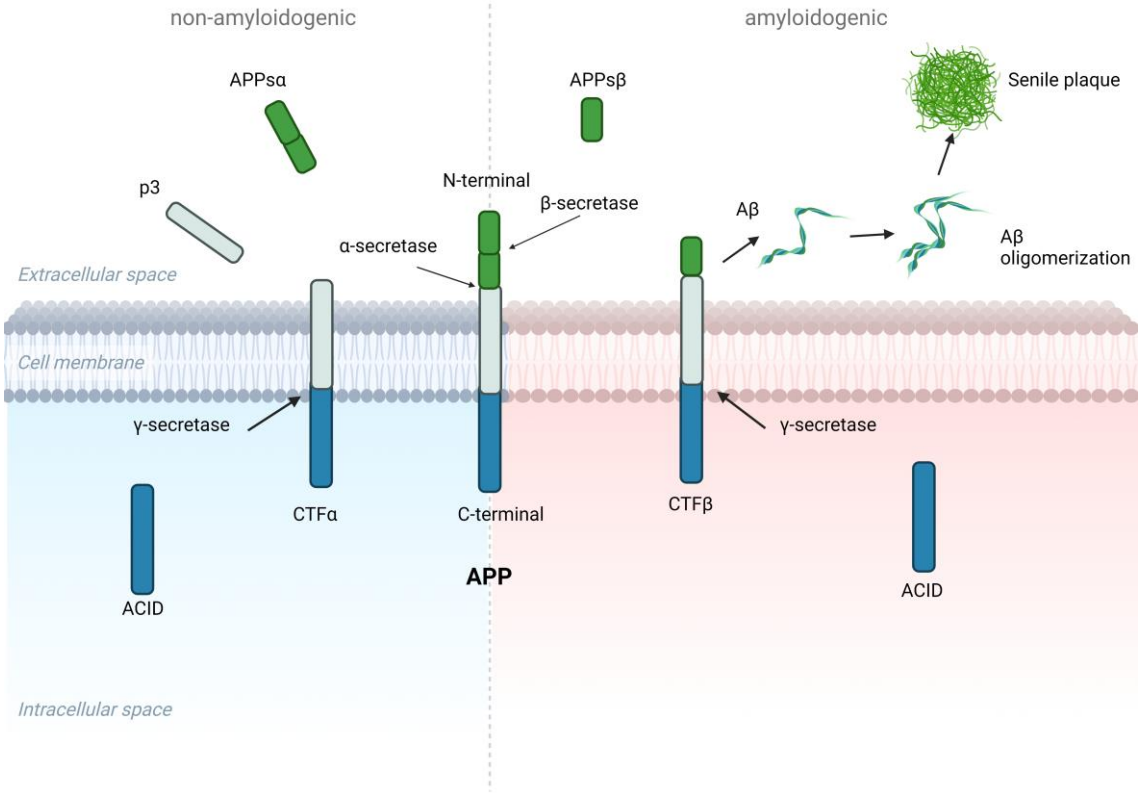

Figure 2: Schematic representation of amyloid precursor protein (APP) processing.
APP processing can occur via the non-amyloidogenic pathway (blue) and the amyloidogenic pathway (red). During the nonamyloidogenic process, APP is cleaved by α- and γ-secretase into APPsα, p3, and ACID. During the amyloidogenic pathway, cleavage occurs by β- and γ-secretase. The cleavage products are APPsβ, AICD, and Aβ. Aβ can then form oligomers and accumulate into amyloid plaques. Aβ (amyloid-β peptide); APP (amyloid precursor protein); sAPP (soluble APP fragment); AICD (intracellular APP domain); CTFα/β (C-terminal fragment α/β). Created with biorender.com (Modified from Spies *et al.* 2012 [48]).

1.1.5 The amyloid hypothesis

Despite many years of research and development of different drugs, the ultimate etiology of AD remains not fully understood and no effective medication is found. There are many descriptive hypotheses regarding the causes of AD, including the tau hypothesis, the inflammatory hypothesis, the cholinergic hypothesis, vascular hypothesis and the oxidative stress hypothesis, but the most common is the amyloid hypothesis [49].

In 1991 the amyloid cascade hypothesis was first described by Selkoe, Hardy and Allsop [50, 51]. They discovered a mutations in *APP* gene and suggested that APP mismetabolism and amyloid-β deposition are the primary events in the disease process. They postulated the pathogenic pathway for the progression of AD as follows: 1.

Altered APP metabolism with increased Aβ production and, in particular, an increased Aβ42/Aβ40 ratio (section 1.1.4); 2. Decreased Aβ clearance and degradation 3. Amyloid deposition; 4. Neuritic plaques and vascular amyloid; 5 Neurofibrillary tangles [50-52]. Subsequently, the amyloid hypothesis has been modified and supplemented by new findings and is now the predominant model of Alzheimer's pathogenesis. Since 2000, it has been suggested that the formation of soluble, ligand-like Aβ42 oligomers (AβO) is also associated with Alzheimer's disease. These AβOs are potent CNS neurotoxins and are regarded as the most toxic and pathogenic form of Aβ [53]. Further, it has been described that AβO can lead to the activation of microglia and astrocytes and thus trigger inflammatory processes such as oxidative stress. Moreover it was shown that, the increase in AβOs cause changes in synaptic function by inhibiting hippocampal long-term potentiation. Last, these events lead to neuronal synapse dysfunction and selective neuron loss with associated neurotransmitter defects [54, 55].

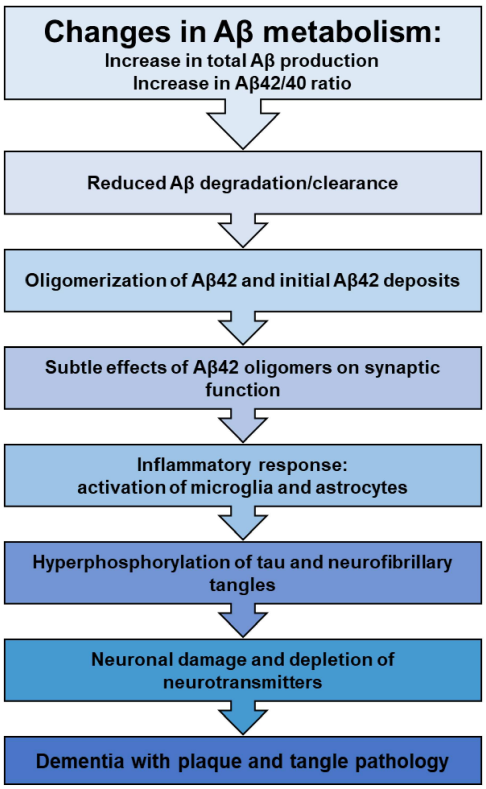

Figure 3: Schematic representation of the amyloid cascade hypothesis.
In this hypothesis, changes in Aβ metabolism, such as the increase in Aβ production, the decrease in Aβ clearance, and the increased ratio of Aβ42 to Aβ40, are considered as the first events in the pathogenesis of AD. Subsequently, the formation of toxic Aβ42 oligomers leads to the activation of microglia and astrocytes and triggers inflammatory processes. Finally, amyloid plaques and neurofibrillary tangles are formed, and neuronal cell loss occurs (Modified from Barage *et al.* 2015 [56]).

1.1.6 The role of inflammation in Alzheimer's disease

Additionally to extracellular amyloid-β plaques and intracellular neurofibrillary tangles, inflammation is another underlying mechanism of AD pathophysiology. Under physiological conditions acute inflammation is a temporary, self-resolving process and essential for the repair process of infection or injury. However, chronic inflammation can be detrimental to brain function. The sustained release of cytotoxic factors and the excessive activation of pro-inflammatory responses are implicated in many neurodegenerative disease, including Alzheimer's disease [57].

Several studies show that AD patients have increased microglial activation in the brain and that some markers of glial activation are elevated even before the development of amyloid deposition [58]. The presence of soluble Aβ is thought to be the primary driver of microglial activation [59]. Activated microglia are able to phagocytose Aβ, however at some point these microglia are no longer able to process Aβ while the capacity for producing pro-inflammatory cytokines is unaffected. This results in an accumulation of Aβ and chronically activated microglia which release many pro inflammatory and toxic products, as reactive oxygen species (ROS), nitric oxide and cytokines which serves to exacerbate neuro-inflammation and contribute to neurodegeneration [60, 61]. Pro-inflammatory cytokines such as TNF-α or IL-1β released from microglia increase Aβ load by upregulating β-secretase and γ-secretase activity, leading to increased Aβ production. Moreover, Aβ can directly stimulate microglial production of TNF-α by activating the transcription factor NFκB [62-65]. These events create a self-repeating cycle in which increased Aβ stress leads to further microglial activation and cytokine production.

Similar to microglia, activated astrocytes are also observed in early stages of AD [66]. Under physiological conditions, astrocytes are important for neurotransmitter secretion and recycling, ion homeostasis, regulation of energy metabolism, synaptic remodeling and modulation of oxidative stress, information processing, and signal transduction [67, 68]. In the presence of amyloid, activated astrocytes begin to degrade Aβ by phagocytosis. However, the constant activation of astrocytes by amyloid manifests itself in an increase in the number, size, and motility of astrocytes. These changes ultimately lead to a disruption of the normal activities, which can then cause cytotoxic damage to neurons [69].

In addition, systemic inflammation can cause changes and compromise the integrity of the blood–brain barrier (BBB), allowing peripheral inflammatory factors to diffuse into the brain. However, the exact mechanisms involved are still unclear and the subject of current research.

Recent studies have shown that cells of the innate immune system contribute to disease development. For example, peripheral macrophages and neutrophils may adhere to cerebral veins, extravagate into the brain parenchyma, and be present in areas of amyloid-β deposition where they exacerbate the effects of sustained inflammation [70-72]. Moreover neutrophils are able to release neutrophil extracellular traps (NETs), consist of chromatin fibers, citrullinated histones, and cytoplasmic enzymes such as myeloperoxidase (MPO) and neutrophil elastase (NE) which could potentially harming the BBB and neural cells [73]. NETs were first described as a first line of defense against infection by tracking and killing bacteria, but in recent years they have also been detected in Alzheimer's patients and in AD mouse models [74]. In addition, Zenaro *et al.* showed that depletion of neutrophils improved cognitive function and reduced the AD pathology in an AD mouse model [70].

1.1.7 Oxidative stress and mitochondria dysfunction in the pathogenesis of Alzheimer’s disease

The occurrence of oxidative stress and mitochondrial dysfunction is strongly associated with the pathogenesis of neurodegenerative diseases [75]. The human brain has a high energy demand and neurons have a limited glycolytic capacity making these cells extremely dependent on mitochondrial energy production [76, 77]. Mitochondria are semi-autonomous organelles and producers of adenosine triphosphate (ATP) by deriving and storing energy through the respiratory chain by oxidative phosphorylation [78]. During this process the unavoidable electron leakage leads to the constant production of superoxide anions. Therefore, mitochondria have an efficient mitochondrial/cellular antioxidant system. Abnormalities in mitochondrial function could lead to less production of ATP but more production of reactive oxygen species (ROS), caused by an imbalance between the generation and detoxification. ROS can act as signaling molecules under carefully controlled conditions, but excess production can cause damage by oxidizing all major biomolecules including nucleic acid (DNA, RNA), proteins, and lipids [79].

To date, mitochondrial dysfunction has been established as an early and prominent feature of AD. Several studies show that neurons of patients suffering from AD or neurons of AD transgenic mouse models exhibit increased ROS generation, resulting in mitochondrial dysfunction [80, 81]. Altered expression of mitochondrial oxidative phosphorylation genes or decreased levels of antioxidant enzymes in patients with AD could cause dysregulation of the mitochondrial respiratory chain, leading to a decrease in ATP production and an increase in ROS [82]. Additionally, in different AD mouse models it were shown, that Aβ can progressively accumulate in neuronal mitochondria.

This event is also associated with reduced oxidative respiration and cell death [83]. In 2004, Aβ was shown to interact with alcohol dehydrogenase in the mitochondria of Alzheimer's patients and transgenic mice, triggering apoptosis and free radical formation in neurons [84]. Thus, increased mitochondrial ROS generation, enhanced oxidative stress and the occurrence of mitochondrial dysfunction, play an essential role in the pathogenesis and progression of AD.

1.1.8 Vascular contribution to Alzheimer's disease: Cerebral amyloid angiopathy

In the last decades many studies suggested that cognitive impairments in the aging brain is also driven by cerebrovascular pathologies [85]. For example Aβ cannot only accumulate in the brain parenchyma, but also within the leptomeninges and small to medium-sized cerebral blood vessels, known as cerebral amyloid angiopathy (CAA) [86]. CAA is increasingly recognized as a major contributor of AD pathogenesis and affects 80% to 95% of all AD patients [87, 88]. The accumulation of amyloid-β could lead to changes in the integrity of the blood-brain barrier, extravasations of plasma proteins, edema formation, release of inflammatory mediators and matrix metalloproteinases (MMPs) which, in turn, produce partial degradation of the basal lamina with the potential to develop hemorrhagic complications [88]. Moreover the Honolulu-Asia Aging Study showed that men with both CAA and AD had greater cognitive impairment than those individuals with either CAA or AD, implicating that CAA may contribute to the clinical presentation of dementia by interacting with other neuronal pathologies [89]. In a mouse model of CAA it was shown that vascular dysfunction reduces perivascular Aβ clearance creating a vicious cycle of vascular and parenchymal Aβ accumulation [90, 91]. Additionally, Aβ can interact with fibrin(ogen), which is inter alia released by platelets and fibrin is the major protein component of blood clots. This interaction leads to increased formation of structurally abnormal Aβ-fibrin clots that are resistant to degradation. Furthermore, fibrin(ogen) is deposited in human and murine CAA-positive vessels and may contribute to vascular occlusion and inflammation [92-94]. Moreover, Cortes-Canteli and colleges showed that fibrin(ogen) is present in areas of dystrophic neurites and that a decrease of fibrinogen levels improves neuronal health and ameliorates amyloid pathology of AD mice [95]. These examples demonstrate the complex interaction between vascular pathologies and AD which could possibly affect neuronal cells and cognition.

1.2 Platelets

1.2.1 Platelet physiology and pathophysiology

Platelets are small (3.6 ± 0.7 µm in diameter), anucleate blood cells which circulate in the bloodstream, numbering of 150.000 – 400.000/µl of blood in healthy individuals and 0.4-1.6 x 10^6/µl in mice [96, 97]. Platelets are derived from megakaryocytes, which are produced in the bone marrow or lung by haematopoiesis [98]. Megakaryocytes are polyploid cells and release 2000-3000 platelets into the bloodstream over their lifespan. After the platelets enter the bloodstream, the pro-platelets are shed into platelets by developing their characteristics, such as high content of α and dense-granules, lysosomes, and the open intracanalicular system. The approximate lifespan of a platelet is ~10 days for human platelets and ~4-5 days for murine platelets [99].Young platelets have a high content of RNA, which decreases during maturation. Therefore, platelets have only a limited capacity for protein synthesis. In the spleen and liver senescent platelets are destroyed by phagocytosis mediated by macrophages [100].

Platelets are originally described as main actors in wound healing and hemostasis through different activation mechanisms (section 1.2.2). Upon vascular injury platelets instantly get activated and form a hemostatic plug in order to prevent massive blood loss. This mechanism requires stringent regulation, as uncontrolled platelet aggregation could lead to vascular occlusion resulting in myocardial infarction and stroke. Without vessel injury, the inhibitory compounds prostacyclin and nitric oxide limit platelets activation and keeps them in a resting (inactivated) state [101]. In the last decades many additional physiological and pathophysiological functions have been reported like angiogenesis, tumor growth, inflammation, and tissue regeneration [102]. In addition, altered platelet activation pathways and dysfunction have recently been described in the context of aging and neurodegenerative diseases, particularly in Alzheimer's disease [103].

1.2.2 Platelet function and signaling in primary hemostasis

There are two main components of hemostasis: Primary and secondary. During the primary hemostasis platelets get activated and an unstable platelet plug is built. During the secondary hemostasis insoluble fibrin is generated by the proteolytic coagulation cascade which forms a mesh that is incorporated into and around the platelet plug resulting in stable thrombus formation [104].

In the event of blood vessel injury, components of the subendothelial extracellular matrix (ECM), such as collagen, laminin or vitronectin are exposed to the blood flow. Consequently the plasma glycoprotein von Willebrand factor (vWF) binds specifically to the exposed collagen type I and III which in turn allows vWF to bind to the platelet glycoprotein-Ib-V-IX (GPIb-V-IX) complex during rapid blood flow. The initial binding cause's platelets to slow down and results in initial platelet activation and adhesion (tethering) to the vessel wall surface. Now the platelet receptor glycoprotein (GP) VI is able to bind to the exposed collagen. These events induce various intracellular signaling pathways: Integrin activation, release of granules, cytoskeletal reorganization and recruitment of more platelets to the site of injury [105].
One essential receptor for stable platelet adhesion and aggregation is the integrin αIIbβ3. Integrin αIIbβ3 is highly expressed in platelets and located at the platelet surface and in α-granules. In resting conditions, integrin αIIbβ3 adopts an inactive conformation. The platelet activation via GPVI induces the externalization of more integrin αIIbβ3 to the platelet surface and the transformation of integrin αIIbβ3 to switch from a low- to high-affinity state for fibrinogen and collagen bound vWF [106]. The ligand binding to integrin αIIbβ3 then promotes outside-in signaling. In detail, one more conformation change results in a trans-phosphorylation of the cytoplasmic tail of the receptor and downstream signaling as well as integrin clustering. This outside-in signaling initiates and amplifies a range of cellular events to drive essential platelet functions such as spreading and fibrin-mediated stabilization as well as platelet aggregation via fibrinogen binding [104].

As mentioned above, the activation of *inter alia* GPVI leads to the release of α- and dense granules. These granules contain platelet agonists which are important for further feedback activation. α-granules contain coagulation factors like vWF, fibrinogen or thrombospondin, but also cytokines like tumour growth factor β 1 (TGF-β1). Moreover, α-granules express the adhesion molecule P-selectin and Integrin- β 3 which are translocated to the plasmamembrane and externalized on the platelet surface during the release [107]. In contrast dense granules store small molecules such as adenosine 5′-diphosphate (ADP), adenosine 5′-triphosphate (ATP), Ca^{2+} and serotonin [108]. Furthermore, platelets immediately generate and release thromboxane A2 (TxA2), converted from arachidonic acid by cyclooxygenase-I [109].
The molecules ADP, TxA2 and thrombin act as secondary mediators to reinforce platelet activation and induce complete platelet activation via stimulation of G protein-coupled receptors. ADP for example activates the two platelets G protein–coupled receptors (GPCRs) $P2Y_1$ and $P2Y_{12}$ [104]. The activation of $P2Y_1$ leads to the activation of phospholipase Cβ and to a subsequent increase in cytosolic calcium [110].

The activation of $P2Y_{12}$ induces the inhibition of adenylyl cyclase and the activation of PI3-kinase. These two events are necessary for platelet activation by ADP, to induce shape change and so stabilizing platelet thrombi *in vivo* [110]. The $P2Y_{12}$ receptor is a target of many clinically effective antithrombotic drugs, like clopidogrel or ticagrelor [111].

TxA2 activates the thromboxane A2 receptor (TP), which is coupled to the G proteins Gq and G12/13. The TP receptor act as a positive feedback loop to promote platelet adhesion, aggregation, degranulation and platelet-induced blood clotting-responses[112].
The transformation of prothrombin to thrombin occurs at the surface of activated platelets [113]. Thrombin is among the most effective activators of platelets and induces the activation of the protease-activated receptors (PAR), PAR1 and PAR4 on human platelets and PAR3 and PAR4 on murine platelets. These receptors link to the G proteins Gq and G12/13 to induce further platelet activation [114].

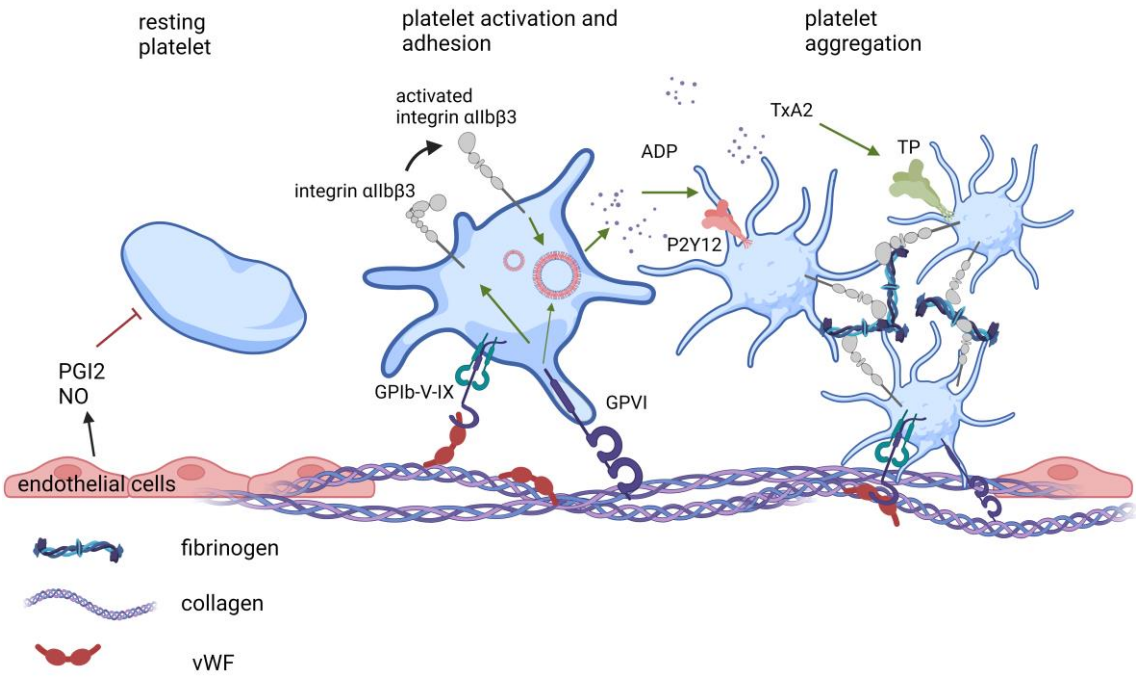

Figure 4: Platelet activation and aggregation during primary hemostasis.
Binding of the GPIb-V-IX complex to the collagen bound vWF and leads to initial platelet adhesion. Binding of the GPIb-V-IX complex to collagen-bound vWF leads to initial platelet adhesion. Binding of GPVI to collagen induces platelet activation through the release of granules and activation of integrin αIIbβ3. Degranulation of α- and dense granules leads to local release of secondary mediators such as ADP and further platelet recruitment. The cross-linking of integrin αIIbβ3 with fibrinogen leads to further platelet aggregation. Created with biorender.com.

1.2.3 The major collagen receptor glycoprotein (GP) VI

The immunoglobulin receptor GPVI was first described in 1989 as the major collagen receptor on the platelet surface with a size of 61-kD [115]. GPVI is selectively expressed on megakaryocytes and platelets. The gene *GP6*, is located at 19q13.4 in the human genome [116]. Today it is known that GPVI binds not only collagen but also a variety of other plasma and vascular proteins, including fibrin, fibrinogen and fibronectin [117-119]. GPVI as a member of the immunoglobulin (Ig)-superfamily of receptors, consists of two Ig domains (D1, D2), an O-glycosylated mucin-like stalk and a cytoplasmic tail containing calmodulin- and Src kinase–binding sites [120]. Intracellular GPVI is associated with the dimeric Fc receptor γ-chain (FcRγ), which has an immunoreceptor tyrosine–based activation motif (ITAM) containing two YxxL sequences.

Collagen is an important physiological ligand that binds to the extracellular D1 domain of GPVI through its recurrent GPO (glycine-proline-hydroxyproline) motif. Collagen binds to dimeric GPVI but not monomeric [121]. To date it is suggested that the dimerization occurs through the D2 domain [122]. The synthetic peptide, known as CRP (collagen-related peptides), mimics the triple-helical structure of collagen by repeating the GPO sequence to trigger platelet activation via GPVI[123].

During GPVI activation, the two Src family kinases, Fyn and Lyn, induce recruitment, docking, and phosphorylation of the SH2 domain of Syk by phosphorylating the two conserved tyrosines in cytosolic ITAM. Syk, in turn, activates an adaptor transmembrane protein, called the linker of activated T cells (LAT). LAT has a long cytosolic tail with 9 tyrosines residues, which get phosphorylated by activation and in turn induces the activation of phospholipase Cγ2 [116, 124]. Downstream of this signaling complex the formation of the secondary messengers like inositol 1,4,5-trisphosphate (IP3) and 1,2-diacylglycerol (DAG) as well as intracellular calcium mobilization occur. These events induce the secretion of intracellular α-granules and dense granules and inside-out activation of platelet integrins, including αIIbβ3, leading to platelet aggregation [116].

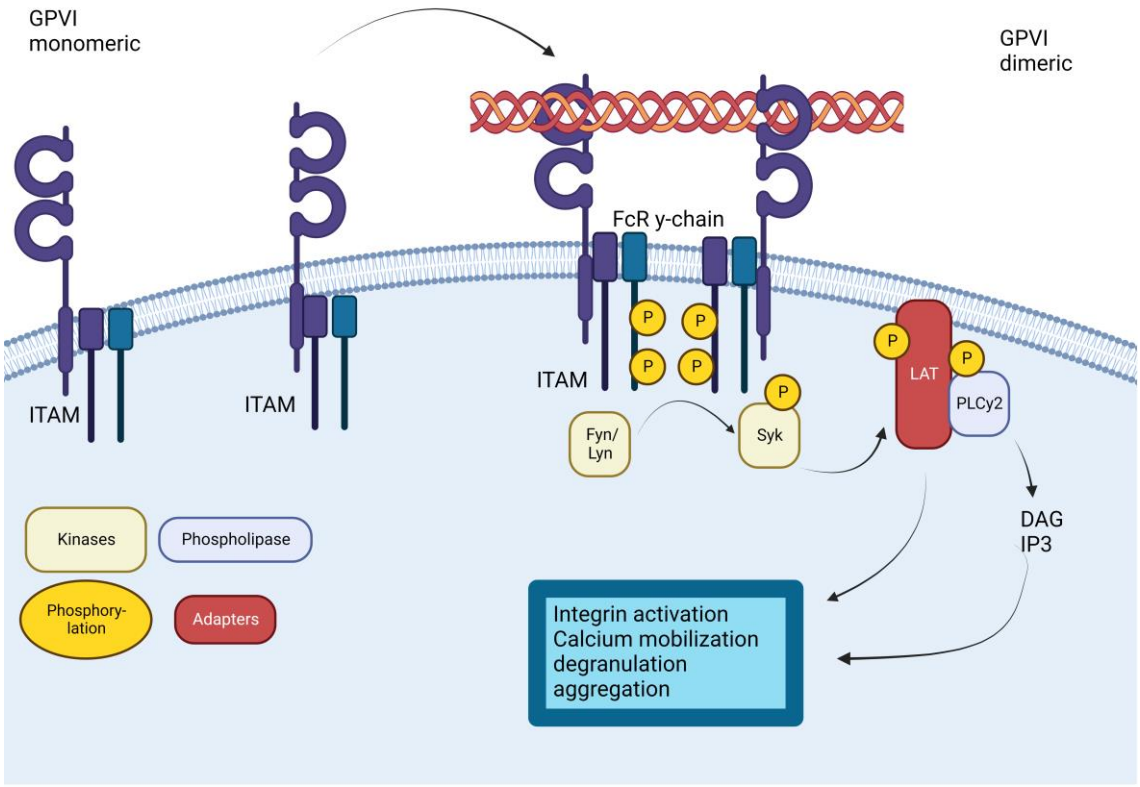

Figure 5: Glycoprotein VI (GPVI) signaling cascade.
GPVI is associated with the Fc receptor γ (FcRγ). Clustering by ligands such as collagen triggers phosphorylation of the FcRγ chain in the ITAM motif by Src family kinases (Fyn/Lyn). These induce recruitment and subsequent activation of splenic tyrosine kinase (Syk). Recruitment of Syk to the ITAM motif initiates a signaling cascade involving numerous kinases, adaptor and effector molecules, including the linker for T cell activation (LAT) and phospholipase C γ2 (PLCγ2), which together with other proteins form the GPVI signalosome. Activation of the GPVI signalosome induces indegrin activation, calcium mobilization, and degranulation, leading to platelet aggregation. Created with biorender.com (Modified from Watson *et al.* 2015 [125]).

1.2.4 Platelets in inflammation

At sites of inflammation, platelets become activated and the release of inflammatory mediators from the granules initiates an inflammatory cascade with the common goal to increase leukocyte recruitment to the endothelium. These mediators include adhesion molecules for example P-selectin or CD40L, fibrinogen as coagulation factor and inflammatory cytokines such as TNF-α, IL-1β, IL-6, IL-8 or TGF-β1. Platelets contribute to about 45 % of TGF-β found in peripheral blood plasma and contain 40 to 100 times more TGF-β than other cells [126, 127]. TGF-β1 acts as a chemoattractant for monocytes, fibroblasts and neutrophils. Sreeramkumar et al. reported that platelets are essential for neutrophil recruitment to sites of inflammation [128]. Especially under increasing shear rates the direct neutrophil adhesion to activated endothelial cells becomes less efficient, making platelets more important. Once activated, platelets are able to form neutrophil-platelet aggregates promoted by the interaction of platelet P-selectin and Glycoprotein Ligand-1 (PSGL-1) on the neutrophil surface [129].

Additionally the release of fibrinogen and the increase expression of the integrin αIIbβ3 receptor on the platelet surface induce a crosslinking with neutrophils. Here, fibrinogen binds to platelet integrin αIIbβ3 receptor and to integrin receptor Mac-1 on neutrophils [130]. Once recruited, neutrophils migrate into the surrounding tissue to carry out their inflammatory functions like phagocytosis, generation of reactive oxygen species or release of NETs [131]. Increased and uncontrolled activation of platelets results in a chronic inflammatory reaction that can induce endothelial cell stress. Endothelial cells in turn could promote more platelet activation and neutrophil recruitment creating a vicious circle that causes increased inflammation [132].

Recent studies have shown that platelet surface GPVI plays a key role in inflammatory and thrombotic pathomechanisms, such as stroke, ischemia-reperfusion or rheumatoid arthritis. Inhibition of GPVI by antibody treatment or with Revacept improves cerebral infarct volume and functional outcome in the MCAO model of stroke. The beneficial effect of GPVI blockade is probably due to a reduction in the inflammatory response, possibly through reduced release of cytokines and attenuation of inflammatory cell recruitment, because inhibition of thrombus formation by αIIbβ3 blockers dramatically increases intracranial hemorrhage and infarct growth without any beneficial effect [133]. Going further, inhibition of platelet GPVI by Revacept has been shown to protect against myocardial injury and reduce the number of leukocytes in reperfused myocardium in a mouse model of ischemia-reperfusion [134] Moreover, in a mouse model of autoimmune rheumatoid arthritis, GPVI was shown to be an important trigger for the formation of pro-inflammatory platelet microparticles in the pathophysiology of arthritis [135]. Interestingly, in humans, increased plasma levels of sGPVI are reported in situations with prothrombotic tendency and during inflammatory processes, such as acute ischemic stroke, thrombotic microangiopathy, or rheumatoid arthritis, suggesting a prominent role of GPVI in thrombotic and inflammatory diseases [136].

1.3 The role of platelets in the progression of Alzheimer's disease

1.3.1 Amyloid precursor protein and Aβ peptides in platelets

The most important function of platelets is to prevent bleeding, but in recent decades it has become increasingly clear that they also play a role in pathological conditions such as AD. Human platelets express high levels of APP and also store *APP* mRNA derived from megakaryocytes [137].

Moreover, platelets express the entire enzymatic machinery for APP metabolism in the form of α-, β-, and γ-secretases and therefore produce metabolites such as sAPPα, sAPPβ, and Aβ. Upon activation by agonists such as thrombin or collagen, platelets are able to release APP and Aβ and thus represent an important peripheral source of circulating APP and Aβ in blood plasma [138].

The physiological role of APP in platelets has not been fully elucidated, but the relatively high concentration of APP in platelets (9300 copies/platelet) suggests a role in events associated with coagulation. Approximately 10 % of APP is expressed as a glycoprotein on the platelet surface where it acts as a receptor for sulfated proteoglycans, laminin, collagen and integrin-like receptors [139]. Recently in our working group it was also shown that platelet APP is an important receptor for Reelin mediating platelet activation by interacting with GPIb and thus has an influence on arterial thrombosis [140]. Moreover APP is cleaved during platelet activation and recent studies implicated an inhibitory effect of soluble APP of the blood coagulation factors IXa, XIa, and Xa [141, 142].

The major Aβ species produced by platelets is Aβ40, and increasing evidence suggests that Aβ40 is capable of inducing platelet activation, adhesion, and aggregation, leading to increased thrombus formation *in vitro* and *in vivo* [103, 143].

In 2014, Gowert et al. showed that treatment of platelets with Aβ40 induced platelet activation in addition to increased ROS formation and stimulated platelet Aβ production. Furthermore, platelets cultured with Aβ40 were able to modulate soluble Aβ40 into fibrillar structures [143]. In 2016, Donner et al demonstrated that monomeric Aβ40 can bind to the integrin-αIIbβ3 receptor on the platelet surface, triggering the release of ADP. ADP, in turn, activates $P2Y_1$ and $P2Y_{12}$ receptors, which further enhances platelet activation and thus increases platelet-induced Aβ aggregation *in vitro*. Furthermore, inhibition of platelet $P2Y_{12}$ receptor with Clopidogrel was shown to reduce platelet-induced Aβ-aggregation *in vitro* [103].

In vivo Gowert *et al.* demonstrated that platelets adhere to vascular amyloid plaques and that sustained platelet recruitment could lead to full occlusion of the vessel in an AD mouse model in cerebral vessels [143]. In addition to binding Aβ40 to integrin-αIIbβ3, fibrinogen can also bind platelet-bound Aβ40, indicating an important role in the occlusion of CAA-affected vessels. More recently Donner *et al.* found that treatment with the platelet activation inhibitor Clopidogrel decreased the CAA burden in an AD mouse model [103]. These findings suggest an important role of platelets in the development of CAA by promoting the formation of Aβ-aggregation.

1.3.2 Platelet alteration in Alzheimer's disease patients and mouse models

Already in 1998 Sevush *et al.* first revealed that platelets of patients with AD exhibit greater unstimulated activation profiles than those of control. Here the number of platelet aggregates, P-selectin expression and leukocyte-platelet complexes were increased [144]. Recently, a one-year follow-up study measured baseline expression of the two platelet activation biomarkers, activated integrin αIIbβ3 and P-selectin, in patients with AD, which correlated positively with the rate of cognitive decline [145]. In 2021 a systematic review and meta-analysis gave evidence that the incidence rate of stroke of all types in patients with AD was higher than in matched controls without AD [146]. Activated platelets act as a catalytic surface for thrombin generation and this leads to thrombus stabilization by an insoluble fibrin plug. As mention above, i*n vitro* and *in vivo* experiments done by Cortes-Canteli and colleagues demonstrated that fibrin clots formed in the presence of Aβ are structurally abnormal and resistant to degradation [147]. Suggesting a mechanism by which the pre-activation state in platelets could be one cause for the increased prevalence of stroke in AD patients. In addition, Johnston *et al* found that platelet β-secretase activity is increased in AD patients, which may lead to increased peripheral Aβ production [148]. Going further, AD patients exhibit a decreased APP 120-130 kDa to 110 kDa ratio, which may be due to increased activity of β-secretase cleavage. This ratio is correlated to the progression of the disease and moreover it is already present in preclinical stages of AD, suggesting that this can be used as a biomarker for AD [149]. As in humans, pre-activated platelets and a pro-thrombotic phenotype were detected in an aged AD mouse model. These mice show increased expression of integrin αIIbβ3 and P-selectin in baseline and after activation with CRP, ADP, or thrombin and increased ATP release on stimulation with CRP, promoting the formation of amyloid-β aggregates *in vitro*. In addition, these mice show accelerated vascular occlusion *in vivo*, indicating an increased risk of arterial thrombosis, which can lead to cardiovascular and cerebrovascular complications, as also observed in Alzheimer's disease patients [150].

Patients in early stages of AD show increased levels of coated platelets. Coated platelets are a subpopulation of cells observed after dual agonist stimulation of platelets with collagen and thrombin. These cells express high levels of several procoagulant proteins including fibrinogen, vWF, phosphatidylserine on their surface and so strongly support prothrombinase activity. Moreover these cells have been shown to potentiate inflammation [151]. As mentioned already inflammatory reaction are a key event in the pathogenesis of AD and platelet activation with consequent degranulation results in secretion of inflammatory mediators like interleukins (IL-1β, IL-7, and IL-8), fibrinogen or CD40 ligand (CD40L).

These mediators could enhance leukocyte adhesion and the release of pro inflammatory cytokines from endothelial cells and trigger CAA related perivascular inflammation [152, 153]. In addition to cytokines, increased ROS levels and decreased cytochrome c oxidase activity in platelet mitochondria have been reported in AD patients. Furthermore, many other platelet changes are observed in AD patients, including alterations in serotonin metabolism, an increase in tau protein, and increased GSK3β activity, which is one of the major tau kinases [154-157].

1.4 Mouse models

1.4.1 The APP23 transgenic mouse as a model for human Alzheimer's disease

Mice are adequate model organisms to investigate genetic and biomedicine questions *in vivo*. The murine genome is between 95 –98% comparably similar to the human genome and since genetically modified mice develop diseases comparable to human diseases, the examination of mouse strains became a more powerful tool for research [158]. Furthermore, the development of AD is a multifactorial neurodegenerative disease in which the initial steps in pathogenesis are often inaccessible in human patients, making it necessary to use model organisms to understand the cause and progression of this disease [159]. The hemizygous APP23 mouse is a widely-used and extensively characterized model of AD. These mice have a 7-fold overexpression of mutant human APP bearing the pathgenic Swedish double mutation K670N/M671L driven by the murine Thy-1 promoter [160]. This mutation is immediately adjacent to the β-secretase cleavage site in *App* gene and results in increased production of total Aβ [161]. The hemizygous APP23 mouse develop an extensive amyloid-β pathology starting at an age of 6-8 months and increase in size and number with age. Congophilic plaques can occupy up to 25% of the neocortex and hippocampus in two-year-old mice and are surrounded by activated microglia, astrocytes, and dystrophic neurites containing hyperphosphorylated tau. This mouse model does not develop neurofibrillary tangles, but neuronal loss in the CA1 region of the hippocampus has been reported [162, 163]. In the Morris water maze, these mice show memory and learning deficits starting at 3 months of age, which increase with age [164, 165]. The APP23 mice also develop a cardiovascular phenotype. At 12 months of age, these mice develop vascular amyloid resembling human CAA. In addition, these mice exhibit cerebral amyloid angiopathy-associated vasculitis and blood vessel ruptures ranging from microbleeds to large hematomas [166].

1.4.2 The ROSA$^{mT/mG}$ PF4-Cre reporter mice

The homozygous ROSA$^{mT/mG}$ Cre reporter mice is a mouse model that can visualize recombinant and non-recombinant cells with a double fluorescent marker system at single cell resolution. These mice exhibit strong red fluorescence in all tissues and cell types by expressing the loxP-flanked tdTomato (mT) cassette with the following stopcodon. When crossed with the megakaryocyte/platelet-specific PF4-Cre mouse, the mT cassette in Cre-expressing tissues (platelets and megakaryocytes) is deleted in the progeny, allowing expression of the membrane-directed EGFP cassette (mG), which is located directly downstream of the mT cassette. In our group, it was shown that in mT/mG; PF4-Cre+ mice, platelets and megakaryocytes can be followed by their specific fluorescence in blood smear, hematopoietic organs and thrombus formation. In addition, the mT/mG; PF4-Cre-positive mice do not exhibit alterations in platelet activation and thrombus formation [167]. For the present study, the mT/mG; PF4-Cre-positive was additionally crossed with the heterozygous APP23 mice, providing a novel phenotypic analysis of platelet localization in an AD mouse model.

1.5 Aim of the study

Despite the most intensive research, there is still no effective therapy that could prevent Alzheimer's disease or effectively attenuates its progression. Numerous clinical trials have failed so far. It is therefore likely that multiple cofactors contribute additively or synergistically to the development of AD, underscoring the importance of new therapeutic strategies. In addition to neuronal changes, processes in the vascular system also contribute to the pathogenesis of AD. In this context, the occurrence of CAA in AD patients, which is characterized by deposits of fibrillary Aβ in cerebral blood vessels, plays an important role in the progression of AD. In recent years, increasing evidence suggests that platelets play an important role in the development of CAA. In our group, platelets have been shown to modulate soluble Aβ40 into fibrils and that Aβ40 can bind to integrin αIIbβ3 resulting in platelet activation and aggregation. Moreover we could show that platelet inhibition with Clopidogrel decreased CAA burden in the APP23 mouse model of AD.

The aim of the present study was to further elucidate the impact of platelets in the pathogenesis of Alzheimer's disease, with the following research topics:

(1) To investigate the influence of Aβ40 on platelets GPVI collagen receptor in terms of amyloid-β fibril formation and platelet activation

(2) Analysis of the influence of Aβ40 on platelet-triggered inflammation and neutrophil recruitment

(3) To analyze the impact of Aβ40 on platelet mitochondrial function and platelet–mediated amyloid-β aggregation in Alzheimer´s disease

(4) Studies on platelet migration into the brain parenchyma in APP23 and WT mice at different ages

2 Material and methods

This section includes only those materials and methods which have not already been described in the publications.

2.1 Material

2.1.1 Experimental animals

For the investigations, mice were either obtained from commercial animal suppliers, generated in the animal facility of the Heinrich Heine University of Düsseldorf (ZETT) backcrossed to C57BL/6 mice (Jackson Laboratory) or provided by J. Ware; University of Arkansas.

Heterozygous APP23 mice and APP noncarrier were used to generate WT and heterozygous APP23 mice. Littermates of APP23 mice were used for used for analyses. Offspring (mT/mG;PF4Cre+) of ROSA mT/mG-Cre mice crossed with PF4Cre+ mice were used to generate the APP23*mT/mG;PF4Cre+;* and the WT*mT/mG;PF4Cre+;* mice by crossing them with heterozygous APP23 mice (1.4.2; Table 1).

All mice had *ad libitum* access to water and a standard chow diet and were kept under standard laboratory specific pathogen-free (SPF) conditions according to the guidelines of FELASA (Federation of European Laboratory Animal Science Association). All animal experiments were conducted according the Declaration of Helsinki and approved by the Ethics Committee of the State Ministry of Agriculture, Nutrition and Forestry State of North Rhine-Westphalia, Germany (reference numbers O 86/12, AZ 84-02.05.40.16.073 AZ 81-02.04.2019.A232 and LANUV AZ 81-02.05.40.21.041).

Table 1: Mouse strains.

Strain	Term	Supplier	Objective
Hemizygous B6.Cg-Tg(Thy1-APP)Somm/J	APP23 WT	The Jackson Laboratory	Breeding Analysis
Mice with targeted deletion of GPVI	*Gp6*$^{-/-}$ WT	provided by J. Ware; University of Arkansas	Breeding Analysis
C57BL/6-Tg(Pf4-icre)Q3Rsko/J	PF4Cre+	The Jackson Laboratory	Breeding
Gt(ROSA)26Sortm4(ACTB-tdTomato,-EGFP)Luo/J	ROSA mT/mG Cre	The Jackson Laboratory	Breeding

PF4-Cre transgenic mice crossbred with ROSA$^{mT/mG}$ Cre	*mT/mG;PF4Cre+ mT/mG;PF4Cre-*	ZETT	Breeding
57BL/6J mice	C57BL/6J	The Jackson Laboratory	Breeding
mT/mG;PF4Cre+ crossbred with APP23	APP23*mT/mG;PF4Cre+;* WT*mT/mG;PF4Cre+;*	ZETT	Breeding Analysis

2.1.2 Ethic vote

The collection of human blood, as well as the experiments, were reviewed and approved by the Ethics Committee of Heinrich Heine University. Volunteers gave informed consent (patient consent) prior to their participation in the study: Permission/Study Number 2018-140-KFogU.

2.1.3 Antibodies

Table 2: Antibodies for flow cytometry.

Antibody	Clone	Cat. number	Company
Human GPVI-PE	HY101	565241	BD BioSciences
Mouse CD42b-APC	Xia.G5	M040-3	Emfret analytics
Mouse CD42b-PE	Xia.G5	M040-2	Emfret analytics
Mouse CD45-APC	30-F11	559864	BD BioSciences
Mouse GPVI-FITC	JAQ1	M011-1	Emfret analytics
Mouse Ly6g-APC	1A8	127614	BioLegend

Table 3: Primary antibodies

Antibody	Term	Cat. number	Company
Anti-NeuN antibody - Neuronal Marker	NeuN	ab104225	abcam
Goat Anti-Mouse IgG Antibody (H+L), Biotinylated, 1.5 mg	IgG	VEC-BA-9200	Biozol
IBA1 Recombinant Rabbit Monoclonal Antibody (JM36-62)	IBA-1	MA5-41239	Invitrogen by Thermo Fisher Scientific
Purified anti-β-Amyloid, 1-16 Antibody	Aβ	803001	Biolegend
Purified Mouse IgG1 κ Isotype Control	IgG-control	554121	BD Biosciences
Purified Rat Anti-Mouse GPIbα (CD42b	GPIb	M42-0	Emfret
Purified Rat Anti-Mouse Ly-6G	Ly6G	551459	BD Biosciences
Purified Rat anti-mouse Platelet endothelial cell adhesion molecule (PECAM1)	CD31	550274	BD Biosciences

Purified Rat IgG2a, κ Isotype Control	IgG-control	553927	BD Biosciences
Rabbit (DA1E) mAb IgG XP® Isotype Control	IgG-control	3900s	Cell Signaling Technology
Recombinant Anti-Myeloperoxidase antibody (human and mouse)	MPO	ab208670	abcam
Recombinant rabbit anti-human GP9 antibody	GPIX	orb167288	biorbyt
Recombinant Rabbit IgG, monoclonal [EPR25A] - Isotype Control	IgG -control	ab172730	abcam
Monoclonal mouse Anti-p-tyrosine clone 4G10	4G10	05-321	Sigmaaldrich

Table 4: Secondary antibodies

Antibody	Cat. number	Company
Alexa Fluor® 488 Goat anti-mouse IgG (minimal x-reactivity) Antibody	A11001	Invitrogen by Thermo Fisher Scientific
Goat anti-Rabbit IgG (H+L) Highly Cross-Adsorbed Secondary Antibody, Alexa Fluor™ Plus 647	A32733	Invitrogen by Thermo Fisher Scientific
Goat anti-Rabbit IgG (H+L) Cross-Adsorbed Secondary Antibody, Alexa Fluor™ 555	A-21428	Invitrogen by Thermo Fisher Scientific
Goat anti-Rabbit IgG (H+L) Cross-Adsorbed Secondary Antibody, Alexa Fluor™ 488	A-11008	Invitrogen by Thermo Fisher Scientific
eBioscience™ Streptavidin eFluor™ 660 Conjugate	50-4317-80	Invitrogen by Thermo Fisher Scientific
Goat anti-Mouse IgG (H+L) Highly Cross-Adsorbed Secondary Antibody, Alexa Fluor™ Plus 660	A21055	Invitrogen by Thermo Fisher Scientific
Goat anti-Rat IgG (H+L) Highly Cross-Adsorbed Secondary Antibody, Alexa Fluor™ Plus 647	A21247	Invitrogen by Thermo Fisher Scientific
Anti-rabbit IgG, HRP-linked Antibody	7074	Cell signaling
Anti-mouse IgG, HRP-linked Antibody	7076	Cell signaling

2.1.4 Enzyme-linked immunosorbent assays kits

Table 5: Enzyme-linked immunosorbent assays kits.

Kit	Catalog No.	Company
Mouse TGF-β Duo Set ELISA	DY1679-05	R&D Systems

Mouse Soluble Glycoprotein VI (SGPVI) ELISA Kit	MBS109240	MyBioSource
Mouse fibrinogen ELISA Kit	MBS721901C	MyBioSource
Mouse Neutrophil Elastade (ELA2)	MELA20	R&D Systems
human Neutrophil Elastease (ELA2)	DY9167-05	R&D Systems
Human Soluble Glycoprotein VI, SGPVI ELISA Kit	MBS9390142	MyBioSource

2.1.5 General devices

Table 6: General devices and equipment

Equipment	Model	Company
Benchtop, pH-Meter	WTW pH526	Xylem Inc.
Bench scale	AE166	Mettler -Toledo
Bench scale	Practum®	Sartorius
Bench scale	Secura®	Sartorius
Centrifuge, cooling	5424-R	Eppendorf
Centrifuge, mini	D-6020	neoLab
Centrifuge, tabletop	5415-C	Eppendorf
Centrifuge, tabletop	2-16	Sigma-Aldrich
Cell culture bottle (250 mL)	658175	Greiner Bio-One™
Laminar flow hood	BSB 3A	Gelaire Flow Laboratories
Magnetic stirrer	RET basic	IKA laboratory technology
Micropipettes	Research plus	Starlab & Eppendorf
Microwave	NN-E201WM	Panasonic
Multichannel pipette	Peqpette	Peqlab
Multipipette	Multipette® plus	Eppendorf
Parafilm	PM-996	Bemis®
Pipettor	Pipetboy acu	Integra Biosciences
Roll mixer	RM5	CAR
Thermo shaker	TS-100C	Biosan
Vortexer	444-0994	VWR
Waterbath 1000W	GFL 1052	GFL

Chemiluminescence imager	Fusion-FX6-EDGE V.070	Vilber Lourmat
Double gel system	PerfectBlue™	Peqlab
Filter paper		Whatman
Horizontal agarose gel	PerfectBlue™ Wide Format Gel System	Peqlab
Microscope, inverse	Axio Observer D1	Zeiss
Microscope- color camera	Axiocam 503 color	Zeiss
Microscope	Axioskop	Zeiss
Microscope- color camera	Axiocam 105 color	Zeiss
Nitrocellulose membrane		GE Healthcare
Semi-Dry blotsystem	PerfectBlue™	Peqlab
Universal power supply	PowerPac™	BioRad Laboratories
Flow cytometer	FACS Calibur	BD BioSciences
Hematology analyzer	KX-21N	Sysmex
Mikrotiter plate reader	GloMax® Multi+	Promega

2.1.6 Chemicals and buffers

Table 7: Chemicals

Chemical	Company
4′,6-diamidino-2-phenylindole (DAPI)	Roche
Acetic acid (CH_3COOH)	Sigma-Aldrich
Acrylamide	Carl ROTH GmbH
Adenosine diphosphate (ADP)	Sigma-Aldrich
Ammonium persulfate (APS 10%)	Sigma-Aldrich
Apyrase	Sigma-Aldrich
Bovine serum albumin	Sigma-Aldrich
Calcium chloride (CaCl)	Sigma-Aldrich
Citric acid ($C_6H_8O_7$)	Sigma-Aldrich
Convulxin (Cvx)	Santa Cruz Biotechnology
Collagen (Horm)	Takeda
Collagen related peptide (CRP)	University of Cambridge, UK
Dithiothreitol (DTT)	Sigma-Aldrich
DMEM (High glucose # 41965062)	Life Technologies
DNaseI recombinant RNAse - free	Roche
EDTA (ethylenediaminetetraacetate)	Sigma-Aldrich
Ethanol 100% (EtOH)	Merck Millipore
Fetal calf serum (FCS)	Life technologies
Glucose	Carl ROTH GmbH

Glycine	Carl ROTH GmbH
Goat serum	Bio & Sell
Heparin-Natrium-25000	Braun
IGEPAL® CA-630	Sigma-Aldrich
Isoflurane	Piramal critical care
L-glutamine	Life technologies
Magnesium chloride (MgCl)	Carl ROTH GmbH
Ethanol 100% (EtOH)	Merck Millipore
Mounting medium #S3023	Dako
Paraformaldehyde 4%	Carl ROTH GmbH
Penicillin/Streptomycin	Life technologies
Phosphate buffered saline (PBS)	Sigma-Aldrich
Ponceau S solution	Sigma-Aldrich
Potassium perrmanganate ($KMnO_4$)	Merck Millipore
Powdered skim milk	Frema Reform
Phorbol myristate acetate (PMA)	Merck Millipore
Precision Plus Protein Dual Color Standards	BioRad Laboratories
Prostaglandin	Merck Millipore
Proteinase-inhibitor (cOmplete Tablets Mini Easy-pack)	Roche
Protein blocking solution #X0909	Dako
Sodium chloride (NaCl)	Sigma-Aldrich
Sodium orthovanadate (Na_3VO_4)	Sigma-Aldrich
Sodium nitroprussid (SNP)	Merck Millipore
Sodium phosphate dibasic (Na_2HPO_4)	Carl ROTH GmbH
Sodium dihydrogenphosphate(NaH_2PO_4)	Carl ROTH GmbH
Sodium acid (NaN_3)	Carl ROTH GmbH
Sodium hydrogencarbonate ($NaHCO_3$)	Merck Millipore
Tetramethylethylenediamine (TEMED)	Carl ROTH GmbH
Thrombin 20U	Roche
Tumor necrosis factor (TNF-α)	Peprotech
Trisodium citrate	Carl ROTH GmbH
Triton™ X-100	Sigma-Aldrich
Trizma®-base	Sigma-Aldrich
Trizma®-HCl	Sigma-Aldrich
Trypsin-EDTA	Life technologies
Tween20	Merck Millipore
0.9% NaCl solution	Fresenius Kabi

Table 8: Buffer and solutions

Buffer/Solution	Recipe
Blot buffer A	36.3 g Trizma-base 200 mL MeOH 800 mL ddH_2O pH 10.4

Blot buffer B	3.03 g Trizma-Base 200 mL MeOH 800 mL ddH_2O pH 10.4
Blot buffer C	5.2 g ε-aminocaproic acid 200 mL MeOH 800 mL ddH_2O
Heparin-solution (20 U/mL)	40 µL heparin natrium 5000 I.E 10 ml PBS
Human Tyrode's buffer	137 mM NaCl 12 mM $NaHCO_3$ 2.8 mM KCl 0.4 mM NaH_2PO_4 5.5 mM glucose pH 7.4
Laemmli (6x)	0.93 g DTT 1 g SDS 7 mL 4x stacking gel buffer 3 mL glycerine 0.02% bromphenol blue
Lysis buffer (human) (5x stock solution)	145 mM NaCl, 20 mM Tris-HCl, 5 mM EDTA, 0.5% sodium deoxycholat, 1% Triton™ X-100 1x Proteaseinhibitor cOmplete plus Roche
Lysis buffer (murine) (5x stock solution)	5 x IP-Puffer (2mL) 5% IGPAL 5 mM Na_3VO_4 1x Proteaseinhibitor cOmplete plus Roche
Murine Tyrode’s buffer	134 mM NaCl 12 mM $NaHCO_3$ 2.9 mM KCl 0.34 mM Na_2HPO_4 20 mM HEPES 10 mM $MgCl_2$ 5 mM glucose 0.2 mM $CaCl_2$ pH 7.35
SDS-PAGE running gel buffer (4x stock solution)	91 g Trizma-Base 400 mL dH_2O pH 8.8 *ad* 500 mL ddH_2O
SDS-PAGE stacking gel buffer (4x stock solution)	6.05 g Trizma-base 80 mL dH_2O pH 6.8

	ad 100 mL ddH_2O 0.4 g SDS
SDS-PAGE-running buffer (5x stock solution)	15.1 g Trizma-base 72 g glycine 5 g SDS *ad* 1 L ddH_2O pH 8.3
TBS-T	100 mL 5x TBS-Puffer 500 µL Tween 400 mL ddH_2O
Tris buffered saline (TBS, 5x stock solution)	15.8 g Trizma-HCl 45 g NaCl *ad* 1 L ddH_2O pH 7.6

2.1.7 Software

Table 9: Software

Software	Company
Microsoft Office 360	Microsoft Corporation
FlowJo Single Cell Analysis v10	FlowJo LLC
ViiA™ 7 Software	Thermo Fisher Scientific
ZEN 2012 (blue)	Zeiss
Biorender	BioRender.com
QuPath 0.4.1 i	Open Software for Bioimage Analysis
Graph Pad Prism 8.0.2	GraphPad Software
Endnote X8	Clarivate

2.2. Methods

2.2.1 Cell biological methods

2.2.1.1 Murine platelet lysate and releasates preparation

For Lysates platelets (50×10^6 cells) from whole blood taken from WT or *GP6*$^{-/-}$ mice were isolated as described by Donner; Toska *et al.* 2020 [3.1; 168] and stimulated with CRP [5 µg/mL] or Aβ40 [20 µM] in Tyrode's buffer (Table 8) for 30 or 120 s at 37 °C and 250 rpm respectively. Platelet activation was stopped by addition of the lysis buffer. Lysis was performed on ice for 30 min. Subsequently, the cell lysates were centrifuged at 10,000x g for 10 minutes at 4°C and the supernatant was collected. For Western blot analyses Laemmli buffer (Table 8) was added.

For releasates platelets (30×10^6 cells) from whole blood taken from WT or *GP6*$^{-/-}$ mice were isolated as described by Donner; Toska *et al.* 2020 [3.1; 168] and stimulated with CRP [5 µg/mL], Aβ40 [10 µM], Aβ16 [10 µM] and Thrombin [0.1 U/ml] in Tyrode's buffer (Table 8) for 10 min at 37 °C and 250 rpm respectively. Platelet activation was stopped by centrifugation at 2800x g, and the supernatant was collected. The supernatant was centrifuged at 13,000x g and stored at -80 °C until analysis by ELISA.

2.2.1.2 Murine neutrophil preparation

Neutrophils were isolated from mouse bone marrow cells. WT mice were sacrificed by cervical dislocation and muscles from the femur and tibia were removed. The bones were placed in a Petri dish containing ice-cold RPMI 1640 1X supplemented with 10% Fetal Bovine Serum (FBS) and 1% Penicillin/streptomycin. The following steps were performed under sterile conditions in a cell culture hood. The epiphyses were cut off from the bones and the bone marrow was flush onto a 50 ml screw top Falcon tube fitted with a 100 µm filter using a 25-gauge needle and a 12 cc syringe filled with RPMI 1640 1X (supplemented with 10% FBS and 2 mM EDTA). The cell suspension was centrifuged at 200 x g for 7 min at 4 °C. The red blood cells were lysed by resuspending the cell pellet in 20 ml of 0.2% NaCl for approximately 20 sec followed by addition of 20 ml of 1.6% NaCl. The cell suspension was centrifuged at 200 x g for 7 min at 4 °C to collect the remaining cells. Cells were washed with RPMI 1640 1X supplemented with 10% FBS and 2 mM EDTA at 200 x g for 7 min at 4 °C. Afterwards bone marrow cells were resuspended in 1 ml of ice-cold sterile PBS. For Density Gradient Centrifugation 3 ml of Histopaque 1119 (density, 1.119 g/ml) was added in a 15-ml conical tube and overlaid with 3 ml of Histopaque 1077 (density, 1.077 g/ml). Afterwards the bone marrow cell suspension was added on the top of the Histopaque 1077. For neutrophil isolation the gradient solution was centrifuged for 30 min at 450 x g at 25 °C without brake. The neutrophils were collected at the interface of the Histopaque 1119 and Histopaque 1077 layers. Two wash steps with RPMI 1640 1X supplemented with 1% Penicillin/streptomycin were performed and the cell count was determined by a hematology analyzer (Sysmex - KX21N, Norderstedt, Germany).

2.2.1.3 Human neutrophil preparation

Fresh EDTA-anticoagulated blood was obtained from healthy volunteers (Ages from 18-50 years). Participants provided their written informed consent to participate in this study according to the Ethic Committee and the Declaration of Helsinki (study number 2018-140-KFogU). In each case, 3 ml of the EDTA-anticoagulated blood was layered on 5 ml of Histopaque 1119 (density, 1.119 g/ml) and centrifuged at 800 g for 20 min at 25 °C without brake.

Granulocytes were collected from interphase, washed with phosphate-buffered saline (PBS), and centrifuged at 450 xg for 8 minutes. To lyse the remaining erythrocytes, 2 ml of ammonium chloride buffer was added to the tube and incubated for 8 minutes. The ammonium chloride buffer was washed out by replenishing with PBS and centrifuged at 450 x g for 8 min. Another washing step with PBS followed. The pellet was resuspended in RPMI 1640 1X supplemented with 1% Penicillin/streptomycin. The cell count was determined by a hematology analyzer (Sysmex - KX21N, Norderstedt, Germany).

2.2.1.4 Co-culture of murine platelets and neutrophils

Platelets (5×10^6 cells) from whole blood taken from WT or *GP6*$^{-/-}$ mice were isolated as described by Donner; Toska et al. 2020 [3.1. 168] and co-incubated with isolated WT neutrophils (180,000 cells) (2.2.1.1) in RPMI 1640 1X (10% FBS and 1% Penicillin/streptomycin) for either 3 h or 16 h at 37 °C in a humidified atmosphere with 5% CO_2. . For inhibition of integrin αIIbβ3 platelets were pre-incubated with the antibody Leo.H4 (3 µg per 1 Mio cells; Emfret; cat.number: M021-1) for 15-30 min at RT. Cells were seeded in a cell culture dish with a glass coverslip bottom. When indicated, platelets were activated with platelet agonist. Neutrophils without platelets stimulated with indicated agonists served as negative controls, TNFα [100 ng/mL] served as a positive control for neutrophil adhesion. After 3 h of incubation the non-adherent remaining cells in the cell culture dish were washed with PBS and the adherent cells were fixed with 4% PFA for 15 min at RT. Afterwards cells were stained with immunofluorescence (Method 2.2.3.1) and adherent neutrophils were counted using quantitative pathology (DAPI positive cells) and bioimage analysis program QuPath (developed at the University of Edinburgh).

For analysis of NET formation, the supernatants of the 16-hour co-culture were transferred to reaction tubes. The non-adherent remaining cells in the cell culture dish were washed with PBS. Supernatants were centrifuged at 10000x g for 10 minutes and assayed for neutrophil elastase by ELISA (2.2.2.1). The adherent cells were fixed with 4% PFA for 15 min at RT. Afterwards cells were stained with immunofluorescence. NETs were visualized by MPO and DAPI staining. NET formation was quantified microscopically by calculating the percentage of NET formation (extracellular DNA) relative to the total number of neutrophils per field of view.

To analyze the amyloid-β aggregate formation in co-culture, the supernatants of the 16-hour co-culture were transferred to reaction tubes. Remaining soluble Aβ was analyzed via SDS-PAGE and Western blotting described in method 2.2.2.3. The remaining cells in cell culture dish were washed with PBS and fixed with 4% PFA for 15 min at RT. Afterwards cells were stained with immunofluorescence against Amyloid-β and GPIb.

2.2.1.5 Co-culture of human platelets and neutrophils

Platelets from whole blood taken from healthy volunteers were isolated as described by Donner; Toska et al. 2020 [168]. 2.5×10^6 platelets were co-incubated with 60,000 Neutrophils (2.2.1.2) in RPMI 1640 1X medium in a cell culture dish with a glass coverslip bottom. The incubation time was 3 h at 37 °C in a humidified atmosphere with 5% CO_2. When indicated, platelets were activated with platelet agonist. Neutrophils without platelets stimulated with indicated agonists served as negative controls, phorbol myristate acetate (PMA) [100 nM] served as a positive control. After co-incubation the remaining cells in cell culture dish were washed with PBS and fixed with 4% PFA for 15 min at RT. Afterwards cells were stained with Immunofluorescence against MPO, DAPI and GPIX. Adherent neutrophils were counted using quantitative Pathology (DAPI positive) and bioimage analysis program QuPath (developed at the University of Edinburgh).

For analysis of NET formation, the supernatants were transferred to new reaction tubes after 3 hours of co-incubation and centrifuged at 10000x g for 10 minutes. Subsequently, the supernatants were analyzed for neutrophil elastase by ELISA (2.2.2.1). The adherent cells were fixed with 4% PFA for 15 min at RT. Afterwards cells were stained with immunofluorescence. NETs were visualized by MPO and DAPI staining. NET formation was quantified microscopically by calculating the percentage of NET formation (extracellular DNA) relative to the total number of neutrophils per field of view.

2.2.1.6 Flow cytometry

Measurements of the GPVI surface expression in human or murine whole blood were performed using a FACSCalibur flow cytometer (BD Biosciences). Data was analyzed using CELLQuest Analysis v10 Software (BD Biosciences). Platelets were gated by SSC vs FSC, the gate was previously established using a platelets specific antibodies for GPIb. Human whole blood was diluted 1:10 in Tyrode's buffer. Heparinized murine blood was washed three times with 500 µL Tyrode's buffer at 650 x g and washed samples were diluted in Tyrode´s buffer supplemented with 1 mM $CaCl_2$. Human and murine samples were incubated for 15 min or 1 h with the indicated agonist and labeled with a specific fluorophore-conjugated GPVI antibody in a ratio of 1:10 and with for 15 min at 37 °C. Reaction was stopped using 400 µL PBS and samples were analyzed.

To measure platelet-neutrophil aggregates murine whole blood were washed three times with 500 µL Tyrode's buffer at 650 x g and resuspended in 100 µl Tyrode´s buffer supplemented with 1 mM $CaCl_2$. Washed whole blood was then stimulated with indicated agonist or kept under resting conditions.

Platelets were labeled with fluorophore-conjugated antibodies for CD42b (Table 2; ratio 1:10) and neutrophils were labeled with fluorophore-conjugated antibodies for Ly6g-APC (Table 2 ratio 1:30). After 15 minutes of incubation, the reaction was stopped with 400 µl of PBS. Samples were measured and the percentage of GPIb/Ly6G-positive cells was analyzed. Measurements were performed using a BD FACSCalibur flow cytometer. Data was analyzed using CELLQuest Analysis v10 Software (BD Biosciences).

To analyze the auto fluorescent of the different blood cell types washed whole blood was incubated with APC-labeled rat anti-mouse (CD45 BD, Heidelberg, Germany, final concentration 20 µg/mL) or APC-labeled rat anti-mouse CD42b (GPIb-APC; ratio 1:10) and a Fc Block antibody (BD Biosciences, ratio1:200). Auto fluorescent was analyzed using the PE and the GFP channel. Platelets were gated by SSC vs FSC, the gate was previously established using a platelets specific antibodies for CD42b. Measurements were performed using a BD FACSymphony™ A1 Cell Analyzer. For analyzing and processing of the flow cytometry data, FlowJO Single Cell Analysis v10 Software was used (BD Biosciences).

2.2.2 Protein biochemical methods

2.2.2.1 Plasma preparation for Enzyme-linked immunosorbent assays

Mouse whole blood of APP23 and WT mice were collected in an EDTA anticoagulant-treated tube by retrobulbar venous plexus puncture under Isoflurane anesthesia. After blood collection, samples were centrifuged for 10 min at 850 x g at 4 °C to sediment all cellular blood components. Plasma was then transferred to new reaction tubes and stored at -80 °C for further analysis.

2.2.2.2 Enzyme-linked immunosorbent assays (ELISA)

To measure soluble substances for example cytokines in mouse plasma (Method 2.2.2.1), cell culture supernatants (Method 2.2.1.3) and platelet releasates (described in Donner; Toska et al. 2020 [168]) the different ELISA kits (Table 5) were used according to the manufacturer's instructions. Prior to ELISA analysis, cell culture supernatants and platelet releasates were centrifuged at 10000 x g for 5 minutes, and the supernatant was transferred to a new reaction tube. The ELISA uses monoclonal antibodies immobilized to a special well plate directed against distinct epitopes of the protein. The protein antigen of the sample specifically binds to the immobilized primary antibody. A second biotin-coupled antibody specifically binds to the antigen of the sample forming an antibody-antigen-antibody complex (= sandwich). By adding a streptavidin-coupled horseradish-peroxidase (HRP) substrate an enzymatic color reaction occurs.

The reaction was stopped by adding 2N sulfuric acid (H_2S0_4). The concentration was determined photometrically with a GloMax microplate reader (Promega) at 450 nm.

2.2.2.3 SDS-PAGE and semi-dry Western blotting

To analyze protein abundance in cell culture supernatants or platelet lysates the SDS-PAGE and Western blotting was used. SDS-PAGE is a method to separate molecules due to their molecular weight in an electric field. The separation takes place in a poly-acrylamide gel. The gel consists of a stacking and a separating part (Table 8). The SDS binds to the hydrophobic residues of the proteins whereby the proteins receive a negative charge proportionally to their sizes. In an electric field the small proteins move faster through the pores of the poly-acrylamide gel than the bigger ones. Laemmli sample buffer with SDS and dithiothreitol (DTT; Table 7) was added to the cell culture supernatants or lysates for protein linearization. For denaturation the samples were boiled for 5 min at 95°C before being loaded onto the SDS gel. Protein samples were separated by electrophoresis for 2 h at 25 mA per gel using running gel buffer (Table 8).

The semi-dry Western blot is a transfer system that allows transfer of proteins from gels to nitrocellulose membranes. Therefore, Whatman filter papers, gels and nitrocellulose membranes were equilibrated and the blotting chamber was constructed as follows: Cathode: six Whatman filter papers in buffer C, nitrocellulose membrane in buffer B, polyacrylamide gel and six Whatman filter papers in buffer A, anode. Transfer was performed in semi-dry transfer buffer for 1 h at 75 mA per gel. After transfer, the membrane was blocked with 5 % skimmed milk powder (SMP) or 5 % BSA dissolved in TBS-Tween (Table 7), in order to reduce Non-specific bindings. Target proteins (Aβ; pTyrosine or β-actin) were coupled to epitope-specific primary antibodies and subsequently with IgG-binding peroxidase-coupled secondary antibodies (Table 4). Unbound antibodies were removed by recurring washing steps with TBS-Tween buffer. For detection, *Western Lightning ECL Pro Kit* or *ECL Ultra Kit* (Perkin Elmer; Waltham, USA) was used. The signal results from the secondary antibody coupled with peroxidase, which oxidates the ECL substrate. Quantification of the bands intensity were performed (Optical density, OD) using the Bio 1d FUSION-FX7 software (Version 18.02; Vilber Lourmat). For platelets lysates relative protein amounts were normalized loading controls (β-actin) of each gel.

2.2.3 Immunofluorescence staining

2.2.3.1 Immunofluorescence (IF) staining from cell culture

Cell culture slides were washed with PBS to remove non-adherent cells. Cells were fixed by adding 4 % PFA for 15 min at RT. For staining the cell culture slides were washed twice with PBS. Slides were blocked and permeabilized with 5% protein blocking solution (#X0909, Dako) and 0.3% Triton X100 (Sigma) for 1 hour at RT. Target proteins (MPO, GPIb, GPIX, Aβ or Ly6G) were coupled to epitope-specific primary antibodies and corresponding IgG controls (Table 3 and 6) and subsequently incubated with the corresponding fluorophore (Alexa488; Alexa555; Alexa647 or Alexa660)-coupled secondary antibodies (Table 4) in 1% blocking solution. Nuclei were stained with 4′, 6-Diamidino-2-phenylindole dihydrochloride (DAPI, #10236276001, Sigmaaldrich, 1:3000). Pictures were taken with the microscope AX10 Observer.D1 HAL100 (Zeiss; 200 x magnification for quantification and 1000 x magnification for representative zoom pictures) and adherent neutrophils were counted using quantitative Pathology (DAPI positive cells) and the bioimage analysis program QuPath (developed at the University of Edinburgh).

2.2.3.2 Blood smear

Whole blood from mice was collected in an EDTA anticoagulant-treated tube by puncture of the retrobulbar arterial venous plexus under isoflurane anesthesia. A drop of blood was placed on a slide. A spreader slide was used to disperse the blood as a monolayer. Blood fixation was performed with methanol for 10 minutes. Nuclei were stained with 4′,6-Diamidine-2′-phenylindole dihydrochloride (DAPI, #10236276001, Roche, 1:3000). Slides were carefully rinsed with PBS before embedding the tissue sections with mounting medium (#S3023, Dako) and stored at 4°C in the dark before further use. Images were taken with the inverted phase contrast fluorescence microscope Zeiss AxioObserver.D1 (400 x magnification, Carl Zeiss, Oberkochem, Germany).

2.2.3.3 Immunofluorescence staining from mouse brain

All mice were sacrificed after anesthesia with ketamine [100 mg/kg] and xylazine [10 mg/kg] by opened the thorax and an incision was made in the right atrium followed by directly purging of 4 ml cold NaCl solution and afterwards 4 ml of cold 4 % PFA solution through the left ventricle of the heart. Brain were directly dissected and stored in 4 % PFA overnight. The next day the brain was stored in 30 % sucrose for two days. Brains were frozen by adding -40° cold isopentane. For longtime store the tissues were stored at -80°. In brains of APP23*mT/mG;PF4Cre+* and WT*mT/mG;PF4Cre+* mice endothelial cells, neuronal nuclei, immunoglobulins or amyloid-β were visualized using IF(Table 10

and 6). The frozen brains were cut in 14 µm large sections using a Cryostat-microtom (Leica CM1950; Leica Biosystems). The tissue sections were transferred onto a 37 °C heating plate for drying. For staining the sections were fixed with ice cold acetone for 10 min and afterwards washed with PBS. Sections were blocked and permeabilized with 5% protein blocking solution (#X0909, Dako) and 0.3% Triton X100 (Sigma) for 1-2 hours at RT, then washed three times with PBS. Target proteins were coupled to epitope-specific primary antibodies and corresponding IgG controls and subsequently incubated with IgG-binding fluorophore (Alexa660 or Alexa647)-coupled secondary antibodies in 1% blocking solution. All secondary antibodies were provided from ThermoFischer (Table 4). Unbound antibodies were removed by recurring washing steps with PBS. Nuclei were stained with 4′,6-Diamidine-2′-phenylindole dihydrochloride (DAPI, #10236276001, Sigmaaldrich, 1:3000). Slides were carefully rinsed with PBS before embedding the tissue sections with mounting medium (#S3023, Dako) and stored at 4°C in the dark before further use. Immunofluorescence images were acquired with the Zeiss LSM780 confocal microscope system or the Zeiss AxioObserv-er.D1 inverted phase-contrast fluorescence microscope (Carl Zeiss, Oberkochem, Germany).

Table 10: Antibodies and conditions used for immunofluorescence staining.

Protein	Name	Supplier	Dilution/ time	Secondary antibody/ dilution/ time
platelet endothelial cell adhesion molecule (PECAM1)	CD31	BD Biosciences	1:75 2 hours at RT	Goat anti-Rat IgG Alexa Fluor 647 1:100 1 hour at RT
Purified anti-β-Amyloid (6E10)	Aβ	Biolegend	1:200 o/n at 4 °C	Goat anti-Mouse IgG Alexa Fluor™ 660 1:250 1 hour at RT
Neuronal nuclear protein	NeuN	Abcam	1:1000 o/n at 4 °C	Goat anti-Rat IgG Alexa Fluor 647 1:250 1 hour at RT
Lymphocyte antigen 6 complex, locus (1A8)	Ly6G	BioLegend	1:75 o/n at 4 °C	Goat anti-Rat IgG Alexa Fluor 647 1:250 1 hour at RT
Anti-Myeloperoxidase	MPO	Abcam	1:100 o/n at 4 °C	Goat anti-Rabbit IgG Alexa Fluor 488 1:250 1 hour at RT
Platelet Glycoprotein Ib (CD42b)	GPIb	Emfret	1:50 o/n at 4 °C	Goat anti-Rat IgG Alexa Fluor 555 1:250 1 hour at RT
Platelet Glycoprotein 9	GPIX	biorbyt	1:50 o/n at 4 °C	Goat anti-Rabbit IgG Alexa Fluor 555 1:250 1 hour at RT

Goat Anti-Mouse IgG Antibody (H+L), Biotinylated	IgG	Vector	1:150 o/n at 4 °C	Streptavidin-660 1:50 1 hour at RT
Ionized calcium-binding adapter molecule 1	IBA1	Invitrogen	1:100 o/n at 4 °C	Goat anti-Rabbit IgG Alexa Fluor 647 1:250 1 hour at RT
Rat IgG2bK isotype control	CD31-IgG	BD Biosciences	1:75 2 hours at RT	Goat anti-Rat IgG Alexa Fluor 647 1:100 1 hour at RT
Mouse IgG1, κ isotype control	Aβ-IgG	Biolegend	1:200 o/n 4 °	Goat anti-Mouse IgG Alexa Fluor™ 660 1:250 1 hour at RT
Rat IgG2a isotype control	NeuN-IgG	Abcam	1:1000 o/n 4	Goat anti-Rat IgG Alexa Fluor 647 1:250 1 hour at RT
Rat IgG1 isotype control	GPIb-IgG	Emfret	1:50 o/n at 4 °C	Goat anti-Rat IgG Alexa Fluor 555 1:250 1 hour at RT
Rabbit IgG1 isotype control	MPO-IgG	Abcam	1:100 o/n at 4 °C	Goat anti-Rabbit IgG Alexa Fluor 488 1:250 1 hour at RT

2.2.3.4 Quantification of Immunofluorescence

For Quantification of the genetically expressed GFP signal of the mT/mG; PF4-Cre positive mice the MFI value was measured in similar regions of the brain with the same exposure time. 100 x magnification was used for quantification and the fluorescence of platelets using a 488 nm laser was evaluated. For the immunoglobulin G the Cy5 signal using a 640 nm laser was measured in similar regions of the brain with the same exposure time. The microscope AX10 Observer.D1 HAL100 (Zeiss) was used and the evaluation was carried out via the program Zen2.6 lite blue.

2.2.4 Software

BIO-1D 15.08b, GraphPadPrims 8, Zen Software, Biorender.com, QuPath (which was developed at the University of Edinburgh), and Microsoft Office 365 were used to analyze and graph the data in this paper and to create the figures.

3. Results

3.1. The collagen receptor glycoprotein VI promotes platelet- mediated aggregation of β-amyloid

Lili Donner[1]*, Laura Mara Toska[1]*, Irena Krüger[1], Sandra Gröniger[1], Ruben Barroso[2], Alice Burleigh[2], Diego Mezzano[3], Susanne Pfeiler[4], Malte Kelm[4], Norbert Gerdes[4], Steve P Watson[2;5], Yi Sun[2;5], Margitta Elvers[1] [168]

[1]Department of Vascular and Endovascular Surgery, Heinrich-Heine University Medical Center, Moorenstrasse 5, 40225 Düsseldorf, Germany.

[2]Institute of Cardiovascular Sciences, IBR Building, College of Medical and Dental Sciences, University of Birmingham, Birmingham B15 2TT, UK.

[3]Department of Hematology and Oncology, School of Medicine, Pontificia Universidad Católica de Chile, Santiago 8330034, Chile.

[4]Division of Cardiology, Pulmonology and Vascular Medicine, Medical Faculty, Heinrich-Heine University, Moorenstrasse 5, 40225 Düsseldorf, Germany.

[5]Centre of Membrane Proteins and Receptors (COMPARE), Universities of Birmingham and Nottingham, The Midlands B12 2TT, UK.

[6]Department of Vascular and Endovascular Surgery, Heinrich-Heine University Medical Center, Moorenstrasse 5, 40225 Düsseldorf, Germany. margitta.elvers@med.uni-duesseldorf.de.

* These authors contributed equally to this work

Published in: Science Signaling in 2020

Impact Factor: 9.517 (2021)

License number for republishing (ISSN): 1937-9145

Own contribution to publication: Western blots 4G10; ATP release in humans and mice; platelet aggregation in humans (except patient data); platelet cell culture for amyloid-β aggregate formation in humans with losartan and WT and *Gp6*$^{-/-}$ mice; pull-down assay; flow cytometric analysis; Western blots of fibrinogen release; platelet cell culture staining of fibrinogen in WT and *Gp6*$^{-/-}$ mice; writing material and methods; writing figure legends, statistical analysis, and contributing to figure design.

SCIENCE SIGNALING | RESEARCH ARTICLE

PHYSIOLOGY

The collagen receptor glycoprotein VI promotes platelet-mediated aggregation of β-amyloid

Lili Donner[1*], Laura Mara Toska[1*], Irena Krüger[1], Sandra Gröniger[1], Ruben Barroso[2], Alice Burleigh[2], Diego Mezzano[3], Susanne Pfeiler[4], Malte Kelm[4], Norbert Gerdes[4], Steve P. Watson[2,5], Yi Sun[2,5], Margitta Elvers[1†]

Cerebral amyloid angiopathy (CAA) and β-amyloid (Aβ) deposition in the brain parenchyma are hallmarks of Alzheimer's disease (AD). We previously reported that platelets contribute to Aβ aggregation in cerebral vessels by secreting the factor clusterin upon binding of Aβ40 to the fibrinogen receptor integrin $\alpha_{IIb}\beta_3$. Here, we investigated the contribution of the collagen receptor GPVI (glycoprotein VI) in platelet-induced amyloid aggregation. Using platelets isolated from GPVI–wild type and GPVI-deficient human donors and mice, we found that Aβ40 bound to GPVI, which induced the release of ATP and fibrinogen, resulting in platelet aggregation. Binding of Aβ40 to integrin $\alpha_{IIb}\beta_3$, fibrinogen, and GPVI collectively contributed to the formation of amyloid clusters at the platelet surface. Consequently, blockade of $\alpha_{IIb}\beta_3$ or genetic loss of GPVI reduced amyloid fibril formation in cultured platelets and decreased the adhesion of Aβ-activated platelets to injured carotid arteries in mice. Application of losartan to inhibit collagen binding to GPVI resulted in decreased Aβ40-stimulated platelet activation, factor secretion, and platelet aggregation. Furthermore, the application of GPVI- or integrin-blocking antibodies reduced the formation of platelet-associated amyloid aggregates. Our findings indicate that Aβ40 promotes platelet-mediated amyloid aggregation by binding to both GPVI and integrin $\alpha_{IIb}\beta_3$. Blocking these pathways may therapeutically reduce amyloid plaque formation in cerebral vessels and the brain parenchyma of patients.

INTRODUCTION

In 2015, there were more than 47 million people living with dementia worldwide. With increasing age and the lack of effective therapeutic strategies, this number is projected to rapidly increase, reaching 135 million people by 2050 (*1*, *2*). Alzheimer's disease (AD) is the most frequent cause of dementia, accounting for 60% of dementia cases (*3*). The pathological hallmarks of AD are elevated misfolding; oligomerization and aggregation of β-amyloid (Aβ) peptides in brain parenchyma and in the cerebral vessels, known as cerebral amyloid angiopathy (CAA); and accumulation of intracellular neurofibrillary tangles in neurons (*4*, *5*). The consequences are neurodegeneration with synaptic and neuronal loss, leading to brain atrophy (*6*, *7*).

Several studies indicate that vascular damage and dysfunction, including reduction of cerebral blood flow (CBF), CAA, and blood-brain barrier (BBB) disturbances, contribute to the onset and progression of AD (*8*). Vascular risk factors such as atherosclerosis, stroke, hypertension, and diabetes lead to vascular damage and are associated with AD. However, whether the processes in the vasculature initiate the pathologic process of Aβ aggregation is still uncertain. Identifying the mechanisms underlying vascular pathophysiology that contribute to neurodegeneration in AD will help identify novel therapeutic targets.

Besides the role of platelets in thrombus formation during hemostasis, it is becoming clear that platelets play a crucial role in a number of other processes within the vasculature such as angiogenesis, inflammation, and cancer (*9*–*11*). Moreover, alterations in platelet function are also observed in diverse neurological diseases such as Parkinson's disease, schizophrenia, autism, and AD (*12*–*15*). A higher baseline expression of platelet activation biomarkers was measured in patients with AD (*16*), and the analysis of the Alzheimer mouse model APP23 showed that these mice have a pro-thrombotic phenotype (*17*, *18*). Moreover, APP23 mice develop CAA and exhibit platelet accumulation at vascular plaques, leading to the reduction of CBF and probably to occlusion of cerebral vessels (*18*). The ability of platelets to modulate soluble, synthetic Aβ40 into fibrillar Aβ in vitro indicates a direct impact of platelets in the aggregation property of Aβ40 peptides (*18*–*20*). Previously, we demonstrated that platelets contribute to Aβ aggregation through the binding of Aβ40 to the fibrinogen receptor integrin $\alpha_{IIb}\beta_3$, leading to outside-in signaling in platelets (*19*, *20*), and we found that the inhibition of integrin $\alpha_{IIb}\beta_3$ on the surface of platelets prevents the aggregation of Aβ40 in cultured cells (*19*). An important indication of the involvement of platelets in Aβ aggregation in vivo was evident through the treatment of APP23 mice with the antiplatelet agent clopidogrel, a $P2Y_{12}$ antagonist. Clopidogrel reduced the incidence of CAA with less adherent platelets at vascular Aβ deposits in transgenic AD mice (*19*). Here, we investigated the involvement of other receptors on the surface of platelets and uncovered a critical role for the collagen receptor glycoprotein VI (GPVI) in platelet-mediated aggregation of Aβ.

RESULTS

Phosphorylation of tyrosine residues in LAT and other proteins by GPVI and integrin $\alpha_{IIb}\beta_3$ in response to Aβ40 stimulation

Binding of collagen to GPVI leads to a series of downstream signals in platelets, resulting in phosphorylation and activation of various signaling proteins, including the adaptor protein LAT (linker of activated

[1]Department of Vascular and Endovascular Surgery, Heinrich-Heine University Medical Center, Moorenstrasse 5, 40225 Düsseldorf, Germany. [2]Institute of Cardiovascular Sciences, IBR Building, College of Medical and Dental Sciences, University of Birmingham, Birmingham B15 2TT, UK. [3]Department of Hematology and Oncology, School of Medicine, Pontificia Universidad Católica de Chile, Santiago 8330034, Chile. [4]Division of Cardiology, Pulmonology and Vascular Medicine, Medical Faculty, Heinrich-Heine University, Moorenstrasse 5, 40225 Düsseldorf, Germany. [5]Centre of Membrane Proteins and Receptors (COMPARE), Universities of Birmingham and Nottingham, The Midlands B12 2TT, UK.
*These authors contributed equally to this work.
†Corresponding author. Email: margitta.elvers@med.uni-duesseldorf.de

T cells) (*21*). The stimulation of human platelets with soluble Aβ40 induced a similar pattern of tyrosine phosphorylation compared to the stimulation of platelets with collagen-related peptide (CRP) as shown by Western blot analysis (Fig. 1A). Aβ40 also induced the phosphorylation of LAT (Fig. 1B) and in a time-dependent manner, with a maximum abundance detected at 90 s of incubation (fig. S1). Previously, we demonstrated that binding of Aβ40 to integrin $\alpha_{IIb}\beta_3$ induces integrin outside-in signaling. To exclude this effect, we performed studies in the presence of the human blocking integrin $\alpha_{IIb}\beta_3$ antibody abciximab. Blocking of integrin $\alpha_{IIb}\beta_3$ decreased the phosphorylation of tyrosine (Fig. 1A) and LAT (Fig. 1B) induced by Aβ40. In addition, we used platelets from patients who lack the GPVI receptor. Human GPVI-deficient platelets did not show phosphorylation of LAT, neither after stimulation with collagen nor by Aβ40 stimulation (Fig. 1C). However, Aβ40-induced phosphorylation of LAT was higher than upon activation with low concentration of collagen. Moreover, we studied the effect of Aβ40 in mouse platelets deficient in GPVI. Compared to wild-type (WT) platelets, GPVI-deficient platelets failed to induce phosphorylation of LAT both upon CRP and Aβ40 activation (Fig. 1D). These results indicate the ability of Aβ40 to activate GPVI in human and mouse platelets.

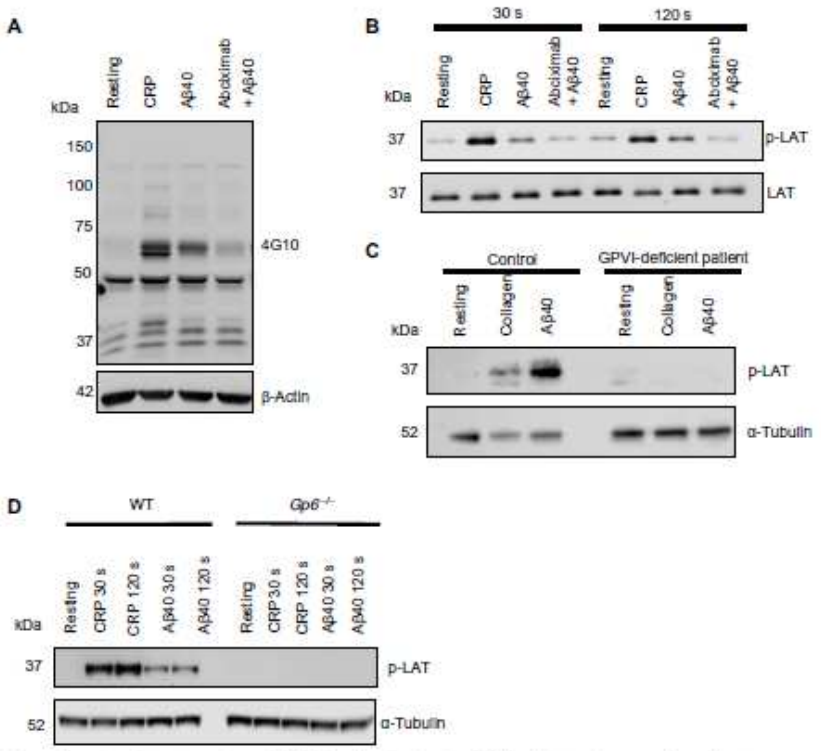

Fig. 1. Aβ40 stimulates tyrosine and LAT phosphorylation in a GPVI- and integrin $\alpha_{IIb}\beta_3$–dependent manner. (**A**) Western blotting for tyrosine phosphorylation (antibody 4G10) in isolated human platelets at rest or upon stimulation with collagen-related peptide (CRP; 5 μg/ml) or Aβ40 (20 μM) for 120 s. In lane 4, as indicated, cultures were pretreated with the integrin $\alpha_{IIb}\beta_3$ antibody abciximab (0.5 μg per 1 Mio cell) for 15 min at room temperature. β-Actin served as loading control; $n = 5$ donors. (**B**) Western blotting for LAT phosphorylation in human platelets treated as described in (A) for 30 or 120 s. Total LAT served as loading control; $n = 5$ donors. (**C**) Western blotting for LAT phosphorylation in platelets isolated from a control donor and a GPVI-deficient patient; cells were unperturbed (resting) or stimulated with collagen (1 μg/ml) or Aβ40 (30 μM). α-Tubulin served as loading control; $n = 2$ GPVI-deficient patients and $n = 2$ healthy controls. (**D**) Western blotting for LAT phosphorylation in isolated *Gp6*$^{-/-}$ and WT platelets stimulated with CRP (5 μg/ml) or Aβ40 (20 μM) for 30 or 120 s. α-Tubulin served as loading control; $n = 6$ to 7 mice per group.

Reduced ATP release of GPVI-deficient platelets in response to Aβ40

Activation of GPVI through collagen induces platelet activation, leading to secretion of granules, inside-out signaling of integrin $\alpha_{IIb}\beta_3$, and platelet aggregation (*22*). To study the consequence of GPVI activation through Aβ40, we measured the release of adenosine 5′-triphosphate (ATP) upon Aβ40 stimulation in human platelets. Previous studies showed that losartan inhibits collagen-induced platelet aggregation through GPVI (*23*, *24*). Therefore, we analyzed the effects of losartan treatment on Aβ40-induced platelet stimulation. Aβ40 induced the release of ATP; however, the amount of ATP was lower compared to CRP stimulation of platelets (Fig. 2, A and B). To test whether Aβ40-induced ATP release is altered by losartan, platelets were preincubated with losartan. The release of ATP was reduced by losartan after stimulation of platelets with either CRP or Aβ40 (Fig. 2, A and B). WT and GPVI-knockout mice were analyzed to confirm that Aβ40 induces a release of ATP via GPVI. The release of ATP in response to CRP or Aβ40 was significantly reduced using GPVI-deficient platelets compared to WT controls. Blocking of integrin $\alpha_{IIb}\beta_3$ using the Leo.H4 antibody in WT platelets resulted in significantly reduced ATP release as well (Fig. 2C). Thus, Aβ40-induced release of ATP is mediated by GPVI and integrin $\alpha_{IIb}\beta_3$. Therefore, blocking of integrin $\alpha_{IIb}\beta_3$ in WT platelets reduced ATP release to resting levels (Fig. 2C).

Strongly reduced aggregation of GPVI-deficient platelets in response to Aβ40

Next, we analyzed platelet aggregation after Aβ40 stimulation. Aβ40-induced platelet aggregation was comparable to that induced by CRP (Fig. 3A). In addition, we analyzed the effect of losartan on Aβ40-induced platelet aggregation (Fig. 3, A and B). In agreement with reported data, losartan significantly inhibited CRP- and Aβ40-induced platelet aggregation (Fig. 3, A and B). To confirm the role of GPVI in Aβ40-induced platelet aggregation, we used platelets from patients with GPVI deficiency. As expected, these platelets showed no platelet aggregation in response to Aβ40 compared to platelets from healthy controls (Fig. 3, C and D). Moreover, we analyzed platelets from WT and GPVI-deficient mice. The aggregation response of WT

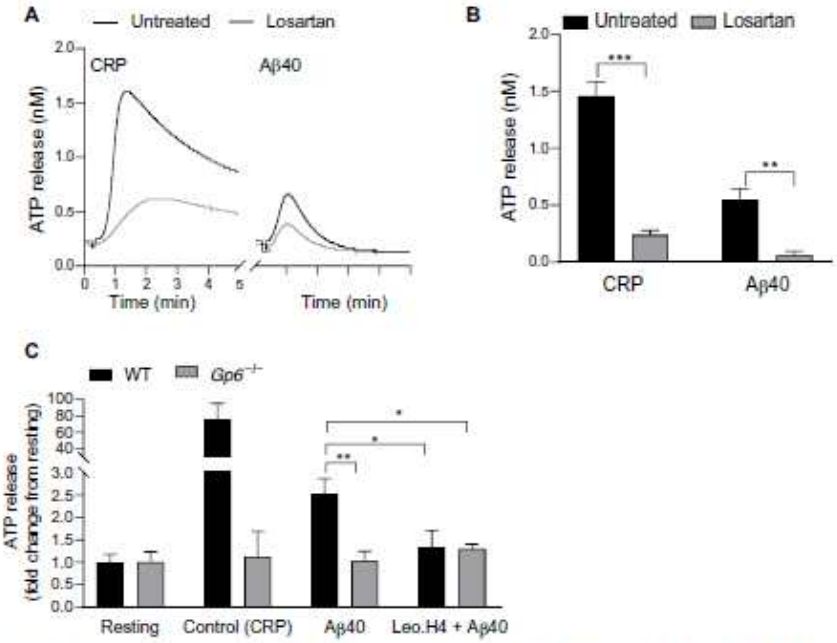

Fig. 2. Reduced ATP release of GPVI-deficient platelets in response to Aβ40. (**A** and **B**) Representative ATP release curves (A) and analysis (B) in human platelets pretreated (gray traces) with losartan (100 μM) for 20 min and then stimulated with CRP (5 μg/ml) or Aβ40 (20 μM). Data are means ± SEM from $n = 5$ donors; two-way ANOVA with Bonferroni's multiple comparison post hoc test: $^{**}P \leq 0.01$ and $^{***}P \leq 0.001$. (**C**) ATP release in WT and *Gp6*$^{-/-}$ platelets at rest, treated with CRP (5 μg/ml), Aβ40 (10 μM), or Aβ40 pretreated with the integrin $\alpha_{IIb}\beta_3$-blocking antibody Leo.H4 for 20 min. Data are means ± SEM from six to seven mice per group; CRP-stimulated platelets served as controls; two-way ANOVA with Bonferroni's multiple comparison post hoc test: $^{*}P < 0.05$ and $^{**}P < 0.01$.

mouse platelets with Aβ40 was comparable to CRP-induced platelet aggregation (Fig. 3, E and F). As expected, GPVI-deficient mouse platelets showed no aggregation upon CRP stimulation. Platelet aggregation upon Aβ40 stimulation was reduced in GPVI-deficient platelets compared to WT platelets (Fig. 3F). In contrast to CRP stimulation, we still measured a slight platelet aggregation of GPVI-deficient platelets in response to Aβ40, suggesting that Aβ40 can induce platelet aggregation without GPVI. These results demonstrated that the activation of GPVI by Aβ40 binding induced platelet aggregation.

Decreased amyloid aggregate formation by GPVI inhibition or genetic deletion in vitro

In our previous study, we showed that platelets are able to modulate soluble Aβ40 to fibrillar Aβ aggregates, whereas blocking of integrin $\alpha_{IIb}\beta_3$ on the surface of platelets prevents Aβ aggregate formation (*19*). To investigate a role of GPVI in platelet-mediated Aβ aggregate formation, we pretreated human platelets with losartan and incubated with soluble, synthetic Aβ40 for 3 days. The formation of fibrillar Aβ aggregates was analyzed by Congo red staining. Although Aβ40-induced platelet aggregation and ATP release were reduced in the presence of losartan, we did not observe alterations in Aβ aggregation in platelet cell culture (Fig. 4A). Neither daily addition nor different concentrations of losartan were able to reduce fibrillar Aβ aggregate formation (fig. S2, A to C).

Because losartan is not a specific GPVI inhibitor, mouse platelet experiments were performed where GPVI was blocked by antibody treatment with JAQ1. In addition, the antibody Leo.H4 was used to block integrin $\alpha_{IIb}\beta_3$ to confirm the essential role of integrin $\alpha_{IIb}\beta_3$ in Aβ aggregate formation. The formation of Aβ aggregates was completely inhibited by blocking of integrin $\alpha_{IIb}\beta_3$ and strongly reduced by blocking of GPVI (Fig. 4B). The inhibitory effect of GPVI blockage in platelet cell culture was dose dependent (fig. S3A). The quantification of remaining soluble Aβ40 in the supernatants of platelet cell culture by Western blot analysis showed significantly increased amounts of Aβ40 when GPVI was blocked compared to untreated platelets, consistent with reduced Aβ aggregate formation (Fig. 4, C and D). To confirm these results, we used platelets from GPVI-deficient mice for cell culture experiments. Cultures of platelets from GPVI-knockout mice displayed markedly reduced Aβ aggregate formation (Fig. 4E). In the supernatants of GPVI-deficient platelets, we measured significantly increased amounts of soluble Aβ40 compared to those from WT platelets (Fig. 4, F and G). The additional blocking of integrin $\alpha_{IIb}\beta_3$ by the antibody Leo.H4 led to increasing amounts of soluble Aβ40 in the supernatant compared to GPVI deficiency alone and to complete inhibition of Aβ aggregates in cell culture (Fig. 4, E to G).

Direct binding of Aβ40 to GPVI

To elucidate the mechanisms by which Aβ40 peptides induce GPVI activation, we investigated the interaction between GPVI and Aβ40. First, we used the microarray AVEXIS (avidity-based extracellular interaction screen) screening assay (*25*). No binding with a control protein (CD200R-BLH) but direct binding of pentameric GPVI to Aβ40 peptides was observed (Fig. 5, A and B). In a second approach, we confirmed the interaction of both proteins by the use of immobilized magnetic beads coated with recombinant GPVI and incubated with soluble Aβ40. After pulldown, the association was visualized by Western blotting using antibodies to GPVI and Aβ (Fig. 4C). When Aβ40 was passed through GPVI-bound beads, a large amount of Aβ was detected along with GPVI. To verify the interaction between GPVI on platelets and Aβ40 in vitro, we incubated murine platelets with Aβ40 peptides and immunoprecipitated GPVI with the antibody JAQ1. Western blot analysis demonstrated that Aβ peptides were coimmunoprecipitated with GPVI (Fig. 4D). To show the relevance of GPVI for Aβ binding to platelets, platelets from GPVI-deficient and WT mice were incubated with Aβ40 peptides. Using flow cytometry, binding of Aβ40 to platelets was detected by fluorescein isothiocyanate (FITC)–labeled Aβ antibody (Fig. 4E). Binding of Aβ to GPVI-deficient platelets was significantly reduced compared to

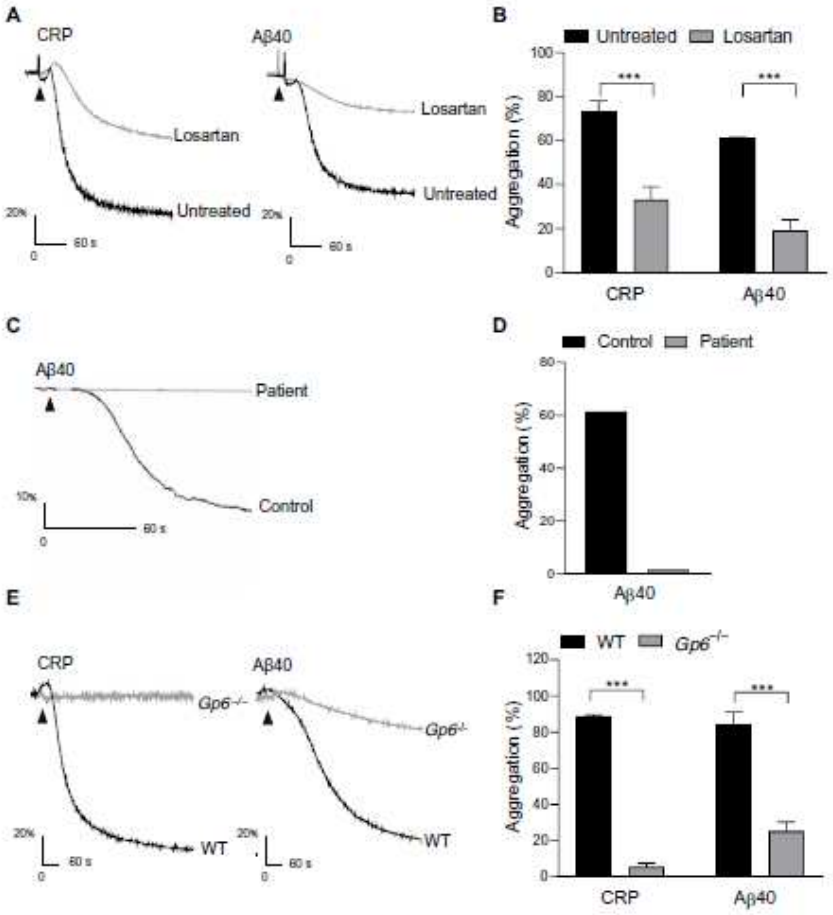

Fig. 3. Reduced aggregation of GPVI-deficient platelets in response to Aβ40. (**A** and **B**) Representative aggregation curves (A) and the quantified maximum aggregation of platelets treated with CRP (5 μg/ml) or Aβ40 (20 μM) in the presence or absence of losartan (100 μM pretreatment for 20 min). Data are means ± SEM from $n = 3$ to 4 donors; two-way ANOVA with Bonferroni's multiple comparison post hoc test: ***$P < 0.001$. (**C** and **D**) As described in (A) and (B) in control donor and GPVI-deficient patient platelets stimulated with Aβ40 (30 μM). Data are means and range from two GPVI-deficient patients and two healthy controls. (**E**) As described in (A) and (B) in platelets isolated from WT and *Gp6*$^{-/-}$ mice and treated with CRP (5 μg/ml) or Aβ40 (10 μM). Data are means ± SEM from $n = 5$ mice per group; two-way ANOVA with Bonferroni's multiple comparison post hoc test: ***$P < 0.001$.

WT platelets. In addition, binding of Aβ to platelets was increased upon stimulation with both CRP and soluble Aβ40 and significantly reduced by integrin $\alpha_{IIb}\beta_3$ blocking in WT platelets. This might be due to an increased number of integrins at the platelet surface after CRP stimulation that allows augmented Aβ40 binding to integrin $\alpha_{IIb}\beta_3$.

Release of fibrinogen through Aβ-induced GPVI activation and colocalization of fibrinogen with Aβ aggregates

The most abundant of platelet secretory granules are α-granules, which contain about 300 proteins, including von Willebrand factor, integrin $\alpha_{IIb}\beta_3$, and fibrinogen (*26*). The release of the α-granule content is important for all platelet functions, including hemostasis, inflammation, and angiogenesis (*27*). In a previously reported study, we showed that monomeric and oligomeric Aβ40 bound to fibrinogen and concluded that fibrinogen bridges Aβ/integrin $\alpha_{IIb}\beta_3$ complexes of platelets and contributes to the occlusion of cerebral vessels in APP23 mice, an AD model (*19*). Thus, we analyzed the release of fibrinogen from platelet α-granules upon Aβ40 stimulation. The release of fibrinogen from platelets in response to Aβ40 was increased and inhibited by losartan, comparable to blocking of integrin $\alpha_{IIb}\beta_3$ (Fig. 6A). In the presence of GPVI-blocking (JAQ1) or $\alpha_{IIb}\beta_3$ integrin–blocking (Leo.H4) antibodies, the release of fibrinogen was strongly reduced in response to Aβ40 (Fig. 6B). To characterize the impact of released fibrinogen on the formation of Aβ aggregates, we incubated murine platelets with Aβ40 for 3 days and analyzed fibrinogen and Aβ localization by immunofluorescence staining, which revealed that fibrinogen and Aβ aggregates colocalized (Fig. 6C). We also observed colocalization of Aβ aggregates and fibrinogen in cultures of human platelets (fig. S4A). Blocking of active factor X with the selective inhibitor arixtra did not alter binding of fibrinogen or amyloid fibril aggregate formation, suggesting that the conversion of fibrinogen to fibrin did not play a role in platelet-mediated amyloid fibril aggregate formation (fig. S5). The inhibition of GPVI on platelets not only led to reduced aggregation of Aβ but also to less accumulation of fibrinogen in cell culture (Fig. 6C, middle). In addition, the inhibition of integrin $\alpha_{IIb}\beta_3$ by blocking antibodies prevented the formation of Aβ aggregates and the accumulation of fibrinogen in cell culture (Fig. 6C, bottom). To confirm the impact of GPVI on the release of fibrinogen upon Aβ40 stimulation of platelets, we used platelets from WT and GPVI-deficient mice. Western blot analysis revealed that GPVI-deficient platelets did not release fibrinogen neither upon stimulation with Aβ40 nor in response to the GPVI agonist CRP (Fig. 6D). Reduced formation of Aβ aggregates was accompanied by reduced fibrinogen in cell culture using GPVI-deficient platelets compared to WT controls (Fig. 6E). Together, these results suggested that Aβ40 induced the release of fibrinogen from platelets via GPVI and the released fibrinogen colocalized with Aβ aggregates in cell culture.

Reduced Aβ-induced platelet adhesion in vivo by blocking or genetically deleting GPVI

Platelet adhesion to vascular Aβ plaques in cerebral vessels of transgenic AD model mice and enhanced Aβ40–triggered platelet adhesion at

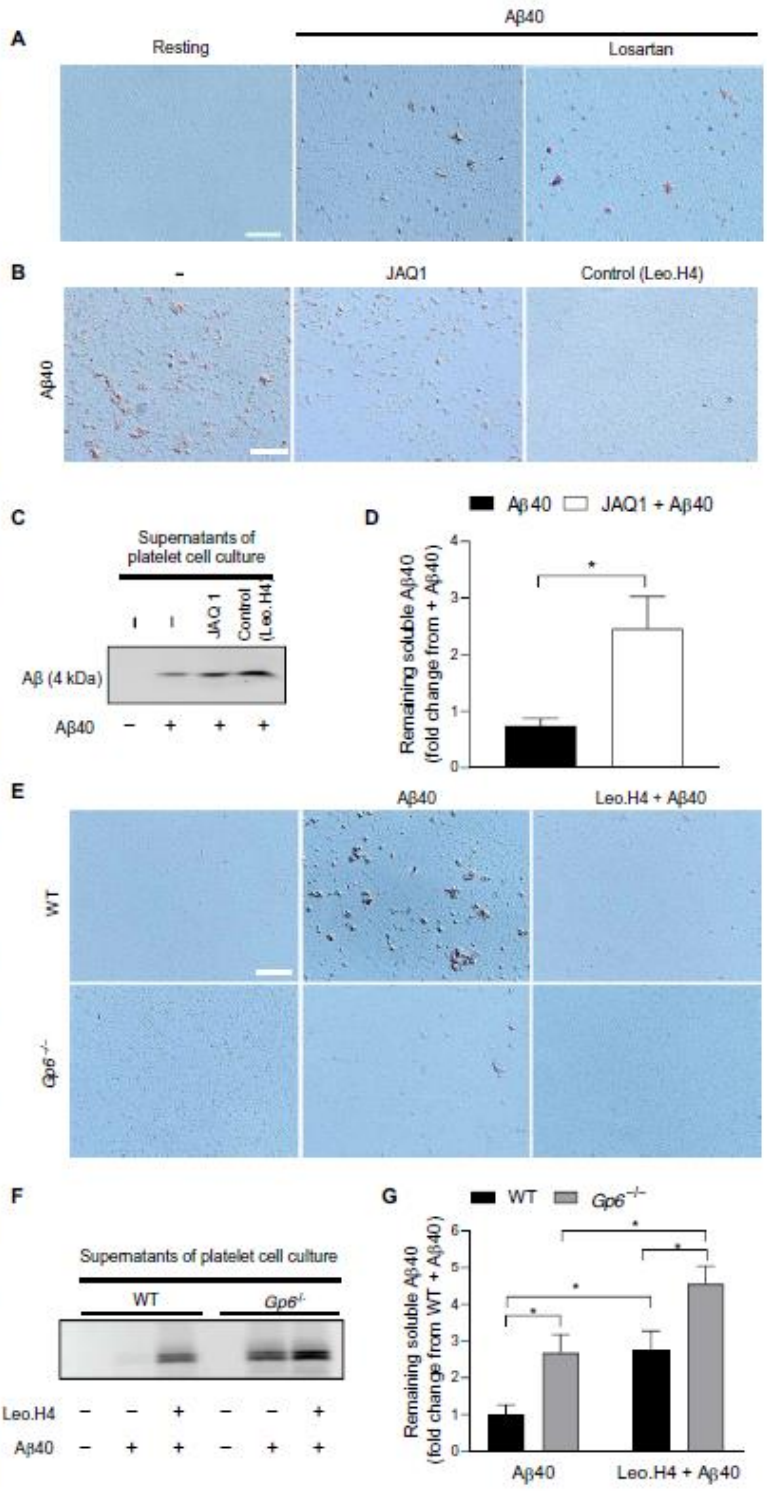

Fig. 4. Inhibition or genetic deletion of GPVI decreases amyloid aggregate formation. (**A**) Isolated human platelets were incubated with Aβ40 (5 μM) at 37°C for 3 days. Afterward, amyloid aggregates were stained by Congo red. Representative pictures of Congo red–stained amyloid aggregates platelet culture in the presence or absence of losartan (100 μM). Scale bar, 50 μm; $n = 5$ experiments. (**B**) Samples of murine platelets treated as in (A) were stained with Congo red to visualize amyloid aggregates in the presence of either the GPVI-blocking antibody JAQ1 or the integrin $\alpha_{IIb}\beta_3$-blocking antibody Leo.H4 (each at 6 μg per 2×10^8 cells). Scale bar, 50 μm; $n = 5$ experiments. (**C** and **D**) Corresponding Western blotting and quantification of soluble Aβ in supernatants from murine platelets cultured as in (B). Leo.H4-treated platelets served as control. Data are means ± SEM from $n = 5$ experiments; Student's t test, $^*P \leq 0.05$. (**E**) Congo red staining of amyloid aggregates in cultures of platelets from WT and *Gp6*$^{-/-}$ mice without Aβ40 and with Aβ40 (5 μM) in the presence or absence of Leo.H4 (6 μg per 2×10^8 cells). Scale bar, 50 μm; $n = 5$ mice per group. (**F** and **G**) Representative Western blots (F) and quantification (G) of soluble Aβ in supernatants from WT and GPVI$^{-/-}$ murine platelet cultures of remaining soluble Aβ. Controls lacking Aβ40 (lane 1 in the blot) were not regarded in the analysis. Data are means ± SEM from $n = 5$ mice per group; two-way ANOVA with Bonferroni's post hoc test, $^*P < 0.05$.

the injured vessels of WT mice in vivo were shown in a previous study (*18*). To explore the inhibitory effects of losartan on Aβ40-enhanced platelet adhesion at the vessel in vivo, we analyzed platelet adhesion at the injured carotid artery by in vivo fluorescence microscopy. Platelets from donor mice were stained with CellTracker Red and activated with Aβ40 in the absence or presence of losartan (Fig. 7A and movies S1 and S2). As expected, Aβ40-induced tethering and stable adhesion of platelets at sites of injury in recipient mice were observed (Fig. 7, A to C). In contrast, treatment of donor platelets with Aβ and losartan led to a statistically significant reduction of tethered (Fig. 7B) and stable adherent (Fig. 7C) platelets at the injured vessel in recipient mice.

To confirm an important role of GPVI on Aβ40-triggered platelet adhesion at the injured vessel in vivo, we used platelets from donor mice lacking GPVI. In vivo fluorescence imaging of platelet adhesion at sites of injury in WT recipient mice showed reduced adhesion of Aβ40-stimulated GPVI-deficient platelets compared to WT controls (Fig. 7, A to C, and movie S3).

DISCUSSION

GPVI is one of the key receptors involved in hemostasis and the prothrombotic state of acute coronary syndrome; thus, targeting GPVI may

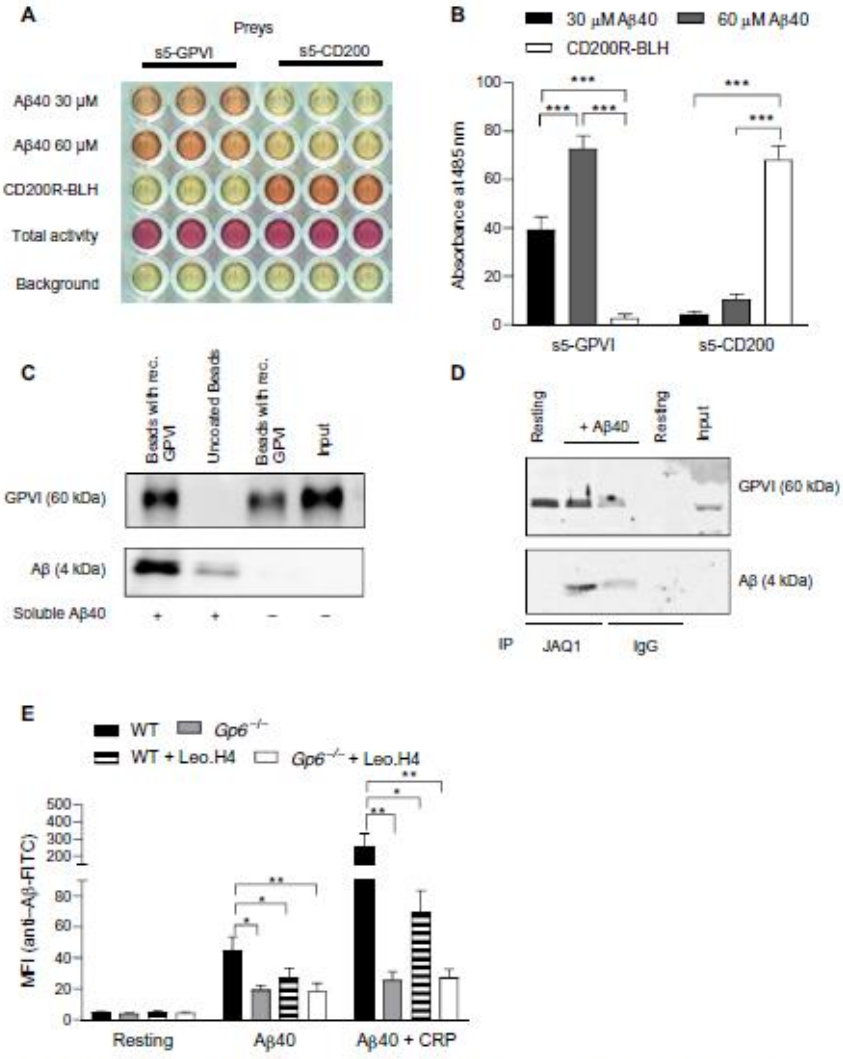

Fig. 5. Aβ40 binds to GPVI. (**A**) Interaction screening using AVEXIS (avidity-based extracellular interaction screen). Biotinylated bait peptides Aβ40 (CD200R-BLH is used as control) are arrayed on the surface of a streptavidin-coated plate and incubated with pentameric prey protein s5-GPVI (s5-CD200 is used as control). Interaction produces a color change to red. (**B**) Corresponding quantification of the colorimetric change after prey binding at 485 nm as represented in (A). $n = 5$ experiments; two-way ANOVA with Bonferroni's post hoc test, $^{***}P < 0.001$ (**C**) Pulldown was accomplished using immobilized GPVI magnetic beads and incubated without and with Aβ40 (20 μM). Uncoated beads served as control. Immunoprecipitates were blotted against Aβ (6E10) and GPVI. Input = cell lysate. $n = 3$ experiments. (**D**) Isolated platelets were stimulated with Aβ40 (20 μM) and immunoprecipitated with GPVI antibody. Immunoprecipitates were analyzed via Western blotting against Aβ and GPVI. Representative of $n = 3$. (**E**) WT and *Gp6*$^{-/-}$ platelets were preincubated with Aβ40 (5 μM), followed by an incubation with anti–Aβ-FITC antibody. When indicated, platelets were pretreated with integrin $\alpha_{IIb}\beta_3$-blocking antibody Leo.H4. Binding of Aβ to platelet surface was measured by flow cytometry ($n = 9$ to 13 mice per group; mean ± SEM; one-way ANOVA with Dunnett's post hoc test within each group: $^{*}P < 0.05$ and $^{**}P < 0.01$).

be therapeutic for thrombosis. Recombinant GPVI-Fc improves left ventricular function after experimental myocardial infarction in mice (*28*). Injection of GPVI-specific antibodies into mice leads to the depletion of the receptor and provides strong protection against arterial thrombosis (*29*, *30*). GPVI is also implicated in vascular integrity during development and inflammation (*31*). Here, our study, using platelets from patients and mice, revealed that GPVI may also contribute to AD through direct interaction with Aβ40 and the consequent release of fibrinogen that amplifies platelet-mediated formation of amyloid fibrils. GPVI-blocking antibodies reduced platelet-associated amyloid aggregate formation. Aβ40 induced tyrosine phosphorylation, including the phosphorylation of LAT, in a GPVI-dependent manner. Platelet aggregation, Aβ40-induced ATP release, and LAT phosphorylation were reduced in GPVI-deficient murine and human platelets. The GPVI-induced release of fibrinogen accounted for amyloid aggregate formation in vitro. In vivo, enhanced platelet accumulation at injured vessels after stimulation of platelets with Aβ40 was markedly reduced when we injected GPVI-deficient platelets into the mice or pretreated the platelets with losartan, a small molecule that has been described to inhibit collagen-induced platelet aggregation in mice (*23*, *24*). Losartan inhibited Aβ40-induced platelet aggregation and ATP and fibrinogen release but had no effect on platelet-mediated amyloid aggregate formation. These results are in line with studies, showing that the use of angiotensin receptor blockers, such as losartan, restore cerebrovascular dysfunction but have no effects on memory decline or AD pathology (as in, specifically, amyloidosis) (*32*, *33*). The selective blocking of the angiotensin IV and its receptor (AngIV/AT4R)–mediated cascade is suggested to represent the underlying mechanism in losartan's benefits. However, our data suggest that the beneficial effect on cerebrovascular function is not restricted to the AngIV/AT4R cascade but rather also includes reduction of GPVI-induced platelet activation and aggregation, demonstrating broader implications of losartan. These results are in line with a study by Elaskalani and colleagues (*34*) who showed reduced platelet aggregation and phospholipase Cγ2 phosphorylation in response to Aβ42 when they block GPVI by losartan.

Besides collagen, several GPVI ligands have been identified; these include diesel exhaust particles and large polysaccharides, such as fucoidan and dextran sulfate (*35*), as well as fibrin (*36*). Here, we provide evidence for Aβ40 binding to GPVI and acting as a regulator of GPVI signaling, including tyrosine

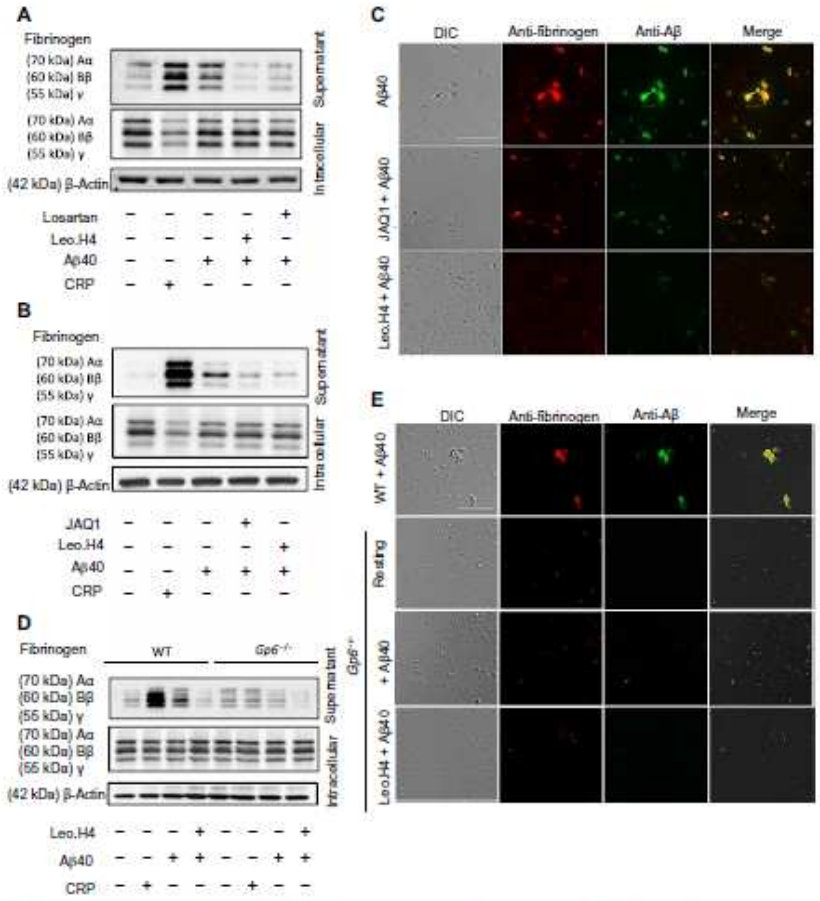

Fig. 6. Fibrinogen release in response to Aβ and colocalization with amyloid aggregates in cell culture. (**A**) Western blotting of fibrinogen release in murine platelets upon stimulation with CRP (5 μg/ml) or Aβ40 (20 μM) [pretreated as indicated with the integrin $\alpha_{IIb}\beta_3$-blocking antibody Leo.H4 (0.5 μg per 1 Mio cell) or with losartan (100 μM)]. β-Actin served as loading control; representative images of $n = 3$ experiments. (**B**) Western blotting of fibrinogen release in murine platelets as described in (A) pretreated with the GPVI-blocking antibody JAQ1 and with the integrin $\alpha_{IIb}\beta_3$-blocking antibody Leo.H4 (each 0.5 μg per 1 Mio cell). Representative Western blot of $n = 3$ experiments. (**C**) Murine platelets were incubated with Aβ40 (5 μM) at 37°C for 3 days. When indicated, platelets were pretreated with the GPVI-blocking antibody JAQ1 or the integrin $\alpha_{IIb}\beta_3$ antibody Leo.H4. Immunostaining against Aβ aggregates (green) and fibrinogen (red) visualizes colocalization. Scale bar, 20 μm. Representative images of $n = 3$ experiments. (**D**) Western blot analysis of fibrinogen release in platelets from WT and *Gp6*$^{-/-}$ mice upon stimulation with CRP (5 μg/ml) or Aβ40 (20 μM). When indicated, platelets were pretreated with integrin $\alpha_{IIb}\beta_3$ antibody Leo.H4. Representative images of $n = 3$ mice per group. (**E**) Platelets from WT and *Gp6*$^{-/-}$ mice were incubated with Aβ40 (5 μM) at 37°C for 3 days in the presence and absence of the integrin $\alpha_{IIb}\beta_3$-blocking antibody Leo.H4. Immunofluorescence staining of fibrinogen (red) and Aβ (green). Scale bar, 20 μm. Representative images of $n = 3$ mice per group.

phosphorylation, ATP and fibrinogen release, and platelet aggregation. Activation of GPVI was induced by direct binding of Aβ40 to the receptor and most likely not as secondary effect of, say, fibrinogen release, conversion of fibrinogen to fibrin, and fibrin-mediated GPVI activation.

To date, there is only one study that has investigated GPVI in AD. Those authors showed that, compared to healthy controls, patients with AD have decreased plasma levels of soluble GPVI (sGPVI) (*37*). This finding is of notable interest in terms of an antithrombotic strategy, given that sGPVI could bind collagen exposed upon vessel injury and thus reduces its binding to platelet GPVI. Reduced sGPVI plasma levels imply increased GPVI exposure at the surface of AD platelets, suggesting an increased number of Aβ40-sensitive receptors at the platelet surface and thus potentially enhanced Aβ40 binding to platelets in patients with AD.

Our data suggest that the binding of Aβ40 to GPVI induces the release of fibrinogen that is then incorporated into amyloid aggregates (Fig. 6). The formation of fibrin might not play a role since treatment of platelets with factor X inhibitor arixtra did not alter platelet-induced amyloid aggregate formation in culture. Studies have shown that fibrinogen only binds to human but not to mouse GPVI (*38*, *39*). Because we did not observe differences in the integration of fibrinogen into Aβ fibrils using either human or mouse platelets, we do not believe that fibrinogen binding to GPVI plays a role in platelet-induced amyloid aggregate formation. Fibrinogen has been identified as possible contributor to the pathology of AD, and reducing fibrinogen decreases neurovascular damage, BBB permeability, and neuroinflammation in AD (*40*). Fibrinogen is a cerebrovascular risk factor that is able to bind to Aβ, thereby altering fibrin clot structure and degradation (*41*, *42*). The interaction of Aβ and fibrinogen induces fibrinogen oligomerization (*42*). Targeting the interaction of Aβ and fibrinogen is a promising new therapeutic approach in AD (*43*). However, the authors had not taken into consideration that platelets might play a role by binding to fibrinogen and/or Aβ. Here, we provide evidence for platelets playing an important role in Aβ40-induced release of fibrinogen via GPVI and integrin $\alpha_{IIb}\beta_3$ and for fibrinogen being involved in platelet-induced amyloid aggregate formation.

We propose that engagement of GPVI and integrin $\alpha_{IIb}\beta_3$ by Aβ40 at the platelet surface induces the formation of an Aβ fibril network that included binding of Aβ40 to GPVI and integrin $\alpha_{IIb}\beta_3$ and fibrinogen binding to Aβ40 and integrin $\alpha_{IIb}\beta_3$ (Fig. 7D). These different binding possibilities might induce the formation of a specific type of "clustering" of GPVI and integrin $\alpha_{IIb}\beta_3$. Therefore, it is feasible that the failure of losartan to prevent platelet-mediated Aβ aggregate formation is due to its inability to

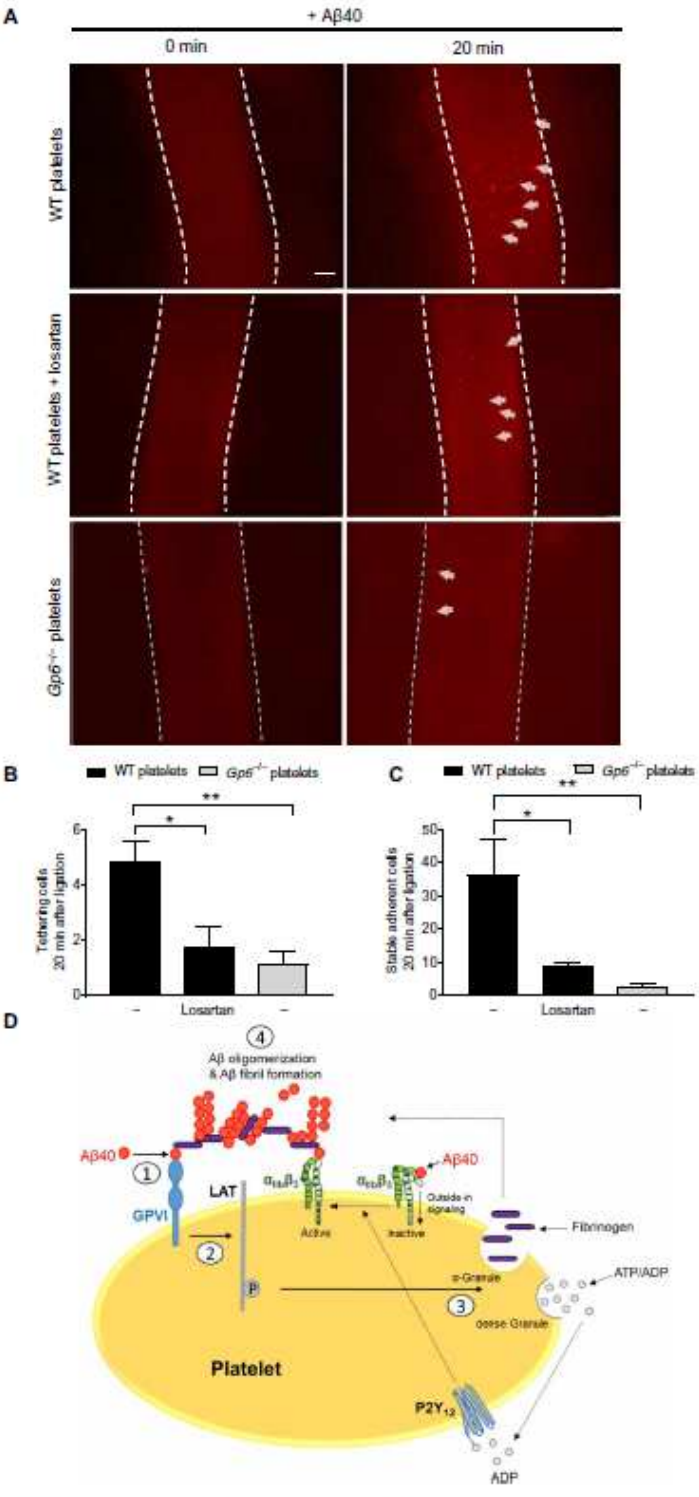

Fig. 7. Blocking or deletion of GPVI reduces Aβ-induced platelet adhesion in vivo. (**A**) Images of stable adherent and tethering Aβ40-activated platelets 20 min after carotid artery ligation in vivo. WT platelets were either incubated only with Aβ40 (top row) or were pretreated with losartan then incubated with Aβ40 (middle row), and *Gp6*$^{-/-}$ platelets were incubated with only Aβ40. Carotid artery vessel wall is outlined using dotted lines. Arrows indicate adherent platelets. $n = 4$ to 5 mice per group. Scale bar, 100 μm. (**B** and **C**) Quantification of tethering (B) and stable adherent (C) Aβ40-activated platelets. Data are means ± SEM; $n = 4$ to 5 mice per group. One-way ANOVA with Dunnett's post hoc test: $^{*}P \leq 0.05$ and $^{**}P \leq 0.01$. (**D**) Tentative schematic illustration. Direct binding of Aβ40 to the collagen receptor GPVI ("1") initiates phosphorylation of LAT ("2"), leading to secretion of granules and thus to the release of ATP, ADP, and fibrinogen ("3"). Activation of GPVI and binding of ADP to the $P2Y_{12}$ receptor induces a shifting of integrin $\alpha_{IIb}\beta_3$ from a closed (inactive) to open (active) form leading to enhanced binding of Aβ to integrin $\alpha_{IIb}\beta_3$. Released fibrinogen bridges binding of soluble Aβ to GPVI and integrin $\alpha_{IIb}\beta_3$ to induce the formation of amyloid aggregates at the platelet surface ("4").

block GPVI clustering, as already shown in the presence of collagen (*24*). However, because we previously did not observe integrin activation in the presence of Aβ40 alone (*19*), binding of Aβ40 to GPVI and integrin $\alpha_{IIb}\beta_3$ probably did not induce integrin inside-out signaling. According to our data, both previously published (*19*) and extended here, Aβ40 binds to nonactivated integrin $\alpha_{IIb}\beta_3$ on the surface of platelets, and this binding is enhanced in the presence of adenosine 5′-diphosphate (ADP) and CRP, probably due to activation-induced up-regulation of $\alpha_{IIb}\beta_3$ at the platelet surface.

Together, our findings reveal that GPVI mediates platelet-induced amyloid aggregate formation through the release of ATP and fibrinogen in response to direct binding of Aβ40 at the platelet surface. Further analysis is needed to validate whether blocking GPVI is beneficial to reduce amyloid plaque formation in cerebral vessels (as in CAA) and in brain parenchyma.

MATERIALS AND METHODS

Chemicals and antibodies

Platelets were activated with CRP (CambCol Laboratories Limited) or soluble Aβ40 (1-40; Bachem Peptide, catalog no. 4014442.1000) sequence single-letter code (DAEFRHDSGYEVHHQKLVFFAEDVGSNKGAIIGLMVGGVV). Aβ1-40 stock solutions with a concentration of 1 mg/ml were solved in sterile H_2O and stored at −20°C. Apyrase (grade II, from potato) and prostacyclin from Calbiochem were used for isolation. Antibodies against phosphotyrosine (Millipore, clone 4G10; catalog no. 05-321), phospho-LAT (p-LAT) (Tyr^{200}; Abcam, catalog no. ab68139), Aβ1-16 (BioLegend, 6E10, catalog no. SIG-39320), and fibrinogen (Dako, catalog no. A0080) were used for immunoblotting. The antibodies to LAT (catalog no. 9166), β-actin (catalog no. 4967), α-tubulin (catalog no. 2144), and horseradish peroxidase (HRP)–linked secondary antibodies (catalog nos. 7074 and 7076) were from Cell Signaling Technology.

Animals

Mice with targeted deletion of GPVI were provided by J. Ware (University of Arkansas for Medical Sciences) and backcrossed to C57BL/6 mice. For the generation of homozygous WT and *Gp6*$^{-/-}$ mice, heterozygous breeding partners were mated. The animals were maintained in an environmentally controlled room at 22° ± 1°C with a 12-hour day-night cycle. Two to five mice were housed in Makrolon cages type III with ad libitum access to food (standard chow diet) and water. All animal experiments were conducted according the Declaration of Helsinki and approved by the Ethics Committee of the State Ministry of Agriculture, Nutrition and Forestry State of North Rhine-Westphalia, Germany (reference numbers AZ 84-02.05.40.16.073 and AZ 81-02.4.2019.A232).

Human platelet preparation

Platelets were prepared, as previously described (*19*). Fresh ACD-anticoagulated blood was obtained from healthy volunteers (age of 18 to 50 years, from the blood bank, not AD or GPVI deficient) and GPVI-deficient patients, as indicated. Participants provided their written informed consent to participate in this study according to the Ethics Committee and the Declaration of Helsinki (study number 2018-140-KFogU). Collected blood was centrifuged at 200*g* for 10 min at room temperature. The supernatant (platelet-rich plasma; PRP) was added to phosphate-buffered saline [PBS; pH 6.5, apyrase (2.5 U/ml) and 1 μM PGI_2 in 1:1 volumetric ratio and centrifuged at 1000*g* for 6 min]. Platelets were resuspended in Tyrode's buffer solution (140 mM NaCl, 2.8 mM KCl, 12 mM $NaHCO_3$, 0.5 mM Na_2HPO_4, and 5.5 mM glucose, pH 7.4).

Murine platelet preparation

Murine blood was acquired by retro bulbar puncture and centrifuged at 250*g* for 5 min. The samples were centrifuged at 50*g* for 6 min to obtain PRP. PRP was washed two times (650*g* for 5 min at room temperature) before the pellet was resuspended in Tyrode's buffer [136 mM NaCl, 0.4 mM Na_2HPO_4, 2.7 mM KCl, 12 mM $NaHCO_3$, 0.1% glucose, and 0.35% bovine serum albumin (BSA; pH 7.4)] supplemented with prostacyclin (0.5 μM) and apyrase (0.02 U/ml). Before use, platelets were resuspended in the same Tyrode's buffer supplemented with 1 mM $CaCl_2$.

Platelet culture, supernatant blotting, and Congo red and immunofluorescent staining

Isolated human or murine platelets were preincubated for 15 min with 6 μg per 2 × 10^6 platelets anti-mouse integrin $\alpha_{IIb}\beta_3$ antibody [Leo.H4/rat immunoglobulin G2b (IgG2b); emfret ANALYTICS, catalog no. M021-0] or 6 μg per 2 × 10^6 platelets anti-mouse GPVI antibody (JAQ1 Rat IgG2a; emfret ANALYTICS, catalog no. M011-0) or 100 μM losartan (Tocris, catalog no. 3798). The final concentration of 2 × 10^6 platelets per well were added to 150 μl of Dulbecco's modified Eagle's medium. Platelets were stimulated with 5 μM Aβ40 or CRP (5 μg/ml) for 3 days at 37°C and 5% CO_2. After 3 days of incubation, unbound platelets were removed by rinsing with PBS. Adherent platelets were fixed with 2% paraformaldehyde and stained against fibrillary Aβ aggregates with Congo red according to the manufacturer's protocol (Millipore catalog no. 101641). For immunofluorescence staining, slides were washed with 100 μl of PBS before being fixed with 2% paraformaldehyde and blocked for 1 hour with 5% goat serum in PBS. Afterward, slides were incubated overnight at 4°C with the primary antibodies against Aβ (mouse anti-human; 6E10), fibrin-[ogen] (rabbit anti-mouse; DAKO) and the IgG controls in a 1:100 dilution containing 1% BSA and 5% goat serum in PBS. The next day, the chamber slide was washed three times with PBS and afterward incubated for 1 hour at room temperature with the secondary antibodies labeled with Alexa Fluor 488 and Alexa Fluor 555 (Life Technologies catalog nos. A32727 and A32790) in a 1:250 dilution containing 1% BSA and 5% goat serum in PBS. For immunoblotting analysis of supernatants, the cell culture supernatants were removed and centrifuged at 10,000*g* for 10 min at 4°C. The supernatant was collected, prepared with reducing sample buffer (Laemmli buffer), and denatured at 95°C for 5 min.

Cell lysis and immunoblotting

Platelets (60 × 10^6) were stimulated with 20 μM soluble Aβ40 or CRP (5 μg/ml) in Tyrode's buffer (pH 7.4) at 37°C for the indicated time. Pretreatment, when indicated, with anti-mouse integrin $\alpha_{IIb}\beta_3$ antibody (Leo.H4; emfret ANALYTICS), anti-mouse GPVI antibody (JAQ1; emfret ANALYTICS), abciximab (Janssen-Cilag GmbH), or losartan (Cayman Chemical company) occurred at 37°C for 15 to 30 min. For separation into supernatant and pellet, platelets were centrifuged at 650*g*. For platelet lysis, human platelets were incubated for 15 min on ice with lysis buffer containing 145 mM NaCl, 20 mM tris-HCl, 5 mM EDTA, 0.5% sodium deoxycholate, 1% Triton X-100, and complete protease inhibitor (PI) cocktail (Roche, catalog no. 5892970001). Murine platelets were incubated for 15 min on ice with lysis buffer containing 15 mM tris-HCl, 155 mM NaCl, 1 mM EDTA (pH 8.05), 0.005% NaN3, 1% IGPAL, and PI. Platelet lysates (30 μl) and supernatants (30 μl) were subjected to SDS–polyacrylamide gel under reducing conditions and transferred onto nitrocellulose blotting membrane (GE Healthcare Life Sciences). Membrane was blocked using 5% BSA or 5% nonfat dry milk in TBST (tris-buffered saline with 0.1% Tween 20) and probed with the appropriate primary antibody (dilution 1:1000 in 5% BSA in TBST) and secondary (dilution 1:2500 in 5% nonfat dry milk in TBST) HRP-conjugated antibody. Band intensities were quantified in relation to untreated platelets using the FUSION FX7 software (Vilber).

p-LAT: Under nonaggregating conditions (apyrase, 0.5 U/ml; lotrafiban, 10 μM; and indomethacin, 10 μM), human and mouse platelets (1.5 × 10^6) were stimulated with 30 μM soluble Aβ40, CRP (5 μg/ml), or collagen (1 μg/ml) in Tyrode's buffer (pH 7.4) for the indicated time at 37°C. Cells were immediately lysed on ice with NP-40 lysis buffer (300 mM NaCl, 20 mM tris, 2 mM EGTA, 2 mM EDTA, and 2% NP-40 detergent) in addition to the protease and phosphatase inhibitors [5 mM sodium orthovanadate, 1 mM AEBSF [4-(2-aminoethyl)benzenesulfonyl fluoride hydrochloride], leupeptin (10 μg/ml), aprotinin (10 μg/ml), and pepstatin (1 μg/ml)]. Platelet lysates were loaded in a gradient gel (NuPAGE 4 to 12%; Invitrogen) under reducing conditions and transferred onto polyvinylidene difluoride blotting membrane (TransBlot Turbo, Bio-Rad). Membrane was blocked using 5% BSA in TBST and probed with the appropriate primary antibody p-LAT (dilution 1:500; Abcam) or α-tubulin (dilution 1:1000; Sigma-Aldrich) and secondary HRP-conjugated antibody anti-mouse IgG (dilution 1:5000; GE Healthcare) or anti-rabbit IgG (dilution 1:5000; GE Healthcare). Band signals were detected using Odyssey Fc imaging system (LI-COR).

Immunoprecipitation

Platelets (1 × 10^9) were stimulated with 20 μM Aβ40 for 30 min at 37°C while being shaken. Platelets without stimulation with Aβ40 were used as a control (resting). Murine resting and 20 μM Aβ40-stimulated platelets were lysed with 5× lysis buffer (as described

in the "Cell lysis and immunoblotting" section) for 10 min on ice. Afterward, the lysate was centrifuged at 10,000*g* for 10 min at 4°C to clear the lysate from remaining cell fragments. The cleared lysate was transferred to a new reaction tube and incubated with GPVI antibody or corresponding IgG control (JAQ1, emfret ANALYTICS; mouse IgG_{2b}, Cell Signaling) for 1 hour at 4°C. Samples were transferred to a new reaction tube and incubated with washed G-sepharose protein overnight at 4°C. Samples were washed three times: first time with immunoprecipitation buffer (15 mM tris-HCl, 155 mM NaCl, 1 mM EDTA, and 0.005% NaN3) additionally containing 1% IGPAL, and second and third times with only immunoprecipitation buffer before adding 2× Laemmli, containing 5% mercaptoethanol, and incubated at 95°C for 5 min. After centrifugation at 10,000*g* for 2 min, supernatants were removed and analyzed via immunoblotting against Aβ (BioLegend, 6E10) and GPVI (R&D Systems, catalog no. AF6758).

Pulldown

Recombinant GPVI (R&D Systems, catalog no. 6758-GP-050) was covalently immobilized to Pierce NHS (N-hydroxysuccinimide)–Activated Magnetic Beads according to the manufacturer's information (Thermo Fisher Scientific, catalog no. 88802). Protein solution with and without 20 μM Aβ40 was added to the GPVI-coupled beads and incubated at room temperature on a rotator for 1 to 2 hours. Beads were collected with the magnetic stand and washed for three times with wash buffer (TBS with 0.05% Tween 20 detergent) and afterward washed with ultrapure water. For protein elution, beads were washed with 100 μl of elution buffer (0.1 M glycine, pH 2.0), and pH was neutralized by adding 10 μl of neutralization buffer (1 M tris, pH 9). Laemmli buffer was added, and samples were analyzed via immunoblotting under reducing conditions against Aβ (BioLegend, 6E10) and GPVI (R&D Systems, catalog no. AF6758).

AVEXIS screening

Aβ40 peptides or CD200R bait proteins were incubated in MaxiSorp 96-well microtiter plates (Nunc) for 1 hour and then blocked with 1% BSA for 30 min. The peptide-coated plate was incubated with full-length recombinant soluble pentameric (s5) GPVI and s5CD200 for 1 hour. Three wash steps were performed between each incubation using PBS with 0.1% Tween 20. After addition of nitrocefin (125 μg/ml; #N005, Toku-e) and incubation for 1 hour, absorbance was measured at 485 nm on a VersaMax microplate reader (Molecular Devices).

Platelet aggregation and ATP release

Aggregation was measured as percentage light transmission compared to Tyrode's buffer (as = 100%) using a Chrono-Log dual-channel lumi-aggregometer (model 700) at 37°C stirring at 1000 rpm. Human ATP release was assessed by applying a luciferin/luciferase bioluminescent assay and calculated using a provided ATP standard protocol (all from Chrono-Log). Murine ATP release was measured using ATP Bioluminescence Assay Kit HS II (Roche, catalog no. 11699709001) according to the manufacturer's information and normalized to resting.

Flow cytometry

Flow cytometry was performed, as described (*18*, *44*). Analysis of Aβ40 binding to platelets surface was carried out using fluorophore-labeled antibodies for Aβ (anti–Aβ-FITC; Santa Cruz Biotechnology, catalog no. sc-28365). Twenty-five microliters of washed blood samples was diluted in Tyrode's buffer with 1 mM $CaCl_2$ and stimulated with indicated agonist [5 μM Aβ40 and CRP (5 μg/ml)] and antibody at room temperature for 15 min. Reaction was stopped using 300 μl of PBS. Samples were analyzed on a FACSCalibur flow cytometer (BD Biosciences).

Carotid artery ligation model

Carotid ligation in mice was performed, as described elsewhere (*18*). Platelets from WT and $Gp6^{-/-}$ donor mice were stained with a CellTracker Red CMTPX (Invitrogen) according to the manufacturer's guidelines and incubated with losartan (100 μM) or vehicle and Aβ (50 μg/ml) for 30 min. WT littermates mice were anaesthetized using ketamine (Zoetis) and xylazine (WDT) and put on a heating pad. The right common carotid artery was prepared, and after intravenous injection of fluorescently labeled and treated platelets, a film of 30 s was taken using a DM6FS microscope (Leica Microsystems, Wetzlar, Germany). Afterward, the carotid artery was ligated vigorously for 5 min, thus inducing vascular injury. The interaction of the fluorescent platelets with the injured vessel wall was visualized 20 min after ligation by in vivo video microscopy. Tethering and adherent cells were counted as means from 10 different pictures throughout the film with the same time span between these pictures, but always in the same phase of vessel pulsation.

Statistical analysis

Data are provided as arithmetic means ± SEM. Significant differences were calculated using the two-way analysis of variance (ANOVA) with Bonferroni's multiple comparison post hoc test, one-way ANOVA with Dunnett's post hoc test, or Student's *t* test as indicated in the figure legends. Outliers were excluded using Grubb's test.

SUPPLEMENTARY MATERIALS

stke.sciencemag.org/cgi/content/full/13/643/eaba9872/DC1

Fig. S1. Time-dependent LAT phosphorylation of human platelets stimulated with Aβ40.
Fig. S2. Different concentrations of losartan on platelet cell cultures.
Fig. S3. Reduced amyloid aggregate formation through GPVI inhibition in a concentration-dependent manner.
Fig. S4. Immunofluorescence staining of fibrinogen and Aβ in human and murine platelet cell cultures.
Fig. S5. No alteration in amyloid fibril formation upon inhibition of active factor Xa.
Movie S1. Adhesion of WT platelets at the injured carotid artery in vivo.
Movie S2. Adhesion of WT platelets at the injured carotid artery in vivo after losartan treatment.
Movie S3. Adhesion of $Gp6^{-/-}$ platelets at the injured carotid artery in vivo.

View/request a protocol for this paper from *Bio-protocol*.

REFERENCES AND NOTES

1. M. Prince, G.-C. Ali, M. Guerchet, A. M. Prina, E. Albanese, Y.-T. Wu, Recent global trends in the prevalence and incidence of dementia, and survival with dementia. *Alzheimers Res. Ther.* **8**, 23 (2016).
2. G. Rakesh, S. T. Szabo, G. S. Alexopoulos, A. S. Zannas, Strategies for dementia prevention: Latest evidence and implications. *Ther. Adv. Chronic Dis.* **8**, 121–136 (2017).
3. A. M. Clarfield, The decreasing prevalence of reversible dementias: An updated meta-analysis. *Arch. Intern. Med.* **163**, 2219–2229 (2003).
4. D. J. Selkoe, J. Hardy, The amyloid hypothesis of Alzheimer's disease at 25 years. *EMBO Mol. Med.* **8**, 595–608 (2016).
5. D. J. Selkoe, Alzheimer's disease. *Cold Spring Harb Perspect. Biol.* **3**, a004457 (2011).
6. H. Braak, E. Braak, D. Yilmazer, R. A. de Vos, E. N. Jansen, J. Bohl, Pattern of brain destruction in Parkinson's and Alzheimer's diseases. *J. Neural Transm.* **103**, 455–490 (1996).
7. A. Serrano-Pozo, M. P. Frosch, E. Masliah, B. T. Hyman, Neuropathological alterations in Alzheimer disease. *Cold Spring Harb. Perspect. Med.* **1**, a006189 (2011).
8. M. Sochocka, E. S. Koutsouraki, K. Gasiorowski, J. Leszek, Vascular oxidative stress and mitochondrial failure in the pathobiology of Alzheimer's disease: A new approach to therapy. *CNS Neurol. Disord. Drug Targets* **12**, 870–881 (2013).

9. M. Z. Wojtukiewicz, E. Sierko, D. Hempel, S. C. Tucker, K. V. Honn, Platelets and cancer angiogenesis nexus. *Cancer Metastasis Rev.* **36**, 249–262 (2017).
10. T. G. Walsh, P. Metharom, M. C. Berndt, The functional role of platelets in the regulation of angiogenesis. *Platelets* **26**, 199–211 (2015).
11. M. R. Thomas, R. F. Storey, The role of platelets in inflammation. *Thromb. Haemost.* **114**, 449–458 (2015).
12. C. Goubau, G. M. Buyse, C. Van Geet, K. Freson, The contribution of platelet studies to the understanding of disease mechanisms in complex and monogenetic neurological disorders. *Dev. Med. Child Neurol.* **56**, 724–731 (2014).
13. E. Asor, D. Ben-Shachar, Platelets: A possible glance into brain biological processes in schizophrenia. *World J. Psychiatry* **2**, 124–133 (2012).
14. M. Padmakumar, E. Van Raes, C. Van Geet, K. Freson, Blood platelet research in autism spectrum disorders: In search of biomarkers. *Res. Pract. Thromb. Haemost.* **3**, 566–577 (2019).
15. M. Behari, M. Shrivastava, Role of platelets in neurodegenerative diseases: A universal pathophysiology. *Int. J. Neurosci.* **123**, 287–299 (2013).
16. K. Stellos, V. Panagiota, A. Kögel, T. Leyhe, M. Gawaz, C. Laske, Predictive value of platelet activation for the rate of cognitive decline in Alzheimer's disease patients. *J. Cereb. Blood Flow Metab.* **30**, 1817–1820 (2010).
17. A. Jarre, N. S. Gowert, L. Donner, P. Münzer, M. Klier, O. Borst, M. Schaller, F. Lang, C. Korth, M. Elvers, Pre-activated blood platelets and a pro-thrombotic phenotype in APP23 mice modeling Alzheimer's disease. *Cell. Signal.* **26**, 2040–2050 (2014).
18. N. S. Gowert, L. Donner, M. Chatterjee, Y. S. Eisele, S. T. Towhid, P. Münzer, B. Walker, I. Ogorek, O. Borst, M. Grandoch, M. Schaller, J. W. Fischer, M. Gawaz, S. Weggen, F. Lang, M. Jucker, M. Elvers, Blood platelets in the progression of Alzheimer's disease. *PLOS ONE* **9**, e90523 (2014).
19. L. Donner, K. Fälker, L. Gremer, S. Klinker, G. Pagani, L. U. Ljungberg, K. Lothmann, F. Rizzi, M. Schaller, H. Gohlke, D. Willbold, M. Grenegard, M. Elvers, Platelets contribute to amyloid-β aggregation in cerebral vessels through integrin $\alpha_{6}\beta_{1}$–induced outside-in signaling and clusterin release. *Sci. Signal.* **9**, ra52 (2016).
20. L. Donner, L. Gremer, T. Ziehm, C. G. W. Gertzen, H. Gohlke, D. Willbold, M. Elvers, Relevance of N-terminal residues for amyloid-β binding to platelet integrin $\alpha_{6}\beta_{1}$, integrin outside-in signaling and amyloid-β fibril formation. *Cell. Signal.* **50**, 121–130 (2018).
21. J. M. Pasquet, B. Gross, L. Quek, N. Asazuma, W. Zhang, C. L. Sommers, E. Schweighoffer, V. Tybulewicz, B. Judd, J. R. Lee, G. Koretzky, P. E. Love, L. E. Samelson, S. P. Watson, LAT is required for tyrosine phosphorylation of phospholipase Cγ2 and platelet activation by the collagen receptor GPVI. *Mol. Cell. Biol.* **19**, 8326–8334 (1999).
22. C. Schulz, N. V. Leuschen, T. Fröhlich, M. Lorenz, S. Pfeiler, C. A. Gleissner, E. Kremmer, M. Kessler, A. G. Khandoga, B. Engelmann, K. Ley, S. Massberg, G. J. Arnold, Identification of novel downstream targets of platelet glycoprotein VI activation by differential proteome analysis: Implications for thrombus formation. *Blood* **115**, 4102–4110 (2010).
23. P. Jiang, S. Loyau, M. Tchitchinadze, J. Ropers, G. Jondeau, M. Jandrot-Perrus, Inhibition of glycoprotein VI clustering by collagen as a mechanism of inhibiting collagen-induced platelet responses: The example of losartan. *PLOS ONE* **10**, e0128744 (2015).
24. M.-B. Onselaer, M. Nagy, C. Pallini, J. A. Pike, G. Perrella, L. G. Quintanilla, J. A. Eble, N. S. Poulter, J. W. M. Heemskerk, S. P. Watson, Comparison of the GPVI inhibitors losartan and honokiol. *Platelets* **31**, 187–197 (2019).
25. Y. Sun, M. Gallagher-Jones, C. Barker, G. J. Wright, A benchmarked protein microarray-based platform for the identification of novel low-affinity extracellular protein interactions. *Anal. Biochem.* **424**, 45–53 (2012).
26. Y. Hou, N. Carrim, Y. Wang, R. C. Gallant, A. Marshall, H. Ni, Platelets in hemostasis and thrombosis: Novel mechanisms of fibrinogen-independent platelet aggregation and fibronectinmediated protein wave of hemostasis. *J. Biomed. Res.* **29**, 437–444 (2015).
27. P. Blair, R. Flaumenhaft, Platelet α-granules: Basic biology and clinical correlates. *Blood Rev.* **23**, 177–189 (2009).
28. T. Schönberger, M. Ziegler, O. Borst, I. Konrad, B. Nieswandt, S. Massberg, C. Ochmann, T. Jürgens, P. Seizer, H. Langer, G. Münch, M. Ungerer, K. T. Preissner, M. Elvers, M. Gawaz, The dimeric platelet collagen receptor GPVI-Fc reduces platelet adhesion to activated endothelium and preserves myocardial function after transient ischemia in mice. *Am. J. Physiol. Cell Physiol.* **303**, C757–C766 (2012).
29. B. Nieswandt, V. Schulte, W. Bergmeier, R. Mokhtari-Nejad, K. Rackebrandt, J.-P. Cazenave, P. Ohlmann, C. Gachet, H. Zimgibl, Long-term antithrombotic protection by in vivo depletion of platelet glycoprotein VI in mice. *J. Exp. Med.* **193**, 459–469 (2001).
30. S. Grüner, M. Prostredna, M. Koch, Y. Miura, V. Schulte, S. M. Jung, M. Moroi, B. Nieswandt, Relative antithrombotic effect of soluble GPVI dimer compared with anti-GPVI antibodies in mice. *Blood* **105**, 1492–1499 (2005).
31. R. H. Lee, W. Bergmeier, Platelet immunoreceptor tyrosine-based activation motif (ITAM) and hemITAM signaling and vascular integrity in inflammation and development. *J. Thromb. Haemost.* **14**, 645–654 (2016).
32. B. Ongali, N. Nicolakakis, X.-K. Tong, T. Aboulkassim, H. Imboden, E. Hamel, Enalapril alone or co-administered with losartan rescues cerebrovascular dysfunction, but not mnemonic deficits or amyloidosis in a mouse model of Alzheimer's disease. *J. Alzheimers Dis.* **51**, 1183–1195 (2016).
33. J. Royea, L. Zhang, X.-K. Tong, E. Hamel, Angiotensin IV receptors mediate the cognitive and cerebrovascular benefits of losartan in a mouse model of Alzheimer's disease. *J. Neurosci.* **37**, 5562–5573 (2017).
34. O. Elaskalani, I. Khan, M. Morici, C. Matthysen, M. Sabale, R. N. Martins, G. Verdile, P. Metharom, Oligomeric and fibrillar amyloid beta 42 induce platelet aggregation partially through GPVI. *Platelets* **29**, 415–420 (2018).
35. O. M. Alshehri, S. Montague, S. Watson, P. Carter, N. Sarker, B. K. Manne, J. L. Miller, A. B. Herr, A. Y. Pollitt, C. A. O'Callaghan, S. Kunapuli, M. Aman, C. E. Hughes, S. P. Watson, Activation of glycoprotein VI (GPVI) and C-type lectin-like receptor-2 (CLEC-2) underlies platelet activation by diesel exhaust particles and other charged/hydrophobic ligands. *Biochem. J.* **468**, 459–473 (2015).
36. O. M. Alshehri, C. E. Hughes, S. Montague, S. K. Watson, J. Frampton, M. Bender, S. P. Watson, Fibrin activates GPVI in human and mouse platelets. *Blood* **126**, 1601–1608 (2015).
37. C. Laske, T. Leyhe, E. Stransky, G. W. Eschweiler, A. Bueltmann, H. Langer, K. Stellos, M. Gawaz, Association of platelet-derived soluble glycoprotein VI in plasma with Alzheimer's disease. *J. Psychiatr. Res.* **42**, 746–751 (2008).
38. P. H. Mangin, M.-B. Onselaer, N. Receveur, N. Le Lay, A. T. Hardy, C. Wilson, X. Sanchez, S. Loyau, A. Dupuis, A. K. Babar, J. L. Miller, H. Philippou, C. E. Hughes, A. B. Herr, R. A. Ariëns, D. Mezzano, M. Jandrot-Perrus, C. Gachet, S. P. Watson, Immobilized fibrinogen activates human platelets through glycoprotein VI. *Haematologica* **103**, 898–907 (2018).
39. A. Slater, G. Perrella, M.-B. Onselaer, E. M. Martin, J. S. Gauer, R.-G. Xu, J. W. Heemskerk, R. A. S. Ariëns, S. P. Watson, Does fibrin(ogen) bind to monomeric or dimeric GPVI, or not at all? *Platelets* **30**, 281–289 (2019).
40. M. Cortes-Canteli, S. Strickland, Fibrinogen, a possible key player in Alzheimer's disease. *J. Thromb. Haemost.* **7**, 146–150 (2009).
41. M. Cortes-Canteli, J. Paul, E. H. Norris, R. Bronstein, H. J. Ahn, D. Zamolodchikov, S. Bhuvanendran, K. M. Fenz, S. Strickland, Fibrinogen and β-amyloid association alters thrombosis and fibrinolysis: A possible contributing factor to Alzheimer's disease. *Neuron* **66**, 695–709 (2010).
42. H. J. Ahn, D. Zamolodchikov, M. Cortes-Canteli, E. H. Norris, J. F. Glickman, S. Strickland, Alzheimer's disease peptide β-amyloid interacts with fibrinogen and induces its oligomerization. *Proc. Natl. Acad. Sci. U.S.A.* **107**, 21812–21817 (2010).
43. H. J. Ahn, J. F. Glickman, K. L. Poon, D. Zamolodchikov, O. C. Jno-Charles, E. H. Norris, S. Strickland, A novel Aβ-fibrinogen interaction inhibitor rescues altered thrombosis and cognitive decline in Alzheimer's disease mice. *J. Exp. Med.* **211**, 1049–1062 (2014).
44. I. Pleines, M. Elvers, A. Strehl, M. Pozgajova, D. Varga-Szabo, F. May, A. Chrostek-Grashoff, C. Brakebusch, B. Nieswandt, Rac1 is essential for phospholipase C-γ2 activation in platelets. *Pflugers Arch.* **457**, 1173–1185 (2009).

Acknowledgments: We thank M. Spelleken for providing outstanding technical assistance. **Funding:** The study was supported by the Deutsche Forschungsgemeinschaft (DFG) grant number EL651/5-1 and the Collaborative Research Center (CRC) 1116 (Project A05) to M.E. and to M.K. (project B06) and N.G. (project B09). S.P.W. is a British Heart Foundation Chair (CH03/003). S.P. and Y.S. acknowledge funding from the COMPARE and the British Heart Foundation (PG/16/53/32242). We acknowledge the support of the Susanne-Bunnenberg-Stiftung at the Düsseldorf Heart Center. **Author contributions:** L.D., L.M.T., I.K., S.G., R.B., A.B., D.M., S.P., M.K., N.G., and Y.S. performed experiments and analyzed the data. D.M. arranged for the acquisition of GPVI-deficient patient samples. L.M.T. discussed the data and helped draft the manuscript. S.P.W. and Y.S. designed and performed experiments and read and edited the manuscript. L.D. and M.E. designed experiments, discussed the data, and wrote the manuscript. A.B. is currently affiliated with the Infection, Inflammation and Rheumatology at UCL Great Ormond Street, Institute of Child Health, London, WC1N 1EH, UK. **Competing interests:** The authors declare they have no competing interests. **Data and materials availability:** All data needed to evaluate the conclusions in the paper are present in the paper or the Supplementary Materials. Additional data related to this paper may be requested from the authors.

Submitted 21 January 2020
Accepted 25 June 2020
Published 4 August 2020
10.1126/scisignal.aba9872

Citation: L. Donner, L. M. Toska, I. Krüger, S. Grüniger, R. Barroso, A. Burleigh, D. Mezzano, S. Pfeiler, M. Kelm, N. Gerdes, S. P. Watson, Y. Sun, M. Elvers, The collagen receptor glycoprotein VI promotes platelet-mediated aggregation of β-amyloid. *Sci. Signal.* **13**, eaba9872 (2020).

Science Signaling

The collagen receptor glycoprotein VI promotes platelet-mediated aggregation of β-amyloid

Lili Donner, Laura Mara Toska, Irena Krüger, Sandra Gröniger, Ruben Barroso, Alice Burleigh, Diego Mezzano, Susanne Pfeiler, Malte Kelm, Norbert Gerdes, Steve P. Watson, Yi Sun and Margitta Elvers

Sci. Signal. **13** (643), eaba9872.
DOI: 10.1126/scisignal.aba9872

Unclogging amyloid from arteries

Cerebral amyloid angiopathy (CAA) is a common feature of Alzheimer's disease in which the deposition of amyloid in vessels in the brain impairs blood flow. Amyloid can activate platelets, which promotes amyloid aggregation. Using platelets from patients and mice, Donner *et al.* found that blocking the collagen receptor GPVI may reduce CAA. Amyloid bound to GPVI on platelets and stimulated the release of fibrinogen that both clustered with soluble amyloid and bound a platelet-surface integrin that further promoted amyloid aggregation. Blockade of GPVI or the integrin reduced amyloid aggregation in platelet cultures, and loss of GPVI reduced the adhesion of amyloid-activated platelets in arteries in mice, revealing a potential therapeutic target to ameliorate CAA in patients.

Science Signaling
AAAS

stke.sciencemag.org/cgi/content/full/13/643/eaba9872/DC1

Supplementary Materials for

The collagen receptor glycoprotein VI promotes platelet-mediated aggregation of β-amyloid

Lili Donner, Laura Mara Toska, Irena Krüger, Sandra Gröniger, Ruben Barroso, Alice Burleigh, Diego Mezzano, Susanne Pfeiler, Malte Kelm, Norbert Gerdes, Steve P. Watson, Yi Sun, Margitta Elvers*

*Corresponding author. Email: margitta.elvers@med.uni-duesseldorf.de

Published 4 August 2020, *Sci. Signal.* 13, eaba9872 (2020)
DOI: 10.1126/scisignal.aba9872

The PDF file includes:

Other Supplementary Material for this manuscript includes the following:

(available at stke.sciencemag.org/cgi/content/full/13/643/eaba9872/DC1)

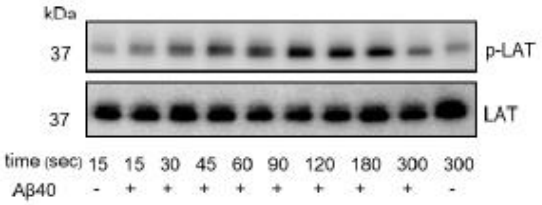

Fig. S1. Time-dependent LAT phosphorylation of human platelets stimulated with Aβ40. Isolated human platelets were stimulated with 20 µM Aβ40 for 15 to 300 sec, and LAT phosphorylation (p-LAT) was analyzed at intervals therein by Western blotting. Total LAT was blotted for reference. Blot is representative of results from n=3 donors.

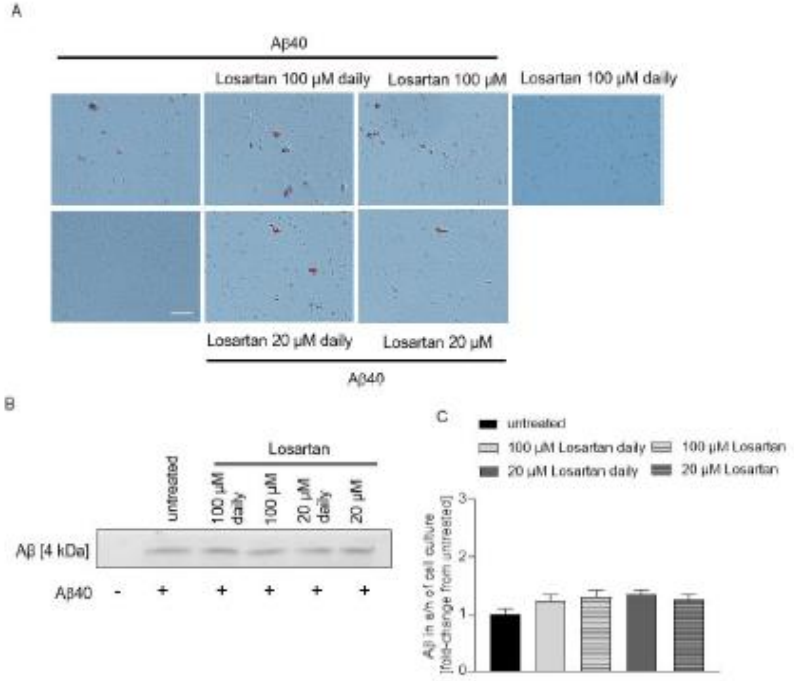

Fig. S2. Different concentrations of losartan on platelet cell cultures. (A) Congo red staining of human platelet cultures incubated with losartan at 20 µM or 100 µM, added either once before incubation with 5 µM Aβ40 for three days or additionally added every day for three days (20 µM daily or 100 µM daily) in the presence of Aβ40. Scale bar, 50 µm. Images are representative of n=5 experiments. **(B and C)** Corresponding representative Western blot (B) of Aβ in supernatants from human platelet culture and (C) its quantification from n=5 experiments; data are mean ± SEM. In (C), "s/n" denotes supernatants.

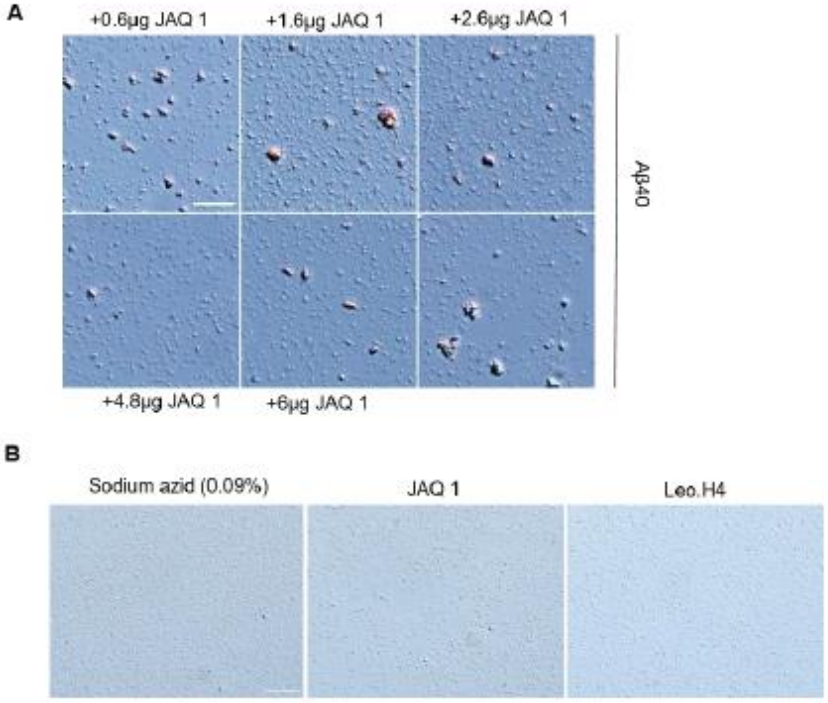

Fig. S3. Reduced amyloid aggregate formation through GPVI inhibition in a concentration-dependent manner. (A) Congo red staining of murine platelet cultures incubated with 5 µM Aβ40 for three days, in the presence of 0.6 µg, 1,6 µg 2.6 µg, 4,8 µg or 6 µg GPVI inhibiting antibody (JAQ1) per $2*10^6$ platelets. Scale bar, 50 µm. N= 3 experiments- (B) Antibody controls. Murine platelet culture was incubated for three days with GPVI-blocking antibody JAQ1 or integrin $\alpha_{IIb}\beta_3$-blocking antibody Leo.H4 (each at 6 µg per $2*10^6$ cells) in the absence of Aβ40. Congo red staining showed no amyloid aggregate formation. N=3 experiments.

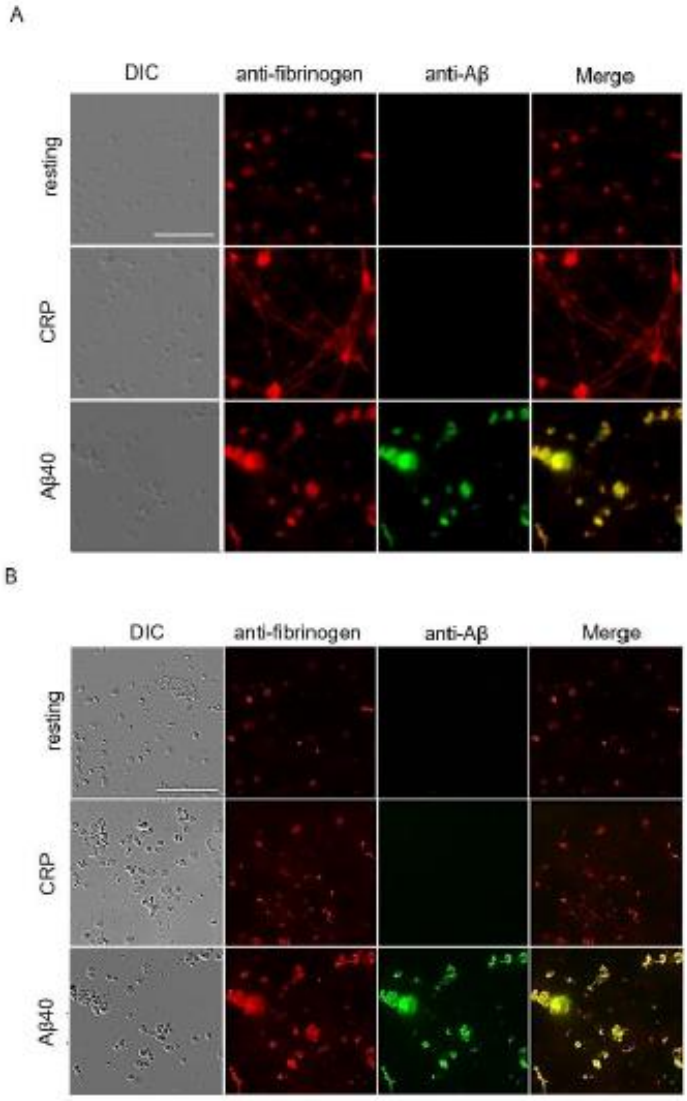

Fig. S4. Immunofluorescence staining of fibrinogen and Aβ in human and murine platelet cell cultures. (**A**) Isolated human platelets were incubated with 5 µg/ml CRP or 5 µM Aβ40 for three days. Fibrinogen (red) and Aβ (green) were stained via immunofluorescence staining. Scale bar, 20 µm. Representative images of n= 4 experiments. (**B**) Isolated murine platelets were incubated with 5 µg/ml CRP or 5 µM Aβ40 for three days. Fibrinogen (red) and Aβ (green) were stained by immunofluorescence staining. Scale bar, 20 µm. Representative images are of n= 4 experiments.

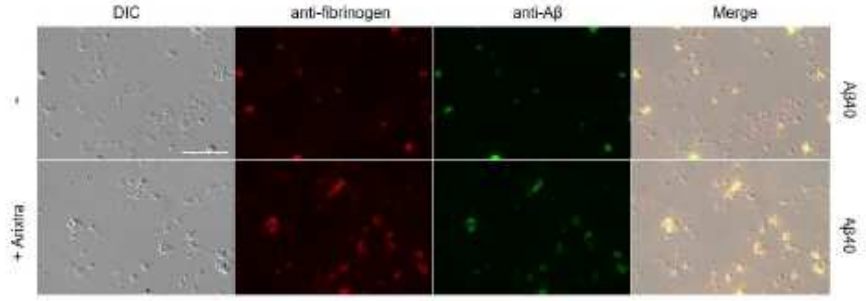

Fig. S5. No alteration in amyloid fibril formation upon inhibition of active factor Xa. Isolated human platelets were incubated with 5 µM Aβ40 for three days in the presence (lower panel) and absence (upper panel) of Arixtra (5 µg/ml). Fibrinogen (red) and Aβ (green) were stained via immunofluorescence. Scale bar, 20 µm. N= 3 experiments.

Movie S1. Adhesion of WT platelets at the injured carotid artery in vivo. Platelet adhesion to the ligated carotid artery was analyzed by intravital fluorescence microscopy. WT platelets from donor mice were stimulated with soluble 50 µg/ml Aβ40 for 30 min and injected into recipient WT mice. Platelet were labeled with CellTracker™ Red CMTPX for visualization and quantification (shown in Fig. 7C). Movie is provided as an mp4 file in the supplementary materials online.

Movie S2. Adhesion of WT platelets at the injured carotid artery in vivo after losartan treatment. Platelet adhesion to the ligated carotid artery was analyzed by intravital fluorescence microscopy. WT platelets from donor mice were pre-treated with losartan, stimulated with soluble Aβ40 and injected into recipient WT mice. Platelet were labeled with CellTracker™ Red CMTPX for visualization and quantification (shown in Fig. 7C). Movie is provided as an mp4 file in the supplementary materials online.

Movie S3. Adhesion of *Gp6*$^{-/-}$ platelets at the injured carotid artery in vivo. Adhesion of GPVI$^{-/-}$ platelets to the ligated carotid artery was analyzed by intravital fluorescence microscopy. GPVI$^{-/-}$ platelets from donor mice were stimulated with soluble Aβ40 and injected into recipient WT mice. Platelet were labeled with CellTracker™ Red CMTPX for visualization and quantification (shown in Fig. 7C). Movie is provided as an mp4 file in the supplementary materials online.

The following section 3.1. contains supplementary results that are not published in the manuscript: The collagen receptor glycoprotein VI promotes platelet-mediated aggregation of amyloid-β (section 3.1).

3.1.1 Murine phosphorylation of tyrosine residues by GPVI in response to Aβ40 stimulation

Binding of collagen or collagen–related peptide (CRP) to GPVI leads to intracellular downstream signaling, including the phosphorylation of tyrosine residues and consequent activation or inhibition of adaptor proteins (section 1.2.3). Thus tyrosine phosphorylation plays a key role in cellular signal transduction following ligation of GPVI. In addition to the analysis of total tyrosine phosphorylation (4G10) upon Aβ40 stimulation in human platelets [168], tyrosine phosphorylation was examined in mouse platelets (Fig. 6). In order to clarify whether mouse platelets exhibit intracellular GPVI-dependent signaling pathways in response to Aβ40 stimulation as observed in human platelets, Western blot analyses were performed with platelets from WT- and *Gp6*$^{-/-}$ mice.

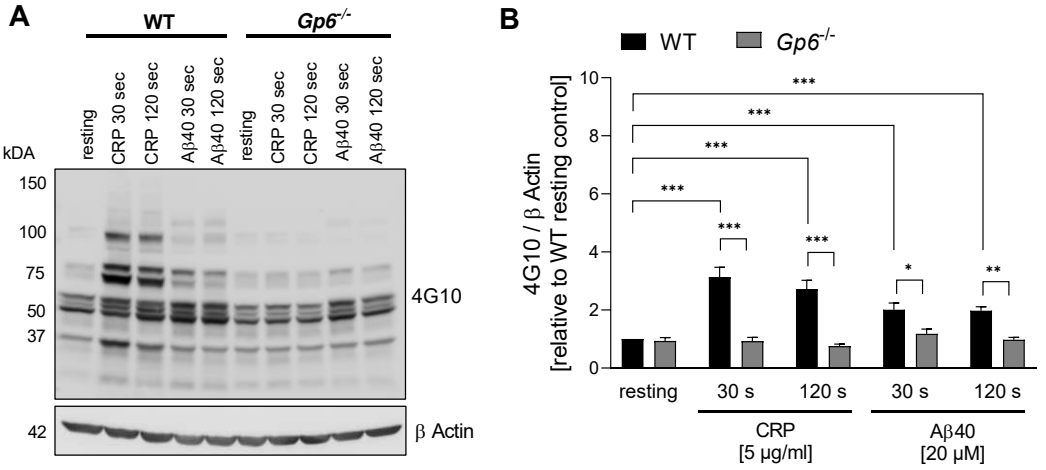

Figure 6: Aβ40 stimulates tyrosine phosphorylation in murine platelets in a GPVI-dependent manner. (A) Representative image and (B) quantification of tyrosine phosphorylation (4G10) via Western blot analysis of isolated platelets from WT and *Gp6*$^{-/-}$ mice activated with 20 µM Aβ40 or 5 µg/ml collagen-related peptide (CRP) for 30 s and 120 s, respectively (n=4). Protein abundance was normalized to WT resting and β-actin. β-actin served as a loading control. Statistical analyses were performed using a two-way ANOVA followed by a Sidak's multiple comparisons post-hoc test. Bar graphs indicate mean values ± SEM, *p < 0.05; **p < 0.005; +**p < 0.001. kDA = kilo Dalton, WT = Wild-type.

Representative image and quantitative analysis revealed an increase in total tyrosine phosphorylation in WT platelets upon CRP (p<0.0001) as well as Aβ40 (30 sec: p=0.0005 and 120 sec: p=0.0007) stimulation compared to their respective resting control. Comparison of genotypes shows a significant reduction in tyrosine phosphorylation in GPVI–deficient platelets after CRP or Aβ40 stimulation compared to

WT mice at each time point (Fig. 6 A+B; CRP: 30 sec and 120 sec $p<0.0001$; Aβ40: 30 sec $p=0.0210$ and 120 sec $p= 0.0042$).

3.1.2 GPVI externalization and shedding upon Aβ40 stimulation in human und murine platelets

In resting state, human GPVI is localized not only at the surface of the plasma membrane but also in membranes of the α-granules and the surface-associated open canalicular system (OCS) of platelets. After activation with GPVI-specific ligands, e.g. CRP, GPVI can be redistributed to the surface membrane during platelet activation [169]. In addition, previous studies have shown that ligand binding to GPVI can lead to metalloproteinase-mediated cleavage of the GPVI ectodomain (GPVI shedding), resulting in the formation of soluble GPVI (sGPVI) in humans and mice [170]. The results in our previous publication (Donner; Toska et al., Sci Signal 2020, 3.1 [168]) showed that Aβ40 can bind to GPVI on the surface of platelets and trigger platelet activation and aggregation. Here, the aim was to address the question whether or not the activation of GPVI by Aβ40 leads to GPVI shedding or enhanced GPVI externalization at the platelet surface. The agonist convulxin (Cvx) and high doses of collagen are known to induce GPVI shedding and hence were used as positive controls for GPVI shedding in this study.

GPVI abundance on the platelet surface was measured by flow cytometry after 15 minutes (min) or one hour (h) stimulation with the indicated agonists using whole blood from healthy volunteers or mice. In addition, sGPVI levels from the supernatant of isolated platelets upon 1 h stimulation with specified agonists were analyzed by ELISA. The incubation with CRP ($p<0.0001$) or Aβ40 (5 µM $p=0.0004$ and 10 µM $p<0.0001$) induced a rapid increase in GPVI externalization in human platelets compared to resting conditions (Fig. 7 A). After 1 h of incubation with 10 µM of Aβ40 ($p=0.0228$) an increased GPVI surface abundance was measured in comparison to resting conditions (Fig. 7 B). Interestingly, stimulation of the protease-activated receptors (PARs) with thrombin leads to a slight increase in GPVI surface abundance after 15 min ($p= 0.0329$) and 1 h ($p= 0.0293$) of incubation. In contrast, the stimulation with Cvx showed a significant reduction of GPVI on the plasma membrane after 1 h ($p=0.0008$) of incubation (Fig. 7 B). The decreased GPVI surface expression is consistent with an increase in sGPVI in the supernatant of Cvx ($p= 0.0292$) stimulated isolated platelets. No increase in sGPVI was detectable upon CRP or Aβ40 incubation, suggesting that neither CRP nor Aβ40 are able to induce GPVI shedding in human platelets (Fig. 7 C). However, high collagen concentrations resulted in an increase in sGPVI ($p= 0.0146$), which is in line with the published literature [171].

Interestingly, GPVI surface expression was not increased in all tested conditions in mouse platelets. Conversely, stimulation with CRP (15 min p=0.0011 and 1 h p<0.0001) or Cvx (15 min p=0.0106 and 1 h p<0.0001) resulted in decreased GPVI surface abundance, indicating GPVI shedding (Fig. 7 D and E). Aβ40 showed no effect on GPVI surface abundance in murine platelets. In addition, plasma from 15-month-old APP23 and WT mice was analyzed for sGPVI. No differences were detected between the two genotypes (Fig. 7 F). Overall, these results show that, although Aβ40 caused an increased externalization of GPVI at the surface but no GPVI shedding in human platelets *in vitro*, murine platelets do not change their GPVI surface abundance in response to Aβ40.

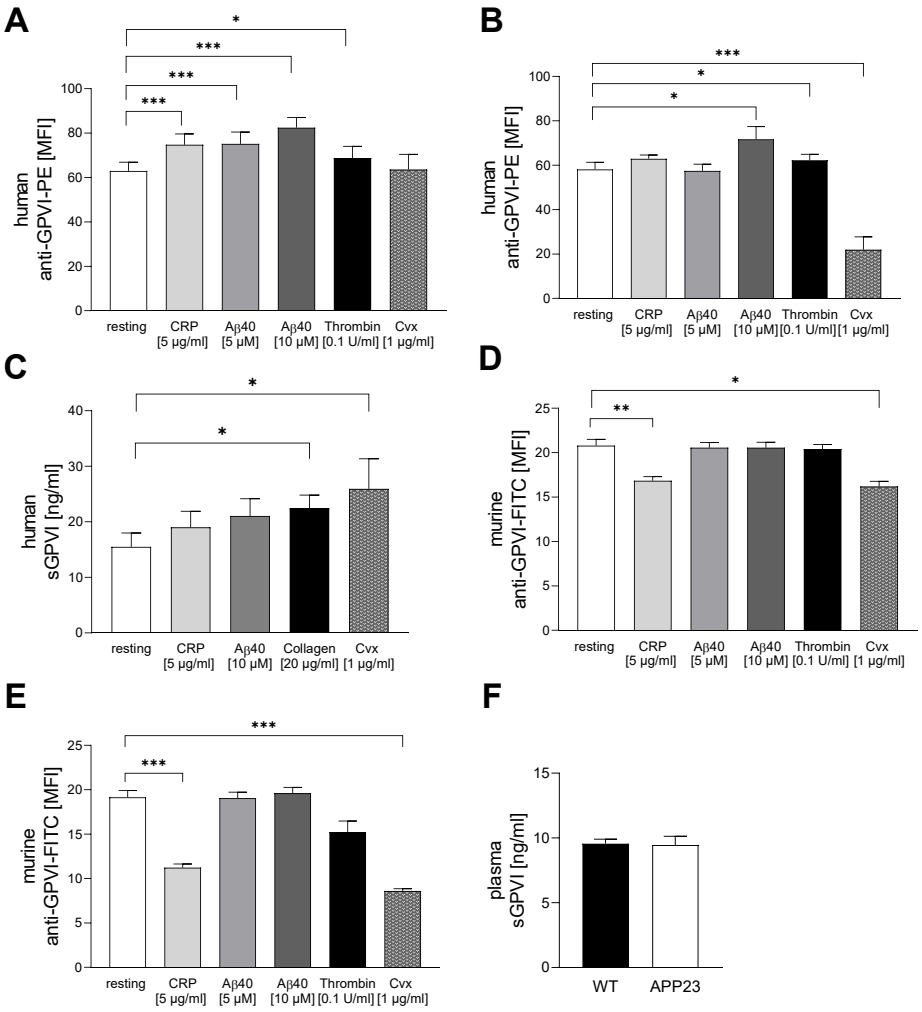

Figure 7: Aβ40 induces an increase in GPVI surface expression in human platelets.
Human whole blood was analyzed by flow cytometry for GPVI surface expression (GPVI-PE) of platelets after stimulation with 5 µg/ml CRP, 5 and 10 µM Aβ40, 0.1 U/ml Thrombin and 1 µg/ml Cvx for 15 min (A) and 1 h (B; n=8). (C) Isolated human platelets were stimulated with the indicated agonists for 1 h, and the supernatant was used for soluble GPVI (sGPVI) by ELISA (n =4). (D and E) Washed whole blood from WT mice was analyzed by flow cytometry to assess GPVI surface expression (GPVI-FITC) after stimulation with 5 µg/ml CRP, 5 and 10 µM Aβ40, 0.1 U/ml thrombin, and 1 µg/ml Cvx for 15 min (D) and 1 h (E), respectively (n=6-7). (F) Plasma sGPVI levels in 15-month-old WT and APP23 mice measured by ELISA (n=9). Statistical analyses were performed using an one-way ANOVA followed by a Dunett's post-hoc test (A-E). Bar graphs indicate mean values ± SEM, *p < 0.05; **p < 0.005; ***p < 0.001. MFI = mean fluorescence intensity, Cvx= Convulxin, CRP = Collagen-related peptide, min = minutes, h= hour, WT = Wildtype.

3.2. Impact of Aβ40 on platelet-mediated inflammation and neutrophil recruitment

3.2.1 Analysis of cytokines and inflammatory markers in APP23 and *Gp6*$^{-/-}$ mice

Many studies indicate that vascular inflammation contributes to neuro-inflammation and leads to neuropathological changes in AD (section 1.1.6). Platelets play a key role in vascular inflammation through the release of fibrinogen, cytokines, etc. and direct interactions with inflammatory cells leading to the recruitment of neutrophils (section 1.2.4). In addition, GPVI on platelets has been shown to play a role in thrombo-inflammatory processes as observed in stroke. In this context, it has been previously described that the inhibition of GPVI interaction with collagen reduced neuronal damage after cerebral reperfusion in the middle cerebral artery occlusion (MCAO) model of experimental stroke, most likely due to reduced inflammatory responses [133].

In this study, plasma fibrinogen, plasma TGF-β1 as well as platelet-neutrophil aggregates (PNAs) were measured in 15-month-old APP23 and age matched WT mice. The results of our previous publication (Donner; Toska et al., Sci Signal 2020, 3.1 [168]) showed that the stimulation of platelets with Aβ40 induces fibrinogen release in a GPVI dependent manner. However, the analysis of the fibrinogen plasma concentration between APP23 and WT mice revealed no differences (Fig. 8 A). In contrast to fibrinogen, TGF-β1 plasma levels were significantly increased in APP23 mice compared to WT mice ($p=0.0006$) (Fig. 8 B). Next, we investigated whether or not Aβ40 is able to induce the release of TGF-β1 in platelets via the GPVI receptor. For this purpose, isolated WT and GPVI deficient platelets were stimulated with Aβ40 and the releasates were analyzed for TGF-β1 levels via ELISA. CRP, as a common GPVI agonist, was used as a positive control. WT platelets showed a significant increase in TGF-β1 release after stimulation with CRP ($p<0.0001$) or Aβ40 ($p=0.0141$). In contrast, in GPVI-deficient platelets, stimulation with CRP or Aβ40 did not result in a significant increase in TGF-β1 release. When Aβ16 was used as a negative control, no TGF-β1 release could be measured neither in GPVI-deficient nor in WT platelets. Thrombin, which induced TGF-β1 release in WT and GPVI-deficient platelets ($p<0.0001$), was used as a control to induce GPVI independent platelet activation via PAR3 and PAR4 receptors (Fig. 8 C). In addition, the concentration of TGF-β1 in whole platelet lysates from *Gp6*$^{-/-}$ and WT mice showed no alterations in total TGF-β1 concentration (Fig. 8 D).

The recruitment of neutrophils to sites of inflammation and the formation of PNAs are fundamental mechanisms of inflammatory processes (section 1.2.4). In acute inflammation such as in response to infection, neutrophils are primarily useful for immunoregulation. However, in chronic sterile inflammation, there is evidence that constant activation of neutrophils may contribute to tissue damage by releasing inflammatory cytokines or NET formation [172]. Furthermore, in 2015, Zenaro et al. demonstrated that neutrophils contribute to Alzheimer's disease pathology by causing vascular and neuronal inflammation [70]. In this study, Aβ40 was previously shown to trigger platelet activation (section 3.1). Activated platelets are able to recruit neutrophils from the bloodstream, leading to neutrophil activation and migration [173]. To study the formation of PNAs upon Aβ40 *in vitro*, washed whole blood was analyzed by flow cytometry. In the resting state, no differences in PNA levels were detected between WT and APP23 mice (Fig. 8 E) and WT and *Gp6*$^{-/-}$ mice (Fig. 8 F). Activation of platelets with CRP leads to an increase in PNA formation in all genotypes except *Gp6*$^{-/-}$ mice. Stimulation with Aβ40 significantly increased PNA formation in all genotypes tested ($p<0.0001$) (Fig. 8 E and F).

Taken together, these results indicate that TGF-β1 is released from platelets upon Aβ40 stimulation in a GPVI-dependent manner. In addition, Aβ40 induces the formation of PNAs suggesting that platelet-mediated inflammation is triggered by Aβ40.

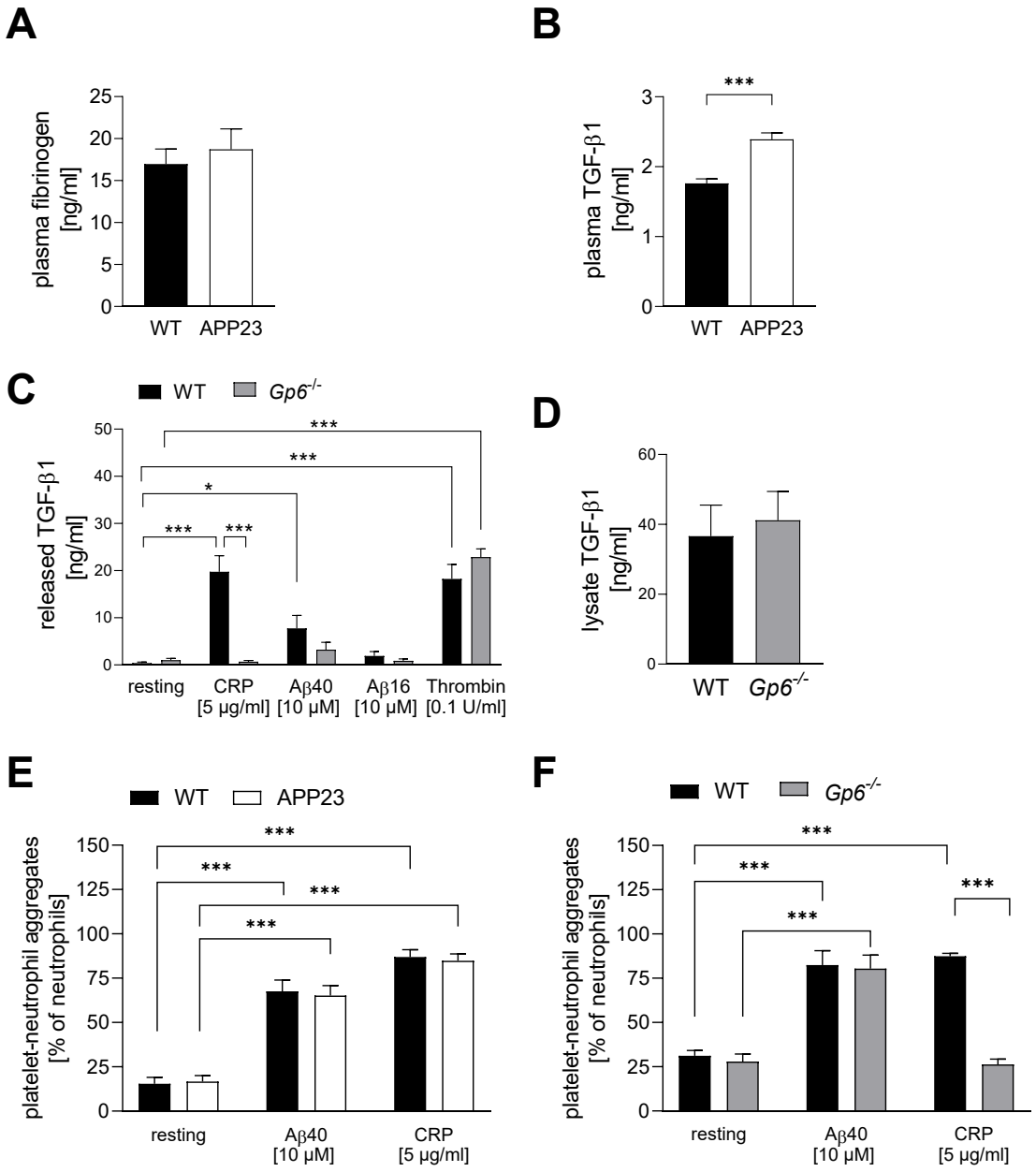

Figure 8: Measurements of an inflammatory cytokine and inflammatory cell recruitment in APP23; *Gp6*$^{-/-}$ and WT mice.

(A and B) Analysis of plasma levels of fibrinogen (n=9) and TGF-β1 (n=5) in APP23 and WT mice at 15 months of age via ELISA. (C) Analyses of TGF-β1 release from platelets in *Gp6*$^{-/-}$ and WT mice upon stimulation with CRP, Aβ40, Aβ16 and thrombin (n=7-8). (D) Analyses of TGF-β1 in platelets lysates of *Gp6*$^{-/-}$ and WT mice. Flow cytometric analyses of platelet (GPIb-PE)-neutrophil (Ly6G-APC) aggregate formation in whole blood from APP23 (E) and *Gp6*$^{-/-}$ (F) mice upon stimulation with Aβ40 or CRP (n=7-9). Statistical analyses were performed using an unpaired t test or two-way ANOVA followed by a Sidak's multiple comparisons post-hoc test. Bar graphs indicate mean values ± SEM, *p < 0.05; ***p < 0.001. MFI = mean fluorescence intensity, CRP = Collagen-related peptide, WT = Wild-type.

3.2.2 Analysis of amyloid-β aggregate formation after co-incubation of platelets with neutrophils *in vitro*

Previously it was shown that platelets are able to modify soluble Aβ40 into fibrillary Aβ aggregates [143] and that inhibition or genetic depletion of GPVI leads to a reduction in fibrillary Aβ aggregates *in vitro* (Donner; Toska *et al*., Sci Signal 2020, 3.1 [168]). Since Aβ40 induces the formation of PNAs, the next step was to analyze whether or not neutrophils play a role in modulating soluble Aβ40 to fibrillar Aβ aggregates or contribute to platelet-mediated aggregation of Aβ40. Therefore isolated murine neutrophils were incubated with Aβ40 and stimulated with ADP for one day. As control, isolated platelets, as well as isolated platelets co-cultured with neutrophils were used. Aβ was visualized by immunofluorescence (IF) staining using the antibody 6E10, platelets were stained with an antibody against GPIb, and neutrophils were labeled with DAPI since they are the only cells with nuclei in this experiment. Single-channel immunofluorescence images are shown in supplemental Figure S1. The supernatant was collected and the remaining soluble Aβ40 was analyzed via Western blot.

In this experimental setup, isolated neutrophils were not able to induce the formation of fibrillar Aβ-aggregates *in vitro*, because no formation of amyloid-β aggregates was observed in cell culture with neutrophils alone. Furthermore the addition of ADP did not result in a significant increase in the formation of fibrillary amyloid-β aggregates (Fig. 9 A). Accordingly, quantification of residual soluble Aβ40 in the supernatant of neutrophil cell culture was significantly increased compared with cell culture experiments where platelets were used (Aβ40: plt vs neu $p= 0.0258$ and neu vs plt + neu $p= 0.0326$; Aβ40 + ADP: plt vs neu $p= 0.0043$ and neu vs plt + neu $p= 0.0089$) indicating that no amyloid-β aggregation had occurred. A co-culture of platelets and neutrophils did not result in increased formation of amyloid-β aggregates compared with platelets alone (Fig. 9 B and C). Quantification of residual soluble Aβ40 in the co-culture compared with platelets alone showed no further reduction. These data suggest that neutrophils, unlike platelets, do not play a role in the formation of amyloid-β fibrils and do not amplify platelet-mediated formation of Aβ40 fibrils *in vitro.*

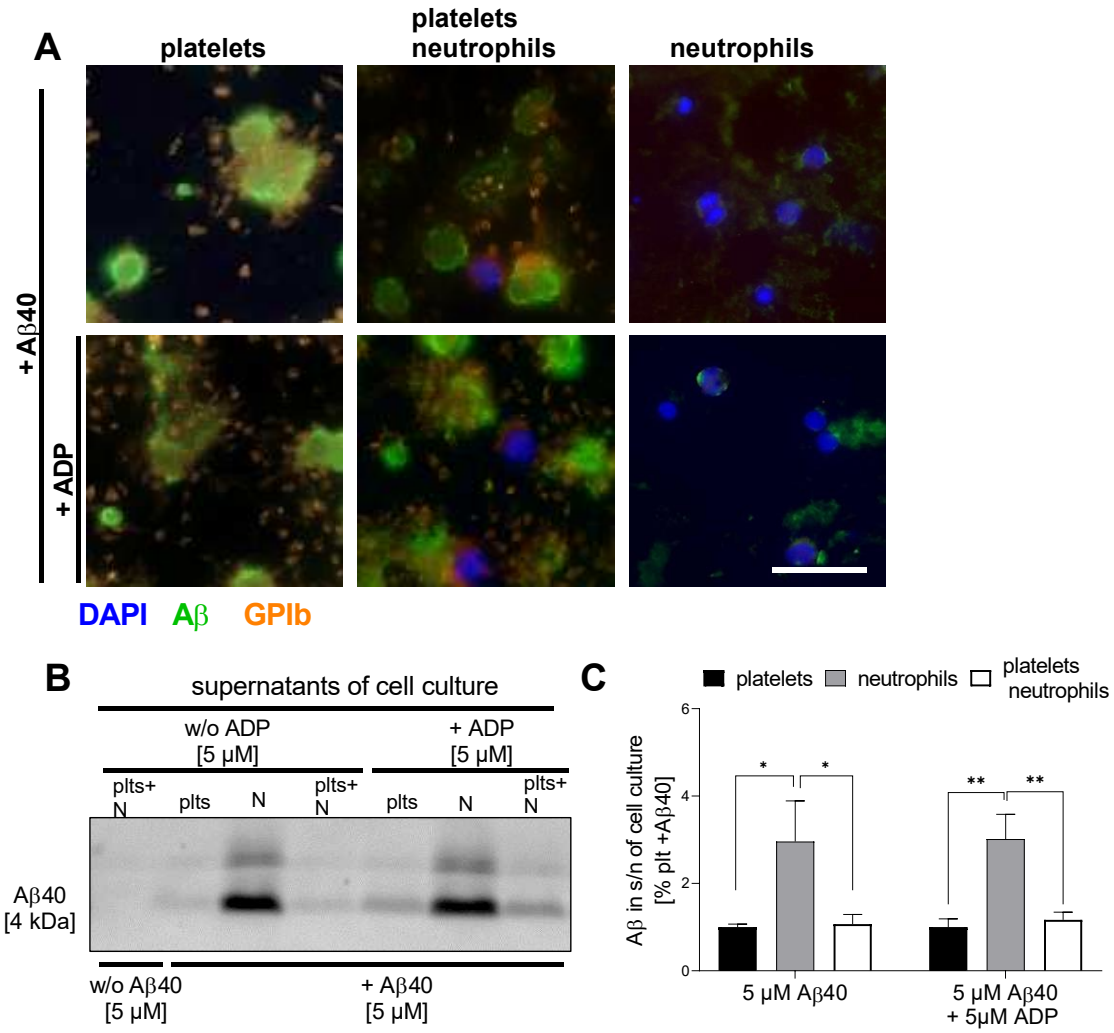

Figure 9: Neutrophils are not involved in the formation of amyloid-β fibrils *in vitro*.
Cell culture experiments were performed with isolated murine platelets and neutrophils in the presence of Aβ40 or Aβ40 and ADP. Supernatants were collected and analyzed via Western blot against remaining soluble Aβ. Amyloid-β aggregates were stained by IF (green=Aβ anti-6E10; orange= plts anti-GPIb) as end-point analysis. (A) Representative images of cell culture experiments. Scale bar = 20 µm. Corresponding Western blot (B) and quantification (C) of soluble Aβ in supernatants from murine cell culture. Scale bar 20 µm. Statistical analyses were performed using a two-way ANOVA followed by a Sidak's multiple comparisons post-hoc test (n= 4-6). Bar graphs indicate mean values ± SEM, *$p < 0.05$; **$p < 0.005$. plts = platelets, N= neutrophils.

3.2.3 Analysis of platelet-induced neutrophil adhesion and extracellular trap formation *in vitro*

Neutrophil accumulation is a characteristic of Alzheimer's disease because it modulates disease-related neuro-inflammatory and vascular signaling pathways [174]. Neutrophil depletion has been shown to improve cognitive abilities in an AD mouse model. Recent studies AD mouse models have shown that the occlusion of capillaries by neutrophils reduces cerebral blood flow and might therefore contribute to the cognitive deficits observed in AD [175]. Here, stimulation with Aβ40 was demonstrated to induce an increase in PNA formation (section 3.2.1). Therefore, we next analyzed whether or not Aβ40 stimulation of platelets is able to support neutrophil adhesion *in vitro.* Murine platelets and neutrophils were co-incubated in the presence of Aβ40 for 3 hours. Adherent neutrophils were visualized via IF staining (myeloperoxidase and DAPI) and quantified using the QuPath bioimage analysis program. Platelets were labeled with the platelet specific marker GPIb.

In order to investigate whether or not the agonists alone exert any effects, neutrophils were incubated with the corresponding agonists in the absence of platelets. No increase in neutrophil adhesion was observed after the addition of CRP, Aβ40, ADP, or a combination of Aβ40 and ADP (supplemental Figure S2). Figure 10 A demonstrates adherent neutrophils in co-culture with platelets after stimulation with indicated agonists as shown by representative images. TNF-α was used as positive control and showed increased neutrophil adhesion compared with resting conditions ($p=0.0047$). The comparison of neutrophil adhesion in the absence and presence of platelets shows no alterations in the absence of any agonist. Interestingly, only CRP ($p=0.0002$) and the combination of ADP and Aβ40 ($p<0.0001$) stimulation leads to an increase in platelet-mediated neutrophil adhesion. Stimulation with either ADP or Aβ40 alone did not alter neutrophil adhesion that might be due to the fact that both ligands are weak platelet agonists (Fig. 10 A and B).

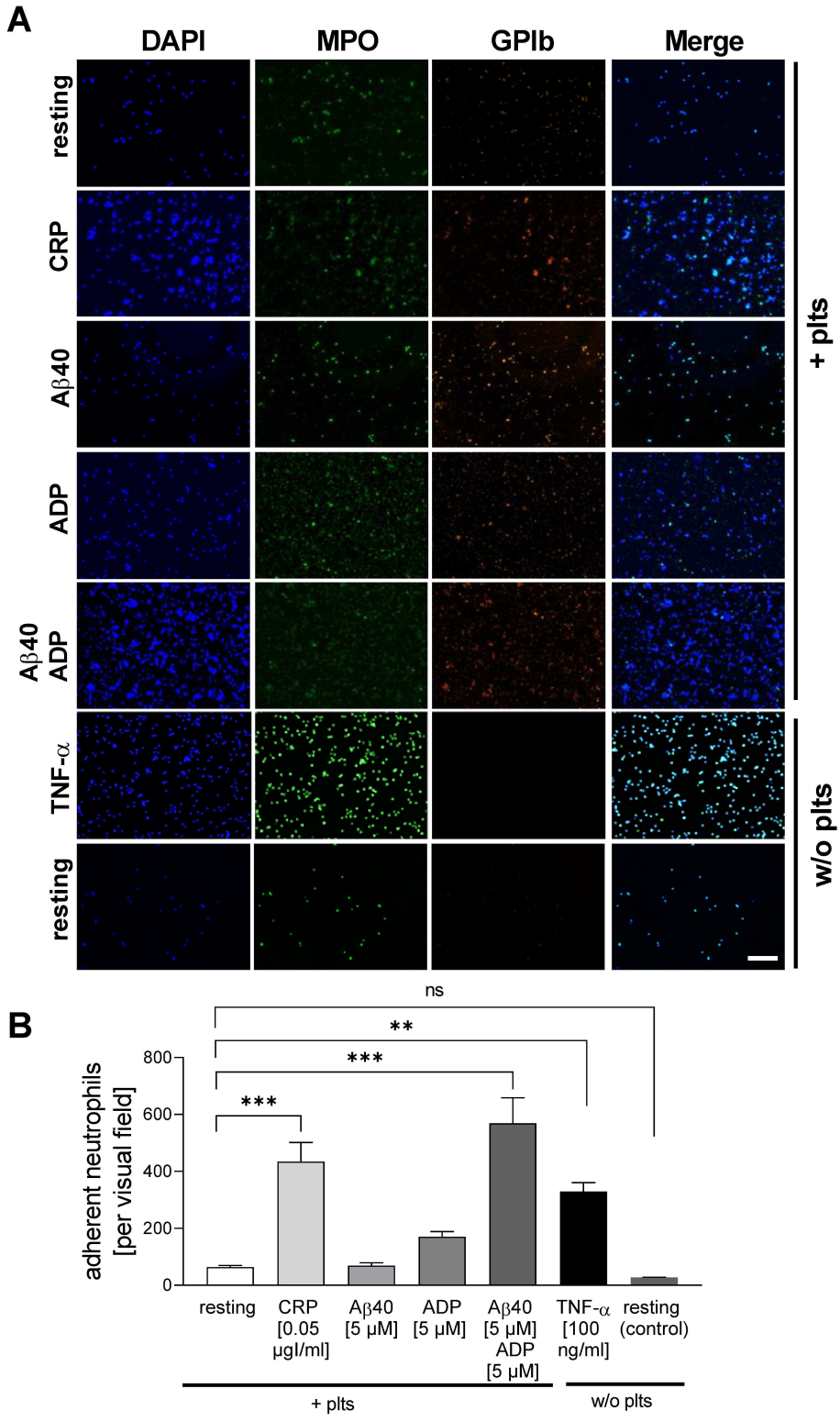

Figure 10: Stimulation of murine platelets with Aβ40 and ADP leads to increased adhesion of neutrophils.

(A) Representative IF images of co-culture experiments with platelets and neutrophils incubated with the indicated agonists for 3 h (MPO=green, GPIb=orange, DAPI=blue). Scale bar = 50 µm. (B) Quantification of neutrophil adhesion when platelets were stimulated with CRP, ADP, Aβ40 or ADP and Aβ40. TNF-α served as a positive control (n=3-11). Statistical analyses were performed using an ordinary one-way ANOVA followed by a Dunnett`s post-hoc test. Bar graphs indicate mean values ± SEM, **p < 0.005; ***p < 0.001, ns= not significant. MPO= Myeloperoxidase.

In addition to the increased accumulation of neutrophils in the vasculature, initial results suggest that neutrophils release extracellular traps (NETs) in the CNS of AD patients and in experimental mouse models [176]. During the formation of NETs, myeloperoxidase (MPO) and neutrophil elastase are released, which can lead to vascular oxidative stress and possible damage the BBB [174]. Therefore, platelet-mediated NET formation with ADP and Aβ40 stimulation was examined *in vitro* in addition to the already observed increase in platelet-mediated neutrophil adhesion (Fig 10).

Isolated platelets were co-incubated with neutrophils and stimulated with the indicated agonists. The supernatant was collected and neutrophil elastase, which is released during NET formation, was measured by ELISA. Neutrophils were stimulated with phorbol 12-myristate 13-acetate (PMA), a known inducer of NET formation that served as positive control. Immunofluorescence microscopy was used to detect NET formation. Representative images of NET formation are depicted in figure 11 A. Single-channel immunofluorescence images are shown in supplemental Figure S3.

Quantification was based on the percentage of neutrophils that formed NETs. PMA induced NET formation in approximately 25% of all neutrophils. In contrast do PMA treatment, NET formation was not observed with all agonists tested in this experiment. Consistently, no increase in neutrophil elastase concentration was measured in respective cell culture supernatants (Fig. 11 C). In addition, the detection of neutrophil elastase in the plasma of 15-month-old APP23 and WT mice revealed no differences between APP23 and WT mice (Fig. 11 D). In conclusion, activation of platelets with ADP and Aβ40 triggers neutrophil adhesion *in vitro*. However, no increased formation of NETs was detected when platelets were stimulated with ADP and Aβ40, suggesting that platelets are not involved in the formation of NETs in AD.

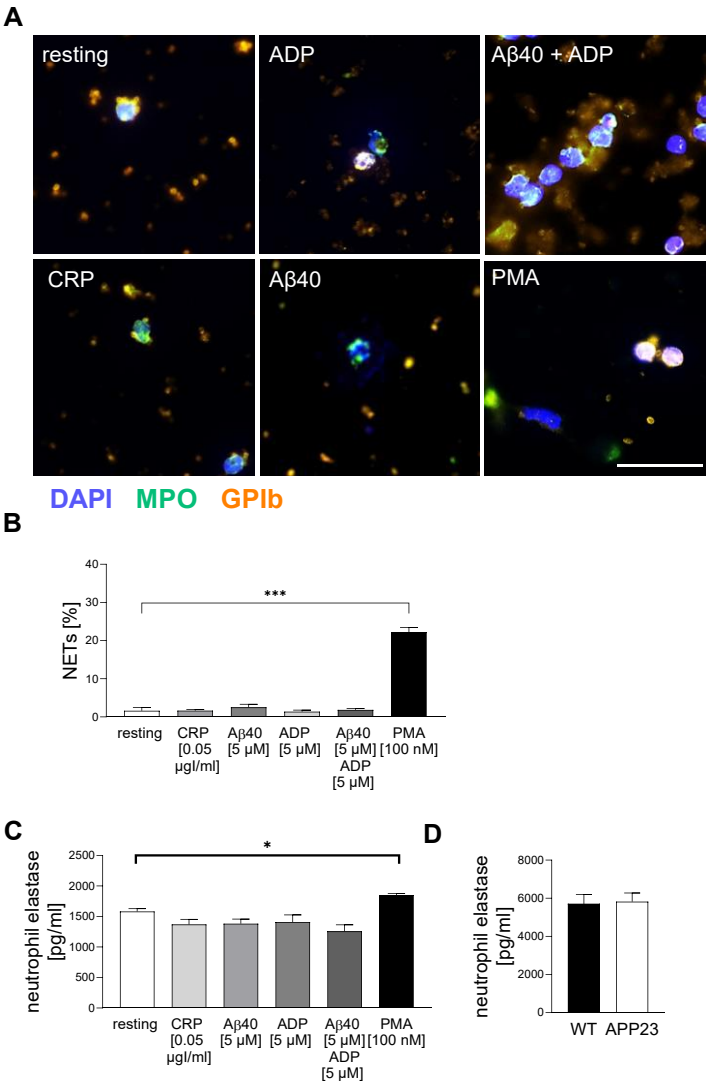

Figure 11: Stimulation of murine platelets with Aβ40 and ADP does not induce NET formation.
(A and B) Analyses of NET formation *in vitro*. Co-culture experiments were performed with the indicated agonists for one day (MPO=green, GPIb=orange, DAPI=blue). (A) Representative images of IF staining from co-culture experiments and (B) quantification of NET formation by calculating the percentage of NET formation related to the total count of neutrophils per visual field. PMA was used as positive control known to induce NET formation (n=3). Scale bar = 30 µm. (C) Quantification of released neutrophil elastase in supernatants from co-culture via ELISA. (E) Measurement of plasma levels of neutrophil elastase in 15-month-old WT and APP23 mice by ELISA (n=5). Statistical analyses were performed using an ordinary one-way ANOVA followed by a Dunnett's post-hoc test. Bar graphs indicate mean values ± SEM, *p < 0.05; **p < 0.005; ***p < 0.001. NETs = Neutrophil extracellular traps, MPO= Myeloperoxidase, PMA= phorbol 12-myristate 13-acetate.

3.2.4 Effects of platelet inhibition on neutrophil adhesion *in vitro*

In this study, Aβ40 was shown to bind to GPVI on the surface of platelets to trigger platelet activation and aggregation (Donner; Toska *et al*., Sci Signal 2020, 3.1 [168]). In addition, Donner *et al.* have already shown that the activation of platelets with ADP and Aβ40 leads to an increase in the expression of activated integrin αIIbβ3 and P-selectin on the platelet surface, which is important for PNA formation (section 1.2.4) [103, 168]. To determine whether platelet-mediated adhesion of neutrophils upon stimulation with ADP and Aβ40 is mediated through GPVI or integrin αIIbβ3, co-cultures were performed in which GPVI-deficient platelets were used or integrin αIIbβ3 was blocked with the inhibitory antibody Leo.H4. Platelets from *Gp6*$^{-/-}$ and WT mice were stimulated with CRP, ADP, Aβ40 or ADP and Aβ40, and where indicated, integrin αIIbβ3 was inhibited with Leo.H4. Neutrophils from WT mice were stained with the specific antibody Ly6G and platelets were labeled with the platelet specific marker GPIb. Representative images of the co-culture are shown in Figure 12 A. Single-channel immunofluorescence images are shown in supplemental Figure S4.

The Quantification reveals that the increase in platelet-mediated neutrophil adhesion after ADP and Aβ40 stimulation was almost completely inhibited when the integrin αIIbβ3 was blocked in platelets of WT mice (663.75± 73.42 in WT platelets vs 95.75 ± 41.43 in WT platelets + Leo.H4) while it was reduced in GPVI-deficient platelets compared to WT platelets (663.75 ± 73.42 in WT platelets vs 263 ± 19.58 in GPVI-deficient platelets). However, stimulation with ADP and Aβ40 of GPVI-deficient platelets still showed an increase in platelet-mediated neutrophil adhesion compared with resting conditions (resting: 62.75 ± 73.42 in GPVI-deficient platelets vs ADP and Aβ40: 263 ± 19.58 in GPVI-deficient platelets). Additional inhibition of platelet integrin αIIbβ3 in GPVI-deficient platelets completely abrogated neutrophil adhesion *in vitro* (resting: 54.5 ± 14.94 in WT platelets; ADP+ Aβ40: 663.75 ± 73.42 in WT platelets vs. 65.5 ± 10.69 in GPVI-deficient platelets + Leo.H4). Stimulation of platelets with CRP leads to an increase in the expression of activated integrin αIIbβ3 and P-selectin and induces the release of fibrinogen via the GPVI receptor on the cell surface [177]. Therefore, CRP as a classical GPVI agonist was used as control. In line with ADP and Aβ40 stimulation of platelets, CRP mediated activation of WT platelets showed an increase in neutrophil adhesion. In contrast, no increase in neutrophil adhesion was measured in GPVI-deficient platelets (Fig. 12 A and B; resting: 62.75 ± 15.46 in GPVI deficient platelets; CRP: 434.25 ± 116.83 in WT platelets vs. 49.5 ± 15.91 in GPVI deficient platelets). Stimulation with ADP or Aβ40 alone showed no increase in neutrophil adhesion in both WT and GPVI deficient platelets (Fig. 12).

In summary, enhanced neutrophil adhesion following platelet stimulation with ADP and Aβ40 is mediated by integrin αIIbβ3 and, in part, by GPVI at the platelet surface.

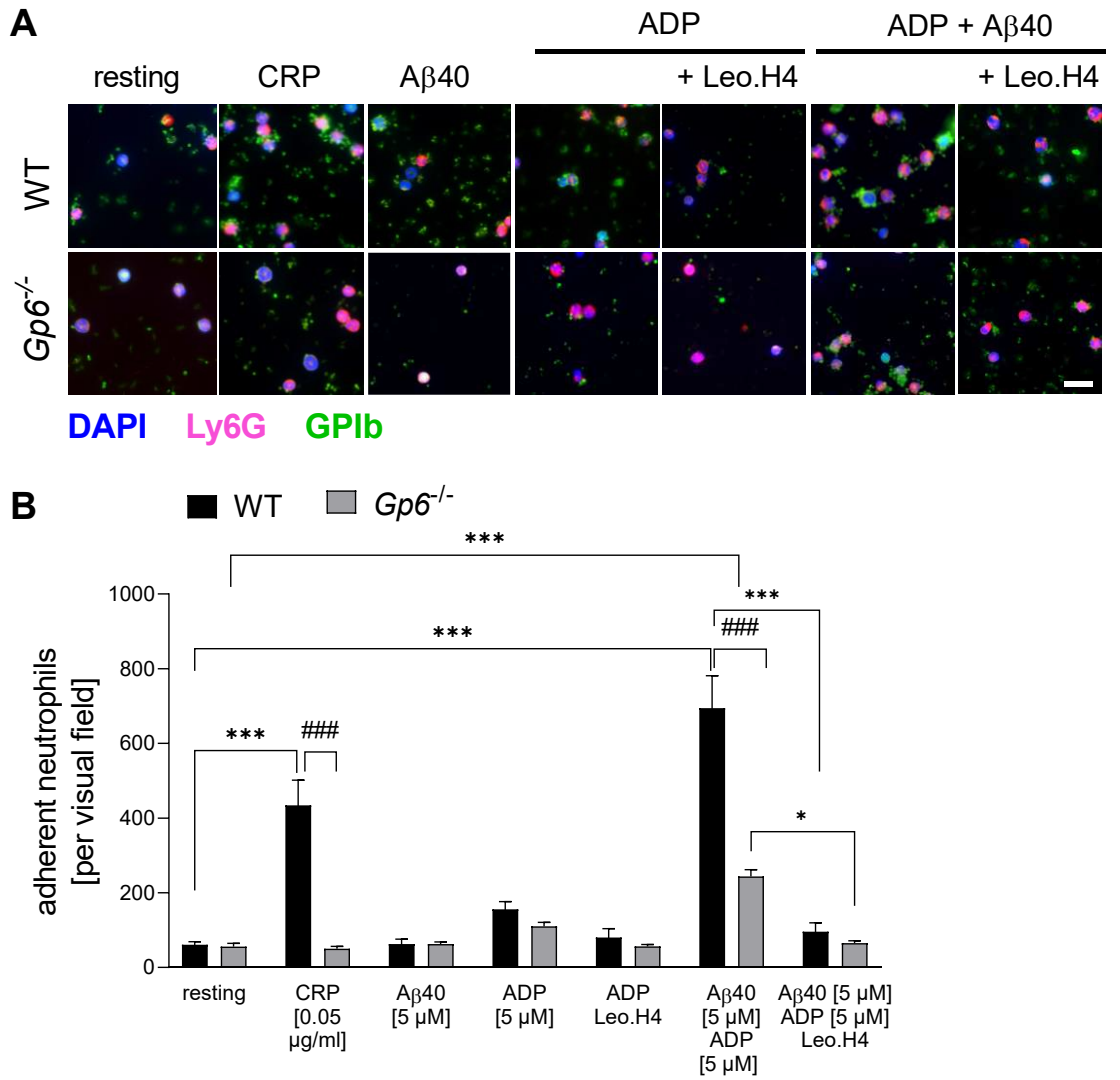

Figure 12: Inhibition of integrin αIIbβ3 or genetic deletion of GPVI reduces neutrophil adhesion *in vitro*.

Representative images of IF staining in co-cultures of platelet and neutrophils (DAPI=blue, Ly6G=purple, GPIb= green). Platelets from WT- and GPVI deficient mice were incubated with the indicated agonists in the presence or absence of the integrin αIIbβ3 inhibitory antibody Leo.H4 and co-cultured with neutrophils from WT mice for 3 hours at 37°C and 5% CO2. (B) Quantification of neutrophil adhesion (n=4-7). Scale bar 20 µm. Statistical analyses were performed using a two-way ANOVA followed by a Sidak's multiple comparisons post-hoc test. ###p < 0.001; ***p < 0.001.

3.2.5 Analysis of human platelet-induced neutrophil adhesion and extracellular trap formation

According to Zenaro *et al*. who demonstrated that neutrophils adhere to brain vessels in AD patients and are also present in the parenchyma where they form NETs [70], we analyzed platelet-mediated adhesion and NET formation of isolated human neutrophils in addition to murine experiments.

The first aim was to investigate whether or not human platelets stimulated with Aβ40 support neutrophil adhesion *in vitro*. Therefore, co-culture experiments were performed using isolated platelets and neutrophils that were stimulated with the indicated agonist for 3 hours. Figure 13 A shows representative images of the co-culture and figure 13 B shows the quantification of the experiments. Similar to murine platelets and neutrophils, the stimulation of human platelets with ADP and Aβ40 led to an increase in platelet-mediated neutrophil adhesion ($p= 0.0024$). Incubation of neutrophils with agonists alone did not amplify neutrophil adhesion and served as negative controls (supplemental Figure S 5). PMA was used as a positive control showing increased NET formation and was therefore not included in the quantification analysis.

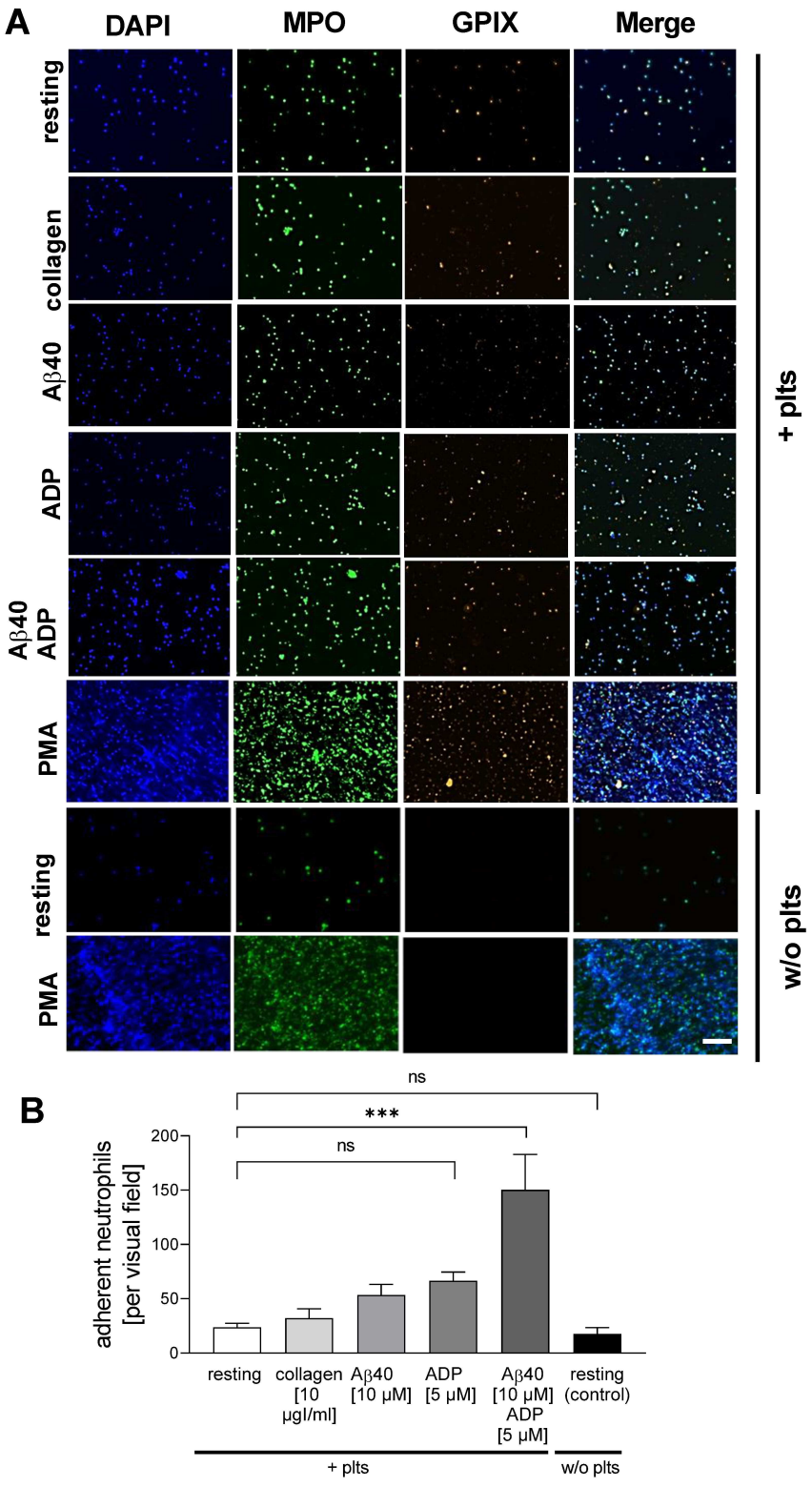

Figure 13: Stimulation of human platelets with Aβ40 and ADP leads to increased adhesion of neutrophils.

(A) Representative images of IF staining from human co-culture experiments with platelets and neutrophils incubated with the indicated agonists for 3 h (MPO=green, GPIb=orange, DAPI=blue). Scale bar = 50 µm. (B) Quantification of neutrophil adhesion after platelet stimulation with collagen, ADP, Aβ40 or ADP and Aβ40. The PMA (positive) control was excluded from the quantification because neutrophil counting was not possible due to increased NET formation. Statistical analyses were performed using ordinary one-way ANOVA multiple comparisons followed by a Dunnett`s post-hoc test n=3-4. Bar graphs indicate mean values ± SEM, *p < 0.05; ***p < 0.001; MPO= Myeloperoxidase, PMA= phorbol 12-myristate 13-acetate.

The second aim was to analyze whether or not human platelets are able to induce the formation of NETs after ADP and Aβ40 stimulation *in vitro*. Representative images of NET formation are depicted in figure 14 A. Single-channel immunofluorescence images are shown in supplemental Figure S 6. Quantification indicate no NET formation of human neutrophils when incubated with platelets after ADP and/or Aβ40 stimulation (Fig. 14 B). In addition to the adhesion experiments, the supernatants were collected from co-cultures and neutrophil elastase levels were analyzed via ELISA (Fig. 14 C). Only the stimulation with PMA (positive control) resulted in an increase in soluble neutrophil elastase ($p<0.0001$), indicating that platelets are not able to induce NET formation after stimulation with Aβ40 in this experimental setup. Consistent with the results of murine experiments, ADP and Aβ40 mediated activation of human platelets stimulates neutrophil adhesion without affecting NET formation.

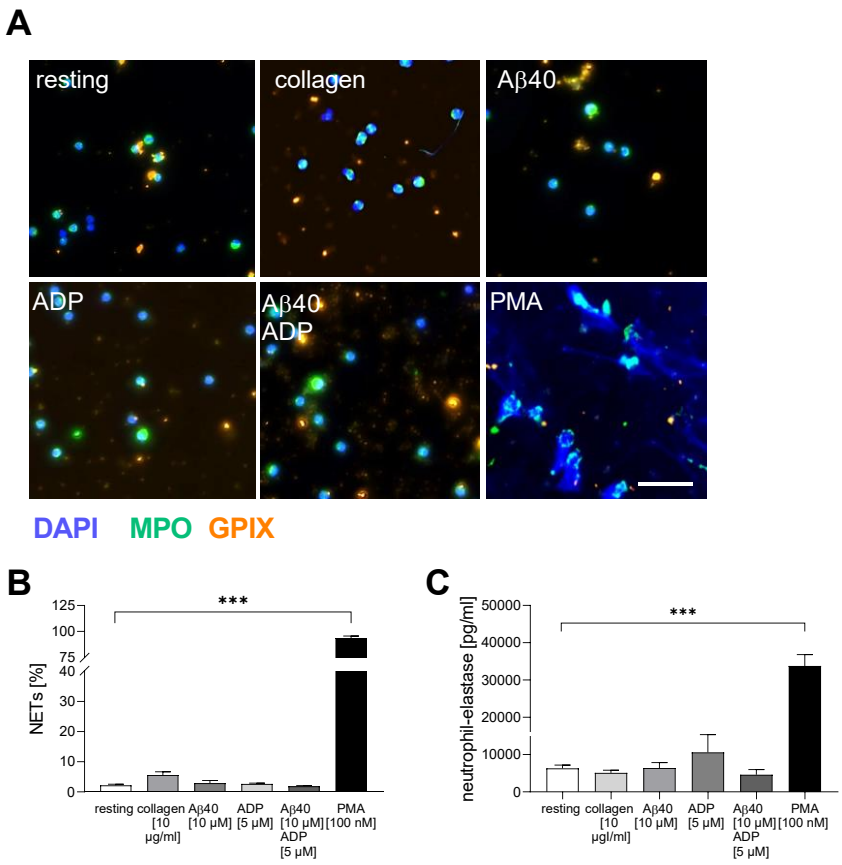

Figure 14: Stimulation of human platelets with Aβ40 and ADP does not induce NET formation.
(A and B) Analyses of NET formation in vitro. Co-culture experiments were performed using the indicated agonists for platelet activation for 3 hours. (A) Representative images of IF staining from co-culture experiments and (B) quantification of NETs as a percentage of adherent neutrophils. PMA was used as positive control to induce NET formation (n=3). Scale bar 20 µm. (C) Quantification of released neutrophil elastase into the supernatant of co-incubated platelets and neutrophils using ELISA. Statistical analyses were performed using an one-way ANOVA followed by a Dunett's post-hoc test n=3-4. Bar graphs indicate mean values ± SEM, ***$p < 0.001$. NETs = Neutrophil extracellular traps, MPO= Myeloperoxidase, PMA= phorbol 12-myristate 13-acetate.

In conclusion, APP23 mice exhibited increased plasma levels of the cytokine TGF-β1, which is released upon platelets stimulation with Aβ40. Moreover the activation of platelets with Aβ40 resulted in the formation of PNAs. Dual stimulation of platelets with ADP and Aβ40 supports neutrophil adhesion *in vitro*, due to the activation of integrin αIIbβ3 and GPVI at the platelet surface. However, platelet activation does not induce NET formation of neutrophils after stimulation with Aβ40 and ADP *in vitro*.

3.3. Impact of amyloid-β on platelet mitochondrial function and platelet–mediated amyloid aggregation in Alzheimer´s disease

Lili Donner[1,*], Tobias Feige[1], Carolin Freiburg[1], Laura Mara Toska[1], Andreas S. Reichert[2], Madhumita Chatterjee[3] and Margitta Elvers[1,*] [178]

1 Department of Vascular and Endovascular Surgery, Experimental Vascular Medicine, Medical Faculty and University Hospital Düsseldorf, Heinrich-Heine University Düsseldorf, 40225 Düsseldorf, Germany

2 Institute of Biochemistry and Molecular Biology I, Medical Faculty and University Hospital Düsseldorf, Heinrich-Heine University Düsseldorf, 40225 Düsseldorf, Germany

3 Department of Cardiology and Angiology, Universitätsklinikum Tübingen, Medizinische Klinik III, 72076 Tübingen, Germany

*Authors to whom correspondence should be addressed

Published in: Int. J. Mol. Sci. 2021

Impact Factor: 6.208

Own contribution to publication: ATP release; platelet aggregation; ROS generation in WT and *Gp6*$^{-/-}$ mice (Figure 5).

International Journal of *Molecular Sciences*

MDPI

Article

Impact of Amyloid-β on Platelet Mitochondrial Function and Platelet–Mediated Amyloid Aggregation in Alzheimer's Disease

Lili Donner [1,*], Tobias Feige [1], Carolin Freiburg [1], Laura Mara Toska [1], Andreas S. Reichert [2], Madhumita Chatterjee [3] and Margitta Elvers [1,*]

[1] Department of Vascular and Endovascular Surgery, Experimental Vascular Medicine, Medical Faculty and University Hospital Düsseldorf, Heinrich-Heine University Düsseldorf, 40225 Düsseldorf, Germany; Tobias.Feige@med.uni-duesseldorf.de (T.F.); Carolin.Freiburg@uni-duesseldorf.de (C.F.); LauraMara.Toska@med.uni-duesseldorf.de (L.M.T.)

[2] Institute of Biochemistry and Molecular Biology I, Medical Faculty and University Hospital Düsseldorf, Heinrich-Heine University Düsseldorf, 40225 Düsseldorf, Germany; reichert@hhu.de

[3] Department of Cardiology and Angiology, Universitätsklinikum Tübingen, Medizinische Klinik III, 72076 Tübingen, Germany; madhumita.chatterjee@med.uni-tuebingen.de

* Correspondence: Lili.Donner@med.uni-duesseldorf.de (L.D.); Margitta.Elvers@med.uni-duesseldorf.de (M.E.)

Abstract: Background: Alzheimer's disease (AD) is characterized by an accumulation of amyloid β (Aβ) peptides in the brain and mitochondrial dysfunction. Platelet activation is enhanced in AD and platelets contribute to AD pathology by their ability to facilitate soluble Aβ to form Aβ aggregates. Thus, anti-platelet therapy reduces the formation of cerebral amyloid angiopathy in AD transgenic mice. Platelet mitochondrial dysfunction plays a regulatory role in thrombotic response, but its significance in AD is unknown and explored herein. Methods: The effects of Aβ-mediated mitochondrial dysfunction in platelets were investigated in vitro. Results: Aβ40 stimulation of human platelets led to elevated reactive oxygen species (ROS) and superoxide production, while reduced mitochondrial membrane potential and oxygen consumption rate. Enhanced mitochondrial dysfunction triggered platelet-mediated Aβ40 aggregate formation through GPVI-mediated ROS production, leading to enhanced integrin $\alpha IIb\beta_3$ activation during synergistic stimulation from ADP and Aβ40. Aβ40 aggregate formation of human and murine (APP23) platelets were comparable to controls and could be reduced by the antioxidant vitamin C. Conclusions: Mitochondrial dysfunction contributes to platelet-mediated Aβ aggregate formation and might be a promising target to limit platelet activation exaggerated pathological manifestations in AD.

Keywords: Alzheimer's disease; platelets; mitochondria dysfunction; Aβ aggregation; cerebral amyloid angiopathy; ROS; GPVI; integrin

Citation: Donner, L.; Feige, T.; Freiburg, C.; Toska, L.M.; Reichert, A.S.; Chatterjee, M.; Elvers, M. Impact of Amyloid-β on Platelet Mitochondrial Function and Platelet-Mediated Amyloid Aggregation in Alzheimer's Disease. *Int. J. Mol. Sci.* **2021**, *22*, 9633. https://doi.org/10.3390/ijms22179633

Academic Editor: Isabella Russo

Received: 20 July 2021
Accepted: 2 September 2021
Published: 6 September 2021

1. Introduction

The most prevalent form of dementia is Alzheimer's disease (AD). AD is characterized by the pathological hallmarks of abnormal accumulation of amyloid β (Aβ) peptides in the brain [1]. One of the earliest pathological alterations in AD is the dysfunction of mitochondria [2]. Mitochondrial abnormalities, such as impaired mitochondrial dynamics (increased fission and reduced fusion), altered morphology and mitochondrial gene expression, increased free radical production and lipid peroxidation, reduced cytochrome c oxidase (COX) activity and ATP production, are typical characteristics of AD. Mitochondrial dysfunction results from these morphological and metabolic alterations during the progression of AD [2–5]. Soluble Aβ enters mitochondria and is responsible for mitochondrial dysfunction that contributes to phosphorylation of tau, increased formation of free radicals, mtDNA damage and interaction of Aβ with Drp1, Aβ-binding alcohol dehydrogenase (ABAD) and cyclophilin D (CypD), loss of cytochrome c oxidase (COX) activity, impaired gating of the mitochondrial permeability transition pore and loss of membrane potential.

In the presence of Aβ, mitochondria are reduced in size due to excessive mitochondrial fragmentation and reduced mitochondrial fusion, but increased in numbers [6–10]. Increased levels of Aβ in the cytoplasm of AD neurons also lead to reduced levels of parkin and PTEN-induced putative kinase1 (PINK1) leading to the inability to clear damaged mitochondria (mitophagy) and other cellular debris from neurons [11]. Persisting mitochondrial dysfunction contributes to synaptic dysfunction because declined mitochondrial biogenesis leads to reduced ATP levels that is essential for delivery of neurotransmitters by synaptic vesicles to the synapse [12]. Furthermore, the loss of COX activates apoptotic pathways, leading to the loss of neurons in the central nervous system [6]. As a compensatory mechanism for dysfunctional energy metabolism, mitochondrial-encoded genes are upregulated in AD transgenic mice [10]. While mitochondrial dysfunction plays a central role in the pathogenesis of AD, the dysregulated mitophagy is causative in worsening disease pathology/severity in AD.

Platelets expose amyloid precursor protein (APP) at the platelet membrane and include all the necessary enzymes for the generation of different Aβ peptides from APP in their alpha granules [13]. Therefore, platelets are a source of Aβ peptides in blood [14]. Furthermore, apoptotic platelets are able to incorporate oligomeric Aβ40 [15]. Different studies have identified pathological alterations in isolated platelets from AD patients, such as a decreased amyloid protein precursor ratio and an increased activity of β-secretase leading to Aβ production [16,17]. Moreover, AD patients exhibit increased basal activation of platelets, denoted by enhanced surface expression of P-selectin and presence of activated integrin $\alpha_{IIb}\beta_3$ [18]. Pre-activated platelets in the circulation are also observed in the AD transgenic mouse model APP23. These platelets adhere to amyloid deposits in cerebral vessels causing vessel occlusion [19]. A subpopulation of coated platelets with high procoagulant activity is elevated in AD patients and correlates with the progression of AD [20]. Interestingly, apart from their ability to generate Aβ peptides, predominantly Aβ40, platelets also modify soluble synthetic Aβ40 into toxic Aβ aggregates in vitro [15]. Platelet-specific receptors, namely integrin $\alpha_{IIb}\beta_3$ and collagen receptor glycoprotein (GP)VI, were identified as direct binding partners of Aβ40 at the platelet membrane that contribute to platelet activation and aggregation of Aβ40 peptides [21–23].

Although platelets contain only five to eight mitochondria per cell [24], they play an important role in energy metabolism and ATP production in platelets. Moreover, mitochondria are also involved in platelet activation and apoptosis [25]. Previous studies have provided evidence for altered mitochondrial function in platelets from AD patients. Compared to platelet mitochondria from healthy volunteers, platelet mitochondria from AD patients exhibit decreased maximal capacity of the electron transport system and reduced respiration rates [26,27]. In addition, platelets from AD patients show decreased COX activity, which is associated with ROS overproduction [28].

Despite the extensive research work in the last decades and the progress that has been made to understand the pathophysiology of AD, there are many open questions in understanding the molecular basis of the disease. However, it is well accepted that AD is a multi-factorial neurodegenerative disease and there is still no drug or therapy available to delay or even prevent dementia in patients with AD. In recent years it has been increasingly recognized that platelets can not only serve as a biomarker for the disease but also substantially contribute to the progression of AD. However, the impact of platelets in AD progression is not fully understood. Therefore, the present study aimed to investigate the effect of Aβ40 peptides on platelet mitochondrial dynamics and its consequences for platelet activation and Aβ40 aggregate formation.

2. Results

2.1. Effects of Aβ40 on Mitochondria in Platelets

Generation of reactive oxygen species (ROS) plays an influential role in pathophysiological platelet functions [29]. To investigate the effect of Aβ40 on intracellular ROS production in platelets, we measured ROS by flow cytometry using the dye DCF-DA.

The cellular ROS level in platelets from healthy donors was significantly increased upon stimulation with Aβ40 (Figure 1A). In contrast, the stimulation with Aβ1-16 (Aβ16, used as negative control) did not lead to increased ROS levels. To determine the impact of Aβ40 on mitochondrial superoxide production, we used the mitochondrial localized ROS sensitive dye MitoSOX-Red. The generation of mitochondrial superoxide was increased upon Aβ40 stimulation and unaltered by Aβ16 (Figure 1B). Using the cationic dye TMRM, we determined whether or not stimulation of platelets with Aβ40 led to a loss of the mitochondrial transmembrane potential (Δψm) (Figure 1C). As shown in Figure 1C, the incubation of platelets with Aβ40 led to significantly reduced Δψm in platelets, whereas Aβ16 showed no effect.

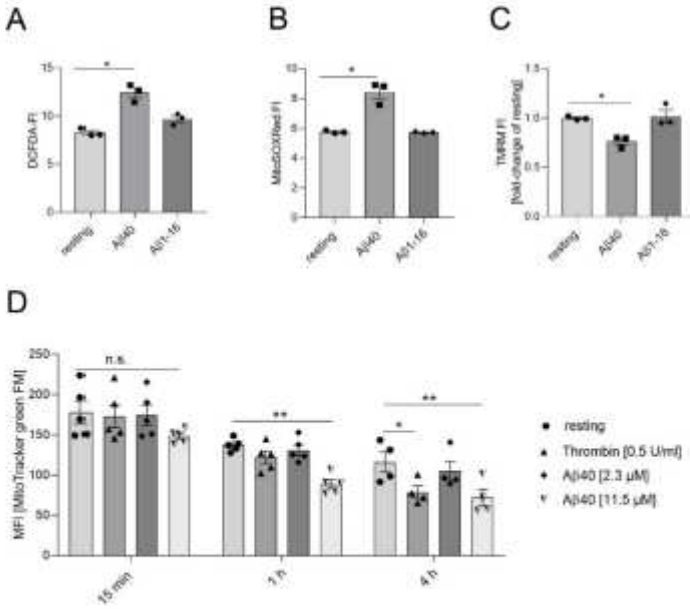

Figure 1. Impact of Aβ on mitochondrial functions in platelets. (**A**) Washed human platelets were incubated for 24 h with 11.5 µM Aβ40 and 11.5 µM Aβ1-16 (as control). Generation of ROS was reported as mean fluorescence intensity of DCF (n = 3). (**B**) MitoSOXRed™-loaded platelets were incubated with 5 µM Aβ40 and 5 µM Aβ1-16 for 30 min and the generation of superoxide was measured as mean fluorescence intensity (n = 3). (**C**) Depolarization of the platelet mitochondrial membrane upon 5 µM Aβ40 and 5 µM Aβ1-16 was observed by decreased TMRM fluorescence intensity (n = 3). (**D**) The mitochondrial dye, MitoTracker™ green FM, was added to platelets to determine the release of mitochondria upon Aβ40 stimulation (n = 4–5). Compared to control (resting). (**A**–**D**) All samples were measured by flow cytometry. Bar graphs depict mean values ± SEM. All analyses were performed using one-way ANOVA and Dunnett's multiple comparisons post-hoc test. ** $p < 0.01$; * $p < 0.05$. n.s.: not significant.

Bourdeau and colleges have shown that activation of platelets induces release of mitochondria to promote inflammatory response [30]. Using a mitochondria-selective, yet membrane potential insensitive, fluorescent dye (MitoTracker™ green FM, Invitrogen), we detected that thrombin activation of platelets led to a reduced mean fluorescence intensity (MFI) consistent with the release of mitochondria after 4 h of incubation (Figure 1D). By contrast, platelets started to release mitochondria upon stimulation with 11.5 µM Aβ40 already after 1 h and continued till 4 h of incubation, while no effects could be seen with lower concentrations of Aβ40 (2.3 µM) (Figure 1D).

2.2. Reduced Mitochondrial Respiration in Platelets Following Aβ40 Treatment

Using the Seahorse Extracellular Flux Analyzer, platelet mitochondrial respiration was investigated after incubation with soluble Aβ40 by measuring the oxygen consumption rate (OCR). Aβ40 or vehicle (medium) was added to platelets for 30 min before measurement. The basal OCR in platelets in the presence of Aβ40 was comparable to resting platelets (control) after 30 min (Figure 2A,B). After injection of collagen related peptide (CRP) to activate the major collagen receptor GPVI, we found a general stimulation of respiration rates (Figure 2A,C). Importantly, a significant relative reduction of OCR in platelets was evident always when Aβ40 was added irrespective of the addition of CRP. A significant reduction of the OCR over time was also found when platelets were incubated with Aβ40 compared to unstimulated platelets (Figure 2A,C). To measure ATP-linked respiration, the ATP synthase inhibitor oligomycin was added subsequently. Again, CRP induced an enhanced OCR compared to non-stimulated platelets. However, in the presence of Aβ40, CRP-induced OCR was significantly reduced (Figure 2A,D). Afterwards, the proton ionophore and uncoupler FCCP was injected to measure maximal respiration (Figure 2A,E). As expected, the injection of FCCP led to increased respiration in CRP-stimulated platelets. Again, the presence of Aβ40 reduced maximal respiration in both resting and in CRP-stimulated platelets. Moreover, the increase of CRP-induced maximal respiration was reduced to basal (resting) levels when platelets were incubated with Aβ40 (Figure 2A,E). Proton leak across the inner mitochondrial membrane was not changed in the presence of Aβ40 (Figure 2A,F). Non-mitochondrial respiration ascertained using the mitochondrial complex inhibitors Antimycin A and Rotenone was not altered between groups (Figure 2A,G). Taken together, these results demonstrate that Aβ40 negatively impacts mitochondrial respiration in resting and CRP-stimulated platelets.

2.3. Impact of Extracellular Aβ40 on Mitochondrial Proteins

To investigate the impact of extracellular Aβ40 on mitochondrial proteins, such as PTEN-induced putative kinase 1 (PINK1), translocase of the inner membrane 23 (TIM23), 60 kDa heat shock protein (Hsp60), optic atrophy-1 (OPA1) and translocase of the outer membrane 20 (TOM20) in platelets, we incubated platelets with different concentrations of Aβ40 for 2 h and analyzed protein expression by Western blot. Non-stimulated platelets were used as negative and CRP-stimulated platelets were used as positive control. The incubation with different concentrations of Aβ40 for 1 h did not induce alterations in the level of the examined proteins (Figure S1). After incubation of platelets with Aβ40 for 2 h, the protein levels of PINK1, TIM23 and Hsp60 were comparable to that of resting platelets (Figure 3A and Figure S2). However, the protein level of TOM20 was significantly reduced when human platelets were stimulated with intermediate and high concentrations of Aβ40 as well as with CRP (Figure 3A,B), suggesting that downregulation of TOM20 is not due to Aβ40 toxicity but due to platelet stimulation. Determination of the ratio of long OPA1/short OPA1 revealed no significant alterations and a trend towards a reduced ratio was only observed when platelets were stimulated with CRP. Addition of Aβ40 did not significantly alter the ratio of long OPA1/short OPA1.

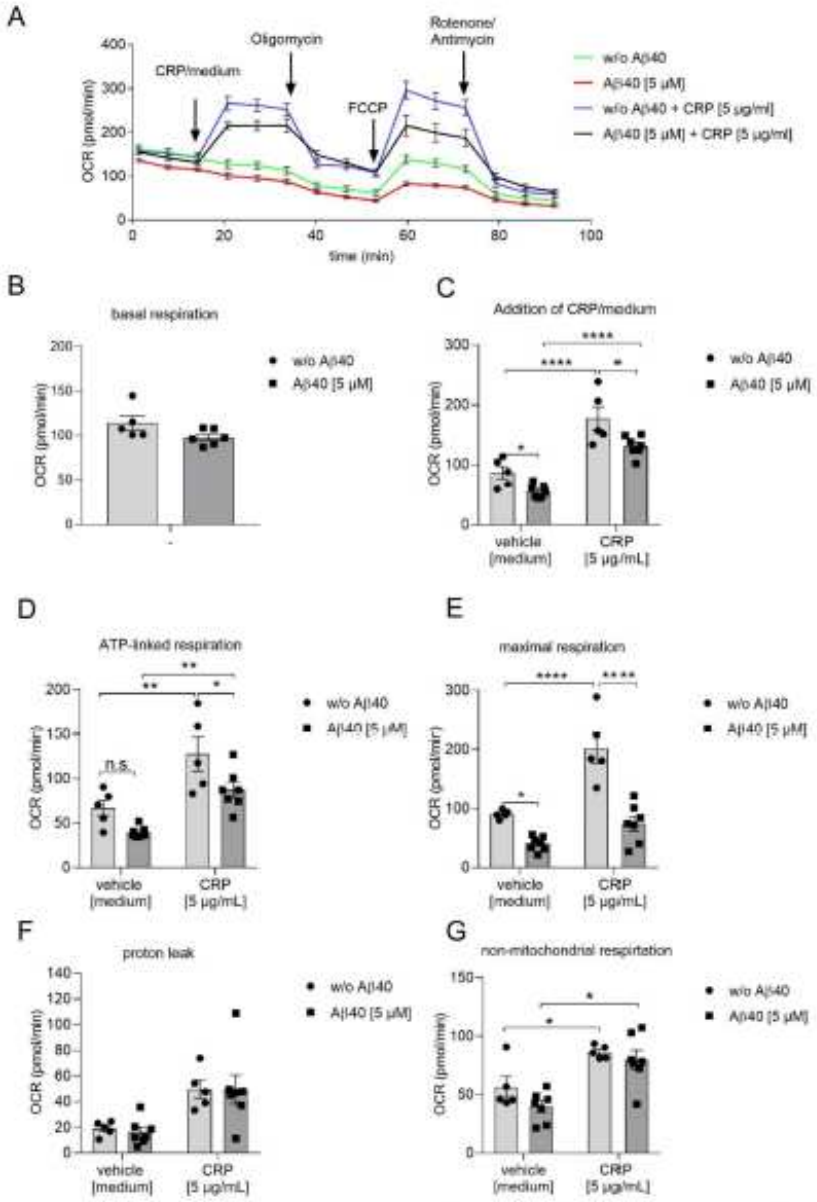

Figure 2. Determination of oxygen consumption rate (OCR) in human platelets upon treatment with Aβ40. (**A**) Determination of the oxygen consumption rate (OCR) after injection of indicated chemicals at indicated time points using a Seahorse XF24 analyzer. (**B**) Basal respiration, (**C**) respiration after addition of collagen-related peptide (CRP) or vehicle (medium), (**D**) ATP-linked respiration, (**E**) maximal respiration, (**F**) proton leak and (**G**) non-mitochondrial respiration. (**A**–**G**) Data represent mean ± SEM from n = 5–7 donors, two-way ANOVA with Holm-Sidak's multiple comparisons test, **** = $p < 0.0001$; ** = $p < 0.01$; * = $p < 0.05$. w/o: Without; n.s.: Not significant.

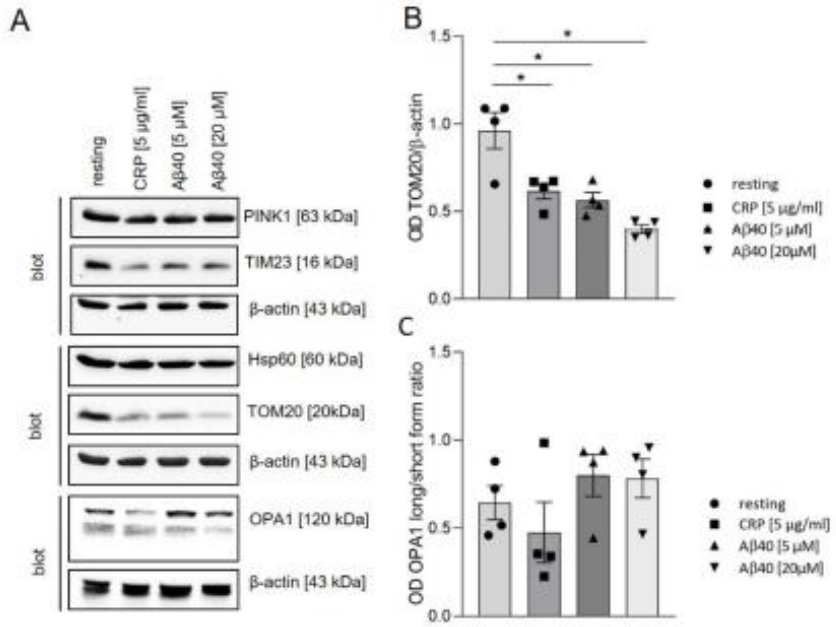

Figure 3. Expression levels of mitochondrial proteins in platelets upon Aβ40 stimulation. (**A**) Human platelets were stimulated with 5 or 20 µM Aβ40 or 5 µg/mL CRP for 2 h. Using Western blot analysis, the expression levels of mitochondrial proteins were detected as indicated. β-actin served as loading control. (**B**,**C**) The intensity of bands was analyzed with ImageJ software. Data represent mean value ± SEM (n = 4). All analyses were performed using one-way ANOVA and Dunnett's multiple comparisons post-hoc test. * = $p < 0.05$.

2.4. *Inhibition of Complex III Leads to Enhanced Platelet Mediated Aβ Aggregate Formation In Vitro*

Platelets are able to modulate soluble, synthetic Aβ40 into forming amyloid aggregates in vitro [15,21–23]. To analyze the role of mitochondria in platelet-mediated Aβ aggregation, we treated human platelets with antimycin A (or with EtOH as vehicle) and incubated the cells with soluble, synthetic Aβ40 for three days. Treatment of platelets with synthetic Aβ40 in presence of antimycin A led to increased Aβ aggregate formation in a concentration-dependent manner (Figure 4A,B). The highest aggregate formation was detected in the presence of 500 and 1000 ng/mL antimycin A. Previously it was demonstrated that complex III-derived ROS triggers the formation of Aβ40 by enhanced amyloidogenic amyloid precursor protein processing in HEK293 cells [31]. To investigate whether or not the inhibition of complex III per se leads to the production of Aβ40 in platelets, we incubated platelets with antimycin A for 24 h. However, as shown in Figure 4C, no increase was detected in Aβ40 levels after inhibition of the mitochondrial respiratory complex III (Figure 4C), suggesting that endogenous Aβ40 production does not significantly contribute to Aβ40 aggregate formation in platelet culture.

Aβ40 induces ROS generation in platelets as shown in Figure 1A. To investigate whether or not elevated ROS levels play a role in platelet-mediated Aβ aggregation, we used the antioxidant vitamin C as ROS scavenger. The presence of vitamin C led to decreased amyloid aggregate formation in platelet cell culture (Figure 4D). To confirm this result, we quantified the remaining soluble Aβ40 in the supernatants of platelet cell culture using Western blot analysis. The remaining amount of Aβ40 was increased when platelets were incubated with vitamin C suggesting that ROS generation plays a crucial role in platelet-mediated Aβ aggregation (Figure 4E).

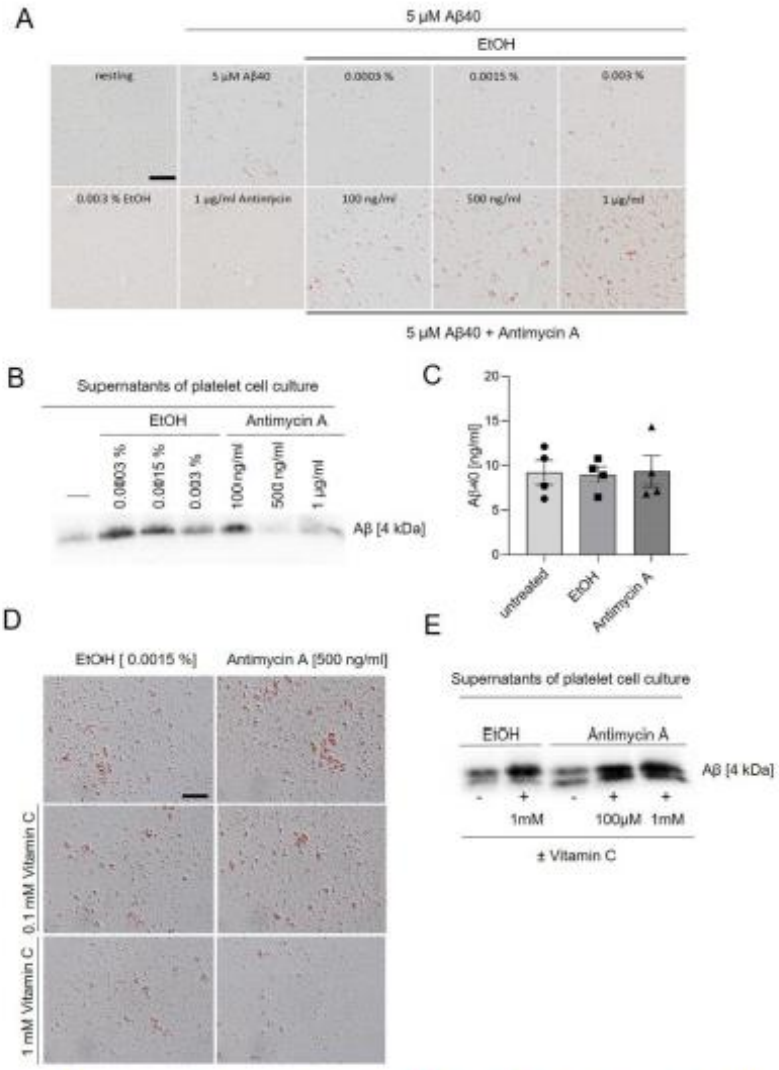

Figure 4. Effects of antimycin A and the antioxidant vitamin C on platelet-mediated Aβ aggregate formation. (**A**) Representative images of congo red-stained Aβ deposits in platelet culture. Platelets were incubated with 5 µM of soluble synthetic Aβ40 and different concentrations of antimycin A for three days at 37 °C and 5% CO_2. EtOH served as the control (vehicle). Scale bar, 50 µm. (**B**) Quantification of remaining soluble Aβ40 in the supernatant of platelet culture using Western blot. (**C**) Isolated platelets were incubated in the absence or presence of antimycin A (500 ng/mL) for 24 h at 37 °C. EtOH (0.0015%) served as solvent control for antimycin A. Aβ40 levels were determined using ELISA (n = 4). (**D**) Platelet culture after incubation with soluble, synthetic Aβ40 for three days. Where indicated, platelets were incubated with antimycin A (500 ng/mL) or antimycin A (500 ng/mL) and different concentrations of vitamin C (100 µM or 1 mM). EtOH served as control (vehicle). Scale bar, 50 µm. (**E**) Quantification of remaining soluble Aβ40 in the supernatant of platelet culture using Western blot (n = 3).

2.5. Aβ Induced GPVI-Mediated ROS Production and Integrin $\alpha_{IIb}\beta_3$ Activation In Vitro

Platelets are metabolically active and display high adenosine triphosphate (ATP) turnover [25]. Luminometric analyses showed a significant reduction of the intracellular ATP level if dysfunction of complex III was induced by antimycin A (Figure 5A). Previously we demonstrated that Aβ40 is able to induce the release of ATP and platelet aggregation [21,23]. Furthermore, ADP/ATP plays an important role in platelet-mediated Aβ aggregation [21] that was enhanced when mitochondrial dysfunction was reinforced by antimycin A (Figure 4A). Therefore, we investigated the effect of complex III dysfunction for Aβ40-induced platelet aggregation and ATP release in the presence of antimycin A. Both, Aβ40 and CRP induced release of ATP from platelets. In the presence of antimycin A, release of ATP was comparable to solvent control EtOH upon CRP (used as positive control) and Aβ40 stimulation (Figure 5B). However, we measured the reduction of the intracellular ATP level (Figure 5A) and of the ATP release (Figure 5B) in response to Aβ40 in the presence of solvent control EtOH. Next, we investigated whether or not the aggregation of platelets is altered by blocking of complex III in platelets. As shown in Figure 5C, platelet aggregation was not altered, either following CRP stimulation or Aβ40 treatment (Figure 5C) when platelets were pre-incubated with antimycin A. Vitamin C was shown to reduce platelet-mediated Aβ aggregation in the presence and absence of antimycin A (Figure 4D), suggesting that ROS generation plays a crucial role in these processes. Moreover, integrin $\alpha_{IIb}\beta_3$ and GPVI play an important role in platelet-mediated Aβ aggregation [21,23]. Therefore, we incubated platelets with 5 and 10 μM Aβ40 and determined ROS generation in GPVI-deficient platelets from *Gp6*$^{-/-}$ mice. As shown in Figure 5D, ROS generation of GPVI-deficient platelets was significantly reduced in response to Aβ40 and CRP (positive control) (Figure 5D), suggesting that GPVI is involved in ROS-mediated Aβ aggregation facilitated by platelets. ROS production regulates integrin $\alpha_{IIb}\beta_3$ activation [32], a major contributor of platelet-mediated Aβ aggregation [21]. Therefore, we next determined integrin activation following Aβ stimulation in the presence and absence of the ROS scavenger vitamin C to investigate, if Aβ-induced ROS production is able to prompt integrin $\alpha_{IIb}\beta_3$ activation (Figure 5E). As shown in Figure 5E, pre-treatment with vitamin C led to reduced Aβ40-induced activation of integrin $\alpha_{IIb}\beta_3$ in ADP-treated platelets (Figure 5E).

2.6. Mitochondrial ROS Production and Mitochondrial Membrane Potential in Platelets from Alzheimer's Disease Transgenic Mice APP23

In our previous studies we showed that aged mice (two years old) from the AD transgenic mouse line APP23, which develop amyloid-β deposits in the brain parenchyma and cerebral vessels at this age, exhibit pre-activated platelets in the blood circulation accompanied by enhanced integrin $\alpha_{IIb}\beta_3$ activation and degranulation of platelets compared to age-matched control mice [19]. Currently we analyzed mitochondria from APP23 mice using platelets from one- and two-year-old mice. Measurements using the ROS sensitive dye MitoSOX-Red showed that superoxide production in resting platelets from APP23 mice is comparable to resting platelets from WT mice (Figure 6A). The generation of mitochondrial superoxide in platelets was significantly increased when platelets were stimulated with 5 μM Aβ40 and even stronger with 20 μM Aβ40, as compared to resting platelets from one- and two-year-old APP23 and WT control mice. However, stimulation with 20 μM Aβ40 led to increased levels of superoxide in platelets from APP23 mice independent of their age, as compared to age-matched control mice (Figure 6A). The mitochondrial transmembrane potential (Δψm) of non-stimulated (resting) platelets was comparable in platelets from one- and two-year-old APP23 and WT mice (Figure 6B). However, stimulation with 5 μM Aβ40 led to reduced mitochondrial transmembrane potential in platelets from WT mice (Figure 6B). Moreover, stimulation with 20 μM Aß40 reduced mitochondrial transmembrane potential in platelets from one- and two-year-old WT mice (Figure 6B).

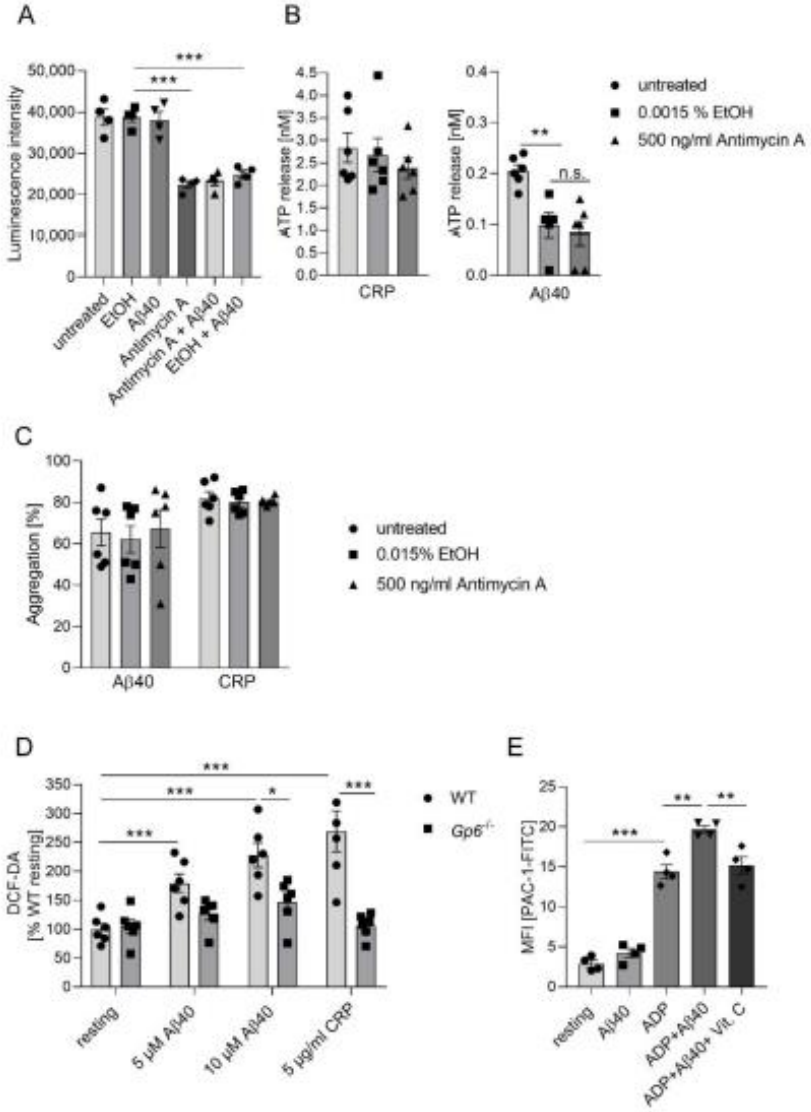

Figure 5. Impact of complex III inhibition on platelet functions following Aβ40 stimulation. (**A**) Detection of intracellular ATP levels after incubation of platelets with Aβ40 (5 µM), antimycin A (12.5 µM) and EtOH (as control, vehicle) for 90 min using Luminescence intensity (n = 4, *** = $p < 0.001$; two-way ANOVA with Tukey's multiple comparisons test). (**B**) Measurement of ATP release from antimycin A-pretreated platelets (EtOH was used in controls as vehicle) following Aβ40 (20 µM) or CRP (1 µg/mL) (n = 5–6). Analyses were performed using one-way ANOVA and Dunnett's multiple comparisons post-hoc test. ** $p < 0.01$; n.s.: not significant. (**C**) Aggregation of antimycin A-pretreated platelets upon Aβ40 (10 µM) or CRP (1µg/mL). EtOH was used as control (vehicle) (n = 5–6). (**D**) Measurement of reactive oxygen species (ROS) generation with DCF-DA in GPVI-deficient platelets upon Aβ40 and CRP (n = 6). Data represent mean value ± SEM; two-way ANOVA with Sidak's multiple comparisons test. *** $p < 0.001$; ** $p < 0.01$; * $p < 0.05$. (**E**) Flow cytometric analysis of integrin activation at the surface of platelets using PAC-1 antibody upon stimulation with Aβ40 (11.5 µM) and ADP (5µM). Where indicated, samples were pre-incubated with vitamin C (1 mM) for 30 min at RT (n = 4). Data represent mean value ± SEM; two-way ANOVA with Tukey's multiple comparisons test. *** $p < 0.001$; ** $p < 0.002$.

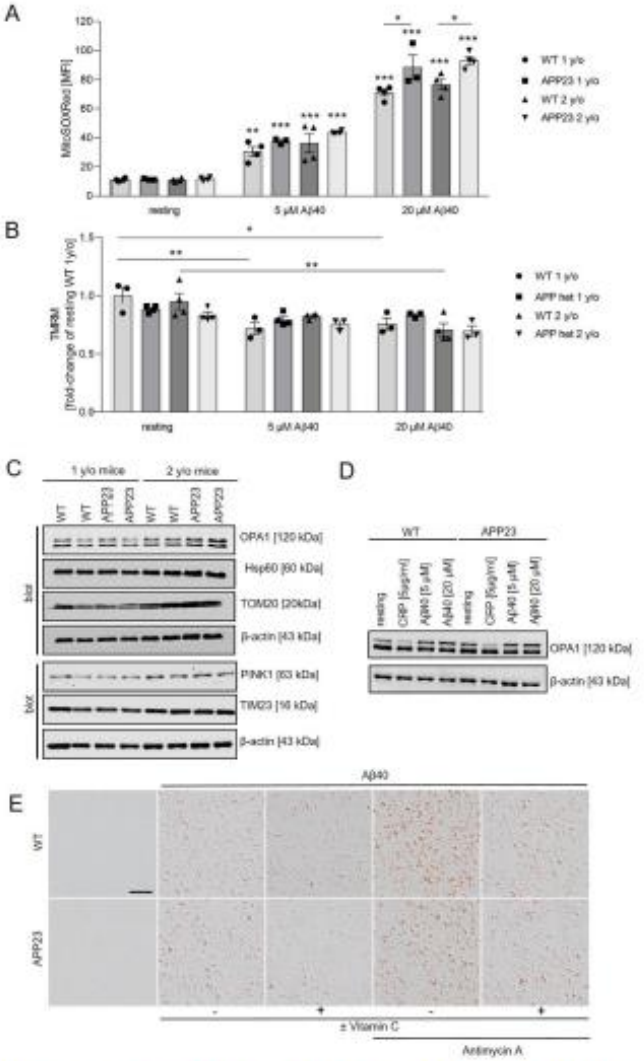

Figure 6. Analysis of mitochondrial function in platelets from APP23 mice. (**A**,**B**) Platelets from one- and two-year-old WT and APP23 mice were incubated with 5 and 20 µM Aβ40 for 30 min. Formation of superoxide was examined using MitoSOX™ Red and depolarization of platelet mitochondrial membrane was observed by decrease in TMRM fluorescence intensity. Data show the mean value ± SEM (n = 3–4), two-way ANOVA with Tukey's multiple comparisons test. *** $p < 0.001$; ** $p < 0.01$; * $p < 0.05$; vs. basal or as indicated. (**C**) Expression levels of mitochondrial proteins in platelets from one- and two-year-old WT and APP23 mice were determined by Western blot analysis. β-actin served as loading control (n = 4). (**D**) Western blot analysis of the mitochondrial protein OPA1 in platelets from two-year-old WT and APP23 mice after stimulation with Aβ40 and CRP. β-actin served as loading control (n = 3). (**E**) Representative images of congo-red stained amyloid aggregates in the culture of platelets after incubation with soluble, synthetic Aβ40 (5 µM) for three days in the presence or absence of antimycin A (500 ng/mL) and vitamin C (100 µM). Platelets from one-year-old WT and APP23 mice were used (n = 3). Scale bar, 50 µm.

Furthermore, we analyzed the levels of mitochondrial proteins in platelets from one- and two-year-old APP23 mice in comparison to age-matched controls. Western blot analysis

revealed that expression of TOM20 and TIM23 was increased in APP23 and WT mice at the age of two years without reaching statistical significance. However, no alterations in protein expression was detected between platelets from different groups at the same age (Figure 6C and Figure S3). The eight splice variants and two proteolytic cleavage sites within mitochondrial OPA1 result in long and short forms of OPA1 with divergent functions in cristae biogenesis and mitochondrial fusion [33]. To investigate whether or not Aβ40 induces the cleavage of OPA1 in platelets from WT and APP23 mice, we stimulated platelets with different concentrations of Aβ40 and CRP as positive control. As shown in Figure 6D, protein levels of the long form of OPA1was slightly increased following stimulation of platelets with Aβ40 as compared to resting platelets but does not reach statistical significance (Figure S4). In contrast, the levels of the long form of OPA1 was slightly reduced in CRP-stimulated platelets but did not reach statistical significance (Figure 6D and Figure S4). We next analyzed platelet-mediated Aβ40 aggregation in cell culture using platelets from age-matched APP23 and control mice. As already observed in cultured human platelets (Figure 4), treatment of murine platelets with antimycin A increased the formation of congo-red positive Aβ40 aggregates, whereas treatment with vitamin C reduced the number of Aβ40 aggregates. However, no differences were observed between platelets from APP23 and WT mice (Figure 6E).

3. Discussion

This study showed that stimulation of human platelets from healthy donors by Aβ40 led to ROS and superoxide production, reduced mitochondrial transmembrane potential, induced the release of mitochondria from platelets and reduced the content of the mitochondrial protein TOM20. Furthermore, the oxygen consumption rate was reduced when we incubated platelets from healthy donors with Aβ40 or Aβ40 and CRP as deciphered by OCR. Enhanced mitochondrial dysfunction induced by antimycin A led to enhanced platelet-mediated Aβ40 aggregate formation. This was due—at least in part—by GPVI- and ADP-mediated ROS production, leading to enhanced integrin $\alpha_{IIb}\beta_3$ activation in the presence of Aβ40. Aβ40 aggregate formation in presence of platelets were comparable between APP23 mice and WT controls, which could be reduced upon treatment with vitamin C.

In line with studies in the past [15], we currently observed that Aβ40 induced ROS and depolarization of the mitochondrial membrane in platelets from healthy donors. In line with previous platelet activation and adhesion studies [22], Aβ1-16 neither induced the formation of ROS and superoxide nor reduced mitochondrial transmembrane potential loss in platelets. This is due to the fact that the RHDS binding sequence of Aβ alone is not sufficient to induce Aβ-mediated alterations in platelets, including Aβ-induced outside-in signaling of integrin $\alpha_{IIb}\beta_3$. Thus, Aβ binding to integrin $\alpha_{IIb}\beta_3$ and integrin outside-in signaling might be important for superoxide production and dysregulation of mitochondrial membrane potential.

Platelet activation, including granular release and aggregation, are energy-dependent processes. Platelets are able to switch between glycolysis and oxidative phosphorylation using either glucose or fatty acids. Activation of platelets promotes a rapid uptake of exogenous glucose and display a glycolytic phenotype coupled with a minor rise in mitochondrial oxygen consumption [34]. To support platelet activation under nutrient limiting conditions, platelets are able to use glucose, glycogen or fatty acids. Thus, platelets have significant metabolic fuel and pathway flexibility, but mostly use glycolysis for ATP generation upon activation [34,35]. Therefore, we analyzed Aβ40-induced release of ATP and platelet aggregation after inducing mitochondrial dysfunction using antimycin A that inhibits complex III of the mitochondrial respiratory chain. Treatment of platelets with antimycin A results in the reduction of the mitochondrial ATP production and supports ROS generation and mitochondrial dysfunction [36]. Treatment of platelets with high dose of antimycin A results in reduced collagen-induced platelet aggregation and strongly reduced dense granule secretion [37]. Here, we used low doses of antimycin A that is

able to amplify platelet-mediated Aβ40 aggregate formation but did not alter platelet aggregation or ATP release, suggesting that ATP content in platelets is still sufficient to allow dense granule release and platelet aggregation.

Platelet-mediated Aβ40 aggregate formation was amplified by mitochondrial dysfunction in a dose-dependent manner using antimycin A (Figures 4 and 6). The reduction of Aβ aggregation by vitamin C strongly indicates that Aβ-induced ROS production in platelets is responsible for platelet-mediated Aβ aggregate formation. Vitamin C is an antioxidant and its protective effects and clinical relevance for AD has been already shown in different studies in the past [38–40]. Treatment of human and murine platelets with vitamin C reduced the formation of Aβ aggregates (Figures 4 and 6). In particular, enhanced Aβ aggregate formation following mitochondrial dysfunction by antimycin A treatment was strongly reduced in the presence of vitamin C, demonstrating that the reduction of free radical generation attenuates platelet-mediated Aβ aggregate formation. Thus, enhanced ROS level in AD patients might be critical for platelet-mediated Aβ aggregate formation in cerebral vessels known as cerebral amyloid angiopathy (CAA) [41]. Our data suggests that vitamin C might reduce platelet-mediated effects on CAA even in the presence of already existing Aβ aggregates, because positive effects of vitamin C on the reduction of Aβ aggregates were also observed with platelets from APP23 mice (Figure 6).

Mitochondrial dysfunction resulting in increased ROS generation accounts for platelet-mediated Aβ aggregate formation in vitro. Similarly, in HEK293 cells, mitochondrial ROS production enhanced the formation of Aβ [31]. In contrast to the present study, the authors provide evidence that ROS induced elevated processing of amyloid precursor protein (APP) and that, in turn, Aβ led to mitochondrial dysfunction and increased ROS levels, suggesting a vicious cycle that contributes to the pathology of AD. Here, we observed that ROS is responsible for Aβ aggregate formation but not for the formation of endogenous Aβ by APP processing in platelets. The source of Aβ40 in plasma is highly discussed among researchers. Chen and colleagues believe that platelets are the primary source of amyloid beta-peptide in human blood [14].Wisniewski and Wegiel think that vascular Aβ originates from a different source to Aβ in plaques and is generated locally, principally in smooth muscle cells [42]. The group of M. Jucker believes that, although several factors may contribute to CAA in humans, the neuronal origin of transgenic APP, high levels of Aβ in cerebrospinal fluid and regional localization of CAA in APP23 transgenic mice indicate that neuron-derived Aβ can migrate to and accumulate in the vasculature far from its production site. Thus, Aβ transport and drainage pathways, rather than local production of Aβ by platelets or smooth muscle cells, are a primary mechanism underlying CAA formation [43,44]. Results of our previous studies demonstrate that platelet-mediated Aβ40 fibril formation and aggregation is not altered when we inhibited the Aβ production from APP precursors using inhibitors. This indicates that Aβ40 of platelet origin does not contribute to Aβ40 aggregation in the platelet culture [15].

We have recently shown that GPVI, ADP and integrin $\alpha_{IIb}\beta_3$ are involved in platelet-mediated Aβ aggregate formation by direct binding of Aβ to GPVI and integrin $\alpha_{IIb}\beta_3$ followed by the release of ATP/ADP [21,23]. Here, our data indicates that GPVI is also responsible for Aβ-induced ROS production and that ROS production is involved in $\alpha_{IIb}\beta_3$ integrin activation induced by ADP and Aβ (Figure 5). Integrin activation of platelets by ROS has already been shown earlier [32]. However, the authors used thrombin to produce ROS in platelets but not soluble Aβ as shown here. GPVI-triggered ROS production and enhanced integrin activation might support Aβ binding to integrin $\alpha_{IIb}\beta_3$ and to GPVI to reinforce platelet-mediated Aβ aggregate formation. Furthermore, the release of mitochondria following treatment of platelets with soluble Aβ might contribute to enhanced platelet activation and inflammation in AD [30].

Mitochondrial dysfunction has been shown to contribute to the pathogenesis of AD and is responsible for the decrease in respiration as observed in platelets from AD patients [26]. However, Fisar and colleagues found no correlation between dysfunctional mitochondrial respiration and changes in plasma Aβ levels as found in patients with

AD [27]. Our data indicates that incubation of platelets from healthy volunteers with Aβ or Aβ and CRP significantly reduced mitochondrial respiration compared to CRP alone, suggesting that Aβ itself is responsible for defects in mitochondrial respiration and that enhanced Aβ plasma levels might affect mitochondrial respiration of circulating platelets in AD transgenic mice and patients.

In AD patients and transgenic mice (APP23), enhanced platelet activation was detected [18,19]. Treatment of APP23 mice with the anti-platelet drug clopidogrel reduced the formation of CAA suggesting that enhanced platelet activation contributes to the pathology of AD [21]. The impact of enhanced platelet activation and mitochondrial dysfunction has already been described in different diseases [45–48]. Patients with sickle cell disease are characterized by decreased mitochondrial respiration, mitochondrial dysfunction that correlates with enhanced platelet activation and hemolysis both contributing to the pathogenesis of the disease [46]. Dengue infection is accompanied by enhanced activation and mitochondrial dysfunction of platelets [47]. In septic patients, Puskarich and colleagues found a correlation between platelet mitochondrial function and organ failure with increased respiratory rates in non-survivors compared to survivors [48]. In diabetes, hyperglycemia was associated with enhanced collagen-induced platelet activation that was triggered by mitochondrial superoxide production [45]. Furthermore, enhanced levels of ROS induced oxidative stress, which plays a crucial role in tissue damage after brain ischemia/reperfusion [49,50].

Taken together, platelet-mediated Aβ40 aggregate formation is enhanced by mitochondrial dysfunction through GPVI-mediated ROS production and elevated integrin $\alpha_{IIb}\beta_3$ activation. Thus, mitochondrial dysfunction contributes to platelet-mediated Aβ aggregate formation, and might be not only a beneficial biomarker but also a promising target to limit platelet activation exaggerated pathological manifestations in AD.

4. Materials and Methods

4.1. Chemicals, Peptides and Antibodies

Platelets were activated with collagen-related peptide (= CRP, Richard Farndale, University of Cambridge, United Kingdom), synthetic Aβ40 (1-40; Bachem, Switzerland, cat no 4014442.1000) sequence single-letter code (DAEFRHDSGYEVHHQKLVFFAEDVGSNKGAIIGLMVGGVV), Aβ16 (Aβ1-16, Bachem, Switzerland) ADP (Sigma-Aldrich). Apyrase (grade II, from potato) and prostacyclin from Calbiochem were used for isolation. Antimycin A (Streptomyces sp., A8674-25MG, Sigma-Aldrich, St. Louis, USA) was solved in 95% EtOH. Vitamin C (L(+)-Ascorbic acid) is from VWR Chemicals. Antibodies: Hsp60 (SAB 4501464; Sigma Aldrich, dilution 1:1000), OPA1 (sc-393296, Santa Cruz, dilution 1:500), PINK1 (D8G Rabbit mAb 6946; Cell Signalling, dilution 1:500), TIM23 (BD 611222; BD Biosciences, dilution 1:500), TOM20 (sc-11415; Santa Cruz, dilution 1:500), Amyloid-β (6E10, SIG-39320; Covance, dilution 1:2000). The antibodies β-actin (cat no 4967) and horseradish peroxidase (HRP)-linked secondary antibodies (cat no 7074 and cat no 7076) were from Cell Signaling Technology.

4.2. Animals

Heterozygous C57BL/6J-TgN(Thy1.2-hAPP751-KM670/671 NL)23 (APP23) were provided by Novartis Pharma AG. Mice with targeted deletion of GPVI were provided by J. Ware (University of Arkansas for Medical Sciences) and backcrossed to C57BL/6 mice. All animal experiments were conducted according the Declaration of Helsinki and approved by the Ethics Committee of the State Ministry of Agriculture, Nutrition and Forestry State of North Rhine-Westphalia, Germany (reference number: AZ 84-02.05.40.16.073). Mice were maintained in a specific pathogen-free environment and fed standard mouse diet ad libitum.

4.3. Murine Platelet Preparation

Platelets were prepared as previously described [23]. Murine blood was taken from the retro-orbital-plexus in a tube containing heparin and centrifuged at 250× g for 5 min at room temperature. Platelet-rich-plasma was obtained by centrifugation at 50× g for 6 min and was washed twice with Tyrode's buffer (136 mM NaCl, 0.4 mM Na_2HPO_4, 2.7 mM KCl, 12 mM $NaHCO_3$, 0.1% glucose, 0.35% bovine serum albumin (BSA, Sigma-Aldrich, St. Louis, MO, USA), pH 7.4) in the presence of prostacyclin (0.5 µM) and apyrase (0.02 U/mL) at 650× g for 5 min at room temperature. Before use, platelet pellets were resuspended in the Tyrode's buffer (without prostacyclin and apyrase) supplemented with 1 mM $CaCl_2$.

4.4. Human Platelet Preparation

Platelets were prepared as previously described [23]. ACD-anticoagulated blood was obtained from healthy volunteers between the ages of 18 und 50 years old from the blood bank. Donors provided written informed consent to participate in this study according to the Ethics Committee and the Declaration of Helsinki (study number 2018-140-KFogU). The blood was centrifuged at 200× g for 10 min at room temperature. The platelet-rich plasma (PRP) was added to phosphate buffered saline (PBS; pH 6.5, apyrase: 2.5 U/mL and 1 µM PGI_2) in 1:1 volumetric ratio and centrifuged at 1000× g for 6 min. Platelets were resuspended in Tyrode's-buffer (140 mM NaCl; 2.8 mM KCl; 12 mM $NaHCO_3$; 0.5 mM Na_2HPO_4; 5.5 mM glucose pH 7.4).

4.5. Human and Murine Platelet Culture

Isolated human or murine platelets at the concentration of 2×10^6 platelets/well were added to 150 µL of DMEM medium (Dulbecco's modified Eagle's medium, 41965-039; Life Technologies). Platelets were incubated with 5 µM synthetic Aβ40 in the presence of antimycin A (or EtOH as solvent control) and Vitamin C for 3 days at 37 °C and 5% CO_2. After 3 days, the supernatants of cell culture were collected for determination of remaining Aβ concentration using immunoblot analysis. The supernatants were prepared with reducing sample buffer (Laemmli buffer) and denatured at 95 °C for 5 min. Unbound platelets were removed by rinsing with PBS and adherent platelets were fixed with 2% paraformaldehyde and stained against fibrillary Aβ aggregates with Congo red according to the manufacturer's protocol (Millipore cat no 101641).

4.6. Measurement of Intracellular ROS Level

Washed platelets were added to DMEM medium (Dulbecco's modified Eagle's medium) and incubated with different concentrations of Aβ40 or Aβ16 (as control) for 24 h at 37 °C. After incubation, platelets were loaded with 10 µM DCF-DA (2′,7′-Dichlor-dihydrofluorescein-diacetat; D6883; Sigma-Aldrich) at 37 °C for 15 min in the dark. Reaction was stopped using PBS. Samples were analyzed on a FACSCalibur flow cytometer (BD Biosciences).

4.7. Measurement of Mitochondrial Superoxide

Washed platelets were pre-incubated with MitoSOX™ Red (M36008; Invitrogen) at room temperature for 30 min in the dark. Then, platelets were stimulated with Aβ40 or Aβ16 (as control) for 30 min at RT. Reaction was stopped using PBS. Samples were analyzed on a FACSCalibur flow cytometer (BD Biosciences).

4.8. Measurement of Mitochondrial Membrane Potential

Isolated platelets were treated with Aβ40 for 30 min at RT and then incubated with 100 nM tetramethylrhodamin methyl ester (TMRM; Sigma-Aldrich) in the dark. The reaction was stopped after 30 min incubation using PBS. Samples were analyzed on a FACSCalibur flow cytometer (BD Biosciences).

4.9. Measurement of Mitochondria Release Using MitoTrackerTM Green FM

Human isolated platelets were incubated with 100 nM MitoTrackerTM green FM (M7514; Invitrogen)for 30 min at 37 °C under exclusion of light. After incubation, platelets were stimulated with thrombin (0.1 U/mL or 0.5 U/mL) or Aβ40 (2.3 µM or 11.5 µM for 15 min, 1 h and 4 h at RT in the dark. The reaction was stopped with PBS. Samples were analyzed on a FACSCalibur flow cytometer (BD Biosciences).

4.10. Cell Lysis and Immunoblotting

Human isolated platelets were stimulated with collagen-related peptide (CRP, 1 µg/mL) or Aβ40 (5 µM or 20 µM) at 37 °C with stirring (250 r.p.m) for 1and 2 h. Stimulation was terminated with 5× ice-cold lysis buffer (100 mM Tris-HCl, 725 mM NaCl, 20 mM EDTA, 5% TritonX-100, complete protease inhibitor (PI) cocktail). Murine platelets were lysed with lysis buffer (15 mM Tris-HCl, 155 mM NaCl, 1 mM EDTA, 0.005% NaN_3, 5% IGPAL and PI). Cell lysates were prepared by boiling a sample of lysate with sodium dodecyl sulfate (SDS) sample buffer. Platelet lysates were then separated by SDS-polyacrylamide gel electrophoresis, electro-transferred onto nitrocellulose blotting membrane (GE Healthcare Life Sciences). Membrane was blocked using 5% nonfat dry milk in TBST (tris-buffered saline with 0.1% Tween20) and probed with the appropriate primary antibody and secondary antibody HRP-conjugated antibody. Immunoreactive bands were visualized with enhanced chemiluminescence detection reagents using FusionFX Chemiluminescence Imager Systems (Vilber) and quantified using the FUSION FX7 software (Vilber).

4.11. Platelet Aggregation

Platelet aggregation was measured as percentage light transmission compared to Tyrode's buffer (=100%) using Chrono-Log dual channel lumi-aggregometer (model 700) at 37 °C stirring at 1000 rpm. Where indicated, the platelets (20×10^3 cells/µL) were pre-treated with 500 ng/mL antimycin A or 0.0015% EtOH (as solvent control) for 1 h at RT. Platelets were then stimulated with 1 µg/mL CRP or 10 µM Aβ40 and aggregation response was examined.

4.12. Measurement of Intracellular ATP Level and ATP Release

Intracellular ATP level was measured using Mitochondrial ToxGlo™ Assay (Promega) following the manufacturer's protocol. Platelets were adjusted to a final concentration of 2×10^2 and incubated with 5 µM Aβ40 und 12.5 antimycin A (EtOH used as control) for 90 min at 37 °C. ATP release was measured using ChronoLume luciferin assay (ChronoLog) on a LumiAggregometer (model 700, ChronoLog) at 37 °C stirring at 1000 rpm. Where indicated, the platelets (20×10^3 cells/µL) were pre-treated with 500 ng/mL antimycin A or 0.0015% EtOH (as solvent control) for 1 h at RT. After 2 min of incubation with luciferase, platelets were stimulated with 1 µg/mL CRP or 20 µM Aβ40 and monitored for ATP release.

4.13. Aβ40 Quantification by Enzyme-Linked Immunosorbent Assay (ELISA)

Platelets were adjusted to a final concentration of 1×10^6/µL and pre-incubated with 500 ng/mL antimycin A or 0.0015% EtOH (as solvent control) for 24 h at 37 °C. Incubation was terminated with 5× ice-cold lysis buffer (100 mM Tris-HCl, 725 mM NaCl, 20 mM EDTA, 5% TritonX-100, complete protease inhibitor (PI) cocktail). After centrifugation, Aβ40 levels in supernatants were measured following the manufacturer's protocol (human Aβ1-40 ELISA Kit, Cat. No: MBS2506221, MyBioSource).

4.14. Measurement of the Oxygen Consumption Rate

Mitochondrial respiration of blood platelets was analyzed by using the Seahorse XFe96 extracellular flux analyzer and the Seahorse XF Cell Mito Stress Test Kit (103015-100, Agilent Technologies), purchased from Agilent (Agilent Technologies, Santa Clara, CA, USA). The Seahorse XF Cell Mito Stress Test Kit allows direct measurement of mitochondrial function

in living cells by monitoring the oxygen consumption rate (OCR) and was performed according to the manufacturers' guidelines. ACD-anticoagulated human whole blood samples were obtained from healthy volunteers. Blood was centrifuged at 200 g for 20 min at 22 °C without brake. The platelet-rich-plasma, PRP thus obtained was separated an added to phosphate buffered saline (PBS, pH 6.5), supplemented with apyrase (2.5 U/mL) and prostaglandin I_2 (PGI_2, 1 µM) in a volumetric ratio of 1:10 and centrifuged at 1000 g for 10 min at 22 °C without brake. Washed platelets were subsequently resuspended in Seahorse XF DMEM medium (containing 5.5 mM D-Glucose, 1 mM Na-Pyruvate, 4 mM L-Glutamine, pH 7.4). Afterwards, platelets were seeded in a density of 2×10^7 cells/well into a Cell-Tak (100 µg/mL) coated XFe96 cell culture microplate in Seahorse XF DMEM medium (containing 5.5 mM D-Glucose, 1 mM Na-Pyruvate, 4 mM L-Glutamine, pH 7.4). To evaluate the impact of Aβ40 on mitochondrial respiration using OCR as a readout, the Seahorse XF DMEM medium was either supplemented with 5 µM Aβ40 or without (Bachem, Switzerland). For optimal adhesion, the seeded platelets were centrifuged in two steps at 143 and 213× *g* respectively for one min each. After centrifugation, the cells were incubated for 30 min in a non-CO_2 incubator at 37 °C, prior the start of the assay. Initially the basal OCR was measured, followed by sequential injections of CRP (5 µg/mL), oligomycin (1 µM), FCCP (0.5 µM) and a mix of antimycin A and rotenone (each 1 µM). ATP-linked respiration is defined as the difference of the last rate measurement before oligomycin injection and the minimum rate measurement after oligomycin injection. Proton leak is defined as the minimum rate measurement after oligomycin minus non-mitochondrial respiration. The OCR measurements were conducted in 3 cycles for each condition. All data were analyzed using the wave software (Agilent Technologies, 2.6.1).

4.15. Flow Cytometry Measurement of PAC-1 Binding

Flow cytometry analysis of platelet activation was performed using fluorophore-labeled antibody PAC-1 (activated integrin $\alpha_{IIb}\beta_3$ receptor marker, BD Biosciences). A total of 5 µL of whole blood was added to tube containing phosphate-buffered saline (PBS), antibody and agonists (ADP and Aβ40). Where indicated, whole blood was pre-incubated with vitamin C (1 mM) for 30 min at RT. After incubation at room temperature for 15 min, the reaction was stopped by the addition of PBS and samples were analyzed on a FACSCalibur flow cytometer (BD Biosciences).

Supplementary Materials: The following are available online at https://www.mdpi.com/article/10.3390/ijms22179633/s1.

Author Contributions: L.D., T.F., L.M.T. and C.F. performed experiments and analyzed the data. L.D. and M.E. designed experiments, discussed the data and wrote the manuscript. A.S.R. discussed experimental designs and data, read and edited the manuscript. M.C. discussed the data, read and edited the manuscript. All authors have read and agreed to the published version of the manuscript.

Funding: This research was funded by grant from the German Research Foundation (Deutsche Forschungsgemeinschaft, DFG, grant number EL651/5-1) and by the *Stiftung für Altersforschung* of the Heinrich-Heine University Düsseldorf) to M.E., and by the *Forschungskommission* of the Medical Faculty Düsseldorf (grant 2020/09) to L.D.

Institutional Review Board Statement: Fresh ACD-anticoagulated blood was obtained from healthy volunteers between the ages of 18 und 50 years old. Participants provided their written informed consent to participate in this study according to the Ethics Committee and the Declaration of Helsinki (study number 2018-140-KFogU). All animal experiments were conducted according the Declaration of Helsinki and approved by the Ethics Committee of the State Ministry of Agriculture, Nutrition and Forestry State of North Rhine-Westphalia, Germany (reference number: AZ 84-02.05.40.16.073).

Informed Consent Statement: Informed consent was obtained from all subjects involved in the study.

Data Availability Statement: The data presented in this study are available on request from the corresponding author.

Acknowledgments: We thank Martina Spelleken for providing outstanding technical assistance and Nahal Brocke-Ahmadinejad and the 'Cellular Metabolism Platform' of the Institute of Bio-chemistry and Molecular Biology I, Medical Faculty, Heinrich-Heine-University Düsseldorf, Germany for introduction into the Seahorse Flux Analyzer.

Conflicts of Interest: The authors declare no conflict of interest.

References

1. Selkoe, D.J.; Hardy, J. The amyloid hypothesis of Alzheimer's disease at 25 years. *EMBO Mol. Med.* **2016**, *8*, 595–608. [CrossRef] [PubMed]
2. Reddy, P.H.; Oliver, D.M. Amyloid Beta and Phosphorylated Tau-Induced Defective Autophagy and Mitophagy in Alzheimer's Disease. *Cells* **2019**, *8*, 488. [CrossRef] [PubMed]
3. Reddy, P.H.; Tripathi, R.; Troung, Q.; Tirumala, K.; Reddy, T.P.; Anekonda, V.; Shirendeb, U.P.; Calkins, M.J.; Reddy, A.P.; Mao, P.; et al. Abnormal mitochondrial dynamics and synaptic degeneration as early events in Alzheimer's disease: Implications to mitochondria-targeted antioxidant therapeutics. *Biochim. Biophys. Acta* **2012**, *1822*, 639–649. [CrossRef] [PubMed]
4. Du, H.; Guo, L.; Yan, S.; Sosunov, A.A.; McKhann, G.M.; Yan, S.S. Early deficits in synaptic mitochondria in an Alzheimer's disease mouse model. *Proc. Natl. Acad. Sci. USA* **2010**, *107*, 18670–18675. [CrossRef]
5. Cai, Q.; Tammineni, P. Alterations in Mitochondrial Quality Control in Alzheimer's Disease. *Front. Cell. Neurosci.* **2016**, *10*, 24. [CrossRef]
6. Shefa, U.; Jeong, N.Y.; Song, I.O.; Chung, H.J.; Kim, D.; Jung, J.; Huh, Y. Mitophagy links oxidative stress conditions and neurodegenerative diseases. *Neural Regen. Res.* **2019**, *14*, 749–756.
7. Manczak, M.; Calkins, M.J.; Reddy, P.H. Impaired mitochondrial dynamics and abnormal interaction of amyloid beta with mitochondrial protein Drp1 in neurons from patients with Alzheimer's disease: Implications for neuronal damage. *Hum. Mol. Genet.* **2011**, *20*, 2495–2509. [CrossRef]
8. Reddy, P.H.; Manczak, M.; Yin, X.; Grady, M.C.; Mitchell, A.; Tonk, S.; Kuruva, C.S.; Bhatti, J.S.; Kandimalla, R.; Vijayan, M.; et al. Protective Effects of Indian Spice Curcumin Against Amyloid-β in Alzheimer's Disease. *J. Alzheimer's Dis.* **2018**, *61*, 843–866. [CrossRef]
9. Reddy, P.H.; Williams, J.; Smith, F.; Bhatti, J.S.; Kumar, S.; Vijayan, M.; Kandimalla, R.; Kuruva, C.S.; Wang, R.; Manczak, M.; et al. MicroRNAs, Aging, Cellular Senescence, and Alzheimer's Disease. *Prog. Mol. Biol. Transl. Sci.* **2017**, *146*, 127–171.
10. Reddy, P.H.; McWeeney, S.; Park, B.S.; Manczak, M.; Gutala, R.V.; Partovi, D.; Jung, Y.; Yau, V.; Searles, R.; Mori, M.; et al. Gene expression profiles of transcripts in amyloid precursor protein transgenic mice: Up-regulation of mitochondrial metabolism and apoptotic genes is an early cellular change in Alzheimer's disease. *Hum. Mol. Genet.* **2004**, *13*, 1225–1240. [CrossRef]
11. Kerr, J.S.; Adriaanse, B.A.; Greig, N.H.; Mattson, M.P.; Cader, M.Z.; Bohr, V.A.; Fang, E.F. Mitophagy and Alzheimer's Disease: Cellular and Molecular Mechanisms. *Trends Neurosci.* **2017**, *40*, 151–166. [CrossRef]
12. Sheng, Z.H.; Cai, Q. Mitochondrial transport in neurons: Impact on synaptic homeostasis and neurodegeneration. *Nat. Rev. Neurosci.* **2012**, *13*, 77–93. [CrossRef] [PubMed]
13. Li, Q.X.; Whyte, S.; Tanner, J.E.; Evin, G.; Beyreuther, K.; Masters, C.L. Secretion of Alzheimer's disease Abeta amyloid peptide by activated human platelets. *Lab. Investig. A J. Tech. Methods Pathol.* **1998**, *78*, 461–469.
14. Chen, M.; Inestrosa, N.C.; Ross, G.S.; Fernandez, H.L. Platelets are the primary source of amyloid beta-peptide in human blood. *Biochem. Biophys. Res. Commun.* **1995**, *213*, 96–103. [CrossRef]
15. Gowert, N.S.; Donner, L.; Chatterjee, M.; Eisele, Y.S.; Towhid, S.T.; Munzer, P.; Walker, B.; Ogorek, I.; Borst, O.; Grandoch, M.; et al. Blood platelets in the progression of Alzheimer's disease. *PLoS ONE* **2014**, *9*, e90523. [CrossRef]
16. Zainaghi, I.A.; Talib, L.L.; Diniz, B.S.; Gattaz, W.F.; Forlenza, O.V. Reduced platelet amyloid precursor protein ratio (APP ratio) predicts conversion from mild cognitive impairment to Alzheimer's disease. *J. Neural Transm.* **2012**, *119*, 815–819. [CrossRef]
17. Johnston, J.A.; Liu, W.W.; Coulson, D.T.; Todd, S.; Murphy, S.; Brennan, S.; Foy, C.J.; Craig, D.; Irvine, G.B.; Passmore, A.P. Platelet beta-secretase activity is increased in Alzheimer's disease. *Neurobiol. Aging* **2008**, *29*, 661–668. [CrossRef]
18. Stellos, K.; Panagiota, V.; Kogel, A.; Leyhe, T.; Gawaz, M.; Laske, C. Predictive value of platelet activation for the rate of cognitive decline in Alzheimer's disease patients. *J. Cereb. Blood Flow Metab.* **2010**, *30*, 1817–1820. [CrossRef]
19. Jarre, A.; Gowert, N.S.; Donner, L.; Munzer, P.; Klier, M.; Borst, O.; Schaller, M.; Lang, F.; Korth, C.; Elvers, M. Pre-activated blood platelets and a pro-thrombotic phenotype in APP23 mice modeling Alzheimer's disease. *Cell Signal.* **2014**, *26*, 2040–2050. [CrossRef]
20. Prodan, C.I.; Ross, E.D.; Vincent, A.S.; Dale, G.L. Rate of progression in Alzheimer's disease correlates with coated-platelet levels—A longitudinal study. *Transl. Res. J. Lab. Clin. Med.* **2008**, *152*, 99–102. [CrossRef] [PubMed]
21. Donner, L.; Falker, K.; Gremer, L.; Klinker, S.; Pagani, G.; Ljungberg, L.U.; Lothmann, K.; Rizzi, F.; Schaller, M.; Gohlke, H.; et al. Platelets contribute to amyloid-beta aggregation in cerebral vessels through integrin alphaIIbbeta3-induced outside-in signaling and clusterin release. *Sci. Signal.* **2016**, *9*, ra52. [CrossRef]
22. Donner, L.; Gremer, L.; Ziehm, T.; Gertzen, C.G.W.; Gohlke, H.; Willbold, D.; Elvers, M. Relevance of N-terminal residues for amyloid-beta binding to platelet integrin alphaIIbbeta3, integrin outside-in signaling and amyloid-beta fibril formation. *Cell Signal.* **2018**, *50*, 121–130. [CrossRef]

23. Donner, L.; Toska, L.M.; Krüger, L.; Gröniger, S.; Barroso, R.; Burleigh, A.; Mezzano, D.; Pfeiler, S.; Kelm, M.; Gerdes, N.; et al. The collagen receptor glycoprotein VI promotes platelet-mediated aggregation of β-amyloid. *Sci. Signal.* **2020**, *13*, eaba9872. [CrossRef]
24. Hayashi, T.; Tanaka, S.; Hori, Y.; Hirayama, F.; Sato, E.F.; Inoue, M. Role of mitochondria in the maintenance of platelet function during in vitro storage. *Transfus. Med.* **2011**, *21*, 166–174. [CrossRef]
25. Melchinger, H.; Jain, K.; Tyagi, T.; Hwa, J. Role of Platelet Mitochondria: Life in a Nucleus-Free Zone. *Front. Cardiovasc. Med.* **2019**, *6*, 153. [CrossRef]
26. Fišar, Z.; Hroudová, J.; Hansíková, H.; Spáčilová, J.; Lelková, P.; Wenchich, L.; Jirák, R.; Zvěřová, M.; Zeman, J.; Martásek, P.; et al. Mitochondrial Respiration in the Platelets of Patients with Alzheimer's Disease. *Curr. Alzheimer Res.* **2016**, *13*, 930–941. [CrossRef]
27. Fišar, Z.; Jirák, R.; Zvěřová, M.; Setnička, V.; Habartová, L.; Hroudová, J.; Vaníčková, Z.; Raboch, J. Plasma amyloid beta levels and platelet mitochondrial respiration in patients with Alzheimer's disease. *Clin. Biochem.* **2019**, *72*, 71–80. [CrossRef] [PubMed]
28. Cardoso, S.M.; Proença, M.T.; Santos, S.; Santana, I.; Oliveira, C.R. Cytochrome c oxidase is decreased in Alzheimer's disease platelets. *Neurobiol. Aging* **2004**, *25*, 105–110. [CrossRef]
29. Masselli, E.; Pozzi, G.; Vaccarezza, M.; Mirandola, P.; Galli, D.; Vitale, M.; Carubbi, C.; Gobbi, G. ROS in Platelet Biology: Functional Aspects and Methodological Insights. *Int. J. Mol. Sci.* **2020**, *21*, 4866. [CrossRef] [PubMed]
30. Boudreau, L.H.; Duchez, A.C.; Cloutier, N.; Soulet, D.; Martin, N.; Bollinger, J.; Pare, A.; Rousseau, M.; Naika, G.S.; Levesque, T.; et al. Platelets release mitochondria serving as substrate for bactericidal group IIA-secreted phospholipase A2 to promote inflammation. *Blood* **2014**, *124*, 2173–2183. [CrossRef] [PubMed]
31. Leuner, K.; Schutt, T.; Kurz, C.; Eckert, S.H.; Schiller, C.; Occhipinti, A.; Mai, S.; Jendrach, M.; Eckert, G.P.; Kruse, S.E.; et al. Mitochondrion-derived reactive oxygen species lead to enhanced amyloid beta formation. *Antioxid. Redox Signal.* **2012**, *16*, 1421–1433. [CrossRef] [PubMed]
32. Begonja, A.J.; Gambaryan, S.; Geiger, J.; Aktas, B.; Pozgajova, M.; Nieswandt, B.; Walter, U. Platelet NAD(P)H-oxidase-generated ROS production regulates alphaIIbbeta3-integrin activation independent of the NO/cGMP pathway. *Blood* **2005**, *106*, 2757–2760. [CrossRef] [PubMed]
33. Del Dotto, V.; Fogazza, M.; Carelli, V.; Rugolo, M.; Zanna, C. Eight human OPA1 isoforms, long and short: What are they for? *Biochim. Biophys. Acta Bioenerg.* **2018**, *1859*, 263–269. [CrossRef] [PubMed]
34. Aibibula, M.; Naseem, K.M.; Sturmey, R.G. Glucose metabolism and metabolic flexibility in blood platelets. *J. Thromb. Haemost.* **2018**, *16*, 2300–2314. [CrossRef] [PubMed]
35. Zharikov, S.; Shiva, S. Platelet mitochondrial function: From regulation of thrombosis to biomarker of disease. *Biochem. Soc. Trans.* **2013**, *41*, 118–123. [CrossRef] [PubMed]
36. Wang, L.; Duan, Q.; Wang, T.; Ahmed, M.; Zhang, N.; Li, Y.; Li, L.; Yao, X. Mitochondrial Respiratory Chain Inhibitors Involved in ROS Production Induced by Acute High Concentrations of Iodide and the Effects of SOD as a Protective Factor. *Oxidative Med. Cell. Longev.* **2015**, *2015*, 217670. [CrossRef]
37. Rusak, T.; Tomasiak, M.; Ciborowski, M. Peroxynitrite can affect platelet responses by inhibiting energy production. *Acta Biochim. Pol.* **2006**, *53*, 769–776. [CrossRef]
38. Heo, J.H.; Hyon, L.; Lee, K.M. The possible role of antioxidant vitamin C in Alzheimer's disease treatment and prevention. *Am. J. Alzheimer's Dis. Other Dement.* **2013**, *28*, 120–125. [CrossRef]
39. Huang, J.; May, J.M. Ascorbic acid protects SH-SY5Y neuroblastoma cells from apoptosis and death induced by beta-amyloid. *Brain Res.* **2006**, *1097*, 52–58. [CrossRef]
40. Engelhart, M.J.; Geerlings, M.I.; Ruitenberg, A.; van Swieten, J.C.; Hofman, A.; Witteman, J.C.; Breteler, M.M. Dietary intake of antioxidants and risk of Alzheimer disease. *JAMA* **2002**, *287*, 3223–3229. [CrossRef]
41. Baloyannis, S.J. Mitochondrial alterations in Alzheimer's disease. *J. Alzheimer's Dis.* **2006**, *9*, 119–126. [CrossRef] [PubMed]
42. Wisniewski, H.M.; Wegiel, J. Beta-amyloid formation by myocytes of leptomeningeal vessels. *Acta Neuropathol.* **1994**, *87*, 233–241. [CrossRef] [PubMed]
43. Calhoun, M.E.; Burgermeister, P.; Phinney, A.L.; Stalder, M.; Tolnay, M.; Wiederhold, K.H.; Abramowski, D.; Sturchler-Pierrat, C.; Sommer, B.; Staufenbiel, M.; et al. Neuronal overexpression of mutant amyloid precursor protein results in prominent deposition of cerebrovascular amyloid. *Proc. Natl. Acad. Sci. USA* **1999**, *96*, 14088–14093. [CrossRef] [PubMed]
44. Herzig, M.C.; Winkler, D.T.; Burgermeister, P.; Pfeifer, M.; Kohler, E.; Schmidt, S.D.; Danner, S.; Abramowski, D.; Stürchler-Pierrat, C.; Bürki, K.; et al. Abeta is targeted to the vasculature in a mouse model of hereditary cerebral hemorrhage with amyloidosis. *Nat. Neurosci.* **2004**, *7*, 954–960. [CrossRef] [PubMed]
45. Yamagishi, S.I.; Edelstein, D.; Du, X.L.; Kaneda, Y.; Guzmán, M.; Brownlee, M. Leptin induces mitochondrial superoxide production and monocyte chemoattractant protein-1 expression in aortic endothelial cells by increasing fatty acid oxidation via protein kinase A. *J. Biol. Chem.* **2001**, *276*, 25096–25100. [CrossRef] [PubMed]
46. Cardenes, N.; Corey, C.; Geary, L.; Jain, S.; Zharikov, S.; Barge, S.; Novelli, E.M.; Shiva, S. Platelet bioenergetic screen in sickle cell patients reveals mitochondrial complex V inhibition, which contributes to platelet activation. *Blood* **2014**, *123*, 2864–2872. [CrossRef]
47. Hottz, E.D.; Oliveira, M.F.; Nunes, P.C.; Nogueira, R.M.; Valls-de-Souza, R.; Da Poian, A.T.; Weyrich, A.S.; Zimmerman, G.A.; Bozza, P.T.; Bozza, F.A. Dengue induces platelet activation, mitochondrial dysfunction and cell death through mechanisms that involve DC-SIGN and caspases. *J. Thromb. Haemost.* **2013**, *11*, 951–962. [CrossRef]

48. Puskarich, M.A.; Cornelius, D.C.; Tharp, J.; Nandi, U.; Jones, A.E. Plasma syndecan-1 levels identify a cohort of patients with severe sepsis at high risk for intubation after large-volume intravenous fluid resuscitation. *J. Crit. Care* **2016**, *36*, 125–129. [CrossRef]
49. Lust, W.D.; Taylor, C.; Pundik, S.; Selman, W.R.; Ratcheson, R.A. Ischemic cell death: Dynamics of delayed secondary energy failure during reperfusion following focal ischemia. *Metab. Brain Dis.* **2002**, *17*, 113–121. [CrossRef]
50. Kalogeris, T.; Bao, Y.; Korthuis, R.J. Mitochondrial reactive oxygen species: A double edged sword in ischemia/reperfusion vs preconditioning. *Redox Biol.* **2014**, *2*, 702–714. [CrossRef]

3.4. Investigation of platelet migration into the brain parenchyma of APP23 mice

3.4.1 Phenotypic analysis of fluorescent blood cells in *WTmT/mG;PF4Cre+* and *APP23mT/mG;PF4Cre+* mice

In this study, the Cre reporter mouse *mT/mG* was crossed with the megakaryocyte/platelet-specific PF4-Cre mouse. These mice exhibit strong red fluorescence in all tissues and cell types by expressing the loxP-flanked tdTomato (*mT*) cassette with the following stopcodon. When crossed with the megakaryocyte/platelet-specific PF4-Cre mouse, the *mT* cassette in Cre-expressing tissues (platelets and megakaryocytes) is deleted in the progeny, allowing expression of the membrane-directed EGFP cassette (mG), which is located directly downstream of the *mT* cassette. The *mT/mG-Pf4-Cre* mouse was then crossed with the APP23 mouse to obtain a novel phenotypic analysis of platelet localization in an AD mouse model (section 1.4.2). In this new knockin reporter mouse line, platelets in *WTmT/mG;PF4Cre+* and in *APP23mT/mG;PF4Cre+* mice express a mGFP (*mG*) signal, whereas the remaining cells express a mTomato (*mT*) signal (Fig. 15 A). To investigate the specificity of the autofluorescence of platelets in this reporter mouse, blood smears were performed and blood cells were analyzes by flow cytometry. Analyses of the blood smear from *WTmT/mG;PF4Cre+, APP23mT/mG;PF4Cre+* and C57BL/6J mice (negative controls) showed that platelets express a GFP signal in *WTmT/mG;PF4Cre+* and *APP23mT/mG;PF4Cre+* as shown by green fluorescence of platelets in the blood smear. In addition, red blood cells and leukocytes express a slight *mT* signal as shown by red fluorescence. In C57BL/6J mice no prominent fluorescence signal was detectable (Fig. 15 B).

Flow cytometric analysis was performed to examine autofluorescence of blood cells in more detail. Figure 15 C shows that approximately 98% of platelets in the *WTmT/mG;PF4Cre+* and *APP23mT/mG;PF4Cre+* mice exhibit a GFP signal and only 0.5% exhibit a *mT* signal (Fig. 15 C). Given that only a limited number of leukocytes or lymphocytes are accessible for analysis in the blood smear, these cells were examined in more detail using flow cytometry. CD45 was used as a marker for all hematopoietic cells, except erythrocytes and platelets [179]. Approximately 85% of CD45-positive cells were found to be *mT*-positive and thus show red fluorescence. However, 0.5% of CD45-positive cells were GFP-positive and approximately 10% were *mG*- and *mT*-positive in *WTmT/mG;PF4Cre+* and *APP23mT/mG;PF4Cre+* mice (Fig. 15 D) confirming recent results from our group and others [167, 180].

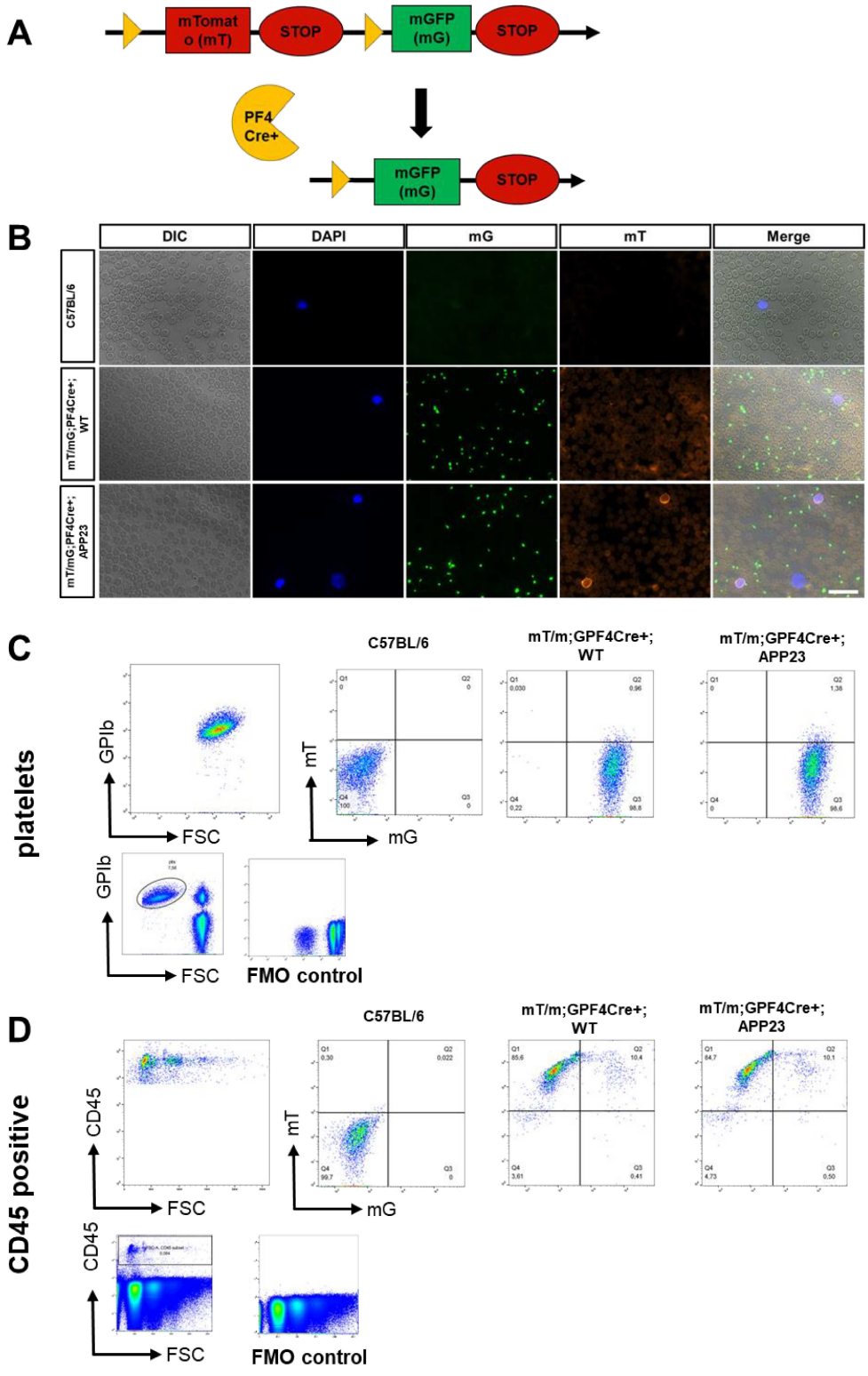

Figure 15: *mT* and *mG* fluorescence of blood cells in *WTmT/mG;PF4Cre+* and *APP23mT/mG;PF4Cre+* reporter mice.

(A) Schematic representation of the genetic construct. (B) Auto fluorescence of cells in the blood smear of C57BL/6J mice, *WTmT/mG;PF4Cre+* and *APP23mT/mG;PF4Cre+* reporter mice Flow cytometric analyses of autofluorescence of (C) platelets and (D) CD45 positive cells from C57BL/6J, *WTmT/mG;PF4Cre+* and *APP23mT/mG;PF4Cre+* mice (n=3-4).

3.4.2 Analysis of platelet localization and abundance in the brain of *WTmT/mG;PF4Cre+* and *APP23mT/mG;PF4Cre+* mice

Vascular inflammation and a disrupted blood-brain barrier (BBB) have been linked to the development of Alzheimer's disease. Moreover, leukocyte subpopulations derived from blood, including neutrophils, have already been detected in the brain of AD patients and in mouse models of AD [70, 181]. Whether platelets migrate into the brain of Alzheimer's patients or transgenic mice is unclear to date. The first aim in this study was to investigate the localization of platelets in the brain of APP23 compared to WT mice at different age (6; 16 and 24 months).

For this purpose, the *WTmT/mG;PF4Cre+* and *APP23mT/mG;PF4Cre+* mouse lines were used in which platelets express a GFP signal (*mG*) and thus show green fluorescence (Fig. 16). Thus specific staining of platelets in brain tissue was not required (section 1.4.2). For better illustration, in the following figures the auto-florescent mTomato channel was not shown because all Cre-non-expressing cells exhibit red fluorescence. To distinguish between vasculature and parenchyma, endothelial cells were stained with an antibody against platelet endothelial cell adhesion molecule-1 (CD31). Two different brain regions were analyzed: First, the hippocampus, which plays an important role in learning and memory and which is affected earliest and most severely in Alzheimer's disease. Second, the cerebral cortex, which is involved in many brain functions such as emotions, thinking, memory, language and consciousness.

Figure 16 A shows representative images of endothelial cell staining in the hippocampus of *WTmT/mG;PF4Cre+* and *APP23mT/mG;PF4Cre+* mice at the age of 6, 16, and 24 months. Single-channel immunofluorescence images are shown in supplemental Figure S 7 and 8. At 6 months of age, platelets were mainly located in the intraluminal space of blood vessels in the hippocampus of *WTmT/mG;PF4Cre+* and *APP23mT/mG;PF4Cre+* mice. At 16 months of age, some platelets were already located outside the vessels (marked with the white arrow head), in *APP23mT/mG;PF4Cre+* but not in *WTmT/mG;PF4Cre+* mice. In 24-month-old *APP23mT/mG;PF4Cre+* and *WTmT/mG;PF4Cre+* mice, a large number of platelets was found outside the blood vessels in the brain parenchyma (Fig.16 A). Quantitative analysis in the hippocampus of different mouse lines in relation to their age revealed that *WTmT/mG;PF4Cre+* and *APP23mT/mG;PF4Cre+* mice had a higher total platelet abundance per brain section at 24 than at 6 months of age ($p<0.0001$ in *WTmT/mG;PF4Cre+* mice and $p=0.0457$ in *APP23mT/mG;PF4Cre+* mice). In *WTmT/mG;PF4Cre+* mice, the platelet abundance was significantly lower at 16 months of age compared with 24 months of age ($p<0.0001$). In *APP23mT/mG;PF4Cre+* mice, there was already a tendency toward a higher platelet abundance observed using 16 months old mice (Fig 16 B). Comparison of genotypes

reveals that the abundance of platelets in the hippocampus is significantly increased in *APP23mT/mG;PF4Cre+* mice compared with *WTmT/mG;PF4Cre+* mice at 16 months of age (p=0.0389; Fig 16 C). These data suggest a time-dependent increase in platelet abundance in the hippocampus in *WTmT/mG;PF4Cre+* and *APP23mT/mG;PF4Cre+* mice, but with an earlier onset in *APP23mT/mG;PF4Cre+* mice.

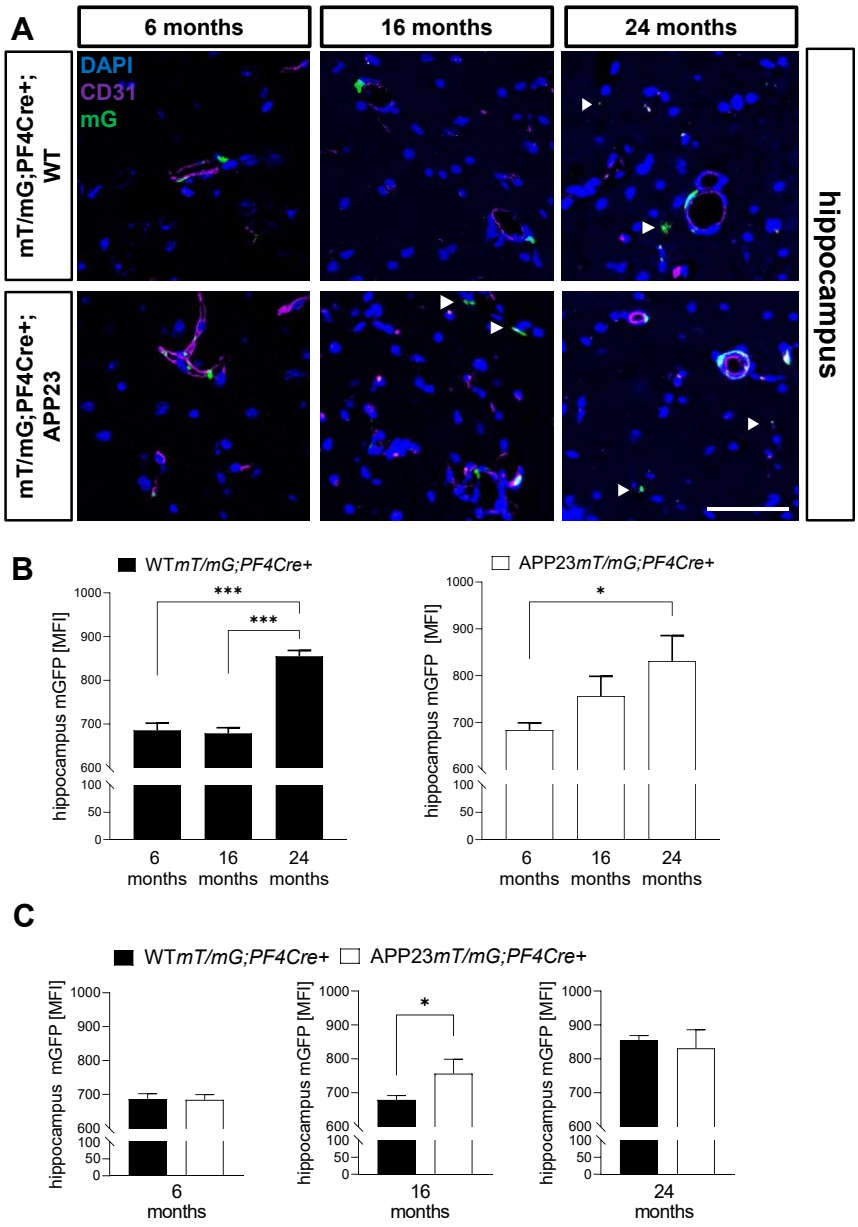

Figure 16: Platelet localization and abundance in the hippocampus of *APP23mT/mG;PF4Cre+* and *WTmT/mG;PF4Cre+* mice at 6, 16, and 24 months of age.

(A) Representative images of immuno-fluorescence staining of endothelial cells (antibody against platelet endothelial cell adhesion molecule 1, CD31; purple) to visualize cerebral vessels in *APP23 mT/mG;PF4Cre+* and WT *mT/mG;PF4Cre+* mice at different age (n=4-5). Platelets express a GFP signal (*mG*; green) and show green fluorscence. Cell nuclei were stained with DAPI (blue). White arrows indicate platelets outside the vasculature. Scale bar = 50 µm (B) Quantification of platelet abundance in the hippocampus of *APP23 mT/mG;PF4Cre+* and *WTmT/mG;PF4Cre+* mice at different age (n=5). For quantification of platelets, the MFI for mGFP was used. (C) Comparison of platelet abundance in the hippocampus of *APP23mT/mG;PF4Cre+* and *WTmT/mG;PF4Cre+* mice of the same age (n=5). Statistical analyses were performed using an ordinary one-way ANOVA followed by a Dunett's post-hoc test (B) or an unpaired t test (C). Bar graphs indicate mean values ± SEM, *p < 0.05; ***p < 0.0001. MFI = mean fluorescence intensity.

Next, platelet localization and abundance was analyzed in the cerebral cortex of *WTmT/mG;PF4Cre+* and *APP23mT/mG;PF4Cre+* mice. Figure 17 A shows representative images of endothelial cell staining in the cortex of *WTmT/mG;PF4Cre+* and *APP23mT/mG;PF4Cre+* mice at the age of 6, 16, and 24 months. In 6-month-old mice, platelets were located in the cerebral cortex within the intraluminal space of blood vessels in both genotypes. In 16-month-old *WTmT/mG;PF4Cre+* and *APP23mT/mG;PF4Cre+* mice, some platelets were found outside the vessels (marked with the white arrow head), while the majority of platelets was detected within vessels (co-localization with CD31). In contrast, in 24-month-old *WTmT/mG;PF4Cre+* and *APP23mT/mG;PF4Cre+* mice, a great number of platelets were localized in the brain parenchyma of the cerebral cortex (Fig. 17 A). Quantification of platelets in the cerebral cortex revealed that *WTmT/mG;PF4Cre+* mice had a higher total platelet abundance at 24 months of age compared with 6 months ($p=0.0002$) and 16 months ($p=0.0007$) of age. *APP23mT/mG;PF4Cre+* mice had a higher total platelet abundance at 24 months of age compared with 6 months of age ($p=0.0219$; Fig. 17 B). In addition, no significant differences were observed between genotypes (Fig. 17 C).

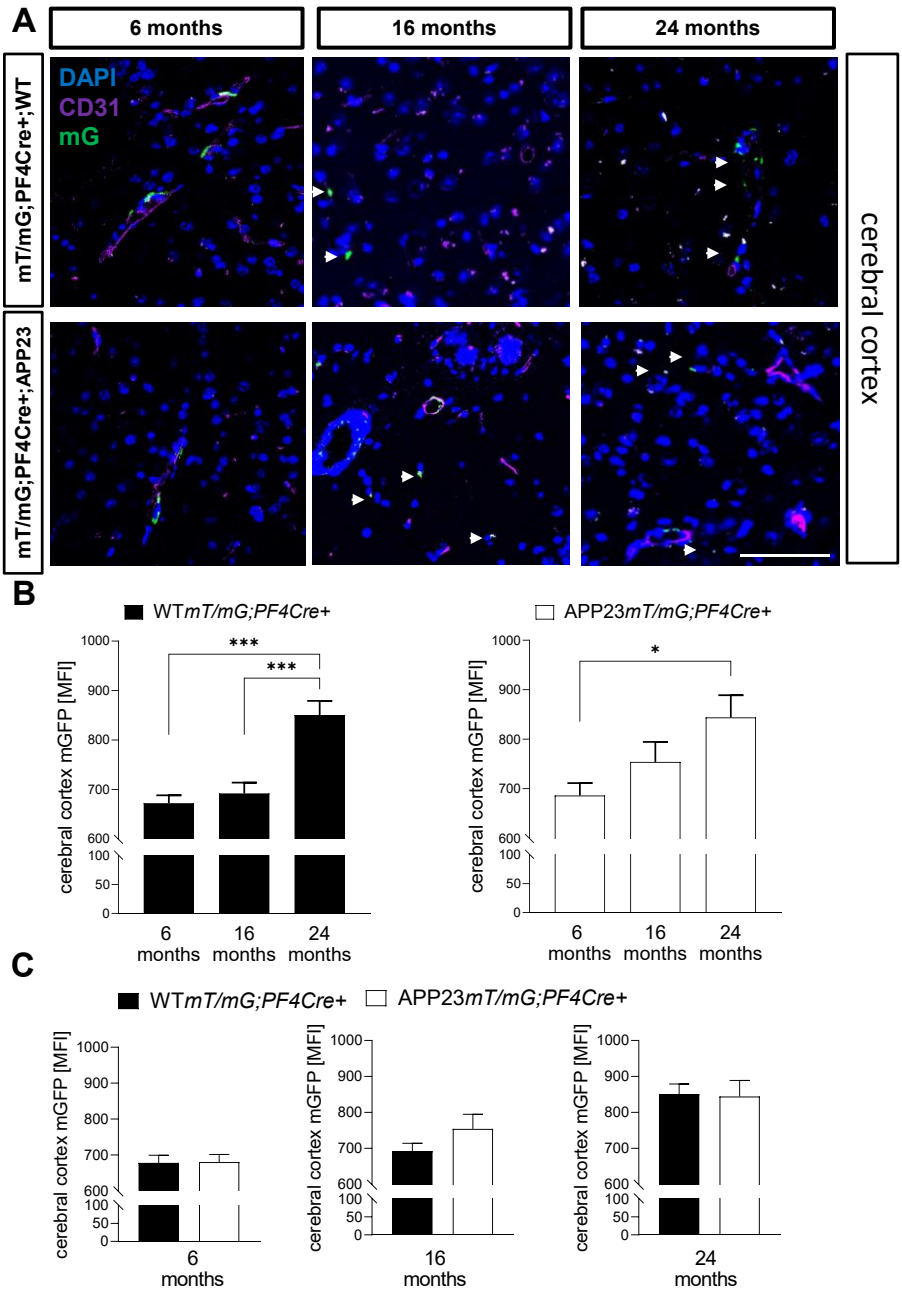

Figure 17: Platelet localization and abundance in the cerebral cortex of *APP23mT/mG;PF4Cre+* and *WTmT/mG;PF4Cre+* mice at the age of 6, 16, and 24 months.

(A) Representative images of immuno-fluorescence staining of endothelial cells (CD31; purple) in *APP23mT/mG;PF4Cre+* and *WTmT/mG;PF4Cre+* mice at different age (n=4-5). Platelets express a GFP signal (mG; green) and show green fluorescence. Cell nuclei were stained with DAPI (blue). White arrows indicate platelets outside the vasculature. Scale bar = 50 µm. (B) Quantification of platelet abundance in the cortex of *APP23mT/mG;PF4Cre+* and *WTmT/mG;PF4Cre+* mice at different age (n=5). For Quantification of platelets in the brain, the MFI for mGFP was used. (C) Comparison of platelet abundance in the cortex between *APP23mT/mG;PF4Cre+* and *WTmT/mG;PF4Cre+* mice of the same age (n=5). Statistical analyses were performed using an ordinary one-way ANOVA followed by a Dunett's post-hoc test (B) or an unpaired t test(C). Bar graphs indicate mean values ± SEM, *p < 0.05; ***p < 0.0001. MFI = mean fluorescence intensity.

3.4.3 Analysis of platelet distribution patterns around amyloid plaques in *APP23mT/mG;PF4Cre+* mice

It has been shown that platelets accumulate and bind to cerebrovascular Aβ deposits and thus may have an impact on Aβ deposition in cerebral vessel and thus contribute to CAA [139]. Furthermore, this work provided first evidence that platelets migrate into the brain parenchyma of *APP23mT/mG;PF4Cre+* mice as early as 16 months of age. To determine whether or not intraparenchymal platelets accumulate in areas with amyloid plaques in the brain, the amyloid plaques were stained with a specific antibody against amyloid-β (6E10) in 16- and 24-month-old *APP23mT/mG;PF4Cre* mice. Mice at 6 months of age were not used for this assay because amyloid pathology is not yet adequately developed at this age in APP23 mice [162]; [182].

Figure 18 A shows the hippocampus and cerebral cortex of *APP23mT/mG;PF4Cre+* mice at 16 and 24 months of age. Single-channel immunofluorescence images are shown in supplemental Figure S 9 and 10. At 16 months of age, only a few platelets were located in close proximity to amyloid plaques. However, the number of platelets around amyloid plaques increased at 24 months of age. The cerebral cortex showed a similar result: With increasing age, the number of platelets that localize to amyloid plaques, increases as well (Fig.18 A).

Quantitative analyses of platelet migration into hippocampal regions of the brain parenchyma showed that in 16-month-old *APP23mT/mG;PF4Cre+* mice, approximately 12% of amyloid plaques had more than 2 mG positive events in their vicinity. In contrast, at 24 months of age, 70% of amyloid plaques were surrounded by more than 2 mG positive events representing migrated platelets. In the cortical brain region of 16-month-old *APP23mT/mG;PF4Cre+* mice, 38% of the amyloid plaques already showed more than 2 mG positive events in their vicinity which further increased up to 67% at 24 months of age (Fig. 18 B). Next, it was examined whether or not there is a relationship between the size of amyloid plaques and the number of mG positive events in the near surrounding. Statistical analysis showed that an increased number of mG positive events correlated positively with the diameter of amyloid plaques (Fig. 18 C; $R=0.7836$; $p< 0.0001$).

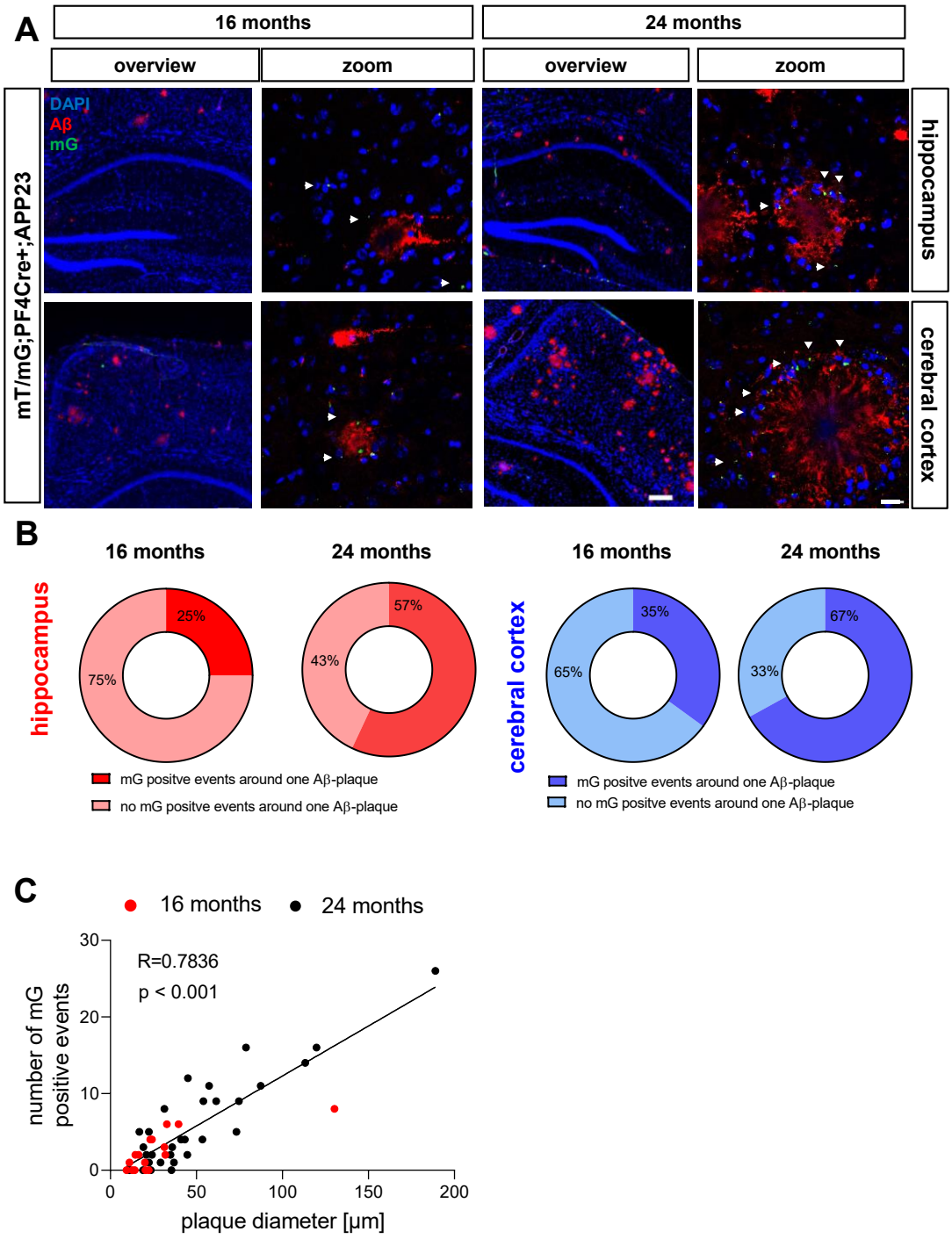

Figure 18: Analysis of platelet localization near to amyloid plaques in the hippocampus and the cortex of *APP23mT/mG;PF4Cre+* mice at the age of 16 and 24 months.

(A) Representative images of immuno-fluorescent staining of amyloid-β (6E10; red) in the hippocampus (upper panel) and the cerebral cortex (lower panel) of 16- and 24-month-old *APP23mT/mG;PF4Cre+* mice. Platelets express a GFP signal (mG; green) and show green fluorescence. Cell nuclei were stained with DAPI (blue). Overview scale bar = 200 µm. Zoom scale bar = 20 µm. White arrows indicate platelets around amyloid plaques. (B) Quantification of platelet abundance around amyloid-β plaques in the hippocampus and cerebral cortex of 16- and 24-month-old *APP23mT/mG;PF4Cre+* (n=5 mice, each with 3-5 plaques). For quantification, the mG positive events around 6E10 positive areas were counted. (C) Spearmen correlation between the diameter of the amyloid plaques and the number of mG positive events in 16 and 24 months old *APP23mT/mG;PF4Cre+* mice (n=5 mice, each with 3- 5 plaques). MFI= mean fluorescence intensity.

3.4.4 Analysis of the interaction of platelets and microglia in the brain of *APP23mT/mG;PF4Cre+* and *WTmT/mG;PF4Cre+* mice

Microglia are innate immune cells of the central nervous system (CNS) that arise from erythromyeloid progenitor cells. Microglia function as resident phagocytes that dynamically monitor the environment and play a critical role in CNS tissue maintenance, response to injury, and defense against pathogens. Amyloid plaques surrounded by activated microglia are part of the inflammatory processes in AD brains [183]. It has been shown that fibrillar Aβ-peptides are able to activate microglia via TLR2 receptors [184]. In addition, microglia are already known to be important for Aβ uptake and degradation. However, continuous activation of microglia by Aβ aggregates or fibrils leads to microglial production of TNFα, IL-1β and other pro-inflammatory cytokines, that may contribute to neurodegeneration [183].

In the present study, immunofluorescence was used to investigate the localization and activation of microglia by IBA-1 staining in relation to platelet localization. Activation of microglia is associated with increased IBA-1 expression, which may be involved in membrane ruffling and phagocytosis. However, it is considered as a marker for all microglia, as non-activated microglia also show IBA-1 protein expression [185]. Single-channel immunofluorescence images are shown in supplemental Figure S 11 and 12.

This study demonstrated that *APP23mT/mG;PF4Cre+* mice display high numbers of IBA-1-positive microglia. High abundance of IBA-1 positive microglia were present in the hippocampus and the cerebral cortex of 24-month-old *APP23mT/mG;PF4Cre+* mice. To a lesser extent, IBA-1 positive microglia were found in 16-month-old *APP23mT/mG;PF4Cre+* mice. In contrast, only low levels of IBA-1-positive microglia were detected in *WTmT/mG;PF4Cre+* mice at 16 and 24 months of age. IBA-1-positive cells are distributed throughout the parenchyma in *WTmT/mG;PF4Cre+* mice. In contrast, IBA-1-positive cells are concentrated in specific regions, most likely around amyloid plaques in *APP23mT/mG;PF4Cre+* mice. Interestingly, in 24 months old *APP23mT/mG;PF4Cre+* mice, platelet positive fluorescent signals directly merge with IBA-1 microglia staining as shown in representative images in Figure 19. This indicates a close proximity of the two cell types in AD transgenic mice (Fig 19).

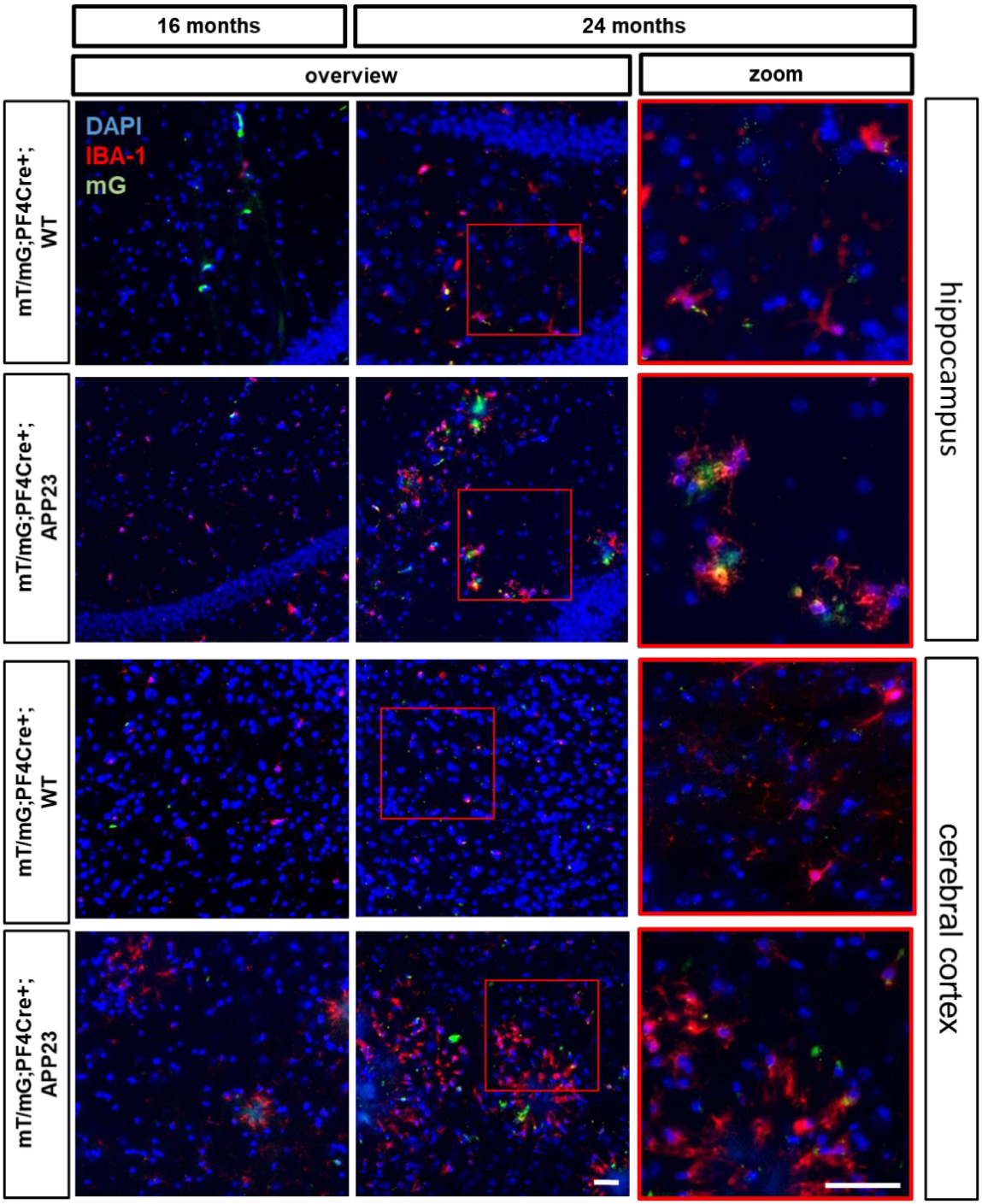

Figure 19: Analysis of platelet interaction with microglia in the hippocampus and the cerebral cortex of APP23mT/mG;PF4Cre+ and WTmT/mG;PF4Cre+ mice at the age of 6, 16 and 24 months.
Representative images of immune-fluorescent staining of microglia (IBA-1; red) in the hippocampus and cerebral cortex of *APP23mT/mG;PF4Cre+* mice. Platelets express a GFP signal (mGFP, green). Cell nuclei were stained with DAPI (blue). Scale bar overview = 50 µm, Scale bar zoom = 50 µm; n=4-5 mice.

3.4.5 Analysis of the interaction of platelets with neurons in the brain of *APP23mT/mG;PF4Cre+* and *WTmT/mG;PF4Cre*$^{+}$ mice

Neuronal loss is a late feature of Alzheimer's disease. In *APP23mT/mG;PF4Cre+* mice, neuronal loss start with 14 -18 months of age and worsens over time [182]. To determine whether or not platelets are located near neurons, neuronal nuclei in 16 and 24-month-old *WTmT/mG;PF4Cre+* and *APP23mT/mG;PF4Cre+* mice were stained with an antibody against neuronal nuclear protein (NeuN; purple). Single-channel immunofluorescence images are shown in supplemental Figure S 13 and 14.

Figure 20 shows an overview and zoom images of the hippocampus and the cerebral cortex of 16 and 24 months old *WTmT/mG;PF4Cre+* and *APP23mT/mG;PF4Cre+* mice. In 16 months old *WTmT/mG;PF4Cre+* mice, almost no platelets were observed near to neuronal nuclei. In contrast, in 16 months old *APP23mT/mG;PF4Cre+* mice and in 24-month-old *WTmT/mG;PF4Cre+* and *APP23mT/mG;PF4Cre+* mice, platelets are partially located near to neurons (Figure 20).

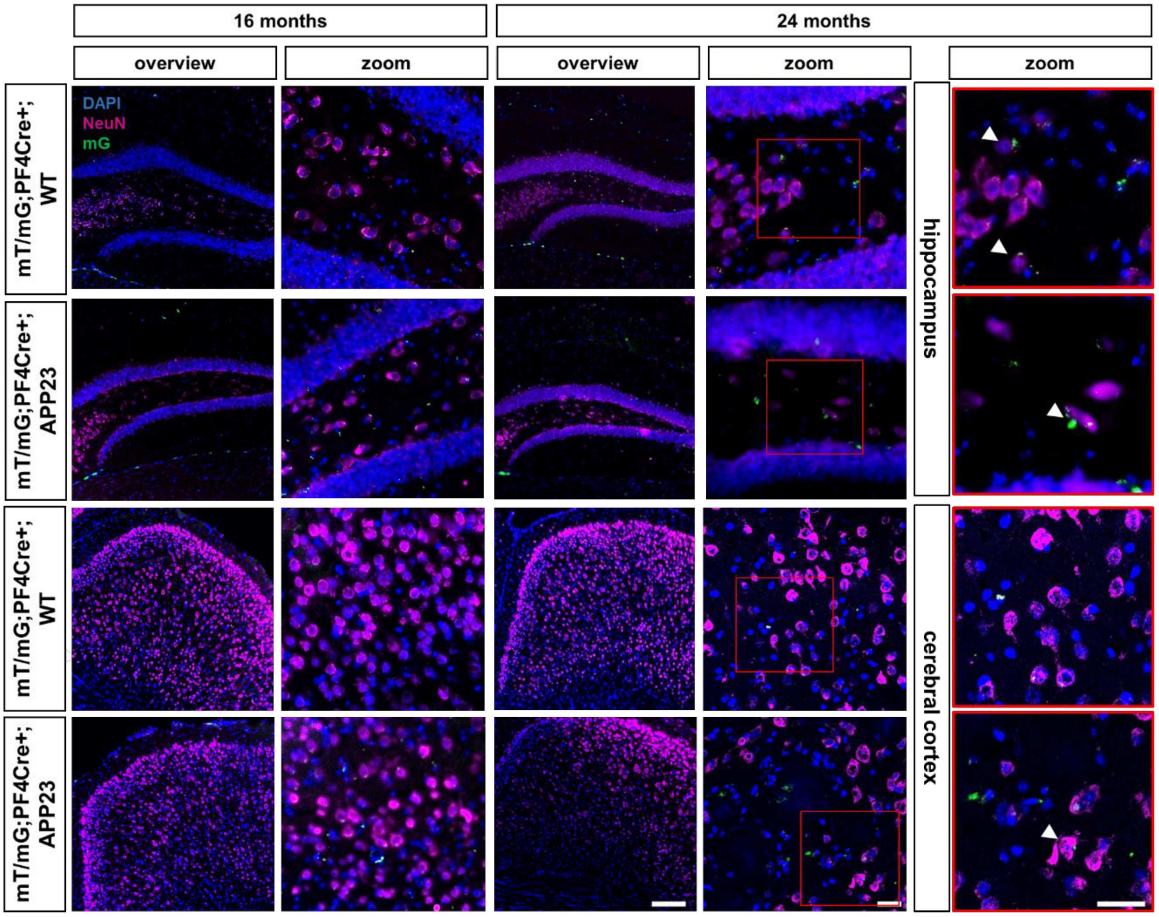

Figure 20: Analysis of platelet interaction with neurons in the hippocampus and the cerebral cortex of *WTmT/mG;PF4Cre+* and *APP23mT/mG;PF4Cre+* mice at 16 and 24 months of age.
Representative images of immune-fluorescent staining of neuronal nuclear protein (NeuN; purble) to detect neurons in the (A) hippocampus and (B) cortex of 16 and 24-month-old *WTmT/mG;PF4Cre+* and *APP23mT/mG;PF4Cre+* mice. Platelets express a GFP signal (mG, green). Cell nuclei were stained with DAPI (blue). Overview scale bar = 200 µm. Zoom scale bar = 20 µm; (n=3).

3.4.6 Analysis of the blood-brain barrier permeability of *APP23mT/mG;PF4Cre+* and *WTmT/mG;PF4Cre+* mice

Another pathological feature of Alzheimer's disease is a disruption of the BBB, characterized, in part, by impaired perivascular Aβ clearance, oxidative stress, and a leaky BBB [186]. To analyze whether the increase in platelet count in the brain parenchyma could be due to impaired BBB, immunoglobulin G (IgG) staining was performed. Anti-IgG staining reveals sites of impaired blood-brain barrier in the brain. Areas with a "leaky" BBB allow serum proteins such as IgGs to enter the brain parenchyma. Single-channel immunofluorescence images are shown in supplemental Figure S 15 and 16.

Images of IgG staining (red) in the cerebral cortex of 6-, 16-, and 24-month-old *WTmT/mG;PF4Cre+* and *APP23mT/mG;PF4Cre+* mice showed increased IgG abundance in 24-month-old mice compared to 6 and 16 month-old mice, indicating a damaged BBB with increasing age in both genotypes (Fig. 21 A and B). A comparison of genotypes showed that the number of IgGs entering the brain was strongly increased in 24-month-old *APP23mT/mG;PF4Cre+* mice compared to 24-month-old *WTmT/mG;PF4Cre+* and tended to increase in 16-month-old *APP23mT/mG;PF4Cre+* mice compared to 16-month-old *WTmT/mG;PF4Cre+* mice. In addition, zoom-in images of the vessel wall indicated a high IgG abundance accompanied by platelet positive green fluorescence (mG signal). This data indicates that the damaged BBB might allow cerebral microbleeding that might be –at least in part- responsible for the presence of platelets in the brain parenchyma, which is in line with previous data shown by Reuter *et al.* [187] (Fig. 21 A).

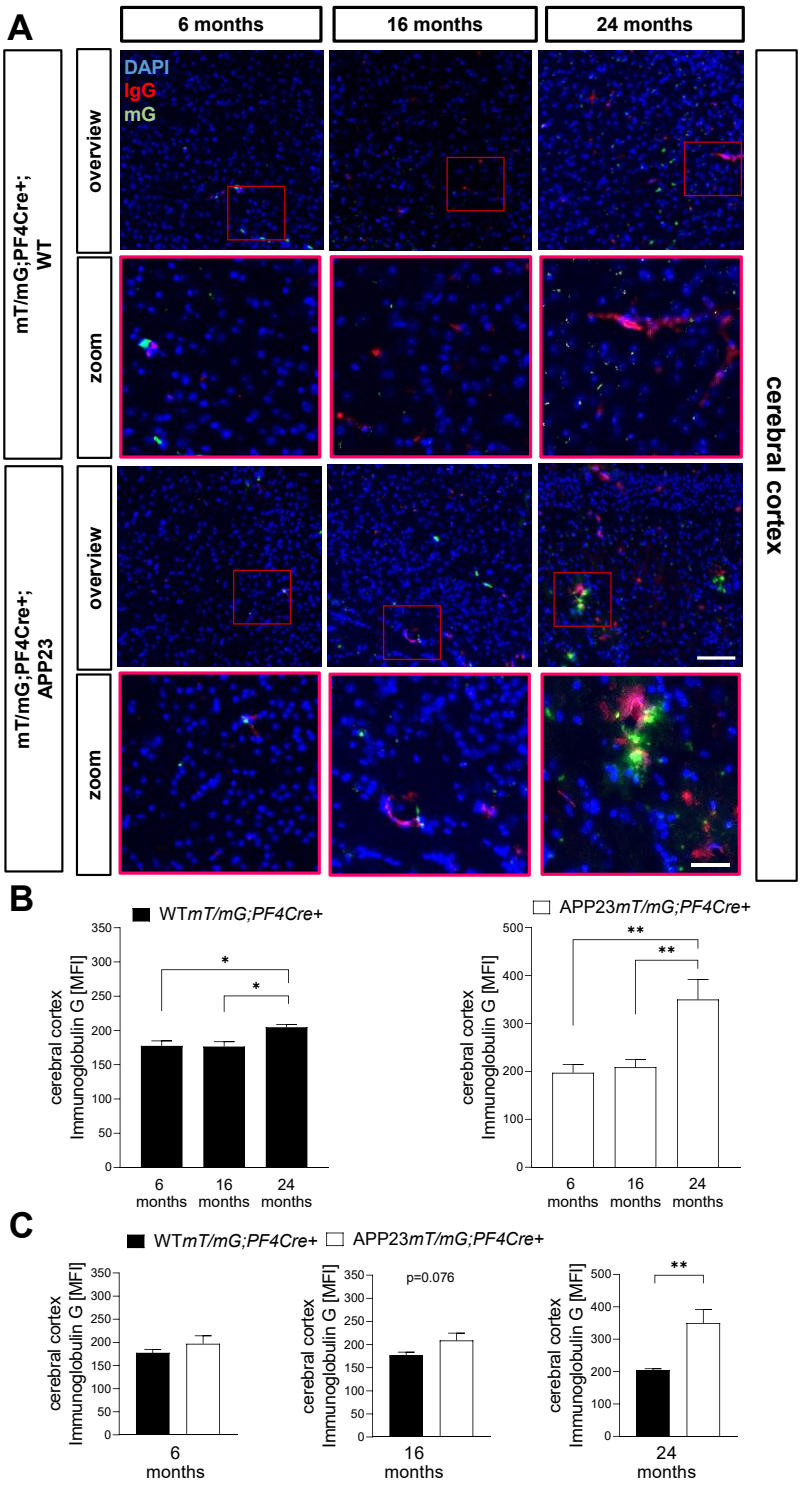

Figure 21: Analysis of blood-brain barrier permeability in the cerebral cortex of *WTmT/mG;PF4Cre+* and *APP23mT/mG;PF4Cre+* mice at 6, 16, and 24 months of age.

(A) Representative images of immuno-fluorescence staining of immunoglubolins G (IgG; red) in the cortex of 6, 16- and 24-month-old APP23mT/mG;PF4Cre+ mice. Platelets express a GFP signal (*mG*). Cell nuclei were stained with DAPI (blue). Scale bar overview = 100 µm. Scale bar zoom = 20 µm (B) Quantification of IgG abundance (MFI) in the cortex of *WTmT/mG;PF4Cre+* and *APP23mT/mG;PF4Cre+* mice at different age (n=5-7). (C) Comparison of IgG abundance (MFI) in the cortex of *WTmT/mG;PF4Cre+* and *APP23mT/mG;PF4Cre+* mice of the same age (n=5-7). Scale bar 100 µm (overview) and 20 µm (zoom). Statistical analyses were performed using an ordinary one-way ANOVA followed by a Dunett's post-hoc test (B) or an unpaired t test (C). Bar graphs indicate mean values ± SEM, *p < 0.05; **p < 0.01. MFI = mean fluorescence intensity.

In addition, the hippocampal region was also examined for BBB permeability using IgG staining. Figure 22 A shows different images of the IgG staining in 6, 16 and 24 months old *WTmT/mG;PF4Cre+* and *APP23mT/mG;PF4Cre+* mice. Only a few IgG-positive areas were observed in the hippocampus, mainly in 24-month-old mice *APP23mT/mG;PF4Cre+* mice.

Figure 22 B shows the corresponding quantification within genotypes with respect to their age. The quantification revealed that IgG abundance was significantly increased in 24-month-old compared to 6- and 16-month-old *APP23mT/mG;PF4Cre+* mice. No significant increase in IgG abundance was observed in *WTmT/mG;PF4Cre+* mice with respect to age. Comparison between genotypes revealed that IgG abundance was greatly elevated in *APP23mT/mG;PF4Cre+* mice at 24 months of age compared to *WTmT/mG;PF4Cre+* mice at the same age (Fig 22 C).

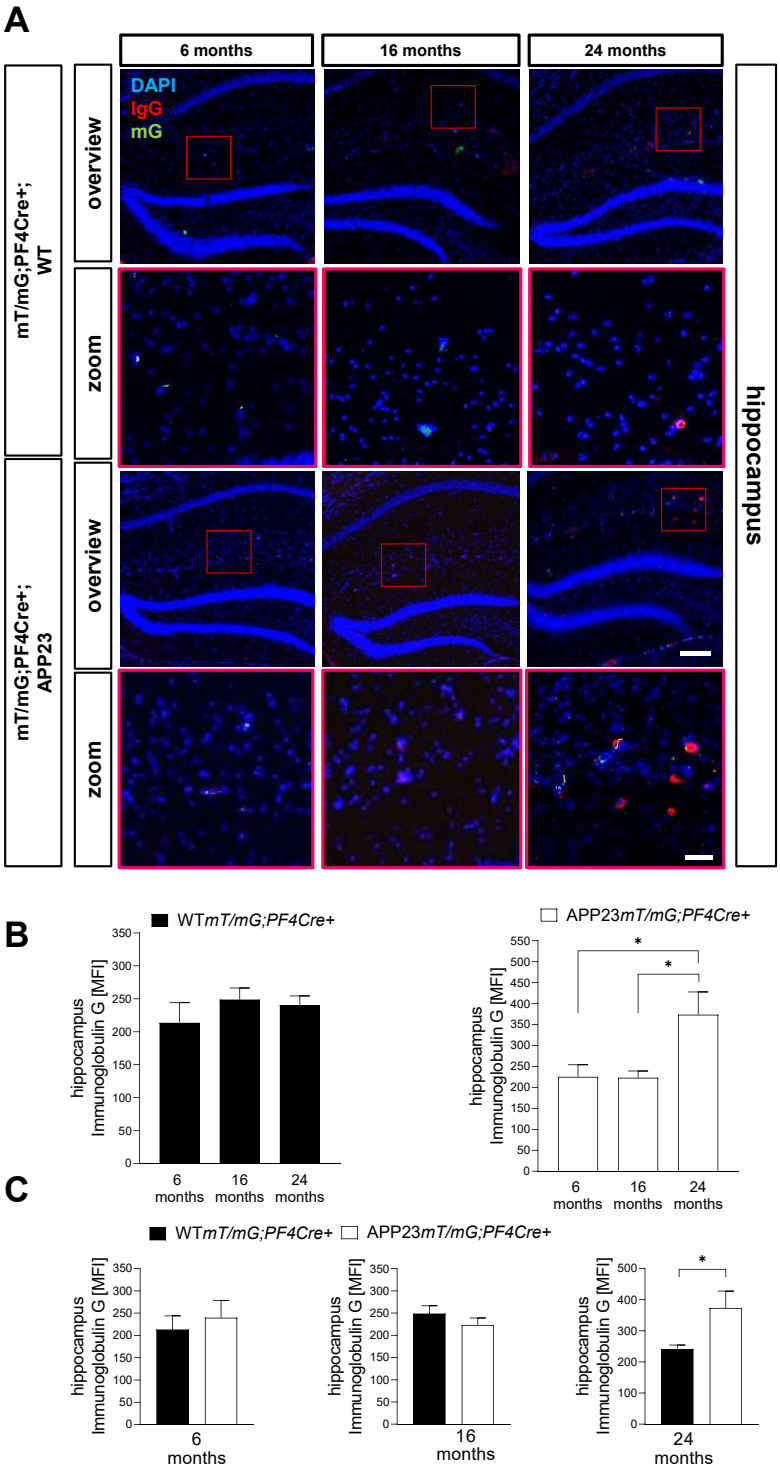

Figure 22: Analysis of blood-brain barrier permeability in the hippocampus of WTmT/mG;PF4Cre+ and APP23mT/mG;PF4Cre+ mice at 6, 16, and 24 months of age.

(A) Representative images of immuno-fluorescence staining of immunoglobulin G (IgG; red) in the hippocampus of 6, 16- and 24-month-old *WTmT/mG;PF4Cre+* and *APP23mT/mG;PF4Cre+* mice. Platelets express a GFP signal (*mG*). Cell nuclei were stained with DAPI (blue). Scale bar overview = 100 µm. Scale bar zoom = 20. (B) Quantification of IgG abundance (MFI) in the hippocampus of *WTmT/mG;PF4Cre+* and *APP23mT/mG;PF4Cre+* mice at different age (n=5-7). (C) Comparison of IgG abundance (MFI) in the hippocampus between genotypes of the same age (n=5-7). Statistical analyses were performed using an ordinary one-way ANOVA followed by a Dunett's post-hoc test (B) or an unpaired t test (C). Bar graphs indicate mean values ± SEM, *p < 0.05. MFI = mean fluorescence intensity.

4 Discussion

4.1 Impact of platelet glycoprotein VI in the progression of Alzheimer's disease

Alzheimer's disease (AD) is the most frequently diagnosed neurodegenerative disease and characterized by the deposition of amyloid-β plaques and neurofibrillary tangles in the brain. In addition to these well-known changes in the brain, there are also cerebrovascular changes seen in many patients with AD. Especially the accumulation of Aβ40 in the vascular walls, called cerebral amyloid angiopathy (CAA), is a commonly observed feature in AD. The presence of CAA in patients with AD increases the rate of decline in cognition and semantic memory. In addition, an increased risk of developing AD was observed after stroke when vascular risk factors such as hypertension or heart disease were already present [188]. This points to a complex relationship between age-related cerebrovascular changes and AD that is not yet fully understood, as many factors may influence each other. For this reason, the elucidation of the pathophysiological mechanisms contributing to the development of AD has been the subject of intensive scientific research for decades.

This study further elucidates the role of platelets in the progression of AD. In the research group Experimental Vascular Medicine (Prof. Elvers) it has already been shown that platelets are able to bind Aβ40 via the integrin αIIbβ3 receptor on the platelet surface and to modify soluble Aβ40 to amyloid-β aggregates *in vitro*. The binding of Aβ40 to the integrin αIIbβ3 receptor induces outside-in signalling and the release of ADP, which induces further activation of platelets by ADP binding to the $P2Y_{12}$ receptor [103]. Moreover, Donner *et al.* already showed that the irreversible inhibition of the $P2Y_{12}$ receptor by clopidogrel reduces CAA burden in APP23 mice, an AD mouse model, and platelet-mediated amyloid-β fibril formation *in vitro* [103]. Epidemiological and imaging studies have demonstrated vascular dysfunction in more than 50% of AD patients, manifested by altered BBB permeability, micro- and macroinfarcts, microhemorrhages, and lacunar strokes [189]. A disadvantage of clopidogrel therapy as a long-term treatment are side effects such as an increased tendency to bleed and, in very rare cases, cerebral hemorrhage [190]. Therefore, in the present study, the effect of Aβ40 on the major collagen receptor GPVI on platelets with regard to amyloid-β fibril formation and platelet activation was analyzed.

The first aim of this study was to investigate the influence of Aβ40 on platelet GPVI and its role in amyloid-β fibril formation and platelet activation. This study demonstrates in different experimental setups that -besides integrin αIIbβ3- Aβ40 also binds to GPVI on the platelet surface (section 3.1). Based on the experiments performed in this study, it was not possible to conclude whether monomeric or oligomeric Aβ40 binds to GPVI. Freshly prepared soluble Aβ40 was used in the experiments, however, Bitan and colleagues have already shown that carefully prepared aggregate-free Aβ40 also exists as monomers, dimers, trimers, and tetramers in rapid equilibrium [191]. These different types of soluble Aβ oligomers have different size ranges, varying from 4 kDa as a monomer, 7 kDa as a dimer, and 11 kDa as a trimer [192]. In this study, some Aβ40 Western blot analyses from cell culture experiments show a small additional band above the 4 kDa band at the level of 10 kDa, suggesting that Aβ40 dimers or trimers were also formed within the experiments (section 3.1). Since collagen, the natural ligand of GPVI, is composed of amino acids bound together in a triple helix of elongated fibrils, one might speculate that the hydrophobic fibrillar Aβ40 binds to GPVI in an increased manner. However in recent years, many other endogenous and exogenous ligands have been shown to activate GPVI, including a number of snake venom toxins such as convulxin or a variety of charged exogenous ligands, including diesel exhaust particles. The conditions and modalities of GPVI activation by these ligands are still unknown [193]. For further elucidation of Aβ40–GPVI interaction, experiments such as surface plasmon resonance (SPR) or Bio-layer interferometry (BLI) can be used to determine the binding kinetics, specificity, affinity, and thermodynamics of biomolecular interactions [194].

In addition to these binding studies, the incubation of human platelets with Aβ40 leads to a rapid externalization of GPVI at the platelet surface (section 3.1.2 Fig.7). This may increase the platelet binding capacity for Aβ40 through an increase in GPVI surface abundance. As early as 2003, Takayama and colleagues reported that activation of human platelets with GPVI-specific ligands induces an increasing redistribution of GPVI to the surface membrane from the membranes of the surface-connected open canalicular system (OCS) and α-granules [169]. Beside increased externalization of GPVI, ligand binding could also induce GPVI shedding and thereby contribute to soluble plasma levels of GPVI [170]. However, no shedding of GPVI after Aβ40 stimulation in either whole blood or isolated platelets was observed (section 3.1.2; Fig.7). This may indicate that Aβ40 does not trigger the activation of ADAM10/ADAM17 metalloproteinases or possibly blocks the GPVI binding side of these cleavage enzymes. Interestingly, Lake *et al.* reported that patients with fully developed AD had significantly lower sGPVI plasma levels as compared to healthy controls [195].

Previously, it was shown that sGPVI can bind to exposed collagen of the injured vessel wall [196]. This suggests that in CAA, inflammatory processes might lead to the injury of the vessel wall and to the exposure of collagen, resulting in the binding of sGPVI. This could be one reason for the decreased sGPVI plasma levels in AD patients. Another reason could be that sGPVI is able to bind to Aβ40 at the vascular wall. Mayeux *et al.* found that Aβ40 and Aβ42 plasma levels are increased in some patients before and during the early stages of AD, but decrease thereafter [197]. Here, one can speculate whether or not plasma Aβ40 is incorporated into CAA and thus binds to platelets via GPVI and inhibits GPVI shedding.

Furthermore, the present study demonstrates that stimulation of platelets with Aβ40 causes platelet activation. This is evidenced by increased tyrosine phosphorylation and LAT activation by phosphorylation (Tyr^{200}), which are both abolished in GPVI-deficient mouse and human platelets (section 3.1 and 3.1.2; Fig 6). Aβ40-induced GPVI activation ultimately leads to ATP release and platelet aggregation in human platelets and is reduced by losartan, which is known to inhibit platelet aggregation after collagen stimulation (section 3.1). In 2017, Elaskalani and colleagues found that oligomeric and fibrillar Aβ42 is able to induce platelet aggregation partially through GPVI. Therefore, they also used losartan, which reduced platelet aggregation upon Aβ42 stimulation [198]. However, the exact mechanism how losartan inhibits collagen-induced platelet aggregation has not been elucidated yet. Jiang *et al.* demonstrated that losartan inhibits the clustering of GPVI but not the binding of recombinant GPVI to collagen [199]. Losartan is classically known as a non-peptidic inhibitor of Ang II AT1 receptors, and platelets also express Ang II AT1 type receptors on their surface [200]. Platelet activation by angiotensin II does not lead to aggregation and can therefore be neglected. However, losartan has also been shown to inhibit platelet aggregation triggered by the thromboxane A2 analog U46619. [201]. Therefore, in addition to losartan, platelets from GPVI-deficient patients and mice were used to provide further evidence that the reduced aggregation and ATP release was due to the interaction of GPVI with Aβ40 rather than nonspecific side effects of losartan. Taken together, Aβ40 stimulation induces an increased externalization of GPVI at the plasma membrane and the release of ATP/ADP in part via GPVI. ADP in turn activates the $P2Y_{12}$ receptor. This leads to a feed-forward-loop of platelet activation and binding of Aβ40 to platelets, resulting in platelet aggregation. With regard to CAA, this mechanism could lead to increased amyloid-β and platelet aggregation in the vasculature and, moreover, to an inflammatory environment and occlusion of cerebral vessels of AD patients, resulting hypoxia and thus could influence neurodegeneration.

In line with studies in the past, this thesis shows that platelets modify soluble Aβ40 into toxic insoluble amyloid-β aggregates *in vitro*.

The present study is the first to demonstrate that GPVI plays a key role in platelet-mediated formation of amyloid-β aggregates by binding Aβ40 (section 3.1). Furthermore, the incubation of platelets with Aβ40 induces ROS production via GPVI (section 3.3). In AD brains, ROS has previously been shown to increase the expression of β-secretase through activation of p38 mitogen-activated protein kinase 23 and to increase abnormal tau phosphorylation through activation of glycogen synthase kinase [202, 203]. In the vascular system, excessive ROS production can lead to vascular cell damage by recruiting inflammatory cells, lipid peroxidation, and activating metalloproteinases [204]. Chronic damage to the vascular cells could further damage the BBB and may be the reason for the increased prevalence of microbleeds in patients with AD [205]. In addition, we could show, that ROS in platelets leads to increased activation of integrin αIIbβ3 in the presence of Aβ40 and thus may increase the formation of amyloid-β aggregates (section 3.3). Vitamin C as a ROS scavenger reduces platelet-mediated amyloid-β aggregate formation (section3.3).

In vitro, inhibition of GPVI by antibody treatment or genetic deletion can significantly reduce platelet-mediated formation of toxic amyloid-β aggregates (section 3.1). It is already known that CAA-positive vessels in the brains of APP23 and patients also contain fibrin(-ogen) deposits [147]. This study could show that stimulation of platelets with Aβ40 induces the release of fibrin(-ogen) in a GPVI depend manner and that platelet-mediated formation of amyloid-β aggregates co-localize with fibrinogen *in vitro* (section 3.1). GPVI inhibition or genetic depletion reduces these amyloid-β fibrinogen aggregates *in vitro*. In 2016, Donner *et al.* showed that Aβ40 binds to fibrinogen [103]. Previously, Ahn *et al.* had also found that Aβ42 and, to a lesser extent, Aβ40 can interact with fibrinogen by binding near the C-terminus of the β-chain of fibrinogen. Furthermore, Ahn *et al*. demonstrated that this interaction leads to abnormal oligomerization of fibrinogen. In addition, blood clots formed in the presence of Aβ have been shown to be more resistant to degradation [206]. Thus, thinking about CAA, one might speculate that binding of Aβ to platelet GPVI and integrin αIIbβ3 induces platelet activation and the release of ATP/ADP, ROS and fibrinogen. Fibrinogen, in turn, binds to integrin αIIbβ3 and Aβ, thereby creating cerebral amyloid aggregates that may be more resistant to degradation. Furthermore, the blocking or deletion of GPVI reduces Aβ40-induced platelet adhesion in the carotid artery ligation model *in vivo* (section 3.1). However, further studies are required to address the question if GPVI inhibition might also reduce CAA burden or even improves cognition *in vivo.* In this study, losartan was used as an off-target GPVI inhibitor in a platelet culture assay. No reduction in amyloid-β aggregate formation was observed *in vitro* (section 3.1). As already mentioned, losartan is not specific for GPVI and probably does not inhibit the direct binding of Aβ40 to GPVI.

Likewise, in 2021, a double-blind, placebo-controlled phase 2 trial demonstrated that 12 months of losartan treatment did not effectively reduce the rate of brain atrophy in individuals with clinically diagnosed mild to moderate AD [207]. Previously, in 2016, Donner *et al.* used aspirin as an antiplatelet agent in platelet cell culture with Aβ40 that also failed to induce a reduction in platelet-mediated amyloid-β aggregate formation [103]. Interestingly, in 2022 in a nested case-control study within a cerebral small vessel disease cohort Pan *et al.* could show that only clopidogrel reduced the risk of dementia while aspirin and cilostazol appeared to have no effect [208]. Platelet inhibition can be achieved either by blocking membrane receptors or by interfering with intracellular signaling pathways. Aspirin and cilostazol inhibit intracellular signaling by blocking platelet cyclooxygenase (aspirin) and phosphodiesterase (cilostazol), resulting in a decreased production of thromboxane A (aspirin) and increased production of cyclic adenosine monophosphate (cAMP; cilostazol) [209, 210]. These findings highlight that platelet inhibition alone may not be sufficient to reduce Alzheimer's risk, but selective blockade of key pathways may be more promising. Overall, our results show that Aβ40 binds GPVI and increase GPVI externalization at the platelet surface. Moreover, Aβ40 triggers platelet aggregation, activation, and the release of ROS, ATP and fibrinogen with GPVI playing an important role in platelet-induced amyloid-β aggregate formation *in vitro*. However, further studies are needed to clarify whether inhibition of GPVI is able to reduce CAA burden *in vivo* and, moreover, whether GPVI may be a promising target for AD.

4.2 Influence of Aβ40 on platelet-triggered inflammation and neutrophil recruitment in the progression of Alzheimer's disease

There is compelling evidence that Alzheimer's disease-related inflammation develops in two distinct but interconnected areas: the blood and the brain. Several reports have suggested that neutrophils may also play a role in the progression of AD beside their role in inflammatory responses under pathological conditions [70, 175]. Zenaro *et al*. demonstrated that depletion of neutrophils reduces Alzheimer's disease neuropathology and improves memory in an Alzheimer's mouse model. [70]. In addition, Hernández *et al.* showed that neutrophil adhesion in brain capillaries reduces cortical blood flow and so impairs memory function in an AD mouse model [175]. Platelets are important for neutrophil recruitment under inflammatory conditions such as thrombosis or stroke [173]. However, the interaction of platelets and neutrophils in AD is not well understood. Therefore, this thesis investigated the interaction between platelets and neutrophils upon Aβ40 stimulation and the influence of Aβ40 on platelet-triggered inflammation.

The results from this study shows that the activation of platelets with Aβ40 induces the formation of platelet-neutrophils aggregates (PNA) in murine whole blood (section 3.2.1; Fig. 8). In this series of experiments, PNA formation appears to be GPVI-independent, as no differences in PNA formation was observed in GPVI-deficient platelets (section 3.2.1; Fig. 8). One possible mechanism of this interaction is that the activation of platelets with Aβ40 triggers integrin αIIbβ3 activation and subsequent fibrinogen binding that allows binding of neutrophils to fibrinogen via integrin αMβ2 (Mac-1) [103]. Several *in vivo* and *in vitro* studies have already shown that platelet activation induces stable binding of platelets and neutrophils [211], but until to date it is not known whether Aβ40 can influence this interaction. In blood samples from AD patients, Dong *et al.* found that neutrophils were hyperactive, which was associated with increased production of ROS and augmented NETosis suggesting systemic, chronic inflammation [74]. This study analyzed 15-month-old APP23 mice to investigate if these mice exhibit increased PNA formation. However, we could not detect differences in PNA abundance in whole blood and in plasma neutrophil elastase concentrations in APP23 compared to WT mice (section 3.2. Fig. 8 and Fig. 11). One reason for these differences could be the different ratio of the leukocyte subgroups between humans and experimental mice. In human blood, neutrophils predominate (50-70% neutrophils, 30-50% lymphocytes), whereas in mouse blood, lymphocytes predominate (75-90% lymphocytes, 10-25% neutrophils) [212]. In addition, important cross-species differences are evident between human and mouse neutrophil activation and signal transduction, such as cytokine release [213], ROS production [214], and cytotoxic granule content [215]. Although there are many differences between mice and humans, it is still important to study this phenomenon in mice as well to better understand the development of AD and to be aware of the differences between AD mouse models and AD patients.

In AD patients it has been reported that fibrinogen levels are positively correlated with Aβ40 and Aβ42 plasma levels [216] and that high fibrinogen levels were associated with an increased risk of both, AD and vascular dementia [217]. This study reveals that binding of Aβ40 to GPVI triggers the release of fibrinogen (section 3.1). Therefore, fibrinogen was measured in the plasma of 15-month-old APP23 and WT mice (section 3.2.1; Fig. 8). In this experiment, no differences in plasma fibrinogen levels were detectable in APP23 compared with WT mice. Previous studies have shown that fibrinogen can enter the brain and accelerate inflammation and neuronal damage [218, 219]. One reason for unchanged plasma fibrinogen levels could be that fibrinogen is consumed upon formation of Aβ plaques in the brain parenchyma and vessel walls.

In APP23 and WT mice, it has already been shown that plasma levels of Aβ40 and Aβ42 decrease after 12 months of age, raising the question whether or not fibrinogen plasma levels also change after a certain time in AD [220].

In addition to fibrinogen, the cytokine TGF-β1 was also measured in plasma. APP23 mice have increased plasma levels of TGF-β1 compared with WT mice (section 3.2.1; Fig. 8). Malaguarnera *et al.* showed that the plasma levels of TGF-β1 were significantly elevated in AD patients compared to non-demented age matched controls [221]. TGF-β1 acts as a chemoattractant for monocytes, fibroblasts, and neutrophils and thus has potent inflammatory activity [222]. Platelets contain 40 to 100 times more TGF-β1 as other cells and are the major source of plasma TGF-β1 [127, 223]. This study demonstrates that stimulation of platelets with Aβ40 leads to an increased release of TGF-β1 that is mediated –at least in part- by GPVI (section 3.2.1 Fig. 8). To date, the effects of TGF-β1 on the development of AD have been discussed controversial. Wyss-Cory *et al*. showed that chronic overproduction of TGF-β1 by astrocytes triggers an accumulation of basement membrane proteins and results in Aβ deposition in cerebral blood vessels and microvascular degeneration [224]. Furthermore, Kato *et al.* have shown that overproduction of TGFβ1 by astrocytes leads to failure of mural cells in the vessel wall, which is accompanied by the dilatation of cerebral vascular lumina [225]. These processes could lead to BBB damage and thus play a major role in the progression of AD. In contrast, recombinant TGF-β1 was also shown to promote microglial Aβ clearance and to reduce parenchymal plaque burden in transgenic mice [226]. These examples demonstrate that controlled production of TGF-β1 has a protective, anti-inflammatory function, but that uncontrolled TGF-β1 production can lead to a proinflammatory environment leading to the damage of vascular cells. However, further studies are needed to determine whether lowering plasma TGF-β1 levels may also have beneficial effects, for example, by reducing the degeneration of cells of the vessel wall. In addition, lowering TGF-β1 plasma levels could influence neutrophil recruitment and reduce the inflammatory burden in vessels.

In addition, the results from this thesis show that dual stimulation of human or murine platelets with ADP and Aβ40 induces an increase in platelet-mediated neutrophil adhesion *in vitro* (section 3.2.3; Fig. 10 anf Fig. 13). One reason for an increase in neutrophil adhesion only with dual stimulation of platelets could be that the initial interaction between neutrophils and platelets are mainly mediated by binding of neutrophil P-selectin glycoprotein ligand-1 (PSGL-1) to platelet P-selectin [227]. Stimulation of murine platelets with either ADP or Aβ40 alone does not significantly increase P-selectin expression on the platelet surface as shown earlier by Gowert *et al*. [143].

In contrast, dual stimulation of platelets with ADP and Aβ40 significantly increases P-selectin expression at the surface of platelets from mice and humans and thus allows binding to PSGL-1 at the neutrophil surface [103, 143, 228]. Another interaction between neutrophils and platelets is mediated by the binding of neutrophil αMβ2 integrin with fibrinogen that is bound to platelet integrin αIIbβ3 as already mentioned above. This work already shows that stimulation of platelets with Aβ40 induces the release of fibrinogen via GPVI and integrin αIIbβ3 activation (section 3.1). Fibrinogen, in turn, can bind to integrin αMβ2 at the surface of neutrophils and thus allows direct interaction of platelets and neutrophils [131]. In contrast to the PNA analyses in murine whole blood, where Aβ40 alone triggers PNA formation, plasma proteins such as fibrinogen are more limited in this cell culture experiment because fibrinogen must be released from activated platelets. Thus, it might be feasible that Aβ40 and fibrinogen, as well as activated platelets with P-selectin exposure at the plasma membrane, provide a matrix for the adhesion of neutrophils. In addition, the inhibition of platelet integrin αIIbβ3 by antibody treatment reduced murine neutrophil adhesion almost to resting levels suggesting that integrin αIIbβ3 is required for platelet neutrophil interaction. GPVI deficiency had a lesser effect on neutrophil adhesion but still showed a significant reduction. This points to an indirect role of GPVI in this process, since activation of GPVI leads to activation of integrin αIIbβ3. Furthermore, other signaling pathways also lead to integrin αIIbβ3 activation, such as activation of $P2Y_{12}$ with ADP, so that GPVI defects could be compensated to some extent. Nonetheless, only dual inhibition of integrin αIIbβ3 and GPVI decreased neutrophil adhesion to resting levels (section 3.2.4 Fig. 12). *In vivo,* GPVI deficiency has already been demonstrated to reduce neutrophil recruitment and leukocyte infiltration in the experimental myocardial ischemia-reperfusion model, thus playing an important role the inflammatory process [229]. More recently, it was also shown that blocking of GPVI reduces neuro-inflammation during middle cerebral artery (MCA) occlusion by reducing neutrophil and T-cell recruitment to the ischemic brain [230]. Further *in vivo* studies are needed to investigate whether or not platelet-induced neutrophil adhesion may also play a role in neutrophil infiltration in AD and if the inhibition of either GPVI or integrin αIIbβ3 has a beneficial effect by reducing the inflammatory response in AD.

As platelets are able to modify soluble Aβ40 into amyloid-β fibrils, this thesis investigated whether murine neutrophils might also play a role in the formation of amyloid-β aggregates *in vitro*. In this experimental setup, only murine neutrophils were used because they have a longer half-life than human neutrophils and the formation of amyloid-β aggregates requires a longer incubation period.

No increase in amyloid-β aggregate formation with neutrophils were detected, suggesting that neutrophils were unable to modify soluble Aβ40 in amyloid-β fibrils or to increase or decrease platelet-mediated amyloid-β aggregate formation *in vitro* (section 3.2.2 Fig. 9). To date, there are few studies published investigating the interaction of Aβ peptides and neutrophils. Park *et al*. found that Aβ40 reduces the apoptotic rate of neutrophils [231]. In 2016, Stock and Kasusu-Jacobi demonstrated that neutrophil granule proteins such as cationic antimicrobial protein of 37 kDa (CAP37), cathepsin G (CG), and neutrophil elastase (NE) directly bind to Aβ42 [232]. In 2021, Kasusu-Jacobi *et al.* showed that neutrophil granule proteins prevent the modulation of Aβ42 aggregation into fibrils. In addition, they showed that the serine proteases CG and NE are able to cleave Aβ42 with different catalytic activities [233]. In this context, it could be speculated that neutrophil may also have beneficial effects on the progression of Alzheimer's disease, for example, by clearing Aβ42 aggregates.

The process of releasing decondensed chromatin decorated with histones and granular antimicrobial proteins, such as neutrophil elastase (NE) or myeloperoxidase (MPO) from neutrophils is termed neutrophil extracellular trap (NET) formation. Classically, NETs represent an important defense mechanism used by neutrophils against pathogens to prevent their systemic dissemination during infection [234]. However, increased and uncontrolled NET formation has the potential to induce significant tissue damage [73]. Zenaro *et al.* showed that in an AD mouse model and in the brain of patients with AD, neutrophils migrate into the brain and produce NETs [70] that possibly enhances neuroinflammation. Moreover, in a mouse model of stroke, neutrophils were shown to produce intravascular and intraparenchymal NETs that damage the blood-brain barrier (BBB) and impair revascularization [73]. Given that increased neutrophil adhesion was observed after platelet stimulation with ADP and Aβ40, the next step in this work was to investigate whether this could trigger the formation of NETs. However, no platelet-induced NET formation was observed with either human or murine platelets with the indicated agonists tested in the *in vitro* experiments (section 3.2.3 and 3.2.5 Fig. 11 and 14). In recent years, several studies have investigated the role of platelets to trigger NET formation. Most of these studies have examined platelet-triggered formation of NETs in the context of acute infectious diseases such as sepsis. For example, Caudriller *et al*. demonstrated that platelets activated by thrombin receptor-activating peptide (TRAP) induce NET formation in a mouse model of transfusion-related acute lung injury [235]. Moreover in a sepsis model, Clark *et al.* demonstrated that LPS-stimulated platelets cause NET formation under flow conditions [236]. Considering that the cell culture experiments performed in this work were conducted under static conditions with healthy human and mouse blood, this could be a reason that no platelet-induced NET formation was observed.

Moreover, the phorbol myristate acetate (PMA) (positive control) induced NET formation in murine neutrophils was only observed in 25% of cells; in contrast, PMA stimulation induced NET formation in almost all human neutrophils. One reason for the lower reactivity of murine neutrophils could be that they originate from the bone marrow and not from the blood. The isolation from bone marrow was necessary because the concentration of neutrophils in murine blood was not sufficient for their isolation. Mice have a large reservoir of functional neutrophils in their bone marrow. However, minor differences were observed between cells derived from the bone marrow and blood, e.g. superoxide production and primary granule release were increased in blood-derived neutrophils [237]. Decreased superoxide production in neutrophils derived from the bone marrow of mice could be a reason for reduced NET formation because this process depends on the formation of ROS [238]. Thus, *in vivo* models might be better suited to further analyze whether or not platelets play a role in the induction of NET formation during inflammatory responses in AD. In this context, one method could be to cross c-mpl knockout mice, which have a 90% decrease in platelet counts, with an AD mouse model to examine the brains for NET formation.

4.3 Migration of platelets into the central nervous system under pathological conditions such as found in Alzheimer's disease

The BBB is a barrier between blood and circulating platelets on the one side and the brain parenchyma on the other side. Several studies have already shown that early dysfunction of the BBB occurs in AD and other neurodegenerative disorders. In this context, increased BBB permeability, microbleeds, perivascular deposition of blood products, and cellular infiltration have been observed [186, 205]. In addition, leukocyte subpopulations from the blood, including neutrophils, have previously been shown to be present in the brain of AD patients and of experimental mice with AD and potentially amplify neuroinflammation [70]. In 2005, Stalder *et al.* demonstrated that hematopoietic cells invade into the brain of aged APP23 mice. However, they could not distinguish between the different cell types because they used a mouse model in which all bone marrow cells were fluorescent [239]. Therefore, it is still unclear whether platelets migrate into the brain under non-pathological and/or pathological conditions as found in AD. To date, there have been published controversial studies on platelet migration into the brain parenchyma in AD. In 2015, a group of researchers led by Prof. Humpel studied platelet migration in a transgenic Alzheimer mouse model by infusing fluorescently labeled red (PKH26 dye) platelets into the vein of the AD mouse model APP-PS1.

They showed that platelets do not migrate into the brain parenchyma but concentrate in the cerebral vasculature. In addition, they also studied platelet migration into the brain of AD patients and could not detect platelets in the brain parenchyma as well [240]. In contrast, Kniewallner *et al.* 2018 showed that 14-month-old APP-PS1 mice had an increased number of platelets outside the blood vessels in the brain parenchyma compared to WT mice [241]. These examples point out that it is yet not clear whether platelets can migrate into the brain parenchyma or not.

For this reason, the current work investigated platelet migration into the brain parenchyma in WT*mT/mG;PF4Cre*+ and APP23*mT/mG;PF4Cre*+ mice at different ages and brain regions, the hippocampus and the cerebral cortex. This study is the first that uses a mouse model in which platelets express a GFP signal, allowing a novel and specific analysis of platelet localization in an AD mouse model (section 3.4.1 Fig. 15). In this model, the presence of platelets in the brain parenchyma of aged WT*mT/mG;PF4Cre*+ and APP23*mT/mG;PF4Cre*+ in the hippocampus and the cerebral cortex was examined. The results provide evidence for a significantly higher platelet count in the hippocampus of 16-month-old APP23*mT/mG;PF4Cre*+ compared to WT*mT/mG;PF4Cre*+ mice. In young mice (6 months), platelets were not detected outside the vessels regardless of the genotype (section 3.4.2 Fig. 16 and 17). These results demonstrate a time-dependent onset of the platelet entry into the brain parenchyma in WT*mT/mG;PF4Cre*+ and APP23*mT/mG;PF4Cre*+ mice that occurs earlier in the hippocampal region of APP23*mT/mG;PF4Cre*+ mice (section 3.4.2 Fig. 16 and 17). However, platelet migration into the brain parenchyma appears to be a common feature of aged brains, at least in mice, as platelets were detected at 24 months of age in WT*mT/mG;PF4Cre*+ and APP23*mT/mG;PF4Cre*+ mice.

It has been previously shown that platelets from AD mouse models including the APP23 mice and from AD patients are in a pre-activated state, resulting in increased P-selectin exposure and enhanced integrin n αIIbβ3 activation at the platelet surface [150, 241, 242]. Activated platelets are able to synthesize and secrete a variety of metalloproteinases (MMPs) and, recruit inflammatory cells to the endothelium, including neutrophil granulocytes, which can also release MMPs or NETs [243]. NETs and MMPs, especially MMP2 and MMP9, are associated with BBB breakdown in neurodegenerative diseases because they degrade the extracellular matrix [73, 244]. AD patients exhibited decreased MMP-2 levels in platelets, possibly indicating increased release of MMP2 during AD progression [245]. In 2018, Kniewallner *et al.* demonstrated that an MMP inhibitor completely counteracted vascular damage and AD indcued platelet vessel penetration in experimental APP_SweDI mice [246].

This AD mouse model expresses the human APP gene containing the Swedish, Dutch, and Iowa mutations and develops amyloid plaque formation along with CAA pathology [247]. Furthermore, isolated platelets from APP_SweDI mice were shown to damage healthy cortical brain vessels. However, no damage to brain vessels was observed with isolated WT platelets [246]. Therefore, it is tempting to speculate that platelets from AD mice actively contribute to vascular damage and inflammation, which could lead to a premature impairment of the BBB and allows early infiltration of platelets into the brain parenchyma of APP23*mT/mG;PF4Cre+* mice.

Interestingly, in 24-month-old mice of both genotypes, platelets were observed in the brain parenchyma (section 3.4.2 Fig. 16 and 17). The question of whether the migration of platelets into the brain parenchyma is active or passive has not yet been completely clarified. In this study, immunoglobulin G (IgG) staining was performed to analyze the leakiness of the BBB. To enter the brain, IgGs have to cross the (damaged) BBB to enter the brain parenchyma. Strongly increased IgG abundance was detected in the cerebral cortex and in the hippocampus of 24-month-old APP23*mT/mG;PF4Cre+* mice and slightly increased IgG abundance was detected in the cerebral cortex but not in the hippocampus of 24-month-old WT*mT/mG;PF4Cre+* mice. In the cerebral cortex of 24 months APP23*mT/mG;PF4Cre*$^{+}$ mice, we also detected IgG-positive areas that associate with high platelet accumulation, indicating passive entry due to microbleeds (section 3.4.6; Fig. 21 and 22). Reuter *et al*. previously showed that cerebral microhemorrhages in the APP23 mouse model occur earliest at 16 months of age and increase exponentially with age. Most of the microhemorrhages were located in the neocortex. However they did not analyzed aged matched WT mice [187]. Xu *et al.* investigated the dynamic changes in vascular size and density in the APP23 and WT mice at 3, 6, 9, 14, and 20 months of age. They could show that in 20-month old APP23 and WT mice, vascular density was significantly decreased, while vascular dilatation and diameter were increased, suggesting that cerebrovascular abnormalities, such as BBB disruption, also occur in WT mice with increasing age. In addition, they could show that APP23 mice exhibited reduced hippocampal vascular density compared to WT mice at 9 months [181]. This suggests that the hippocampus is the most susceptible brain region in AD and may be another reason for the higher platelet abundance in the hippocampus of 16-month-old APP23 *mT/mG;PF4Cre+* mice (section 3.4.2 Fig. 16). In AD patients, the entorhinal area, which is the main entry and exit structure of the hippocampus, is the first region where amyloid plaques and tangles are deposited [248]. These examples may provide evidence that platelet migration into the brain is passively due to BBB disruption. Nevertheless, the group of Prof. Massberg provided evidence for active platelet migration as an autonomous platelet function at sites of vascular injury and inflammation [249].

Recently, paracrine effects of migrating monocytes were shown to influence the ability of platelets to migrate and aggregate through an activated endothelium [250]. Most of these experiments were performed in cell cultures of murine or human microvascular endothelial cells and by mouse ear microvascular injury. Depending on which organs the capillaries supply, they regulate the transport of solutes between the blood and the tissues very differently. The microvasculature of the central nervous system has unique properties in being continuous, non-fenestrated vessels with a strong barrier capacity that tightly regulates the movement of molecules, ions, and cells between the blood and the CNS. However, under inflammatory conditions such as AD, this barrier function is disturbed and BBB dysfunction occurs [251]. The extent to which platelets are involved in this process requires further investigation.

Once platelets enter the brain parenchyma, the question arises whether they play a functional role in amyloid formation in the brain parenchyma or in promoting neuroinflammation and thus progression of AD. Platelets are already associated with enhanced neuroinflammation in various neurological disorders, particularly in response to injuries such as subarachnoid hemorrhage or stroke [133, 252]. Moreover in a mouse model of multiple sclerosis it has been shown that extravascular platelets in the brain promote leukocyte infiltration as well as CNS inflammation [253]. In the present study, it was clearly shown that platelets are located around amyloid plaques in the brain parenchyma. Interestingly, with increasing amyloid plaque diameter and increasing age of APP23*mT/mG;PF4Cre+* mice, platelet abundance around the amyloid plaques increased as well (section 3.4.3; Fig. 18). Platelets carry the amyloid precursor protein and are able to release Aβ40 upon activation. In contrast to diffuse plaques, which consist only of Aβ42 and do not show neuritic dystrophy, senile plaques contain a small amount of Aβ40 [254]. In addition, other studies have previously shown that fibrinogen co-localizes with Aβ deposits outside the vessels in the cerebral cortex of APP23 mice and in human AD brains [255, 256]. Fibrinogen is mainly produced by liver hepatocyte cells and released into the blood. Platelets are known to take up and store fibrinogen, and release it upon activation [257]. Thus, it is tempting to speculate that platelets release Aβ40 and/or fibrinogen near amyloid plaques after entering the brain parenchyma and thus contribute to the growth of senile plaques. However, beside platelets as a source of fibrinogen, it cannot be excluded that fibrinogen enters the brain parenchyma via the leaky BBB and accumulates around amyloid plaques. Interestingly, in a mouse model of systemic shock, platelets were found to deposit in the brain and return to the circulation after degranulation of serotonin [258]. Whether platelets contribute to the enlargement of amyloid plaques in the brain parenchyma by releasing Aβ40 and/or fibrinogen has to be further investigated.

However, short-term treatment of APP23 mice with the antiplatelet agent clopidogrel has already been shown to reduce CAA burden [103]. Thus, long-term treatment of APP23 mice with clopidogrel has to be performed to investigate if anti-platelet therapy is able to reduce parenchymal amyloid plaque formation in experimental AD mice as well.

Interestingly, Bian *et al.* recently showed that fibrinogen accumulates in NeuN- and Tuj-1-positive neurons in APP23 mice with chronic cerebral hypoperfusion [255]. In the present study, it has been shown that some platelets from 24-month-old APP23*mT/mG;PF4Cre*+ mice were located around NeuN-positive neurons (section 3.4.5 Fig. 20), suggesting that platelets might contribute to fibrinogen accumulation in the brain parenchyma. Furthermore, Schleicher *et al.* 2015 demonstrated that platelets trigger apoptosis in human and mouse neuronal cells via exposure of the Fas ligand [259]. In addition to Fas ligand induced (extrinsic) apoptosis, ROS formation is also known to trigger neuronal cell death and cell apoptosis. In this study it has already been shown that platelets release ROS upon Aβ40 stimulation (section 3.3). Therefore, in the vicinity of neurons activated platelets could be a part of the imbalance between ROS production and detoxification, and thus might contribute to neuronal cell damage. Furthermore, fibrinogen has been shown to induce rapid and sustained microglial responses via the microglial integrin receptor CD11b/CD18 [260]. In addition to Aβ40 or fibrinogen (section 3.1), platelets can also release a variety of inflammatory mediators such as TGF-β1 [127] (section 3.2.1 Fig 8). Inflammatory stimuli induce microglia activation to morph from a ramified to an amoeboid shape. Activated microglia become highly motile, secrete inflammatory cytokines, and phagocytose apoptotic cells or damaged neurons, and thus contribute to neuron loss [261]. In this thesis, platelets have been shown to co-localize with activated microglia in 24-month-old APP23*mT/mG;PF4Cre*+ mice (section 3.4.4 Fig. 19). One reason for this co-localization might be that activated microglia are able to clear platelets from the brain parenchyma by phagocytosis. In 2018, Kniewallner *et al.* demonstrated that platelets in APP-SweDI mice recruit and activate microglia, leading to increased TNF-α levels and promoting an inflammatory environment [246]. Whether platelets are able to activate microglia and thus promote neuroinflammation and neurodegeneration in AD remains elusive. However, microglia are capable of clearing cell debris, and it cannot yet be ruled out that the migrated platelets detected in the brain parenchyma of APP23*mT/mG;PF4Cre*+ mice are already apoptotic or nonfunctional platelets containing the GFP signal.

In conclusion, this study provides strong evidence for platelet migration into aged mouse brains and platelet accumulation around amyloid plaques in the here established reporter knockin mouse model, the APP23*mT/mG;PF4Cre*+ mice. Further studies on human AD brains are pending.

However, the presence of platelets in the brain may indicate a new role for platelets in AD progression. Understanding of the mechanisms that modulate platelet activation and migration in the brain and how platelets affect AD pathology could provide new, promising therapies for AD and many other neuroinflammatory diseases.

4.4 Conclusion and Outlook

Platelets are an emerging issue in neurodegenerative diseases, such as AD. However, the functional role of platelets and the underlying molecular and cellular mechanisms are not fully understood to date. Therefore, this thesis investigated the role of platelets and the major platelet collagen receptor GPVI in the progression of Alzheimer's disease with regard to amyloid-β aggregation and platelet-mediated inflammation. It has been clearly demonstrated that the major platelet collagen receptor GPVI binds Aβ40 and thereby triggers platelet activation and aggregation. In addition, platelets from patients and mice with GPVI deficiency do not aggregate upon Aβ40 stimulation. *In vitro*, GPVI was identified as a key regulator of platelet-mediated formation of amyloid-β aggregates. Moreover, this study provides first evidence that GPVI may be involved in the inflammatory response triggered by Aβ40 through the release of TGF-1β, ROS and, in part, by stimulation the adhesion of neutrophils. To further analyze whether blocking of GPVI has a beneficial effect not only *in vitro* but also *in vivo*, the next approach would be to analyze APP23 mice with GPVI deficiency. In this *in vivo* model, inflammatory plasma markers as well as the amyloid load, CAA, neuro-inflammation and neurodegeneration in the brain can be studied. The overall aim is to determine whether antiplatelet therapy, in this case genetic loss of GPVI, can improve cognition and moreover reduce the progression of AD. Therefore, in further analysis, behavioral studies such as Morris water maze (MWM), Y maze, elevated plus maze, light-dark test, and open-field test might be of great interest. The combination of these studies might provide a broad picture not only of cognitive development but also of neuropsychiatric symptoms such as alterations in mood, including anxiety and depression. In addition, it may be of future interest to investigate the impact of the GPVI inhibitor glenzocimab on Aβ40 induced platelet activation and amyloid-β aggregate formation. Glenzocimab is a Fab fragment of a humanized anti-GPVI monoclonal antibody and has been in a Phase II clinical trial since 2021 to gain insights into its safety, tolerability and efficacy in the treatment of acute ischemic stroke [262, 263]. In a second part, this thesis analyzed the age-dependent migration of platelets into the brain parenchyma of APP*23mT/mG;PF4Cre+* and WT*mT/mG;PF4Cre+* mice. An increased number of platelets were found in the brain parenchyma of 24-month-old APP23*mT/mG;PF4Cre+* and WT*mT/mG;PF4Cre+* mice.

In addition, at 16 months of age, more platelets were present in the hippocampus of APP23*mT/mG;PF4Cre+* compared to WT*mT/mG;PF4Cre+* mice, indicating premature BBB dysfunction in the experimental AD mice. These data raise the question of whether or not the inhibition of platelet activation could reduce inflammatory vascular processes leading to decreased vascular cell degradation and disruption of the BBB, which in turn might result in less entry of platelets and/or blood components into the brain parenchyma. Therefore, it may be of interest to analyze platelet migration in APP23 mice receiving antiplatelet therapy. In addition, this study was the first to show that platelets accumulate around amyloid plaques in the new reporter knockin APP23*mT/mG;PF4Cre+* mouse model. In future, it will be of interest to determine whether platelets are also found in the parenchyma and around amyloid plaques in the brain of AD patients. In this study the accumulation of immunoglobulins G in the brain suggest a leaky BBB or even microbleeds in aged APP23*mT/mG;PF4Cre+* mice. However, the overall prevalence of microbleeds is consistently higher in people with CAA and AD compared to non-demented elderly people [264]. This observation needs to be carefully considered when using antiplatelet agents for the treatment of AD, as they might increase the risk and frequency of microbleeds. Microbleeds differ from stroke in both, their extent and effects. Whereas stroke is considered a so-called macro event, usually affecting only one hemisphere of the brain and having immediate effects, microbleeds can occur over a longer time period throughout the brain and thus have a cumulative effect. In this context, GPVI might be an interesting target for the treatment of AD because it has already been shown that depletion of GPVI improves the outcome in experimental stroke without increasing the risk of cerebral hemorrhages [133].

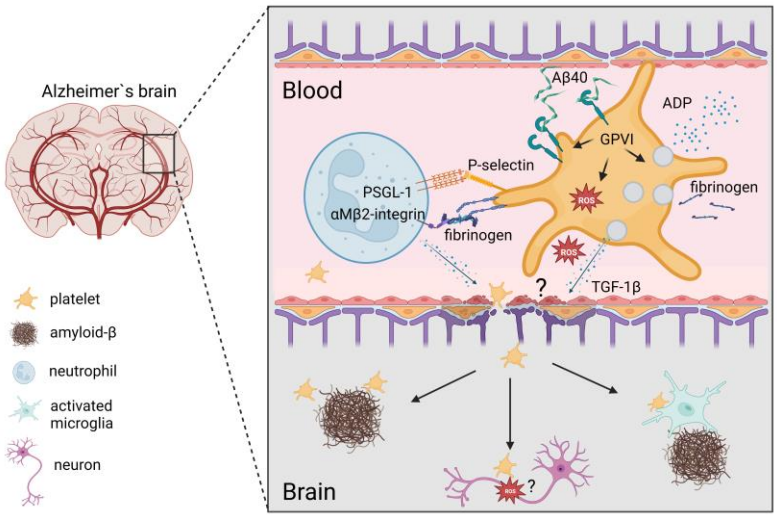

Figure 23: Graphical abstract.
Binding of Aβ40 to GPVI on the surface of platelets leads to externalization of GPVI and the release of ROS, ADP, fibrinogen, and TGF-1β. In addition, Aβ40 stimulation of platelets leads to the recruitment of neutrophils. Neutrophils, TGF-1β, and ROS are proinflammatory stimuli and presumably may damage the BBB, thus permitting platelets to invade into the brain parenchyma. In APP23 mice, platelets were localized near amyloid plaques, microglia, and neurons. The influence of platelets in the brain remains to be elucidated in further detail in future.

5 References

1. WHO. *Key facts Dementia*. 2021; Available from: https://www.who.int/news-room/fact-sheets/detail/dementia.
2. Gesellschaft, D.A. *Die Häufigkeit von Demenzerkrankungen*. 2020; Available from: https://www.alzheimer-bw.de/fileadmin/AGBW_Medien/AGBW-Dokumente/Infoblaetter-DAIzG/infoblatt1_haeufigkeit_demenzerkrankungen_dalzg_2020.pdf.
3. Butterfield, D.A. and B. Halliwell, *Oxidative stress, dysfunctional glucose metabolism and Alzheimer disease.* Nat Rev Neurosci, 2019. **20**(3): p. 148-160.
4. REPORT, A.S.A., *2020 Alzheimer's disease facts and figures.* Alzheimer's & Dementia, 2020. **16**(3): p. 391-460.
5. Winston Wong, P., *Economic Burden of Alzheimer Disease and Managed Care Considerations.* Supplements and Featured Publications, 2020. **26**(8).
6. Huang, L.-K., S.-P. Chao, and C.-J. Hu, *Clinical trials of new drugs for Alzheimer disease.* Journal of Biomedical Science, 2020. **27**(1): p. 18.
7. Williams, M.E., et al., *Genetic and environmental influences on Alzheimer's disease neuroimaging signatures.* Alzheimer's & Dementia, 2021. **17**(S4): p. e054708.
8. Tiedt, H.O., et al., *Phenotypic Variability in Autosomal Dominant Familial Alzheimer Disease due to the S170F Mutation of Presenilin-1.* Neurodegenerative Diseases, 2018. **18**(2-3): p. 57-68.
9. Wu, L., et al., *Early-Onset Familial Alzheimer's Disease (EOFAD).* Canadian Journal of Neurological Sciences / Journal Canadien des Sciences Neurologiques, 2012. **39**(4): p. 436-445.
10. Bekris, L.M., et al., *Genetics of Alzheimer disease.* Journal of geriatric psychiatry and neurology, 2010. **23**(4): p. 213-227.
11. Giau, V.V., et al., *Genetic analyses of early-onset Alzheimer's disease using next generation sequencing.* Scientific Reports, 2019. **9**(1): p. 8368.
12. Mendez, M.F., *Early-onset Alzheimer Disease and Its Variants.* Continuum (Minneap Minn), 2019. **25**(1): p. 34-51.
13. Kang, J., et al., *The precursor of Alzheimer's disease amyloid A4 protein resembles a cell-surface receptor.* Nature, 1987. **325**(6106): p. 733-736.
14. Doran, E., et al., *Down Syndrome, Partial Trisomy 21, and Absence of Alzheimer's Disease: The Role of APP.* J Alzheimers Dis, 2017. **56**(2): p. 459-470.
15. Karch, C.M. and A.M. Goate, *Alzheimer's disease risk genes and mechanisms of disease pathogenesis.* Biol Psychiatry, 2015. **77**(1): p. 43-51.
16. Van Cauwenberghe, C., C. Van Broeckhoven, and K. Sleegers, *The genetic landscape of Alzheimer disease: clinical implications and perspectives.* Genetics in Medicine, 2016. **18**(5): p. 421-430.
17. Misra, A., S.S. Chakrabarti, and I.S. Gambhir, *New genetic players in late-onset Alzheimer's disease: Findings of genome-wide association studies.* Indian J Med Res, 2018. **148**(2): p. 135-144.
18. Bennet, A.M., et al., *Association of apolipoprotein E genotypes with lipid levels and coronary risk.* Jama, 2007. **298**(11): p. 1300-11.
19. Corder, E.H., et al., *Gene dose of apolipoprotein E type 4 allele and the risk of Alzheimer's disease in late onset families.* Science, 1993. **261**(5123): p. 921-3.
20. Kathiresan, S., et al., *Polymorphisms associated with cholesterol and risk of cardiovascular events.* N Engl J Med, 2008. **358**(12): p. 1240-9.
21. Cechetto, D.F., V. Hachinski, and S.N. Whitehead, *Vascular risk factors and Alzheimer's disease.* Expert Rev Neurother, 2008. **8**(5): p. 743-50.
22. Flicker, L., *Modifiable lifestyle risk factors for Alzheimer's disease.* J Alzheimers Dis, 2010. **20**(3): p. 803-11.

23. Alzheimer, A., et al., *An English translation of Alzheimer's 1907 paper, "Uber eine eigenartige Erkankung der Hirnrinde".* Clin Anat, 1995. **8**(6): p. 429-31.
24. Suppiah, S., M.-A. Didier, and S. Vinjamuri, *The Who, When, Why, and How of PET Amyloid Imaging in Management of Alzheimer's Disease-Review of Literature and Interesting Images.* Diagnostics (Basel, Switzerland), 2019. **9**(2): p. 65.
25. Ebenau, J.L., et al., *ATN classification and clinical progression in subjective cognitive decline.* The SCIENCe project, 2020. **95**(1): p. e46-e58.
26. Thal, D.R., et al., *The development of amyloid beta protein deposits in the aged brain.* Sci Aging Knowledge Environ, 2006. **2006**(6): p. re1.
27. Dickson, D.W., *The pathogenesis of senile plaques.* J Neuropathol Exp Neurol, 1997. **56**(4): p. 321-39.
28. Yamaguchi, H., et al., *Diffuse type of senile plaques in the brains of Alzheimer-type dementia.* Acta Neuropathol, 1988. **77**(2): p. 113-9.
29. Iwatsubo, T., et al., *Visualization of A beta 42(43) and A beta 40 in senile plaques with end-specific A beta monoclonals: evidence that an initially deposited species is A beta 42(43).* Neuron, 1994. **13**(1): p. 45-53.
30. Aamodt, E.J. and R.C. Williams, Jr., *Microtubule-associated proteins connect microtubules and neurofilaments in vitro.* Biochemistry, 1984. **23**(25): p. 6023-31.
31. von Bergen, M., et al., *Assembly of tau protein into Alzheimer paired helical filaments depends on a local sequence motif ((306)VQIVYK(311)) forming beta structure.* Proc Natl Acad Sci U S A, 2000. **97**(10): p. 5129-34.
32. Köpke, E., et al., *Microtubule-associated protein tau. Abnormal phosphorylation of a non-paired helical filament pool in Alzheimer disease.* J Biol Chem, 1993. **268**(32): p. 24374-84.
33. Nixon, R.A., *Autophagy, amyloidogenesis and Alzheimer disease.* Journal of Cell Science, 2007. **120**(23): p. 4081-4091.
34. Zhang, T., D. Chen, and T.H. Lee, *Phosphorylation Signaling in APP Processing in Alzheimer's Disease.* International Journal of Molecular Sciences, 2020. **21**(1).
35. Matsui, T., et al., *Expression of APP pathway mRNAs and proteins in Alzheimer's disease.* Brain Res, 2007. **1161**: p. 116-23.
36. Smith, R.P. and G.J. Broze, Jr., *Characterization of platelet-releasable forms of beta-amyloid precursor proteins: the effect of thrombin.* Blood, 1992. **80**(9): p. 2252-60.
37. Canobbio, I., et al., *Platelet amyloid precursor protein is a modulator of venous thromboembolism in mice.* Blood, 2017. **130**(4): p. 527-536.
38. Cacace, R., K. Sleegers, and C. Van Broeckhoven, *Molecular genetics of early-onset Alzheimer's disease revisited.* Alzheimers Dement, 2016. **12**(6): p. 733-48.
39. Priller, C., et al., *Synapse Formation and Function Is Modulated by the Amyloid Precursor Protein.* The Journal of Neuroscience, 2006. **26**(27): p. 7212-7221.
40. Klevanski, M., et al., *The APP Intracellular Domain Is Required for Normal Synaptic Morphology, Synaptic Plasticity, and Hippocampus-Dependent Behavior.* The Journal of Neuroscience, 2015. **35**(49): p. 16018-16033.
41. Deyts, C., G. Thinakaran, and A.T. Parent, *APP Receptor? To Be or Not To Be.* Trends Pharmacol Sci, 2016. **37**(5): p. 390-411.
42. Kuhn, P.H., et al., *ADAM10 is the physiologically relevant, constitutive alpha-secretase of the amyloid precursor protein in primary neurons.* Embo j, 2010. **29**(17): p. 3020-32.
43. Hefter, D., et al., *Amyloid Precursor Protein Protects Neuronal Network Function after Hypoxia via Control of Voltage-Gated Calcium Channels.* The Journal of Neuroscience, 2016. **36**(32): p. 8356-8371.
44. Corrigan, F., et al., *sAPPα rescues deficits in amyloid precursor protein knockout mice following focal traumatic brain injury.* Journal of Neurochemistry, 2012. **122**(1): p. 208-220.

45. Müller, U.C., T. Deller, and M. Korte, *Not just amyloid: physiological functions of the amyloid precursor protein family.* Nature Reviews Neuroscience, 2017. **18**(5): p. 281-298.
46. Zhang, Y.W., et al., *APP processing in Alzheimer's disease.* Mol Brain, 2011. **4**: p. 3.
47. Haass, C., et al., *Trafficking and proteolytic processing of APP.* Cold Spring Harb Perspect Med, 2012. **2**(5): p. a006270.
48. Spies, P.E., et al., *Reviewing reasons for the decreased CSF Abeta42 concentration in Alzheimer disease.* Front Biosci (Landmark Ed), 2012. **17**(6): p. 2024-34.
49. Du, X., X. Wang, and M. Geng, *Alzheimer's disease hypothesis and related therapies.* Translational Neurodegeneration, 2018. **7**(1): p. 2.
50. Hardy, J. and D. Allsop, *Amyloid deposition as the central event in the aetiology of Alzheimer's disease.* Trends in Pharmacological Sciences, 1991. **12**: p. 383-388.
51. Selkoe, D.J., *The molecular pathology of Alzheimer's disease.* Neuron, 1991. **6**(4): p. 487-98.
52. Hardy, J. and D.J. Selkoe, *The amyloid hypothesis of Alzheimer's disease: progress and problems on the road to therapeutics.* Science, 2002. **297**(5580): p. 353-6.
53. Hayden, E.Y. and D.B. Teplow, *Amyloid β-protein oligomers and Alzheimer's disease.* Alzheimers Res Ther, 2013. **5**(6): p. 60.
54. Selkoe, D.J. and J. Hardy, *The amyloid hypothesis of Alzheimer's disease at 25 years.* EMBO Molecular Medicine, 2016. **8**(6): p. 595-608.
55. Walsh, D.M., et al., *Naturally secreted oligomers of amyloid β protein potently inhibit hippocampal long-term potentiation in vivo.* Nature, 2002. **416**(6880): p. 535-539.
56. Barage, S.H. and K.D. Sonawane, *Amyloid cascade hypothesis: Pathogenesis and therapeutic strategies in Alzheimer's disease.* Neuropeptides, 2015. **52**: p. 1-18.
57. Chaney, A., S.R. Williams, and H. Boutin, *In vivo molecular imaging of neuroinflammation in Alzheimer's disease.* Journal of Neurochemistry, 2019. **149**(4): p. 438-451.
58. Sheng, J.G., et al., *Overexpression of the Neuritotrophic Cytokine S100β Precedes the Appearance of Neuritic β-Amyloid Plaques in APPV717F Mice.* Journal of Neurochemistry, 2000. **74**(1): p. 295-301.
59. Meda, L., et al., *Activation of microglial cells by β-amyloid protein and interferon-γ.* Nature, 1995. **374**(6523): p. 647-650.
60. Tamboli, I.Y., et al., *Statins Promote the Degradation of Extracellular Amyloid β-Peptide by Microglia via Stimulation of Exosome-associated Insulin-degrading Enzyme (IDE) Secretion *.* Journal of Biological Chemistry, 2010. **285**(48): p. 37405-37414.
61. Bolmont, T., et al., *Dynamics of the Microglial/Amyloid Interaction Indicate a Role in Plaque Maintenance.* The Journal of Neuroscience, 2008. **28**(16): p. 4283-4292.
62. Chang, R., K.-L. Yee, and R.K. Sumbria, *Tumor necrosis factor α Inhibition for Alzheimer's Disease.* Journal of Central Nervous System Disease, 2017. **9**: p. 1179573517709278.
63. Perry, R.T., et al., *The role of TNF and its receptors in Alzheimer's disease.* Neurobiology of Aging, 2001. **22**(6): p. 873-883.
64. Yamamoto, M., et al., *Interferon-γ and Tumor Necrosis Factor-α Regulate Amyloid-β Plaque Deposition and β-Secretase Expression in Swedish Mutant APP Transgenic Mice.* The American Journal of Pathology, 2007. **170**(2): p. 680-692.
65. Liao, Y.-F., et al., *Tumor Necrosis Factor-α, Interleukin-1β, and Interferon-γ Stimulate γ-Secretase-mediated Cleavage of Amyloid*

*Precursor Protein through a JNK-dependent MAPK Pathway *.* Journal of Biological Chemistry, 2004. **279**(47): p. 49523-49532.
66. Chun, H., et al., *Severe reactive astrocytes precipitate pathological hallmarks of Alzheimer's disease via H2O2− production.* Nature Neuroscience, 2020. **23**(12): p. 1555-1566.
67. Henneberger, C., et al., *Long-term potentiation depends on release of d-serine from astrocytes.* Nature, 2010. **463**(7278): p. 232-236.
68. Halassa, M.M. and P.G. Haydon, *Integrated Brain Circuits: Astrocytic Networks Modulate Neuronal Activity and Behavior.* Annual Review of Physiology, 2010. **72**(1): p. 335-355.
69. Sanchez-Mico, M.V., et al., *Amyloid-β impairs the phagocytosis of dystrophic synapses by astrocytes in Alzheimer's disease.* Glia, 2021. **69**(4): p. 997-1011.
70. Zenaro, E., et al., *Neutrophils promote Alzheimer's disease–like pathology and cognitive decline via LFA-1 integrin.* Nature Medicine, 2015. **21**(8): p. 880-886.
71. Pietronigro, E.C., et al., *NETosis in Alzheimer's Disease.* Frontiers in immunology, 2017. **8**: p. 211-211.
72. Jay, T.R., et al., *TREM2 deficiency eliminates TREM2+ inflammatory macrophages and ameliorates pathology in Alzheimer's disease mouse models.* Journal of Experimental Medicine, 2015. **212**(3): p. 287-295.
73. Kang, L., et al., *Neutrophil extracellular traps released by neutrophils impair revascularization and vascular remodeling after stroke.* Nature Communications, 2020. **11**(1): p. 2488.
74. Dong, Y., et al., *Neutrophil hyperactivation correlates with Alzheimer's disease progression.* Ann Neurol, 2018. **83**(2): p. 387-405.
75. Guo, C., et al., *Oxidative stress, mitochondrial damage and neurodegenerative diseases.* Neural Regen Res, 2013. **8**(21): p. 2003-14.
76. Weber, B. and L.F. Barros, *The Astrocyte: Powerhouse and Recycling Center.* Cold Spring Harb Perspect Biol, 2015. **7**(12).
77. Watts, M.E., R. Pocock, and C. Claudianos, *Brain Energy and Oxygen Metabolism: Emerging Role in Normal Function and Disease.* Frontiers in Molecular Neuroscience, 2018. **11**.
78. Siesjö, B.K., *Brain energy metabolism*. 1978: John Wiley & Sons.
79. Lin, M.T. and M.F. Beal, *Mitochondrial dysfunction and oxidative stress in neurodegenerative diseases.* Nature, 2006. **443**(7113): p. 787-95.
80. Wang, X., et al., *Oxidative stress and mitochondrial dysfunction in Alzheimer's disease.* Biochim Biophys Acta, 2014. **1842**(8): p. 1240-7.
81. Yao, J., et al., *Mitochondrial bioenergetic deficit precedes Alzheimer's pathology in female mouse model of Alzheimer's disease.* Proceedings of the National Academy of Sciences, 2009. **106**(34): p. 14670-14675.
82. Manczak, M., et al., *Differential expression of oxidative phosphorylation genes in patients with Alzheimer's disease: implications for early mitochondrial dysfunction and oxidative damage.* Neuromolecular Med, 2004. **5**(2): p. 147-62.
83. Manczak, M., et al., *Mitochondria are a direct site of Aβ accumulation in Alzheimer's disease neurons: implications for free radical generation and oxidative damage in disease progression.* Human Molecular Genetics, 2006. **15**(9): p. 1437-1449.
84. Lustbader, J.W., et al., *ABAD Directly Links Aß to Mitochondrial Toxicity in Alzheimer's Disease.* Science, 2004. **304**(5669): p. 448-452.
85. Greenberg, S.M., et al., *Cerebral amyloid angiopathy and Alzheimer disease - one peptide, two pathways.* Nat Rev Neurol, 2020. **16**(1): p. 30-42.
86. Farkas, E. and P.G. Luiten, *Cerebral microvascular pathology in aging and Alzheimer's disease.* Prog Neurobiol, 2001. **64**(6): p. 575-611.
87. Vinters, H.V., *Emerging concepts in Alzheimer's disease.* Annu Rev Pathol, 2015. **10**: p. 291-319.

88. Ghiso, J., et al., *CEREBRAL AMYLOID ANGIOPATHY AND ALZHEIMER'S DISEASE.* Hirosaki igaku = Hirosaki medical journal, 2010. **61**(Suppl): p. S111-S124.
89. Pfeifer, L.A., et al., *Cerebral amyloid angiopathy and cognitive function: the HAAS autopsy study.* Neurology, 2002. **58**(11): p. 1629-34.
90. Deane, R., et al., *apoE isoform-specific disruption of amyloid beta peptide clearance from mouse brain.* J Clin Invest, 2008. **118**(12): p. 4002-13.
91. Fryer, J.D., et al., *Human apolipoprotein E4 alters the amyloid-beta 40:42 ratio and promotes the formation of cerebral amyloid angiopathy in an amyloid precursor protein transgenic model.* J Neurosci, 2005. **25**(11): p. 2803-10.
92. Strickland, S., *Blood will out: vascular contributions to Alzheimer's disease.* The Journal of Clinical Investigation, 2018. **128**(2): p. 556-563.
93. Cortes-Canteli, M., et al., *Fibrinogen and β-Amyloid Association Alters Thrombosis and Fibrinolysis: A Possible Contributing Factor to Alzheimer's Disease.* Neuron, 2010. **66**(5): p. 695-709.
94. Hultman, K., S. Strickland, and E.H. Norris, *The APOE ε4/ε4 genotype potentiates vascular fibrin(ogen) deposition in amyloid-laden vessels in the brains of Alzheimer's disease patients.* Journal of cerebral blood flow and metabolism : official journal of the International Society of Cerebral Blood Flow and Metabolism, 2013. **33**(8): p. 1251-1258.
95. Cortes-Canteli, M., et al., *Fibrin deposited in the Alzheimer's disease brain promotes neuronal degeneration.* Neurobiol Aging, 2015. **36**(2): p. 608-17.
96. Jirouskova, M., A.S. Shet, and G.J. Johnson, *A guide to murine platelet structure, function, assays, and genetic alterations.* J Thromb Haemost, 2007. **5**(4): p. 661-9.
97. Gremmel, T., A.L. Frelinger, 3rd, and A.D. Michelson, *Platelet Physiology.* Semin Thromb Hemost, 2016. **42**(3): p. 191-204.
98. Lefrançais, E., et al., *The lung is a site of platelet biogenesis and a reservoir for haematopoietic progenitors.* Nature, 2017. **544**(7648): p. 105-109.
99. Lebois, M. and E.C. Josefsson, *Regulation of platelet lifespan by apoptosis.* Platelets, 2016. **27**(6): p. 497-504.
100. Mason, K.D., et al., *Programmed anuclear cell death delimits platelet life span.* Cell, 2007. **128**(6): p. 1173-86.
101. Broos, K., et al., *Platelets at work in primary hemostasis.* Blood Reviews, 2011. **25**(4): p. 155-167.
102. Camilli, M., et al., *Platelets: the point of interconnection among cancer, inflammation and cardiovascular diseases.* Expert Rev Hematol, 2021. **14**(6): p. 537-546.
103. Donner, L., et al., *Platelets contribute to amyloid-β aggregation in cerebral vessels through integrin αIIbβ3-induced outside-in signaling and clusterin release.* Sci Signal, 2016. **9**(429): p. ra52.
104. Gale, A.J., *Continuing education course #2: current understanding of hemostasis.* Toxicol Pathol, 2011. **39**(1): p. 273-80.
105. Koupenova, M., et al., *Thrombosis and platelets: an update.* European Heart Journal, 2016. **38**(11): p. 785-791.
106. Jurk, K. and B.E. Kehrel, *Platelets: physiology and biochemistry.* Semin Thromb Hemost, 2005. **31**(4): p. 381-92.
107. Blair, P. and R. Flaumenhaft, *Platelet alpha-granules: basic biology and clinical correlates.* Blood Rev, 2009. **23**(4): p. 177-89.
108. Ambrosio, A.L. and S.M. Di Pietro, *Storage pool diseases illuminate platelet dense granule biogenesis.* Platelets, 2017. **28**(2): p. 138-146.
109. Arita, H., T. Nakano, and K. Hanasaki, *Thromboxane A2: its generation and role in platelet activation.* Prog Lipid Res, 1989. **28**(4): p. 273-301.
110. Hardy, A.R., et al., *P2Y1 and P2Y12 receptors for ADP desensitize by distinct kinase-dependent mechanisms.* Blood, 2005. **105**(9): p. 3552-3560.

111. O'Connor, S., G. Montalescot, and J.P. Collet, *The P2Y(12) receptor as a target of antithrombotic drugs.* Purinergic Signal, 2011. **7**(3): p. 325-32.
112. Smyth, E.M., *Thromboxane and the thromboxane receptor in cardiovascular disease.* Clinical Lipidology, 2010. **5**(2): p. 209-219.
113. Wood, J.P., et al., *Prothrombin activation on the activated platelet surface optimizes expression of procoagulant activity.* Blood, 2011. **117**(5): p. 1710-8.
114. Offermanns, S., *Activation of Platelet Function Through G Protein–Coupled Receptors.* Circulation Research, 2006. **99**(12): p. 1293-1304.
115. Moroi, M., et al., *A patient with platelets deficient in glycoprotein VI that lack both collagen-induced aggregation and adhesion.* The Journal of clinical investigation, 1989. **84**(5): p. 1440-1445.
116. Rayes, J., S.P. Watson, and B. Nieswandt, *Functional significance of the platelet immune receptors GPVI and CLEC-2.* J Clin Invest, 2019. **129**(1): p. 12-23.
117. Alshehri, O.M., et al., *Fibrin activates GPVI in human and mouse platelets.* Blood, 2015. **126**(13): p. 1601-1608.
118. Mangin, P.H., et al., *Immobilized fibrinogen activates human platelets through glycoprotein VI.* Haematologica, 2018. **103**(5): p. 898-907.
119. Bültmann, A., et al., *Impact of glycoprotein VI and platelet adhesion on atherosclerosis—A possible role of fibronectin.* Journal of Molecular and Cellular Cardiology, 2010. **49**(3): p. 532-542.
120. Nieswandt, B. and S.P. Watson, *Platelet-collagen interaction: is GPVI the central receptor?* Blood, 2003. **102**(2): p. 449-61.
121. Miura, Y., et al., *Analysis of the interaction of platelet collagen receptor glycoprotein VI (GPVI) with collagen. A dimeric form of GPVI, but not the monomeric form, shows affinity to fibrous collagen.* J Biol Chem, 2002. **277**(48): p. 46197-204.
122. Horii, K., M.L. Kahn, and A.B. Herr, *Structural basis for platelet collagen responses by the immune-type receptor glycoprotein VI.* Blood, 2006. **108**(3): p. 936-42.
123. Niedergang, F., et al., *Convulxin Binding to Platelet Receptor GPVI: Competition with Collagen Related Peptides.* Biochemical and Biophysical Research Communications, 2000. **273**(1): p. 246-250.
124. Pasquet, J.M., et al., *LAT is required for tyrosine phosphorylation of phospholipase cgamma2 and platelet activation by the collagen receptor GPVI.* Mol Cell Biol, 1999. **19**(12): p. 8326-34.
125. WATSON, S.P., et al., *GPVI and integrin αIIbβ3 signaling in platelets.* Journal of Thrombosis and Haemostasis, 2005. **3**(8): p. 1752-1762.
126. Assoian, R.K., et al., *Transforming growth factor-beta in human platelets. Identification of a major storage site, purification, and characterization.* Journal of Biological Chemistry, 1983. **258**(11): p. 7155-7160.
127. Meyer, A., et al., *Platelet TGF-β1 contributions to plasma TGF-β1, cardiac fibrosis, and systolic dysfunction in a mouse model of pressure overload.* Blood, 2012. **119**(4): p. 1064-1074.
128. Sreeramkumar, V., et al., *Neutrophils scan for activated platelets to initiate inflammation.* Science, 2014. **346**(6214): p. 1234-1238.
129. Moore, K.L., et al., *P-selectin glycoprotein ligand-1 mediates rolling of human neutrophils on P-selectin.* Journal of Cell Biology, 1995. **128**(4): p. 661-671.
130. Weber, C. and T.A. Springer, *Neutrophil accumulation on activated, surface-adherent platelets in flow is mediated by interaction of Mac-1 with fibrinogen bound to alphaIIbbeta3 and stimulated by platelet-activating factor.* The Journal of Clinical Investigation, 1997. **100**(8): p. 2085-2093.
131. Page, C. and S. Pitchford, *Neutrophil and platelet complexes and their relevance to neutrophil recruitment and activation.* International Immunopharmacology, 2013. **17**(4): p. 1176-1184.

132. Hamilos, M., S. Petousis, and F. Parthenakis, *Interaction between platelets and endothelium: from pathophysiology to new therapeutic options.* Cardiovasc Diagn Ther, 2018. **8**(5): p. 568-580.
133. Kleinschnitz, C., et al., *Targeting Platelets in Acute Experimental Stroke.* Circulation, 2007. **115**(17): p. 2323-2330.
134. Goebel, S., et al., *The GPVI-Fc Fusion Protein Revacept Improves Cerebral Infarct Volume and Functional Outcome in Stroke.* PLOS ONE, 2013. **8**(7): p. e66960.
135. Boilard, E., et al., *Platelets Amplify Inflammation in Arthritis via Collagen-Dependent Microparticle Production.* Science, 2010. **327**(5965): p. 580-583.
136. Perrella, G., et al., *Platelet GPVI (Glycoprotein VI) and Thrombotic Complications in the Venous System.* Arteriosclerosis, Thrombosis, and Vascular Biology, 2021. **41**(11): p. 2681-2692.
137. Li, Q.X., et al., *Membrane-associated forms of the beta A4 amyloid protein precursor of Alzheimer's disease in human platelet and brain: surface expression on the activated human platelet.* Blood, 1994. **84**(1): p. 133-42.
138. Skovronsky, D.M., V.M.Y. Lee, and D. Praticò, *Amyloid Precursor Protein and Amyloid β Peptide in Human Platelets: ROLE OF CYCLOOXYGENASE AND PROTEIN KINASE C *.* Journal of Biological Chemistry, 2001. **276**(20): p. 17036-17043.
139. Evin, G. and Q.X. Li, *Platelets and Alzheimer's disease: Potential of APP as a biomarker.* World J Psychiatry, 2012. **2**(6): p. 102-13.
140. Gowert, N.S., et al., *Loss of Reelin protects mice against arterial thrombosis by impairing integrin activation and thrombus formation under high shear conditions.* Cell Signal, 2017. **40**: p. 210-221.
141. Smith, R.P., D.A. Higuchi, and G.J. Broze, Jr., *Platelet coagulation factor XIa-inhibitor, a form of Alzheimer amyloid precursor protein.* Science, 1990. **248**(4959): p. 1126-8.
142. Schmaier, A.H., et al., *Factor IXa inhibition by protease nexin-2/amyloid beta-protein precursor on phospholipid vesicles and cell membranes.* Biochemistry, 1995. **34**(4): p. 1171-8.
143. Gowert, N.S., et al., *Blood platelets in the progression of Alzheimer's disease.* PLoS One, 2014. **9**(2): p. e90523.
144. Sevush, S., et al., *Platelet activation in Alzheimer disease.* Arch Neurol, 1998. **55**(4): p. 530-6.
145. Laske, C., et al., *Amyloid-β Peptides in Plasma and Cognitive Decline After 1 Year Follow-Up in Alzheimer's Disease Patients.* Journal of Alzheimer's Disease, 2010. **21**: p. 1263-1269.
146. Pinho, J., et al., *Incident stroke in patients with Alzheimer's disease: systematic review and meta-analysis.* Scientific Reports, 2021. **11**(1): p. 16385.
147. Cortes-Canteli, M., et al., *Fibrinogen and beta-amyloid association alters thrombosis and fibrinolysis: a possible contributing factor to Alzheimer's disease.* Neuron, 2010. **66**(5): p. 695-709.
148. Johnston, J.A., et al., *Platelet β-secretase activity is increased in Alzheimer's disease.* Neurobiology of Aging, 2008. **29**(5): p. 661-668.
149. Borroni, B., et al., *Blood cell markers in Alzheimer Disease: Amyloid Precursor Protein form ratio in platelets.* Exp Gerontol, 2010. **45**(1): p. 53-6.
150. Jarre, A., et al., *Pre-activated blood platelets and a pro-thrombotic phenotype in APP23 mice modeling Alzheimer's disease.* Cell Signal, 2014. **26**(9): p. 2040-50.
151. DALE, G.L., *REVIEW ARTICLE: Coated-platelets: an emerging component of the procoagulant response.* Journal of Thrombosis and Haemostasis, 2005. **3**(10): p. 2185-2192.
152. Suo, Z., et al., *Alzheimer's beta-amyloid peptides induce inflammatory cascade in human vascular cells: the roles of cytokines and CD40.* Brain Res, 1998. **807**(1-2): p. 110-7.

153. Zhang, W., W. Huang, and F. Jing, *Contribution of blood platelets to vascular pathology in Alzheimer's disease.* J Blood Med, 2013. **4**: p. 141-7.
154. Neumann, K., et al., *Human Platelets Tau: A Potential Peripheral Marker for Alzheimer's Disease.* Journal of Alzheimer's Disease, 2011. **25**: p. 103-109.
155. Elyaman, W., et al., *In vivo activation and nuclear translocation of phosphorylated glycogen synthase kinase-3β in neuronal apoptosis: links to tau phosphorylation.* European Journal of Neuroscience, 2002. **15**(4): p. 651-660.
156. Forlenza, O.V., et al., *Increased platelet GSK3B activity in patients with mild cognitive impairment and Alzheimer's disease.* Journal of Psychiatric Research, 2011. **45**(2): p. 220-224.
157. Mészáros, Z., et al., *Platelet MAO-B activity and serotonin content in patients with dementia: effect of age, medication, and disease.* Neurochem Res, 1998. **23**(6): p. 863-8.
158. Perlman, R.L., *Mouse models of human disease: An evolutionary perspective.* Evol Med Public Health, 2016. **2016**(1): p. 170-6.
159. Carreiras, M.C., et al., *The multifactorial nature of Alzheimer's disease for developing potential therapeutics.* Curr Top Med Chem, 2013. **13**(15): p. 1745-70.
160. Sturchler-Pierrat, C., et al., *Two amyloid precursor protein transgenic mouse models with Alzheimer disease-like pathology.* Proceedings of the National Academy of Sciences, 1997. **94**(24): p. 13287-13292.
161. Citron, M., et al., *Mutation of the β-amyloid precursor protein in familial Alzheimer's disease increases β-protein production.* Nature, 1992. **360**(6405): p. 672-674.
162. Sturchler-Pierrat, C., et al., *Two amyloid precursor protein transgenic mouse models with Alzheimer disease-like pathology.* Proc Natl Acad Sci U S A, 1997. **94**(24): p. 13287-92.
163. He, P., et al., *Deletion of tumor necrosis factor death receptor inhibits amyloid beta generation and prevents learning and memory deficits in Alzheimer's mice.* J Cell Biol, 2007. **178**(5): p. 829-41.
164. Van Dam, D., et al., *Age-dependent cognitive decline in the APP23 model precedes amyloid deposition.* Eur J Neurosci, 2003. **17**(2): p. 388-96.
165. Kelly, P.H., et al., *Progressive age-related impairment of cognitive behavior in APP23 transgenic mice.* Neurobiol Aging, 2003. **24**(2): p. 365-78.
166. Winkler, D.T., et al., *Spontaneous hemorrhagic stroke in a mouse model of cerebral amyloid angiopathy.* J Neurosci, 2001. **21**(5): p. 1619-27.
167. Krüger, I., et al., *Genetic Labeling of Cells Allows Identification and Tracking of Transgenic Platelets in Mice.* Int J Mol Sci, 2021. **22**(7).
168. Donner, L., et al., *The collagen receptor glycoprotein VI promotes platelet-mediated aggregation of β-amyloid.* Sci Signal, 2020. **13**(643).
169. Suzuki, H., et al., *Intracellular localization of glycoprotein VI in human platelets and its surface expression upon activation.* Br J Haematol, 2003. **121**(6): p. 904-12.
170. Bender, M., et al., *Differentially regulated GPVI ectodomain shedding by multiple platelet–expressed proteinases.* Blood, 2010. **116**(17): p. 3347-3355.
171. Stephens, G., et al., *Platelet activation induces metalloproteinase-dependent GP VI cleavage to down-regulate platelet reactivity to collagen.* Blood, 2005. **105**(1): p. 186-191.
172. Herrero-Cervera, A., O. Soehnlein, and E. Kenne, *Neutrophils in chronic inflammatory diseases.* Cellular & Molecular Immunology, 2022. **19**(2): p. 177-191.
173. Pitchford, S., D. Pan, and H.C. Welch, *Platelets in neutrophil recruitment to sites of inflammation.* Curr Opin Hematol, 2017. **24**(1): p. 23-31.
174. Smyth, L.C.D., et al., *Neutrophil-vascular interactions drive myeloperoxidase accumulation in the brain in Alzheimer's disease.* Acta Neuropathologica Communications, 2022. **10**(1): p. 38.

175. Cruz Hernández, J.C., et al., *Neutrophil adhesion in brain capillaries reduces cortical blood flow and impairs memory function in Alzheimer's disease mouse models.* Nat Neurosci, 2019. **22**(3): p. 413-420.
176. Pietronigro, E.C., et al., *NETosis in Alzheimer's Disease.* Front Immunol, 2017. **8**: p. 211.
177. Bender, M., et al., *Combined In Vivo Depletion of Glycoprotein VI and C-Type Lectin-Like Receptor 2 Severely Compromises Hemostasis and Abrogates Arterial Thrombosis in Mice.* Arteriosclerosis, Thrombosis, and Vascular Biology, 2013. **33**(5): p. 926-934.
178. Donner, L., et al., *Impact of Amyloid-β on Platelet Mitochondrial Function and Platelet-Mediated Amyloid Aggregation in Alzheimer's Disease.* Int J Mol Sci, 2021. **22**(17).
179. Donovan, J.A. and G.A. Koretzky, *CD45 and the immune response.* J Am Soc Nephrol, 1993. **4**(4): p. 976-85.
180. Muzumdar, M.D., et al., *A global double-fluorescent Cre reporter mouse.* Genesis, 2007. **45**(9): p. 593-605.
181. Xu, X., et al., *Dynamic changes in vascular size and density in transgenic mice with Alzheimer's disease.* Aging (Albany NY), 2020. **12**(17): p. 17224-17234.
182. Calhoun, M.E., et al., *Neuron loss in APP transgenic mice.* Nature, 1998. **395**(6704): p. 755-6.
183. Hansen, D.V., J.E. Hanson, and M. Sheng, *Microglia in Alzheimer's disease.* J Cell Biol, 2018. **217**(2): p. 459-472.
184. Jana, M., C.A. Palencia, and K. Pahan, *Fibrillar amyloid-beta peptides activate microglia via TLR2: implications for Alzheimer's disease.* J Immunol, 2008. **181**(10): p. 7254-62.
185. Hopperton, K.E., et al., *Markers of microglia in post-mortem brain samples from patients with Alzheimer's disease: a systematic review.* Molecular Psychiatry, 2018. **23**(2): p. 177-198.
186. Sweeney, M.D., A.P. Sagare, and B.V. Zlokovic, *Blood-brain barrier breakdown in Alzheimer disease and other neurodegenerative disorders.* Nat Rev Neurol, 2018. **14**(3): p. 133-150.
187. Reuter, B., et al., *Development of Cerebral Microbleeds in the APP23-Transgenic Mouse Model of Cerebral Amyloid Angiopathy-A 9.4 Tesla MRI Study.* Front Aging Neurosci, 2016. **8**: p. 170.
188. Honig, L.S., et al., *Stroke and the risk of Alzheimer disease.* Arch Neurol, 2003. **60**(12): p. 1707-12.
189. Iadecola, C. and R.F. Gottesman, *Cerebrovascular Alterations in Alzheimer Disease.* Circ Res, 2018. **123**(4): p. 406-408.
190. https://www.ema.europa.eu/en/documents/product-information/plavix-epar-product-information_de.pdf. 2022.
191. Bitan, G., et al., *Amyloid β-protein (Aβ) assembly: Aβ40 and Aβ42 oligomerize through distinct pathways.* Proceedings of the National Academy of Sciences, 2003. **100**(1): p. 330-335.
192. Libeu, C.P., et al., *Structural and functional alterations in amyloid-β precursor protein induced by amyloid-β peptides.* J Alzheimers Dis, 2011. **25**(3): p. 547-66.
193. Clark, J.C., et al., *Structure-function relationship of the platelet glycoprotein VI (GPVI) receptor: does it matter if it is a dimer or monomer?* Platelets, 2021. **32**(6): p. 724-732.
194. Singh, A.N., K. Ramadan, and S. Singh, *Chapter 8 - Experimental methods to study the kinetics of protein–protein interactions*, in *Advances in Protein Molecular and Structural Biology Methods*, T. Tripathi and V.K. Dubey, Editors. 2022, Academic Press. p. 115-124.
195. Laske, C., et al., *Association of platelet-derived soluble glycoprotein VI in plasma with Alzheimer's disease.* Journal of Psychiatric Research, 2008. **42**(9): p. 746-751.

196. Massberg, S., et al., *Soluble glycoprotein VI dimer inhibits platelet adhesion and aggregation to the injured vessel wall in vivo.* Faseb j, 2004. **18**(2): p. 397-9.
197. Mayeux, R., et al., *Plasma Aβ40 and Aβ42 and Alzheimer's disease.* Relation to age, mortality, and risk, 2003. **61**(9): p. 1185-1190.
198. Elaskalani, O., et al., *Oligomeric and fibrillar amyloid beta 42 induce platelet aggregation partially through GPVI.* Platelets, 2018. **29**(4): p. 415-420.
199. Jiang, P., et al., *Inhibition of Glycoprotein VI Clustering by Collagen as a Mechanism of Inhibiting Collagen-Induced Platelet Responses: The Example of Losartan.* PLOS ONE, 2015. **10**(6): p. e0128744.
200. Al-Majed, A.R., et al., *Losartan: Comprehensive Profile.* Profiles Drug Subst Excip Relat Methodol, 2015. **40**: p. 159-94.
201. López-Farré, A., et al., *Angiotensin II AT1 receptor antagonists and platelet activation.* Nephrology Dialysis Transplantation, 2001. **16**(suppl_1): p. 45-49.
202. Giraldo, E., et al., *Aβ and tau toxicities in Alzheimer's are linked via oxidative stress-induced p38 activation: Protective role of vitamin E.* Redox Biology, 2014. **2**: p. 873-877.
203. Xiong, Y.-S., et al., *Inhibition of glycogen synthase kinase-3 reverses tau hyperphosphorylation induced by Pin1 down-regulation.* CNS & Neurological Disorders-Drug Targets (Formerly Current Drug Targets-CNS & Neurological Disorders), 2013. **12**(3): p. 436-443.
204. Chen, Q., et al., *Reactive oxygen species: key regulators in vascular health and diseases.* Br J Pharmacol, 2018. **175**(8): p. 1279-1292.
205. Benedictus, M.R., et al., *Microbleeds, mortality, and stroke in Alzheimer disease: the MISTRAL study.* JAMA neurology, 2015. **72**(5): p. 539-545.
206. Ahn, H.J., et al., *Alzheimer's disease peptide β-amyloid interacts with fibrinogen and induces its oligomerization.* Proceedings of the National Academy of Sciences, 2010. **107**(50): p. 21812-21817.
207. Kehoe, P.G., et al., *Safety and efficacy of losartan for the reduction of brain atrophy in clinically diagnosed Alzheimer's disease (the RADAR trial): a double-blind, randomised, placebo-controlled, phase 2 trial.* Lancet Neurol, 2021. **20**(11): p. 895-906.
208. Pan, D., et al., *Anti-platelet Therapy Is Associated With Lower Risk of Dementia in Patients With Cerebral Small Vessel Disease.* Front Aging Neurosci, 2022. **14**: p. 788407.
209. Gresele, P., S. Momi, and E. Falcinelli, *Anti-platelet therapy: phosphodiesterase inhibitors.* British Journal of Clinical Pharmacology, 2011. **72**(4): p. 634-646.
210. Schrör, K., *Aspirin and platelets: the antiplatelet action of aspirin and its role in thrombosis treatment and prophylaxis.* Semin Thromb Hemost, 1997. **23**(4): p. 349-56.
211. Zarbock, A., K. Singbartl, and K. Ley, *Complete reversal of acid-induced acute lung injury by blocking of platelet-neutrophil aggregation.* The Journal of Clinical Investigation, 2006. **116**(12): p. 3211-3219.
212. Mestas, J. and C.C.W. Hughes, *Of Mice and Not Men: Differences between Mouse and Human Immunology.* The Journal of Immunology, 2004. **172**(5): p. 2731-2738.
213. Tecchio, C., A. Micheletti, and M.A. Cassatella, *Neutrophil-derived cytokines: facts beyond expression.* Frontiers in immunology, 2014. **5**: p. 508.
214. Condliffe, A.M., et al., *Sequential activation of class IB and class IA PI3K is important for the primed respiratory burst of human but not murine neutrophils.* Blood, 2005. **106**(4): p. 1432-1440.
215. Eisenhauer, P.B. and R.I. Lehrer, *Mouse neutrophils lack defensins.* Infection and immunity, 1992. **60**(8): p. 3446-3447.
216. Fan, D.Y., et al., *The Correlations Between Plasma Fibrinogen With Amyloid-Beta and Tau Levels in Patients With Alzheimer's Disease.* Front Neurosci, 2020. **14**: p. 625844.

217. Oijen, M.v., et al., *Fibrinogen Is Associated With an Increased Risk of Alzheimer Disease and Vascular Dementia.* Stroke, 2005. **36**(12): p. 2637-2641.
218. Paul , J., S. Strickland , and J.P. Melchor *Fibrin deposition accelerates neurovascular damage and neuroinflammation in mouse models of Alzheimer's disease.* Journal of Experimental Medicine, 2007. **204**(8): p. 1999-2008.
219. Cortes-Canteli, M., et al., *Fibrinogen and Altered Hemostasis in Alzheimer's Disease.* Journal of Alzheimer's Disease, 2012. **32**: p. 599-608.
220. Kuo, Y.-M., et al., *The Evolution of Aβ Peptide Burden in the APP23 Transgenic Mice: Implications for Aβ Deposition in Alzheimer Disease.* Molecular Medicine, 2001. **7**(9): p. 609-618.
221. Malaguarnera, L., et al., *Interleukin-18 and transforming growth factor-beta 1 plasma levels in Alzheimer's disease and vascular dementia.* Neuropathology, 2006. **26**(4): p. 307-312.
222. Reibman, J., et al., *Transforming growth factor beta 1, a potent chemoattractant for human neutrophils, bypasses classic signal-transduction pathways.* Proc Natl Acad Sci U S A, 1991. **88**(15): p. 6805-9.
223. Ahamed, J., et al., *In vitro and in vivo evidence for shear-induced activation of latent transforming growth factor-β1.* Blood, 2008. **112**(9): p. 3650-3660.
224. Wyss-Coray, T., et al., *Chronic Overproduction of Transforming Growth Factor-β1 by Astrocytes Promotes Alzheimer's Disease-Like Microvascular Degeneration in Transgenic Mice.* The American Journal of Pathology, 2000. **156**(1): p. 139-150.
225. Kato, T., et al., *Excessive Production of Transforming Growth Factor β1 Causes Mural Cell Depletion From Cerebral Small Vessels.* Front Aging Neurosci, 2020. **12**: p. 151.
226. Wyss-Coray, T., et al., *TGF-β1 promotes microglial amyloid-β clearance and reduces plaque burden in transgenic mice.* Nature Medicine, 2001. **7**(5): p. 612-618.
227. Li, J., et al., *Platelet–neutrophil interactions under thromboinflammatory conditions.* Cellular and Molecular Life Sciences, 2015. **72**(14): p. 2627-2643.
228. Donner, L., et al., *Relevance of N-terminal residues for amyloid-β binding to platelet integrin α(IIb)β(3), integrin outside-in signaling and amyloid-β fibril formation.* Cell Signal, 2018. **50**: p. 121-130.
229. Pachel, C., et al., *Inhibition of Platelet GPVI Protects Against Myocardial Ischemia-Reperfusion Injury.* Arterioscler Thromb Vasc Biol, 2016. **36**(4): p. 629-35.
230. Bieber, M., et al., *Targeting platelet glycoprotein VI attenuates progressive ischemic brain damage before recanalization during middle cerebral artery occlusion in mice.* Experimental Neurology, 2021. **344**: p. 113804.
231. Park, H.-Y., et al., *Modulation of neutrophil apoptosis by β-amyloid proteins.* International Immunopharmacology, 2006. **6**(7): p. 1061-1069.
232. Stock, A.J., et al., *The Role of Neutrophil Proteins on the Amyloid Beta-RAGE Axis.* PLoS One, 2016. **11**(9): p. e0163330.
233. Kasus-Jacobi, A., et al., *Neutrophil Granule Proteins Inhibit Amyloid Beta Aggregation and Neurotoxicity.* Curr Alzheimer Res, 2021. **18**(5): p. 414-427.
234. Brinkmann, V., et al., *Neutrophil Extracellular Traps Kill Bacteria.* Science, 2004. **303**(5663): p. 1532-1535.
235. Caudrillier, A., et al., *Platelets induce neutrophil extracellular traps in transfusion-related acute lung injury.* The Journal of Clinical Investigation, 2012. **122**(7): p. 2661-2671.
236. Clark, S.R., et al., *Platelet TLR4 activates neutrophil extracellular traps to ensnare bacteria in septic blood.* Nature Medicine, 2007. **13**(4): p. 463-469.
237. Boxio, R., et al., *Mouse bone marrow contains large numbers of functionally competent neutrophils.* J Leukoc Biol, 2004. **75**(4): p. 604-11.

238. Kirchner, T., et al., *The impact of various reactive oxygen species on the formation of neutrophil extracellular traps.* Mediators Inflamm, 2012. **2012**: p. 849136.
239. Stalder, A.K., et al., *Invasion of hematopoietic cells into the brain of amyloid precursor protein transgenic mice.* J Neurosci, 2005. **25**(48): p. 11125-32.
240. Kniewallner, K.M., et al., *Platelets in the Alzheimer's disease brain: do they play a role in cerebral amyloid angiopathy?* Curr Neurovasc Res, 2015. **12**(1): p. 4-14.
241. Kniewallner, K.M., et al., *Platelets in Amyloidogenic Mice Are Activated and Invade the Brain.* Front Neurosci, 2020. **14**: p. 129.
242. Ciabattoni, G., et al., *Determinants of platelet activation in Alzheimer's disease.* Neurobiology of aging, 2007. **28**(3): p. 336-342.
243. Seizer, P. and A.E. May, *Platelets and matrix metalloproteinases.* Thromb Haemost, 2013. **110**(11): p. 903-909.
244. Weekman, E.M. and D.M. Wilcock, *Matrix Metalloproteinase in Blood-Brain Barrier Breakdown in Dementia.* Journal of Alzheimer's Disease, 2016. **49**: p. 893-903.
245. Hochstrasser, T., et al., *Matrix metalloproteinase-2 and epidermal growth factor are decreased in platelets of Alzheimer patients.* Curr Alzheimer Res, 2012. **9**(8): p. 982-9.
246. Kniewallner, K.M., B.M. Foidl, and C. Humpel, *Platelets isolated from an Alzheimer mouse damage healthy cortical vessels and cause inflammation in an organotypic ex vivo brain slice model.* Scientific Reports, 2018. **8**(1): p. 15483.
247. Davis, J., et al., *Early-onset and robust cerebral microvascular accumulation of amyloid beta-protein in transgenic mice expressing low levels of a vasculotropic Dutch/Iowa mutant form of amyloid beta-protein precursor.* J Biol Chem, 2004. **279**(19): p. 20296-306.
248. Knierim, J.J., *The hippocampus.* Curr Biol, 2015. **25**(23): p. R1116-21.
249. Gaertner, F., et al., *Migrating Platelets Are Mechano-scavengers that Collect and Bundle Bacteria.* Cell, 2017. **171**(6): p. 1368-1382.e23.
250. Huilcaman, R., et al., *Endothelial transmigration of platelets depends on soluble factors released by activated endothelial cells and monocytes.* Platelets, 2021. **32**(8): p. 1113-1119.
251. Zlokovic, B.V., *The Blood-Brain Barrier in Health and Chronic Neurodegenerative Disorders.* Neuron, 2008. **57**(2): p. 178-201.
252. Frontera, J.A., et al., *The Role of Platelet Activation and Inflammation in Early Brain Injury Following Subarachnoid Hemorrhage.* Neurocrit Care, 2017. **26**(1): p. 48-57.
253. Langer, H.F., et al., *Platelets Contribute to the Pathogenesis of Experimental Autoimmune Encephalomyelitis.* Circulation Research, 2012. **110**(9): p. 1202-1210.
254. Walker, L.C., *Aβ Plaques.* Free Neuropathol, 2020. **1**.
255. Bian, Z., et al., *Accelerated accumulation of fibrinogen peptide chains with Aβ deposition in Alzheimer's disease (AD) mice and human AD brains.* Brain Res, 2021. **1767**: p. 147569.
256. Ryu, J.K. and J.G. McLarnon, *A leaky blood-brain barrier, fibrinogen infiltration and microglial reactivity in inflamed Alzheimer's disease brain.* J Cell Mol Med, 2009. **13**(9a): p. 2911-25.
257. Rondina, M.T. and A.S. Weyrich, *Arf6 arbitrates fibrinogen endocytosis.* Blood, 2016. **127**(11): p. 1383-4.
258. Cloutier, N., et al., *Platelets release pathogenic serotonin and return to circulation after immune complex-mediated sequestration.* Proceedings of the National Academy of Sciences, 2018. **115**(7): p. E1550-E1559.
259. Schleicher, R.I., et al., *Platelets induce apoptosis via membrane-bound FasL.* Blood, 2015. **126**(12): p. 1483-93.

260. Davalos, D., et al., *Fibrinogen-induced perivascular microglial clustering is required for the development of axonal damage in neuroinflammation.* Nature Communications, 2012. **3**(1): p. 1227.
261. Fu, R., et al., *Phagocytosis of microglia in the central nervous system diseases.* Mol Neurobiol, 2014. **49**(3): p. 1422-34.
262. Alenazy, F.O., et al., *GPVI inhibition by glenzocimab synergistically inhibits atherosclerotic plaque-induced platelet activation when combined with conventional dual antiplatelet therapy.* European Heart Journal, 2021. **42**(Supplement_1).
263. Wichaiyo, S., W. Parichatikanond, and W. Rattanavipanon, *Glenzocimab: A GPVI (Glycoprotein VI)-Targeted Potential Antiplatelet Agent for the Treatment of Acute Ischemic Stroke.* Stroke, 2022. **53**(11): p. 3506-3513.
264. Viswanathan, A. and S.M. Greenberg, *Cerebral amyloid angiopathy in the elderly.* Ann Neurol, 2011. **70**(6): p. 871-80.

6 Appendix

6.1. Supplemental Figures

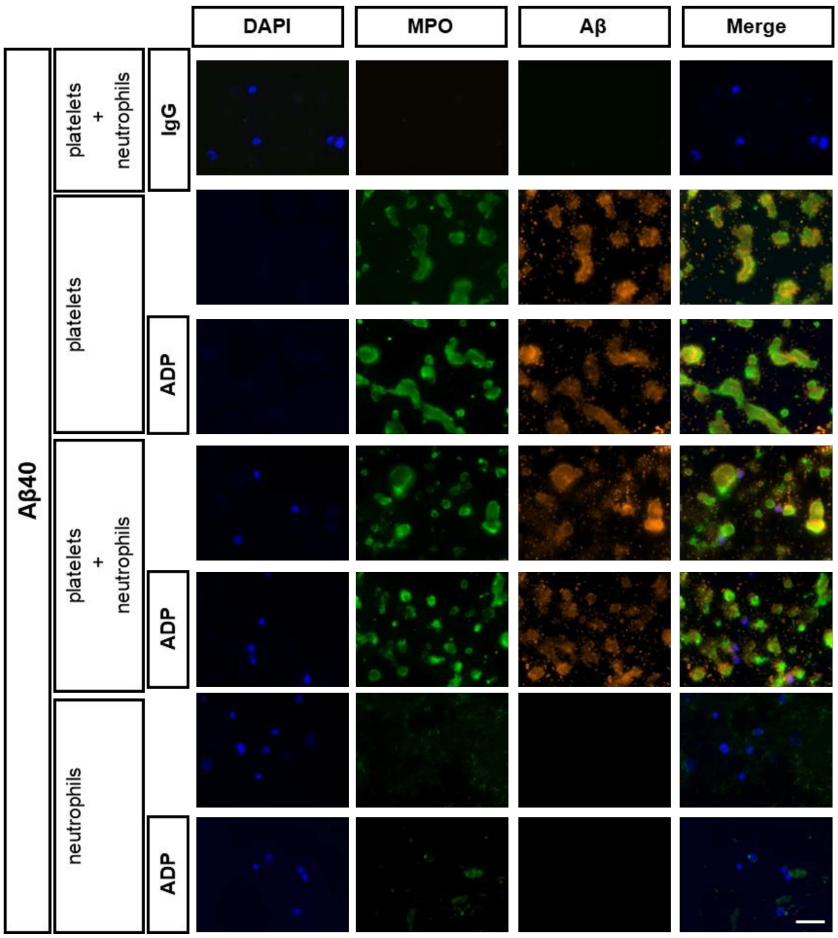

Figure S 1: Formation of amyloid aggregates in co-culture of platelets and neutrophils.
Single channel immuno-fluorescence images of neutrophils and platelets with corresponding IgG control (green= 6E10; orange=GPIb and blue=DAPI).

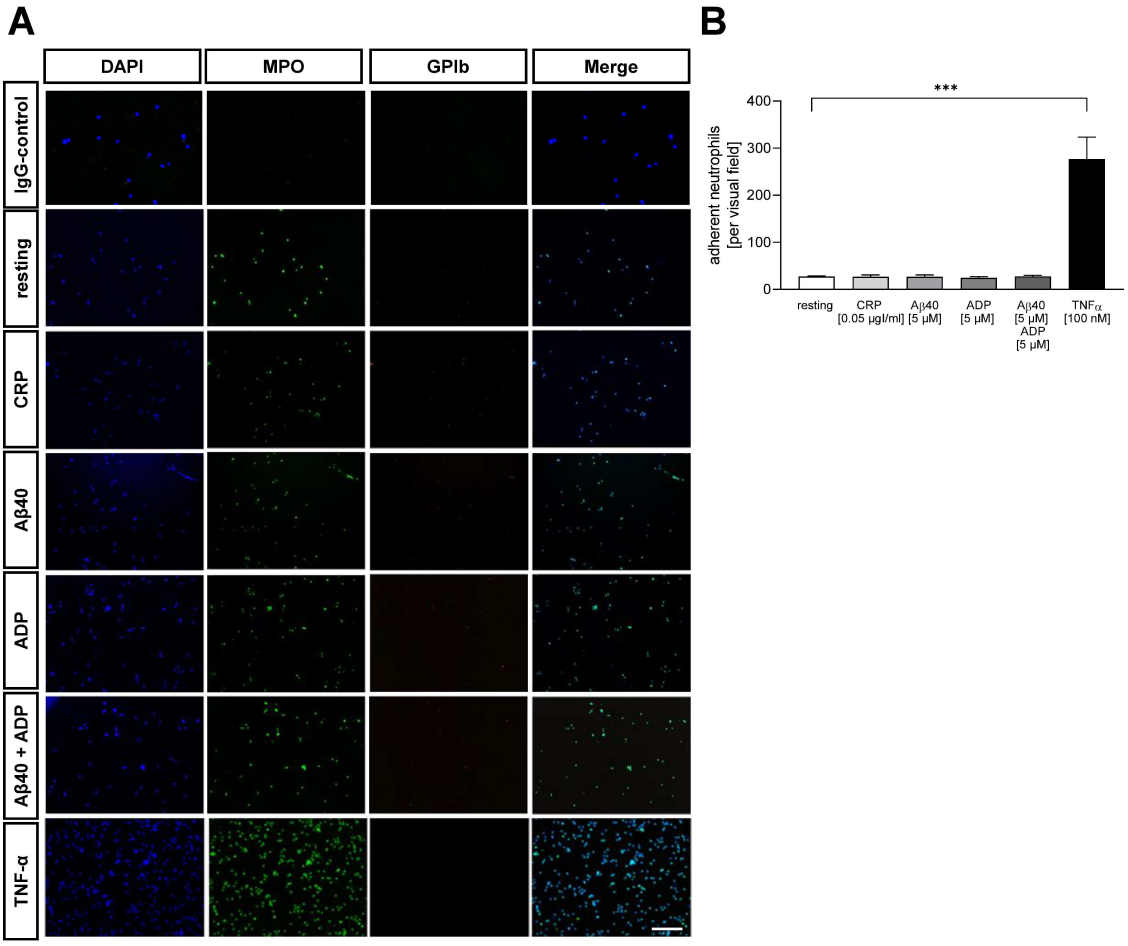

Figure S 2: Control experiment stimulation of murine neutrophils with the indicated agonist without platelets.
(A) Representative images of immunofluorescence staining and IgG control. (B) Quantification of neutrophils. Statistical analyses were performed using an ordinary one-way ANOVA followed by a Sidak`s post-hoc test. Bar graphs indicate mean values ± SEM (n=3) ***p < 0.001.

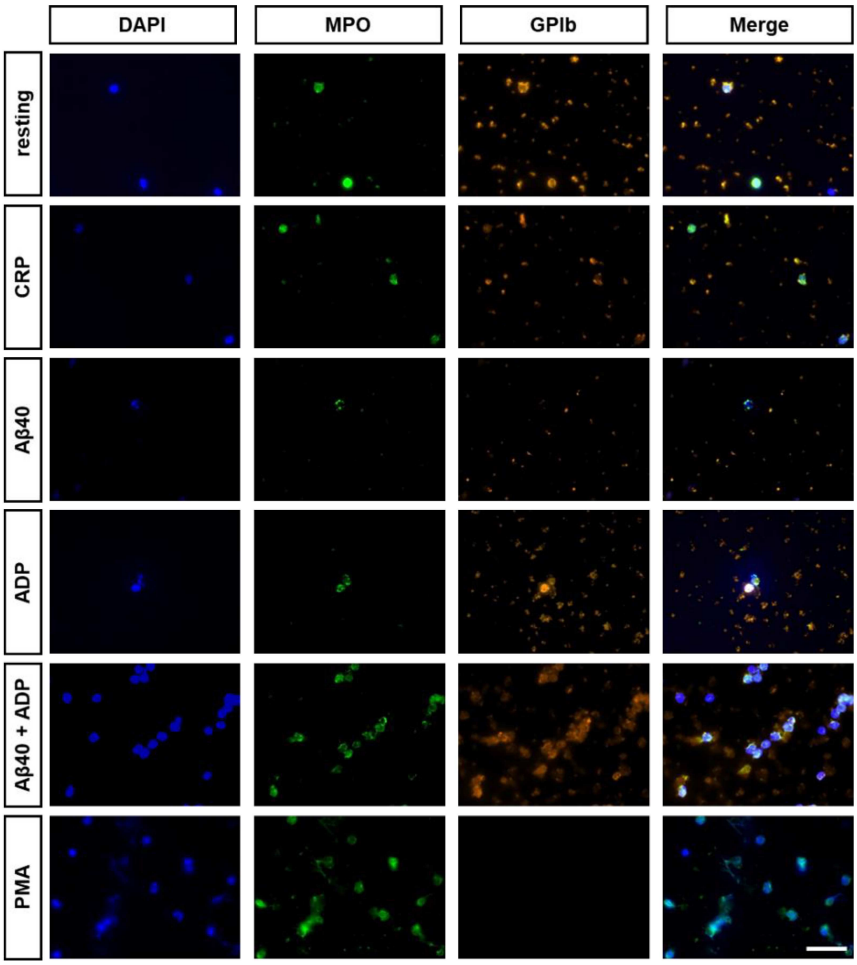

Figure S 3: Representative single channel images of immunofluorescence staining from analysis of murine NET formation *in vitro*
(MPO=green, GPIb=orange, DAPI=blue).

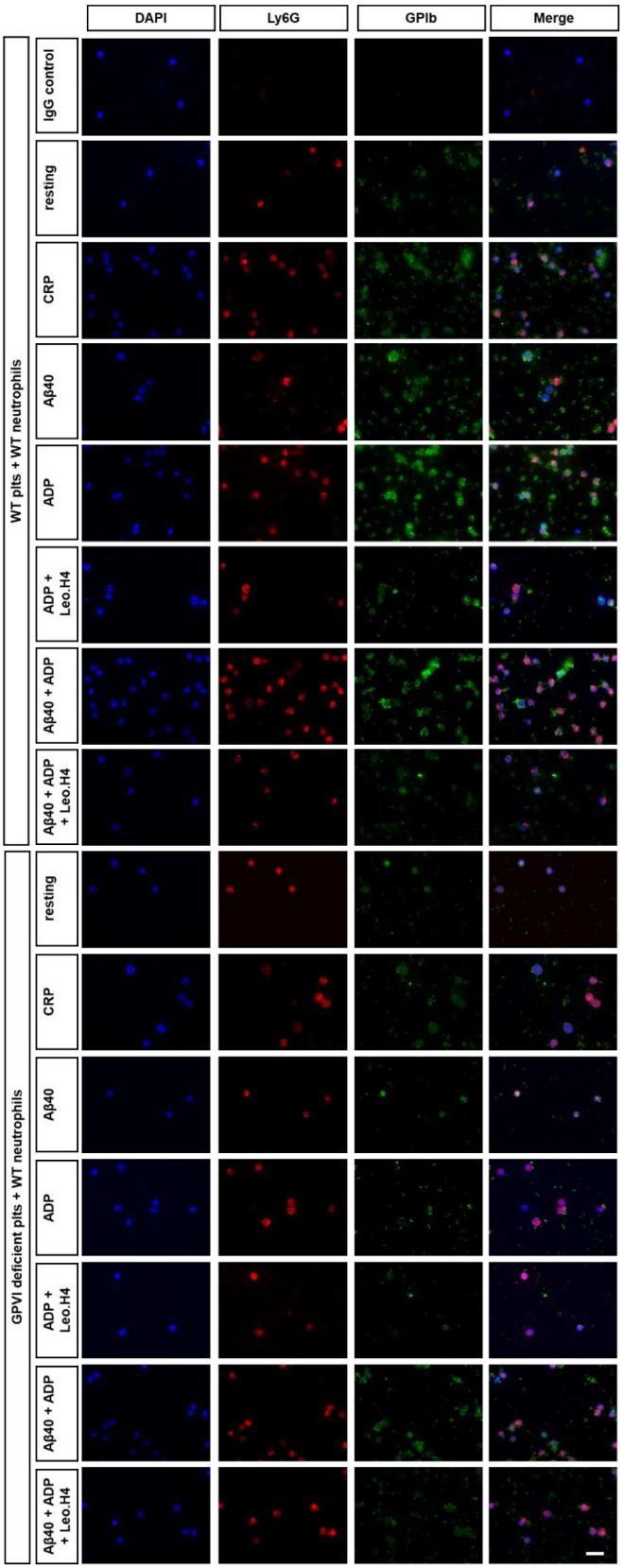

Figure S 4: Single channel immunofluorescence images of WT and GPVI deficient platelets with WT neutrophils co-culture with the indicated agonists.
Scale bar= 20 µm. (blue=DAPI; red=Ly6G; green= GPIb).

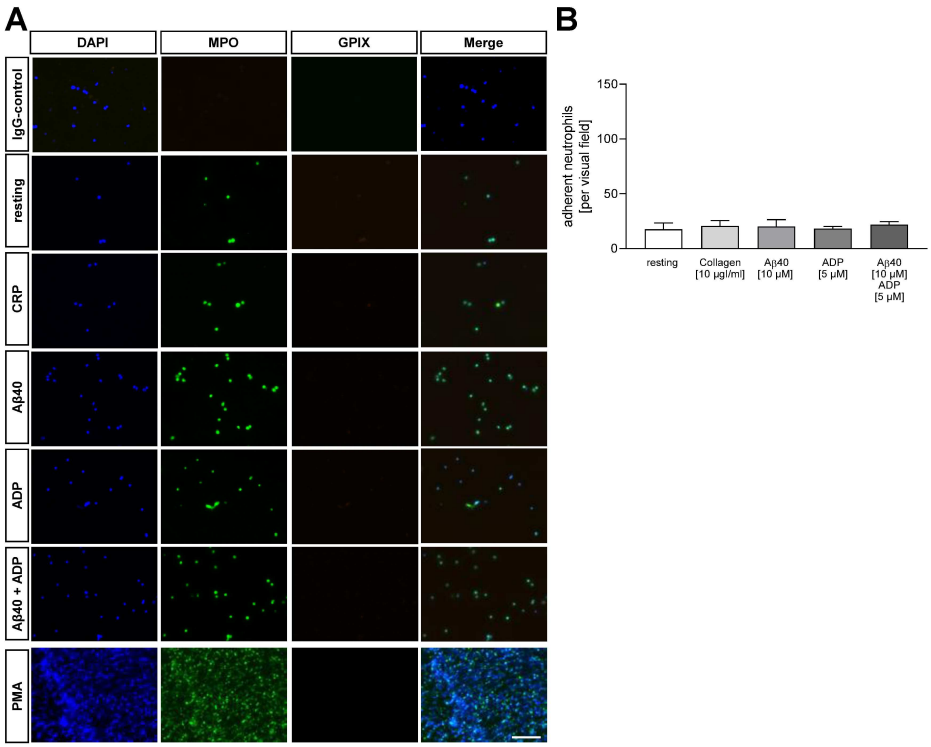

Figure S 5: Control experiment stimulation of human neutrophils with the indicated agonist without platelets.

Representative images of immunofluorescence staining and IgG controls (MPO= green; DAPI= blue; GPIX = orange). (B) Quantification of neutrophils. Data are **re**presented as mean ± SEM (n=3).

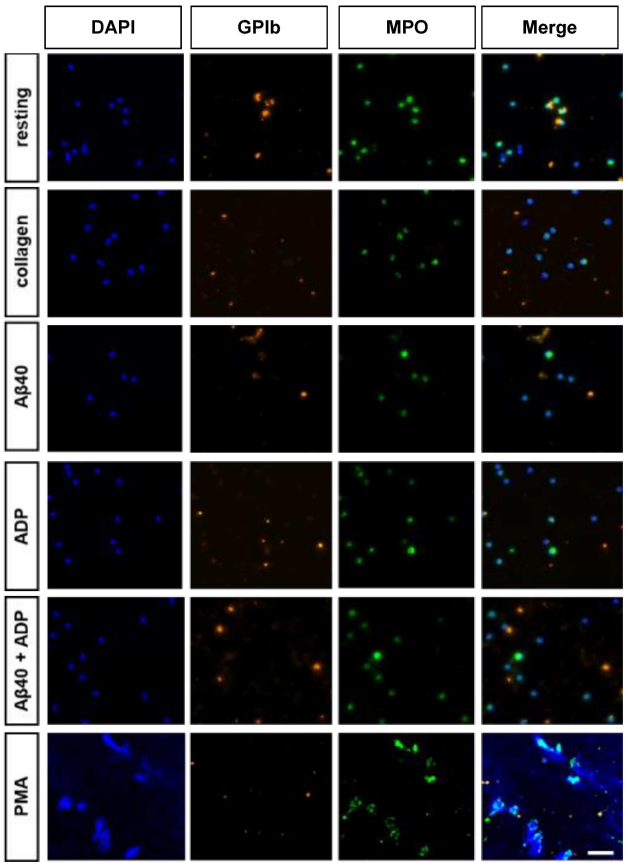

Figure S 6: Representative single channel images of immunofluorescence staining from analysis of human NET formation *in vitro.*

(MPO=green, GPIX=orange, DAPI=blue).

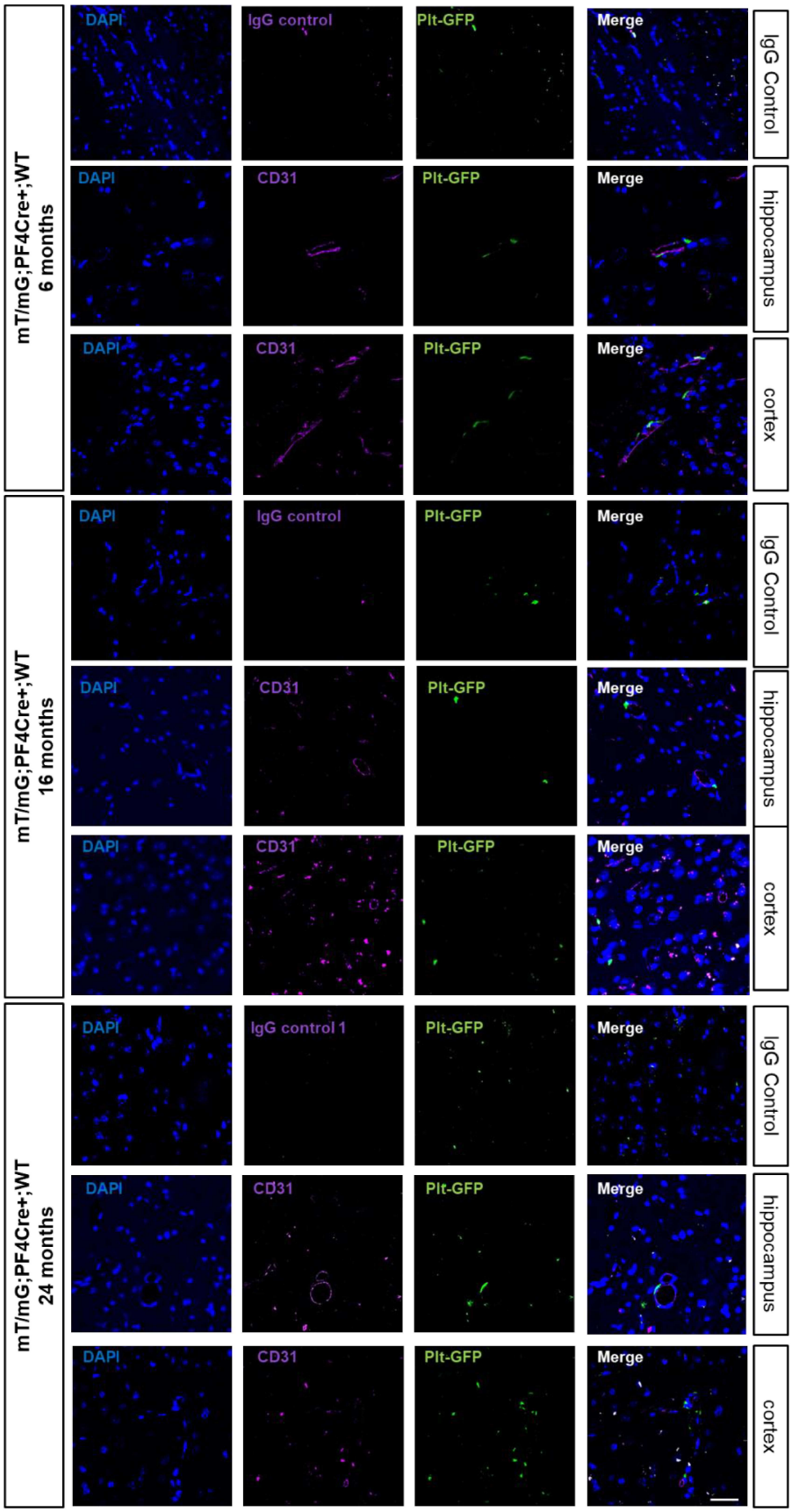

Figure S 7: Single channel immunofluorescence images of CD31 with corresponding IgG control of *WTmT/mG;PF4Cre+.*

Scale bar= 50 µm.

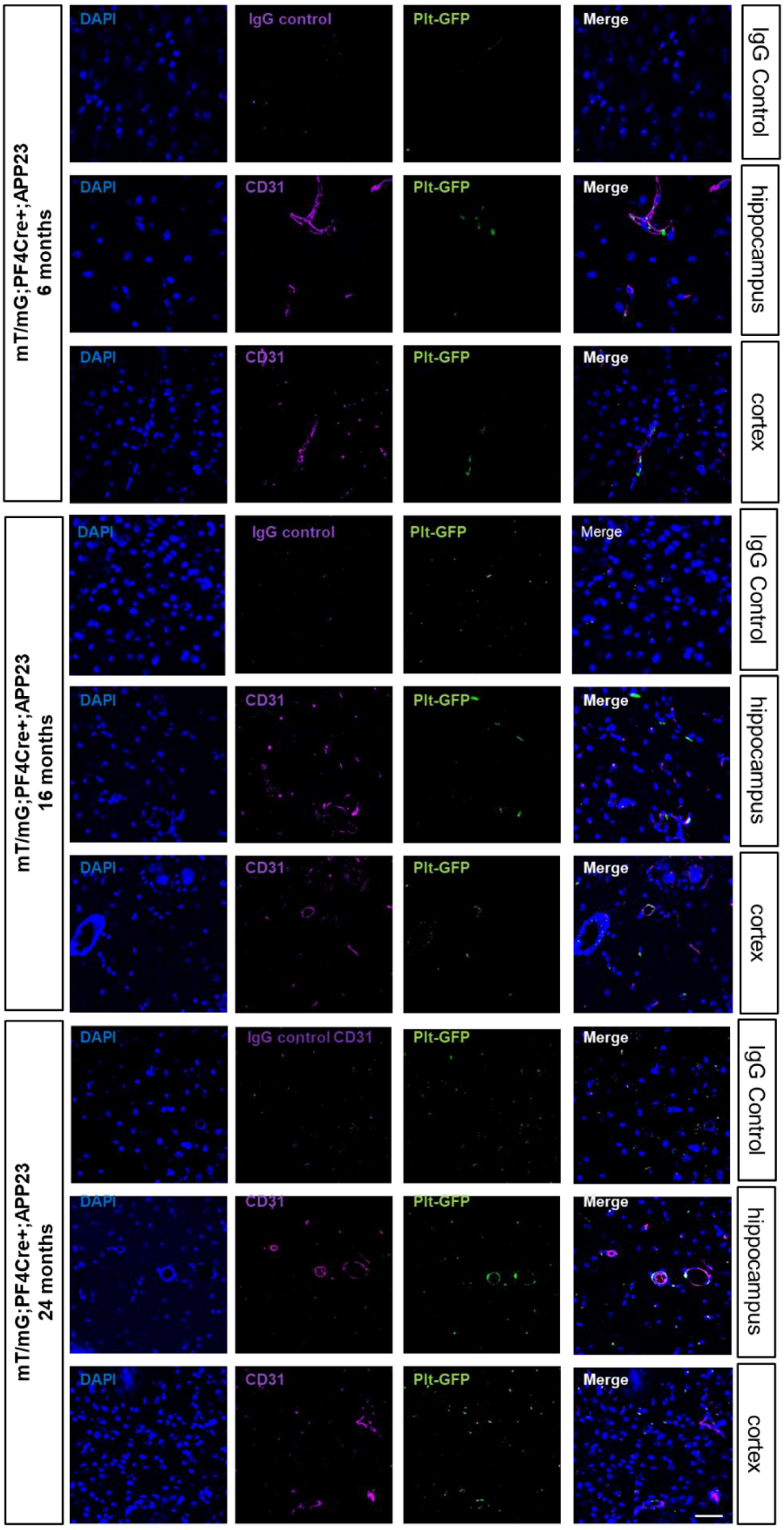

Figure S 8: Single channel immunofluorescence images of CD31 with corresponding IgG control of *APP23mT/mG;PF4Cre+.*

Scale bar= 50 µm.

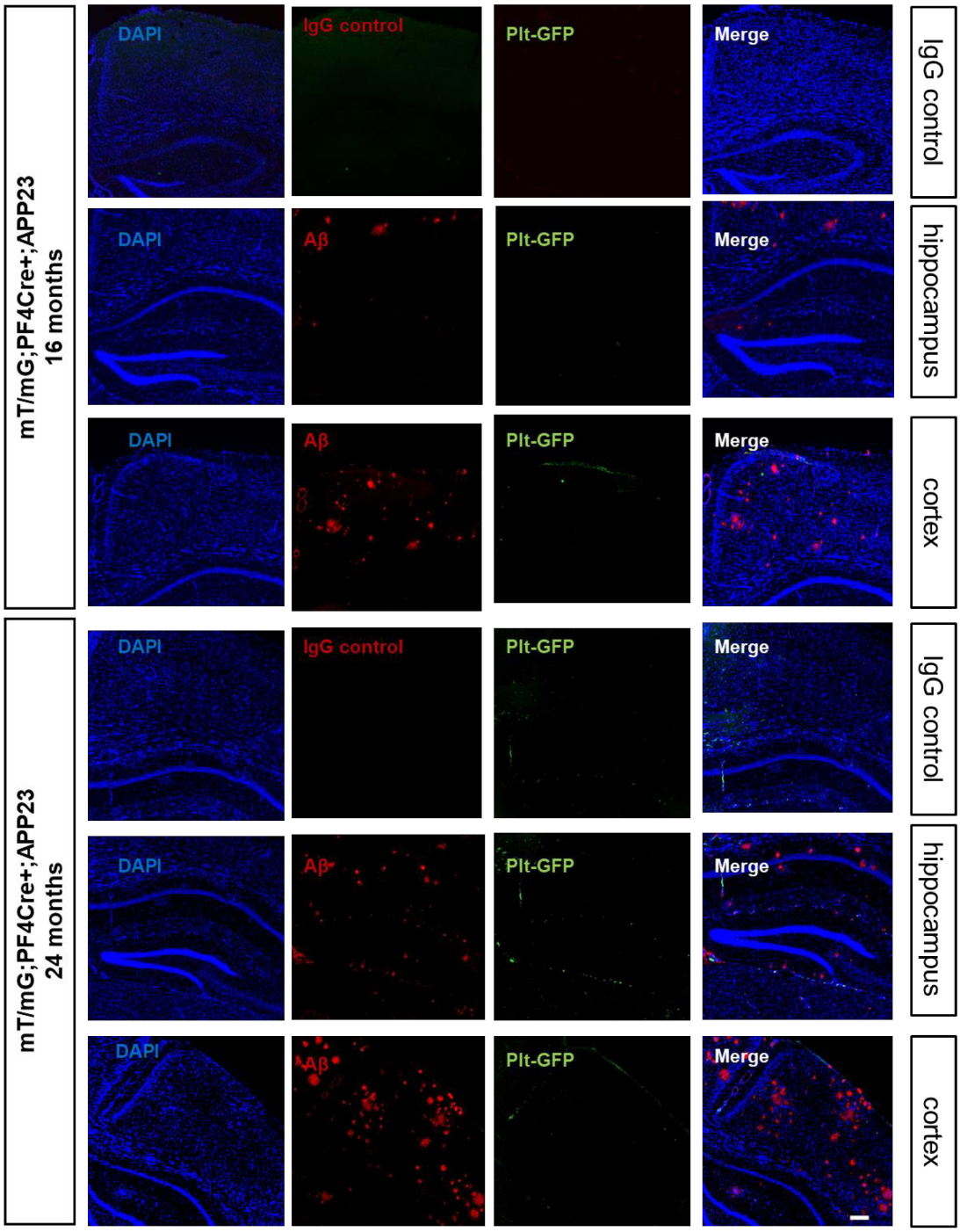

Figure S 9: Single channel immunofluorescence images from the Aβ (6E10) overview staining with corresponding IgG control of *APP23mT/mG;PF4Cre+.*

Scale bar= 200 µm.

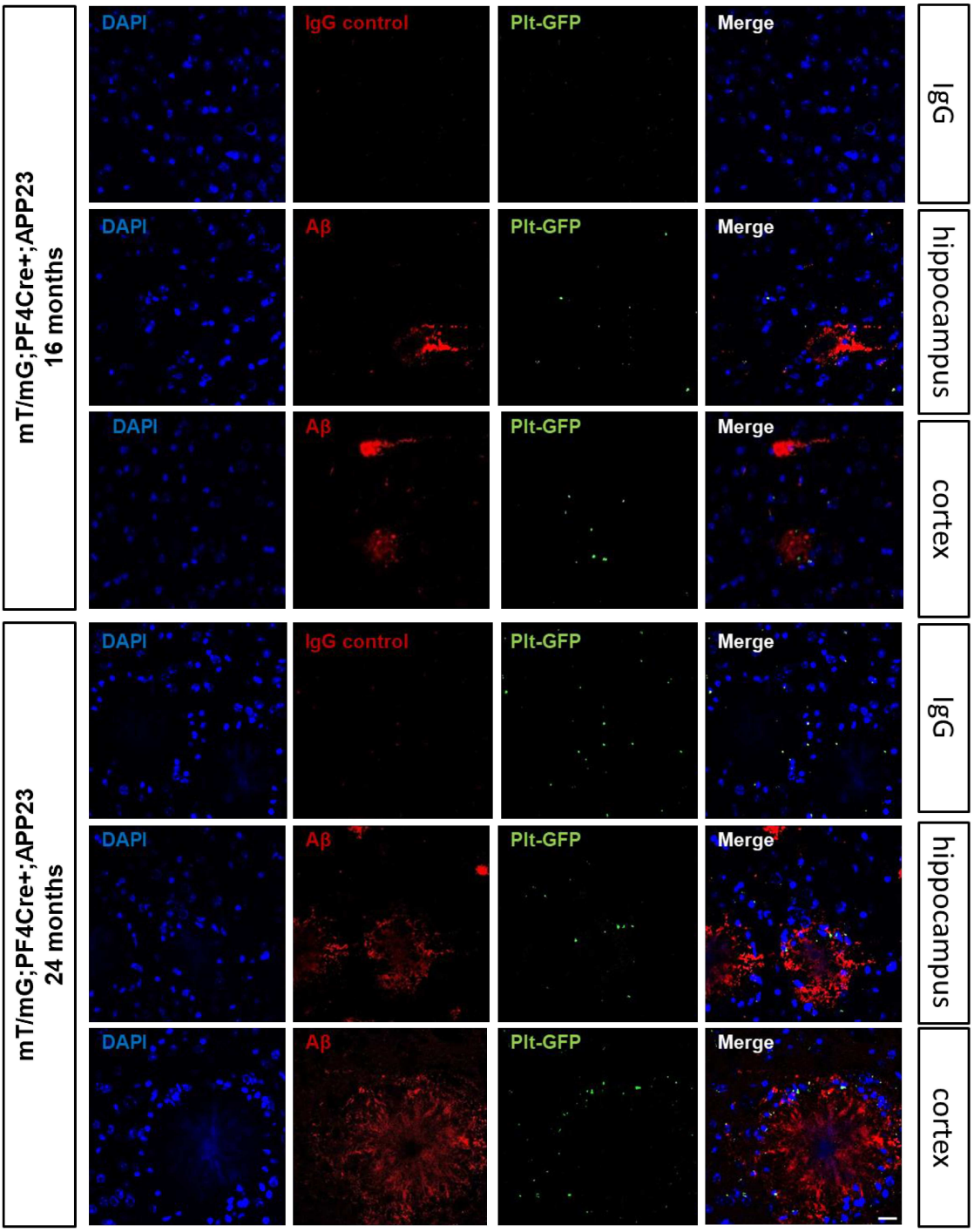

Figure S 10: Single channel immunofluorescence images of Aβ (6E10) zoom staining with corresponding IgG control of *APP23mT/mG;PF4Cre+*.

Scale bar= 20 µm.

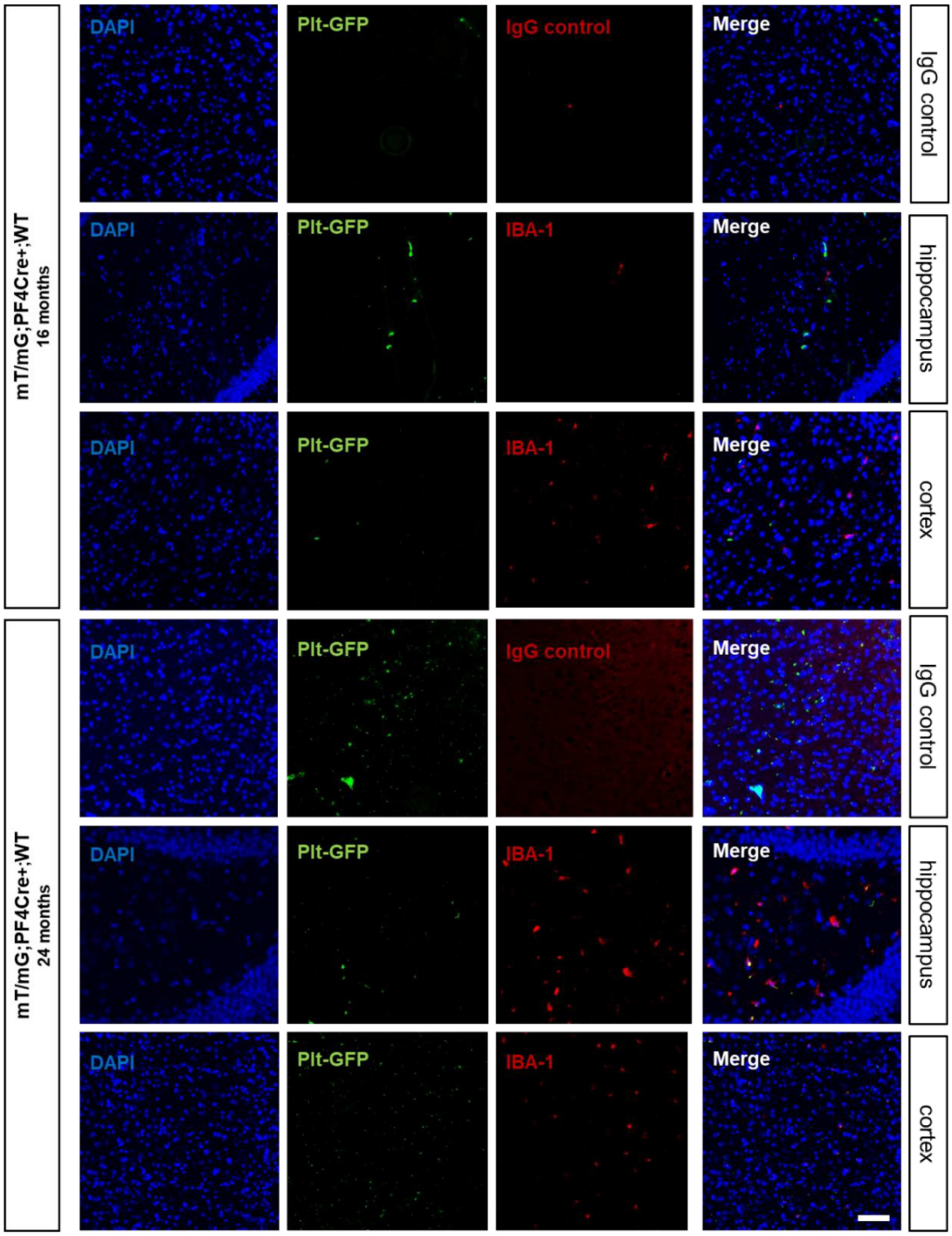

Figure S 11: Single channel immunofluorescence images of IBA-1 with corresponding IgG control of *WTmT/mG;PF4Cre+.*

Scale bar= 50 µm.

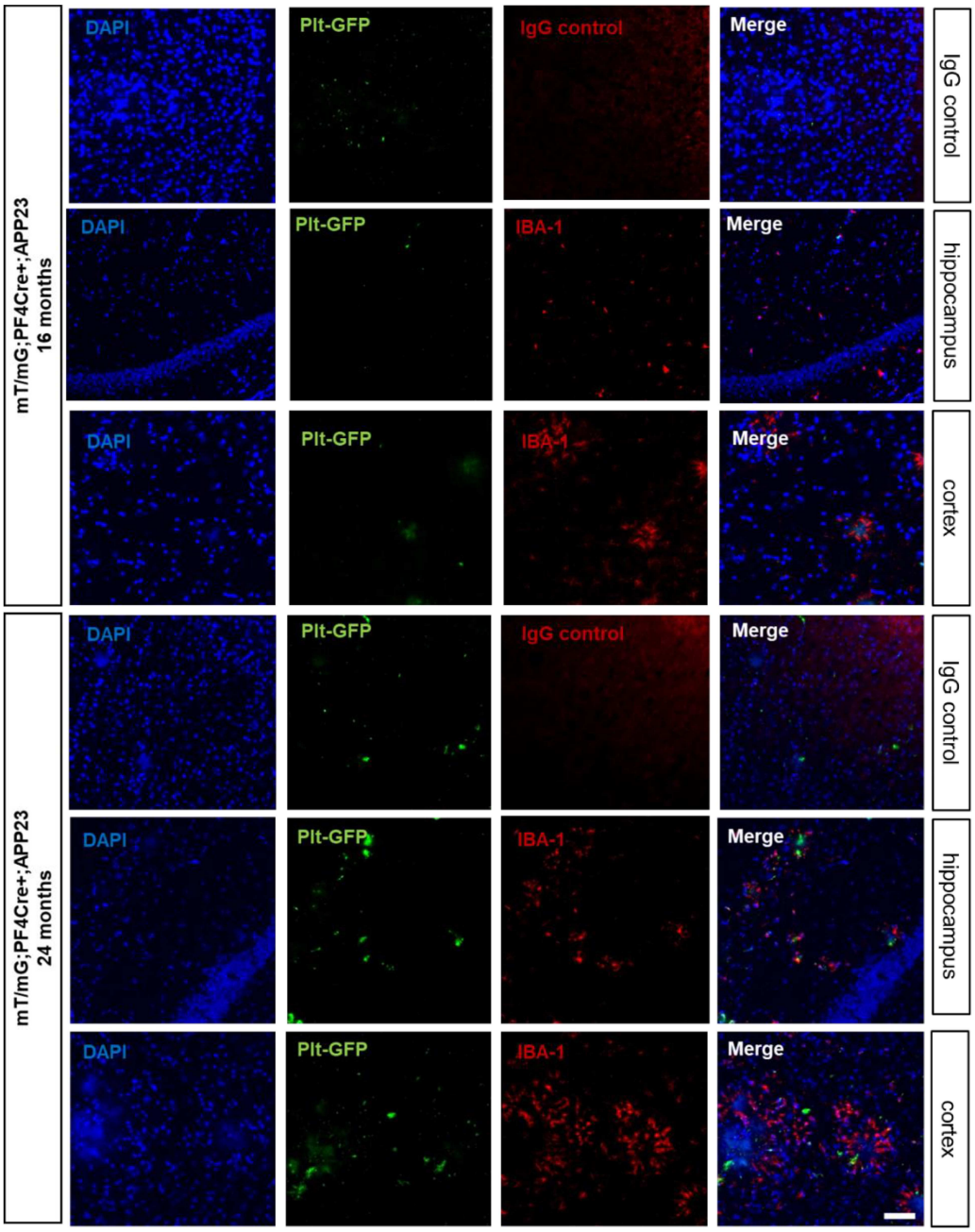

Figure S 12: Single channel immunofluorescence images of IBA-1 with corresponding IgG control of *APP23mT/mG;PF4Cre+.*

Scale bar= 50 µm.

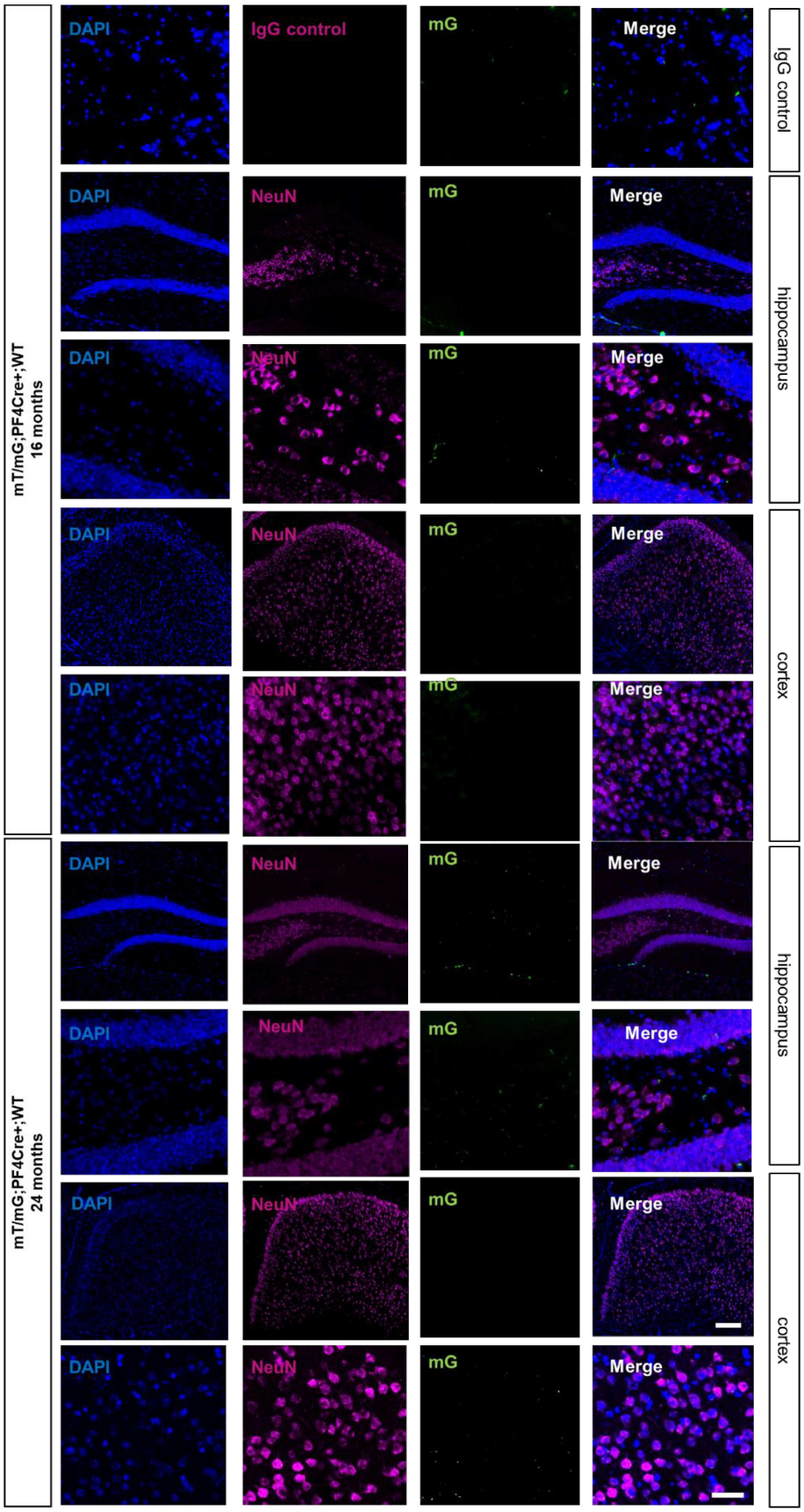

Figure S 13: Single channel immunofluorescence images of NeuN with corresponding IgG control of *WTmT/mG;PF4Cre+.*

Scale bar= 200 µm and 20 µm.

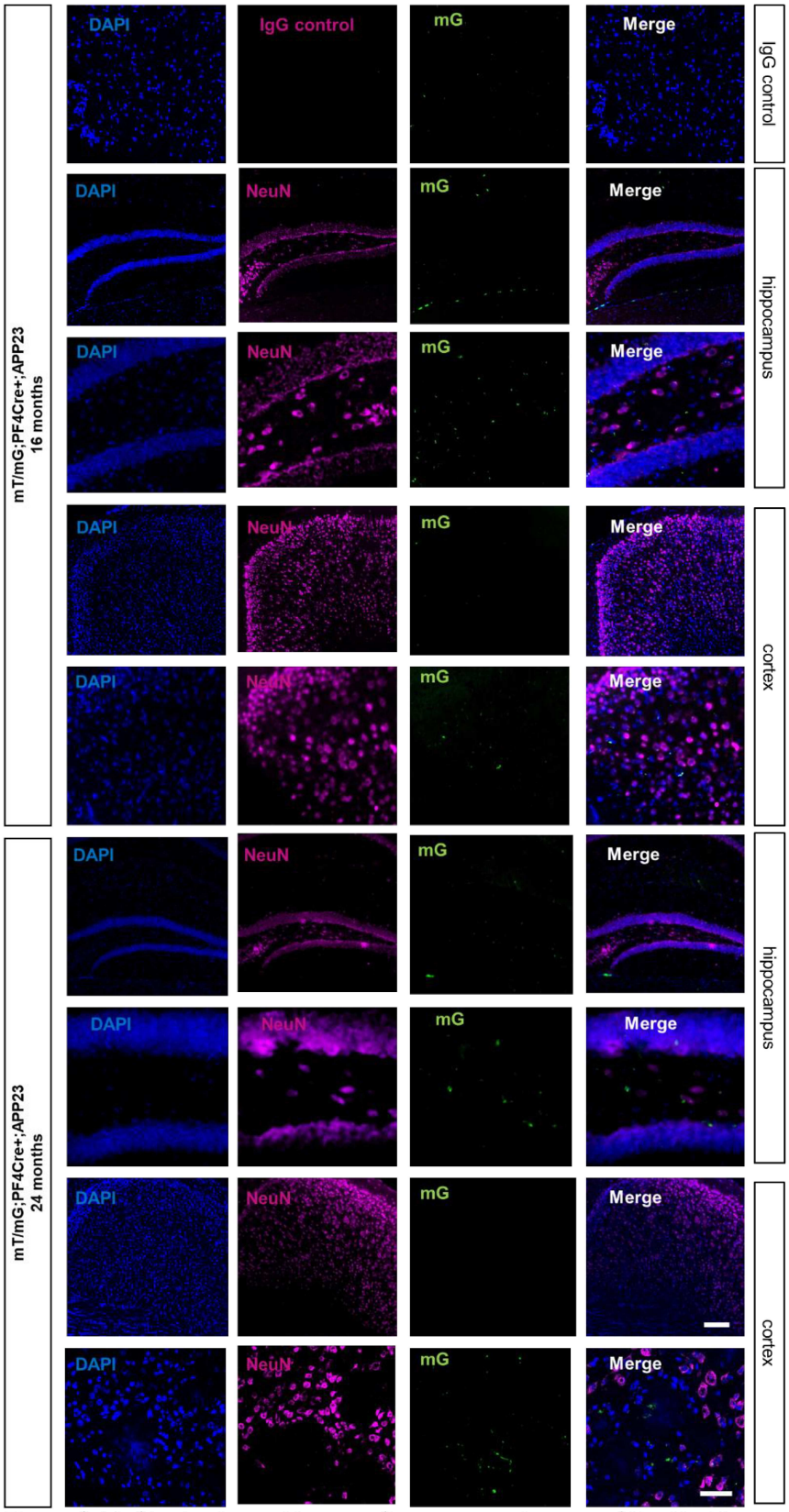

Figure S 14: Single channel immunofluorescence images of NeuN with corresponding IgG control of *APP23mT/mG;PF4Cre+.*

Scale bar= 200 µm and 20 µm.

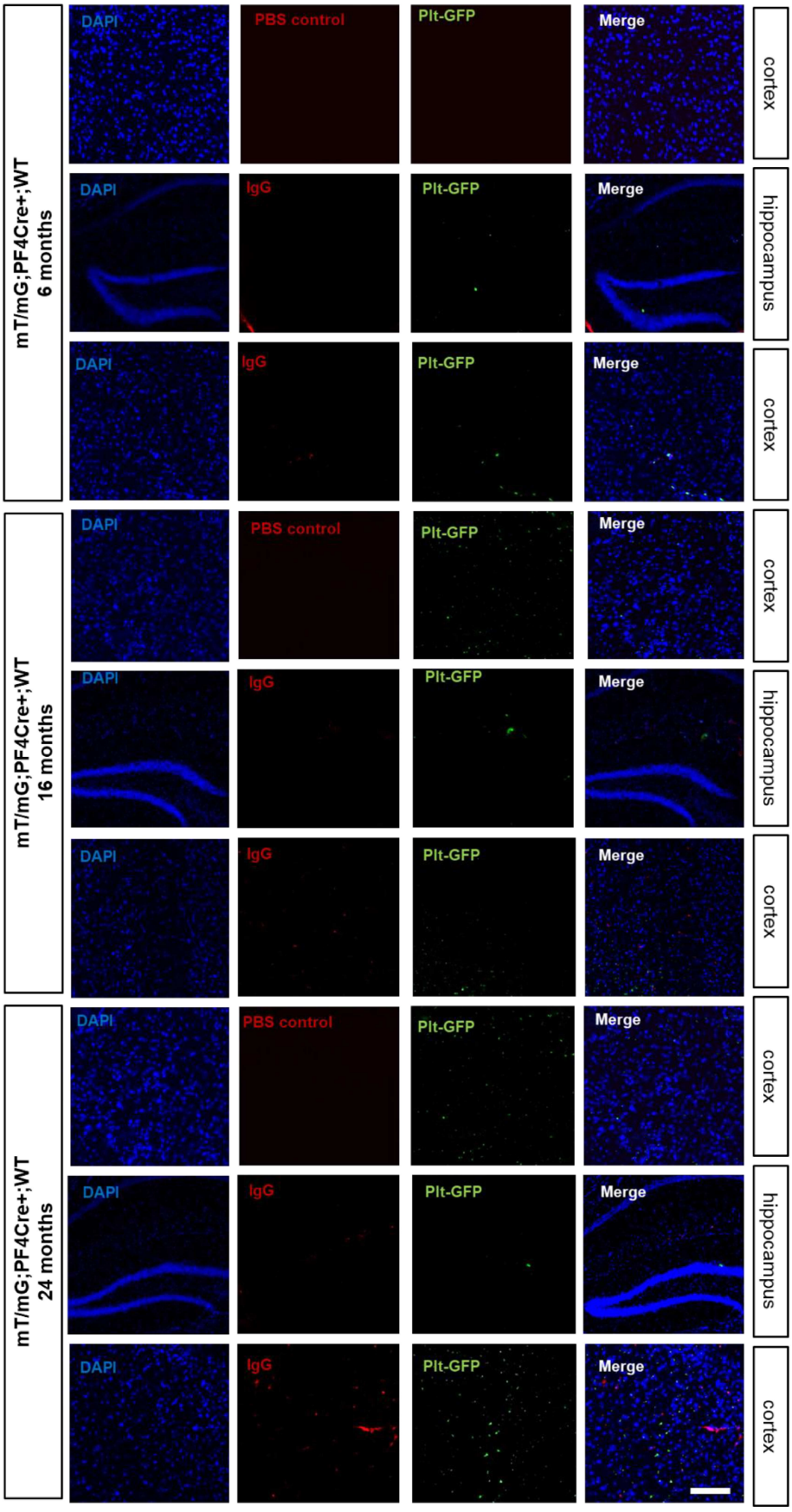

Figure S 15: Single channel immunofluorescence images from immunoglobulin G staining and PBS control (secondary antibody control) of *WTmT/mG;PF4Cre+.*

Scale bar= 200 µm.

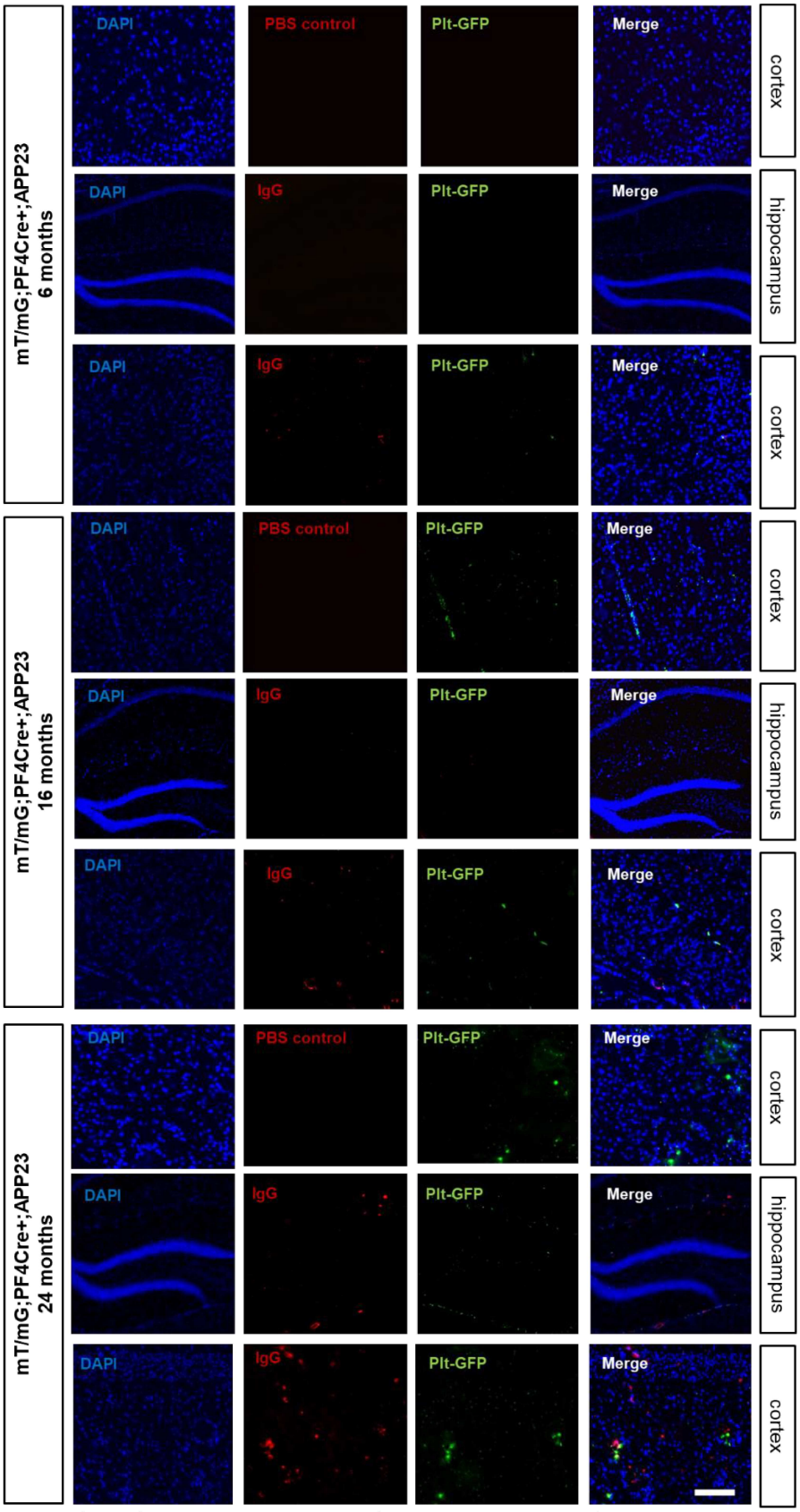

Figure S 16: Single channel immunofluorescence images from immunoglobulin G staining and PBS control (secondary antibody control) of *APP23mT/mG;PF4Cre+.*

Scale bar= 200 µm.

6.2. List of publications

(1) 09/2021 **Impact of Amyloid-β on Platelet Mitochondrial Function and Platelet-Mediated Amyloid Aggregation in Alzheimer's disease.**
Lili Donner, Tobias Feige, Carolin Freiburg, **Laura Mara Toska**, Andreas S Reichert, Madhumita Chatterjee, Margitta Elvers. Int J Mol Sci. 2021 Sep 6;22(17):9633. doi: 10.3390/ijms22179633

(2) 10/2020 **Molecular Drivers of Platelet Activation: Unraveling Novel Targets for Anti-Thrombotic and Anti-Thrombo-Inflammatory Therapy.**
Madhumita Chatterjee, Agnes Ehrenberg**, Laura Mara Toska**, Lisa Maria Metz, Meike Klier, Irena Kruege, Friedrich Reusswig, Margitta Elvers. Int J Mol Sci. 2020 Oct 24;21(21):E7906. doi: 10.3390/ijms21217906

(3) 08/2020 **The collagen receptor glycoprotein VI promotes platelet-mediated aggregation of β-amyloid.**
*Lili Donner, ***Laura Mara Toska**, Irena Krüger, Sandra Gröniger, Ruben Barroso, Alice Burleigh, Diego Mezzano, Susanne Pfeiler, Malte Kelm, Norbert Gerdes, Steve P Watson, Yi Sun, Margitta Elvers. Sci Signal. 2020 Aug 4;13 (643):eaba9872. doi: 10.1126/scisignal.aba9872
*These authors contributed equally to this work.

Publications (3) and (1) are reprinted in this dissertation. (3) Permission and license was granted by Sci Signal, ISSN: 1937-9145. (1) No special permission is required to reuse all or part of an article published by MDPI.

6.3. International conferences

03/2022	**Poster presentation**: *Interaction between amyloid-β and platelet collagen receptor Glycoprotein VI* AD/PD™ 2023 Alzheimer's & Parkinson's Diseases Conference, online and in Barcelona, Spain
02/2020	**Poster presentation**: *Involvement of Glycoprotein VI in Platelet mediated Amyloid-β Fibril Formation* 64th annual meeting from the GTH (Society for Thrombosis and Hemostasis) in Bremen, Germany
11/2019	**Poster presentation**: *Involvement of Glycoprotein VI in Platelet mediated Amyloid-β Fibril Formation* Düsseldorf-Jülich Symposium on Neurodegenerative Diseases 2019, in Düsselddorf, Germany

6.4. Affidavit

I declare in lieu of an oath that the dissertation has been written by me independently and without unauthorized outside help, in compliance with the "Principles for Ensuring Good Scientific Practice at the Heinrich Heine University of Düsseldorf".
Furthermore, I confirm that this thesis has not yet been submitted as part of another examination process neither in identical nor in similar.

Düsseldorf, February 2023

6.5. Eidesstattliche Erklärung

Ich versichere an Eides Statt, dass die Dissertation von mir selbständig und ohne unzulässige fremde Hilfe unter Beachtung der „Grundsätze zur Sicherung guter wissenschaftlicher Praxis an der Heinrich-Heine-Universität Düsseldorf“ erstellt worden ist.
Ich erkläre außerdem, dass die Dissertation weder in gleicher noch in ähnlicher Form bereits in einem anderen Prüfungsverfahren vorgelegen hat.

Düsseldorf, Februar 2023

Danksagung

An dieser Stelle möchte ich mich bei all denjenigen bedanken, die mich während der Anfertigung dieser Dissertationsschrift begleitet und unterstützt haben.

Mein Dank gilt Frau Prof. Margitta Elvers, die mir die Möglichkeit gab, meine Dissertation in ihrer Arbeitsgruppe zu schreiben, und die mir ein so interessantes Thema und die Möglichkeit zur Teilnahme an internationalen Konferenzen bot. Darüber hinaus danke ich Frau Prof. Patricia Hidalgo für die Betreuung meiner Dissertation als Erstgutachterin.

Besonderer Dank gilt auch Lili Donner für ihre Unterstützung, Hilfsbereitschaft und Engagement in allen Bereichen dieser Arbeit. Ohne die hilfreichen Anregungen und die konstruktive Kritik wäre die Arbeit in dieser Form nicht möglich gewesen.

Der gesamten Arbeitsgruppe des Instituts für „Experimentellen vaskulären Medizin“ möchte ich danken für die Freude und Hilfsbereitschaft. Durch euch wurde eine tolle Arbeitsatmosphäre geschaffen, in der ich mich jederzeit wohlgefühlt habe. Vielen Dank an Lili, Lisa, Friedrich, Agnes, Tobi, Kim, Dennis, Sevgi und last but not least Martina.

Danken möchte ich auch meiner Familie und insbesondere meinen Eltern, die mich in allen privaten und beruflichen Belangen immer unterstützt haben und immer für mich da sind. Bedanken möchte ich mich bei meinen Freunden, insbesondere bei Lina und Christopher, mit denen ich viele Jahre während meiner Arbeit zusammenlebte und mit denen ich so manches Freud und Leid am Küchentisch teilen durfte. Größen Dank möchte ich auch meinem Freund Paco aussprechen der immer für mich da ist, mich zum Lachen bring und mir so viel Zuversicht und Liebe schenkt.